Regulation and Organisation of Glycogen Metabolism in *Synechocystis* sp. PCC 6803: Insights from *in vitro* Reconstitutions

Dissertation

der Mathematisch-Naturwissenschaftlichen Fakultät

der Eberhard Karls Universität Tübingen

zur Erlangung des Grades eines

Doktors der Naturwissenschaften

(Dr. rer. nat.)

vorgelegt von

Kenric Lee

aus Singapur

Tübingen

2026

Gedruckt mit Genehmigung der Mathematisch-Naturwissenschaftlichen Fakultät der Eberhard Karls Universität Tübingen.

Tag der mündlichen Qualifikation:	12.03.2026
Dekan:	Prof. Dr. Thilo Stehle
1. Berichterstatter/-in:	Prof. Dr. Karl Forchhammer
2. Berichterstatter/-in:	Prof. Dr. Hannes Link

Erklärung

Hiermit erkläre ich, dass ich die zur Promotion eingereichte Arbeit eigenständig verfasst habe. Dabei habe ich ausschließlich die angegebenen Quellen und Hilfsmittel verwendet. Alle Stellen, die wörtlich oder sinngemäß aus den Arbeiten anderer Autorinnen und Autoren übernommen wurden, sind als solche kenntlich gemacht. Eine genaue Abgrenzung meiner eigenen Beiträge von denen meiner Kooperationspartner ist in der „Declaration of Author Contribution“ dargelegt.

Tübingen, den _____

Kenric Lee

世間如酒舎
yo wa marude sakaba no you da

歳月是故客
toki wa furui kyaku no you da

長途風雪苦
nagaki tabi kaze yuki kurushi

良友笑歌行
yoki tomo warai utai yuku

歸家燈火暖
ie ni kaeri tomoshibi atatakai

平生一夢成
heizei no hitotsu no yume naru

Contents

Abbreviations

Abbreviation	Meaning
µE	µmol photons /m^2/s
2-OG	2-oxoglutarate
2-PGA	2-phosphoglycerate
3-PGA	3-phosphoglycerate
Ab	Rabbit polyclonal antibodies
ABC	Ammonium bicarbonate
ACN	Acetonitrile
ADP-Glc	ADP-glucose
ARTO	Alternative respiratory terminal oxidase
C/N	Carbon/Nitrogen
CBB cycle	Calvin–Benson–Bassham cycle
CCM	Carbon concentrating mechanism
CEF	Cyclic electron flow
COX	Cytochrome c oxidase
cyt b_6f	Cytochrome b_6f complex
FA	Formic acid
FNR	Ferredoxin–$NADP^+$ reductase
Fru-6P	Fructose-6-phosphate
GG	Glucosylglycerol
Glc-1P	Glucose-1-phosphate
Glc-6P	Glucose-6-phosphate
GlgA	Glycogen synthase
GlgB	Branching enzyme
GlgC	Glucose-1-phosphate adenylyltransferase
GlgP	Glycogen phosphorylase
GlgX	Debranching enzyme
GS	Glutamine synthetase
HCO_3^-	Bicarbonate
IAA	Iodoacetamide
LDH	Lactate dehydrogenase
LEF	Linear electron flow
NDH	NAD(P)H dehydrogenase
OEC	Oxygen-evolving complex
PEP	Phosphoenolpyruvate
PEPC	Phosphoenolpyruvate carboxylase
PGAM	Phosphoglycerate mutase
PGM	Phosphoglucomutase
PHB	Polyhydroxybutyrate
Pi	Inorganic phosphate / orthophosphate
PK	Pyruvate kinase
PM	Plasma membrane
PPi	Pyrophosphate
PPiase	Pyrophosphatase

PQ	Plastoquinone
PRP	Pentapeptide repeat proteins
PSII	Photosystem II
RTO	Respiratory terminal oxidases
RuBisCO	Ribulose-1,5-bisphosphate carboxylase/oxygenase
RuBP	Ribulose-1,5-bisphosphate
SDH	Succinate dehydrogenases
Synechocystis	*Synechocystis* sp. PCC 6803
TCA cycle	Tricarboxylic acid cycle
TFA	Trifluoroacetic acid
TM	Thylakoid membrane
TrxA	Thioredoxin A

Zusammenfassung

Cyanobakterien nutzen Glykogen als ihren wichtigsten Kohlenstoff- und Energiespeicher, um tageszeitliche und stressbedingte Schwankungen abzufedern. Die zugrunde liegenden Regulationsprinzipien des Glykogenstoffwechsels in *Synechocystis* sp. PCC 6803 konnten jedoch bislang nicht vollständig verstanden werden. Diese kumulative Dissertation untersucht die Steuerungsarchitektur von Glykogensynthese und -abbau durch die Kombination quantitativer Enzymkinetik, *in vitro* rekonstruierter Stoffwechselwege, kinetischer Modellierung, Proteomik und physiologischer Analysen.

Zunächst wird die Glucose-1-phosphat-Adenylyltransferase (GlgC) als streng reguliertes, 3-Phosphoglycerat- (3-PGA)/Pi-verhältnissensitives Regulationselement charakterisiert, das Änderungen der photosynthetischen Leistung und der Phosphatverfügbarkeit in die Bereitstellung von ADP-Glucose übersetzt und so eine ausgeprägte tageszeitliche Asymmetrie der Glykogensynthese erzwingt. Die beiden Glykogen-Synthasen (GlgA1 und GlgA2) weisen vergleichbare intrinsische katalytische Effizienzen auf, arbeiten jedoch in unterschiedlichen Regimen, die durch Primer Architektur und Verzweigungsgrad definiert sind. Zusammen mit dem Verzweigungsenzym GlgB erzeugen sie Glykogenpartikel mit unterschiedlichen Kettenlängenverteilungen und Verzweigungsmustern und offenbaren damit eine funktionelle Arbeitsteilung zwischen Flusskapazität und Polymerarchitektur.

Der Glykogenabbau erweist sich als redox- und stresssensitives Modul. GlgP2 fungiert als Haupt-Glykogen-Phosphorylase unter Standard- und Dunkelbedingungen, während GlgP1 als redoxkontrollierte Reserve unter oxidierenden, stressassoziierten Zuständen aktiviert wird. Die effiziente Mobilisierung von Glykogen bei langanhaltender Dunkelheit und während der Erholung aus der Chlorose hängt entscheidend von der durch GlgX1 vermittelten Entzweigung ab. Pulldown- und Co-Immunpräzipitations-Experimente stützen zudem ein glykogenzentriertes Proteinmilieu, das GlgC–GlgA–GlgB mit GlgP/GlgX verknüpft. Insgesamt etablieren diese Befunde den Glykogenstoffwechsel in *Synechocystis* als räumlich organisiertes Kontrollsystem, das Licht-, Phosphat-, Redox- und Stickstoffsignale integriert und eine mechanistische Grundlage für die gezielte Gestaltung der Kohlenstoffspeicherung in Cyanobakterien liefert.

Summary

Cyanobacteria rely on glycogen as their principal carbon and energy reserve to buffer Diel and stress-induced fluctuations, yet the regulatory logic of glycogen metabolism in *Synechocystis* sp. PCC 6803 has remained incompletely understood. This cumulative work dissects the control architecture of glycogen synthesis and degradation by combining quantitative enzyme kinetics, *in vitro* pathway reconstitution, kinetic modelling, proteomics, and physiological analysis.

First, glucose-1-phosphate adenylyltransferase (GlgC) is characterised as a tightly regulated 3-phosphoglycerate (3-PGA)/Pi ratio-sensing gate that converts changes in photosynthetic output and phosphate availability into ADP-glucose supply, enforcing a strong Diel asymmetry of glycogen synthesis. Second, the two glycogen synthases (GlgA1 and GlgA2) are shown to have comparable intrinsic catalytic efficiencies but distinct operating regimes dictated by primer architecture and branching. Together with the branching enzyme GlgB, they generate glycogen particles with different chain-length distributions and branching patterns, revealing a division of labour between throughput and architecture.

Third, glycogen catabolism is resolved into a redox- and stress-responsive module. GlgP2 emerges as the main glycogen phosphorylase under standard and nocturnal conditions, whereas GlgP1 acts as a redox-controlled reserve activated under oxidising, stress-associated states. Deep mobilisation of glycogen during prolonged darkness and resuscitation from chlorosis critically depends on GlgX1-mediated debranching. Pulldown and co-immunoprecipitation experiments further support a glycogen-centred protein neighbourhood linking GlgC–GlgA–GlgB with GlgP/GlgX.

Together, these findings establish glycogen metabolism in *Synechocystis* as a spatially organised, multi-layered control system that integrates light, phosphate, redox and nitrogen signals, providing a mechanistic framework for rational engineering of cyanobacterial carbon storage.

Publications

1. Accepted publications

Publication 1: Lee K, Doello S, Hagemann M & Forchhammer K (2025) Deciphering the tight metabolite-level regulation of glucose-1-phosphate adenylyltransferase (GlgC) for glycogen synthesis in cyanobacteria. The FEBS Journal 292, 759–775.

Publication 2: Lee K, Bekiari D, Doello S & Forchhammer K (2026) The (Glg)ABCs of cyanobacteria--modelling of glycogen synthesis and functional divergence of glycogen synthases in *Synechocystis* sp. PCC 6803. FEBS Letters

2. Submitted manuscripts

Publication 3: Neumann N, Doello S, **Lee K**, Kauderer B & Forchhammer K (2025) Redox control and substrate specificity of the glycogen catabolic isoenzymes in *Synechocystis* sp. PCC 6803. doi: https://doi.org/10.1101/2022.11.21.517384

3. Declaration of author contribution

Publication 1: *Deciphering the tight metabolite-level regulation of glucose-1-phosphate adenylyltransferase (GlgC).*

I designed and conducted all the experiments and analyses in the study, except for the mass photometry experiment shown in Figure 8, and the construction of the GlgC-long expression plasmid. The paper was written with the feedback and supervision of Prof. Dr. Forchhammer.

Publication 2: *The (Glg)ABCs of cyanobacteria--modelling of glycogen synthesis and functional divergence of glycogen synthases in Synechocystis sp. PCC 6803.*

I designed and conducted all other experiments and analyses in the study except for data shown in Figure 7. For those, I only designed the experiments and analysed the results. The paper was written with the feedback and supervision of Prof. Dr. Forchhammer.

Publication 3: *Redox control and substrate specificity of the glycogen catabolic isoenzymes in Synechocystis sp. PCC 6803.*

I designed and conducted the physiological experiments data shown in Figures 5 and 6F. I also generated fresh knockout mutants of GlgP1, GlgP2 and the GlgP1/GlgP2 double mutant used in the study.

Chapter I. Introduction

1. Cyanobacteria

1.1. In the beginning, there were Cyanobacteria

Cyanobacteria, also known as Cyanophyta, constitute a phylum of Gram-negative prokaryotes within the domain Bacteria and are regarded as some of the most ancient organisms on Earth, with fossil evidence indicating their existence as early as 2.7 to 2.45 billion years ago. Notably, cyanobacteria are the only prokaryotes capable of performing oxygenic photosynthesis, a groundbreaking metabolic innovation that fundamentally transformed Earth's biosphere. Approximately 2.45 billion years ago, the advent of oxygenic photosynthesis by cyanobacteria catalyzed the Great Oxidation Event, converting Earth's atmosphere from a reducing to an oxidizing state. This pivotal environmental transition not only precipitated a massive extinction event but also laid the foundation for the evolution of complex, aerobic life forms [1–3].

Since their emergence, cyanobacteria have demonstrated extraordinary ecological versatility, enabling them to colonize a vast array of terrestrial and aquatic habitats worldwide [4]. Today, they represent a diverse and ecologically critical group of prokaryotes, serving as essential primary producers responsible for approximately one quarter to one third of global CO_2 fixation. Beyond their role in carbon cycling, certain cyanobacterial strains possess the enzymatic machinery necessary for biological nitrogen fixation [5]. Through the action of the nitrogenase enzyme complex within specialized cells known as heterocysts, these organisms convert atmospheric nitrogen (N_2) into bioavailable ammonium, thus significantly contributing to the global nitrogen cycle and supporting the productivity of numerous ecosystems.

Morphologically, cyanobacteria exhibit considerable diversity and are classified into five major sections based on characteristics of cell organization and modes of reproduction [6,7]. Section I encompasses unicellular cyanobacteria that reproduce by binary fission or budding. Section II includes unicellular strains capable of multiple fission, resulting in the formation of baeocytes. Section III is composed of filamentous strains that divide in a single plane and do not differentiate specialized cell types. Section IV contains filamentous cyanobacteria that can develop specialized cells, such as heterocysts for nitrogen fixation, akinetes for dormancy, and hormogonia for motility. Section V also comprises filamentous cyanobacteria with specialized cells but is distinguished by the ability to divide in more than one plane. Collectively, cyanobacteria remain indispensable to global biogeochemical cycles as primary biomass producers and nitrogen fixers, with a profound and continuing impact on ecosystem function and evolutionary history.

1.2. The model cyanobacterium Synechocystis sp. PCC 6803

Synechocystis sp. PCC 6803 (hereafter *Synechocystis*) is a unicellular cyanobacterium from Section I, first isolated from a freshwater lake in Berkeley in 1968 [8]. It tolerates freshwater and near-coastal high-salinity environments and was the first fully sequenced photoautotrophic organism, with natural competence for uptake of exogenous DNA facilitating genetic modification [9,10]. *Synechocystis* is metabolically versatile, capable of mixotrophic and light-activated heterotrophic growth using external carbon sources. It is non-diazotrophic, relying on combined nitrogen sources, and adapts to nitrogen limitation by entering a dormant-like state [11].

Under stress, *Synechocystis* produces storage polymers such as glycogen, polyhydroxybutyrate, cyanophycin, and polyphosphate, highlighting its biotechnological potential [11–15]. These features make it a valuable model for studying photosynthesis, metabolism, stress responses, and biotechnological applications.

2. Bioenergetic processes in *Synechocystis* sp. PCC 6803

In Cyanobacteria, the earliest oxygenic phototrophs, photosynthesis and respiration are intricately interconnected. The model organism *Synechocystis* primarily grows photoautotrophically, deriving its energy from oxygenic photosynthesis when light and nutrients are abundant. However, it exhibits facultative mixotrophy, enabling the simultaneous utilization of exogenous organic carbon sources, such as glucose, alongside photosynthetic activity. Under dark conditions, energy production is maintained exclusively through respiration [16].

Both photosynthetic and respiratory reactions in *Synechocystis* are localized mainly within the thylakoid membranes, which serve as the central site for electron transport, as shown below in **Figure 1**. A simplified respiratory chain also exists in the plasma membrane [17]. Uniquely, cyanobacteria possess overlapping components within their photosynthetic and respiratory electron transport chains—an evolutionary feature not found in other organisms [17–19]. The thylakoid electron transport chain establishes a proton motive force across the membrane, which drives ATP synthesis via the F_0F_1-ATP synthase complex. This process represents the universal mechanism of cellular energy conversion, coupling photochemical or respiratory electron transport to ATP generation.

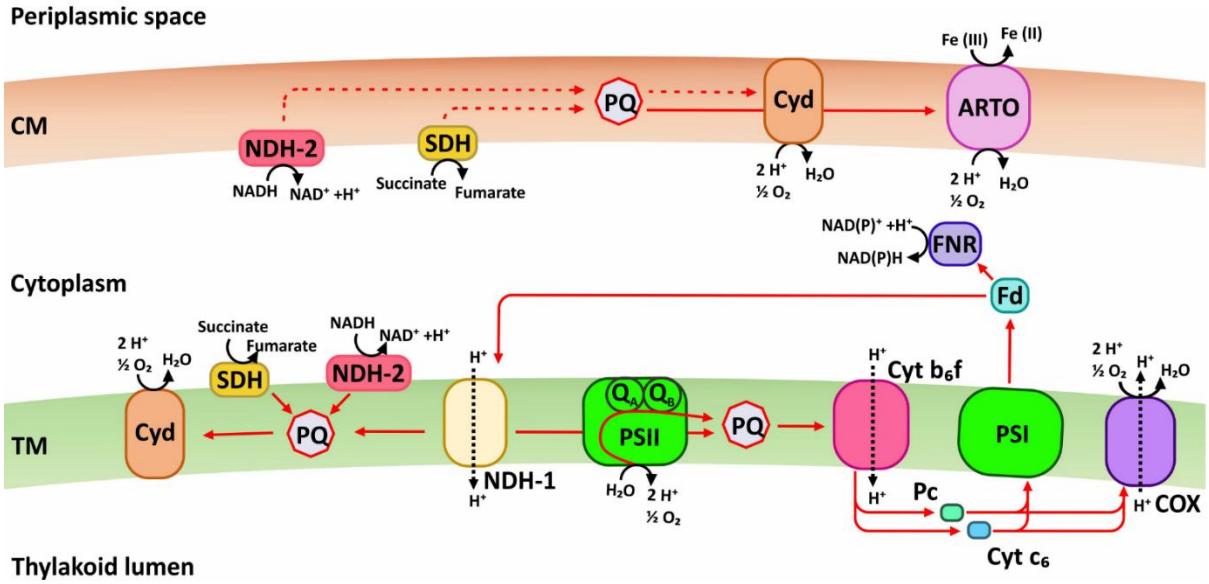

Figure 1: Schematic depiction of the cyanobacterial electron transport chain within the cytoplasmic membrane (CM) and thylakoid membrane (TM). Adapted from Krömer et al (2025). Red arrows indicate the direction of electron transport, dashed red lines indicate electron transport pathways that are not experimentally verified, and black dotted arrows indicate the direction of proton transport across the TM.

RTO: respiratory terminal oxidase; PS I/II: photosystem I/II; OEC: oxygen evolving complex; Fd: ferredoxin; FNR: ferredoxin-NADP+ reductase; PQ: plastoquinol; cyt b_6f: cytochrome b6f; PC: plastocyanin; cyt-c6: cytochrome c6; ARTO: alternative respiratory terminal oxidase; COX: cytochrome c oxidase; SDH: succinate dehydrogenase; NDH: NAD(P)H dehydrogenase.

2.1. Oxygenic photosynthesis

Oxygenic photosynthesis is a cornerstone of global primary productivity, driving the conversion of light energy into chemical energy, carbohydrates, and molecular oxygen that collectively sustain nearly all life on Earth. This process comprises two interconnected phases: the light-dependent reactions, in which absorbed solar energy is transformed into ATP and reducing equivalents such as NADPH, and the light-independent (carbon) reactions, in which these energy-rich compounds power the fixation of atmospheric CO_2 into organic carbon. The light-dependent reactions initiate at photosystem II (PSII), a pigment–protein complex composed of a light-harvesting antenna, a reaction center, and an oxygen-evolving complex (OEC). In cyanobacteria such as *Synechocystis*, light is captured primarily by phycobilisomes, large hemi-discoidal structures consisting of phycobiliproteins—phycoerythrin, phycocyanin, phycoerythrocyanin, and allophycocyanin—that efficiently transfer excitation energy to the chlorophyll a molecule P680 in the PSII reaction center [20–22]. Upon photon absorption, P680 becomes photooxidized, transferring an electron to a plastoquinone acceptor, which is subsequently reduced to plastoquinol while the OEC restores P680 by oxidizing water molecules. The oxidation of two water molecules yields four electrons, four protons, and one molecule of oxygen, thereby contributing to the proton gradient across the thylakoid membrane [21,23]. The reduced plastoquinol diffuses within the thylakoid membrane and transfers electrons to the cytochrome b_6f complex (cyt b_6f) via the Q cycle—a series of redox reactions that release protons into the thylakoid lumen and deliver electrons to the soluble carriers plastocyanin or cytochrome c_6. Under conditions of over-reduction or high light intensity, excess plastoquinol may also react with molecular oxygen, leading to the formation of reactive oxygen species (ROS)[24].

In *Synechocystis*, plastocyanin serves as the primary electron carrier, while cytochrome c_6 is synthesized under copper-limited conditions. These carriers subsequently deliver electrons to photosystem I (PSI), where excitation of the P700 chlorophyll a by light results in electron transfer to ferredoxin, the terminal electron acceptor of the photosynthetic chain. The oxidized P700 is reduced again by plastocyanin or cytochrome c_6, completing the transfer sequence. Reduced ferredoxin donates electrons to the ferredoxin–$NADP^+$ reductase (FNR), facilitating the formation of NADPH [24]. This sequence of reactions constitutes linear electron flow (LEF), producing both ATP and NADPH that fuel the carbon fixation reactions. Alternatively, electrons can be recycled around PSI through cyclic electron flow (CEF), wherein NADPH is reoxidized by the NAD(P)H dehydrogenase (NDH) complex, transferring electrons back to cyt b_6f and reinforcing the proton gradient without additional NADPH formation [25]. The interplay between LEF and CEF provides a crucial regulatory mechanism, allowing photosynthetic organisms to adjust the ATP/NADPH production ratio in response to varying metabolic and environmental conditions. The resulting proton motive force across the thylakoid membrane is harnessed by the F_0F_1-ATP synthase complex to drive ATP synthesis, representing the universal mechanism of biological energy transduction [26–28]. The subsequent fixation of CO_2 into carbohydrates, utilizing the ATP and NADPH generated in these light-dependent reactions, is discussed later in section *3.1*.

2.2. Oxidative respiration

Respiration, also known as oxidative phosphorylation, constitutes the metabolic counterpart to oxygenic photosynthesis, utilizing the energy-rich products of photosynthesis together with molecular oxygen to generate ATP, CO_2, and water. In cyanobacteria, respiratory and

photosynthetic electron transport chains are intricately intertwined and share several components, making these organisms unique in combining both pathways within the same thylakoid membrane system [19]. Most respiratory activity occurs in the thylakoid membranes, where electron transport reactions establish an electrochemical proton gradient that drives ATP synthesis via the F_0F_1-ATP synthase complex, similar to that of photosynthesis [28]. Respiratory electron transport is initiated primarily by type I NADPH dehydrogenases (NDH-1) and succinate dehydrogenases (SDH), which oxidize NAD(P)H and succinate, respectively, and transfer the resulting electrons to the plastoquinone (PQ) pool. Reduced plastoquinol subsequently donates electrons to the cytochrome b_6f complex (cyt b_6f), which channels electrons to the soluble carriers plastocyanin and cytochrome c_6 while simultaneously translocating protons into the thylakoid lumen via the Q cycle. The terminal step of respiration involves the respiratory terminal oxidases (RTOs), which reduce molecular oxygen to water and contribute further to the proton motive force [19,24,29]. In *Synechocystis*, three major RTOs have been identified: the cytochrome c oxidase (COX, aa_3-type), which receives electrons from cyt b_6f; the bd-type quinol oxidase; and the alternative respiratory terminal oxidase (ARTO), both of which accept electrons directly from plastoquinol [30]. Although the mechanisms of energy transduction in photosynthesis and respiration are closely related, these two processes are typically separated in time to prevent interference, a phenomenon known as the Kok effect [31,32]. In addition to the thylakoid membrane, *Synechocystis* also harbours a more rudimentary respiratory chain within the plasma membrane, comprising SDH, type II NAD(P)H dehydrogenases (NDH-2)—encoded by ndbA, ndbB, and ndbC—plastoquinone, and ARTO. While plasma membrane respiration contributes minimally to ATP generation under normal growth conditions, it plays important physiological roles in processes such as motility, nutrient uptake, and efflux pump function [33]. Under certain conditions, such as resuscitation from chlorosis or when proton translocation is energetically unfavourable, the plasma membrane can also employ a sodium motive force to sustain ATP synthesis [34]. Together, these respiratory systems provide *Synechocystis* with remarkable metabolic flexibility, enabling efficient energy conversion under fluctuating environmental conditions.

3. Carbon Storage and metabolism

3.1. Carbon fixation

A defining feature of cyanobacterial physiology is their ability to alternate between autotrophic and heterotrophic metabolism in response to the day–night cycle. During the light period, photosynthetic activity drives carbon fixation and the accumulation of storage compounds, whereas during darkness, these stored reserves are mobilized through respiration to sustain essential cellular functions in the absence of photosynthetic energy generation.

The central pathway for carbon fixation in cyanobacteria is the Calvin–Benson–Bassham (CBB) cycle. Within this cycle, the enzyme ribulose-1,5-bisphosphate carboxylase/oxygenase (RuBisCO) catalyses the incorporation of carbon dioxide (CO_2) into ribulose-1,5-bisphosphate (RuBP), yielding two molecules of 3-phosphoglycerate (3-PGA). These intermediates can either re-enter the CBB cycle to regenerate RuBP or serve as precursors for a wide variety of biosynthetic processes, including amino acid, lipid, and carbohydrate synthesis [5]. However, RuBisCO is characterized by a relatively low specificity for CO_2 and can also catalyse an oxygenation reaction in which O_2 is used as a substrate, producing one molecule of 3-PGA and one of 2-phosphoglycolate. The latter is a toxic compound that must be recycled through

photorespiration—an energetically expensive process that consumes ATP and reducing power while releasing previously fixed carbon [35]. Consequently, photorespiration represents a major limitation to photosynthetic efficiency and growth, particularly under low-CO_2 or high-O_2 conditions.

To overcome the inherent inefficiency of RuBisCO, cyanobacteria have evolved a sophisticated carbon concentrating mechanism (CCM) that enhances CO_2 availability at the site of fixation and suppresses photorespiration. The CCM integrates multiple inorganic carbon uptake and conversion systems, enabling cells to accumulate CO_2 and bicarbonate (HCO_3^-) far above ambient concentrations [5,36,37]. Five major transporter systems contribute to this process: the CO_2 uptake complexes NDH-I_3 and NDH-I_4, which are associated with the thylakoid membrane, and three HCO_3^- transporters—BCT1, SbtA, and BicA—located in the plasma membrane. These transporters differ in their affinities, transport kinetics, and energy requirements, ensuring efficient carbon acquisition across a wide range of environmental conditions. Once inside the cytoplasm, HCO_3^- is delivered to specialized polyhedral microcompartments known as carboxysomes. Within these proteinaceous structures, carbonic anhydrase converts HCO_3^- into CO_2, which is then immediately fixed by RuBisCO. The carboxysome shell is selectively permeable, allowing the diffusion of small metabolites such as RuBP and 3-PGA while preventing CO_2 leakage, thus maintaining a microenvironment with elevated CO_2 concentrations that promote carboxylation efficiency.

In addition to the CBB cycle, cyanobacteria possess an auxiliary carbon fixation route mediated by phosphoenolpyruvate carboxylase (PEPC). This enzyme catalyses the β-carboxylation of phosphoenolpyruvate (PEP) to produce oxaloacetate, a key intermediate that feeds into the tricarboxylic acid (TCA) cycle and supports nitrogen assimilation. PEPC may contribute up to 20% of total carbon fixation, underscoring its physiological importance as an anaplerotic and regulatory node in central metabolism [38]. Together, the CBB and PEPC pathways provide cyanobacteria with the metabolic flexibility to maintain carbon balance and adapt to changing environmental CO_2 availability.

3.2. Carbon utilisation pathways

Cyanobacterial carbon metabolism is tightly regulated to ensure optimal partitioning of resources between anabolic and catabolic processes. The transition between light-dependent CO_2 fixation and dark-dependent respiration is coordinated by complex regulatory networks that integrate signals from multiple sources, including the cellular redox state, the carbon-to-nitrogen (C/N) ratio, and environmental light conditions. Central to this regulation is the circadian clock, which synchronizes metabolic activities with the day–night cycle [39,40]. These signalling systems collectively ensure that carbon fixation, storage, and degradation occur in a temporally and energetically balanced manner.

The degradation of carbon reserves becomes particularly crucial during the dark phase, when photosynthesis ceases and energy must be derived from internal stores. Glycogen serves as the principal carbon reserve in cyanobacteria, and its catabolism begins with the formation of glucose-6-phosphate (Glc-6P). This metabolite is produced either through glycogen breakdown or by the phosphorylation of imported glucose via glucokinase. In *Synechocystis*, glucose-6P acts as a central hub connecting multiple glycolytic and biosynthetic pathways. It can be metabolized through three distinct routes highlighted in **Figure 2**: the Embden–Meyerhof–Parnas (EMP) pathway, the Entner–Doudoroff (ED) pathway, and the oxidative pentose

phosphate (OPP) pathway [37,41]. Although all three pathways contribute to energy generation and the production of reducing equivalents, they differ significantly in their metabolic outputs and cofactor balances. The EMP pathway provides the highest ATP yield and generates NADH but does not supply pentose sugars, which are essential for nucleotide and nucleic acid synthesis. These pentoses are instead produced via the OPP pathway, which primarily generates NADPH and enables the complete oxidation of glucose-6P to CO_2. Each run of the OPP pathway releases one molecule of CO_2 and produces NADPH, making it an efficient source of reducing power for biosynthetic reactions and respiration. The ED pathway, an active glycolytic route in *Synechocystis* is also particularly advantageous under conditions in which photosynthesis and carbohydrate degradation must proceed simultaneously, as it reduces the competition for enzymes shared between the CBB and EMP/OPP pathways [42]. The coordinated regulation of these metabolic routes ensures a balanced distribution of carbon flux between energy generation, biomass synthesis, and storage. Such regulation is essential for maintaining metabolic homeostasis during the transitions between day and night and for adapting to environmental changes such as nutrient availability or light intensity.

Altogether, the intricate network of carbon fixation, storage, and degradation pathways highlights the evolutionary optimization of cyanobacterial metabolism. By integrating multiple layers of regulation, cyanobacteria maintain a fine-tuned balance between autotrophic and heterotrophic states [37]. This metabolic adaptability not only supports their ecological success but also makes them promising model organisms for the study of photosynthetic regulation and for biotechnological applications aimed at sustainable carbon capture and bioresource production.

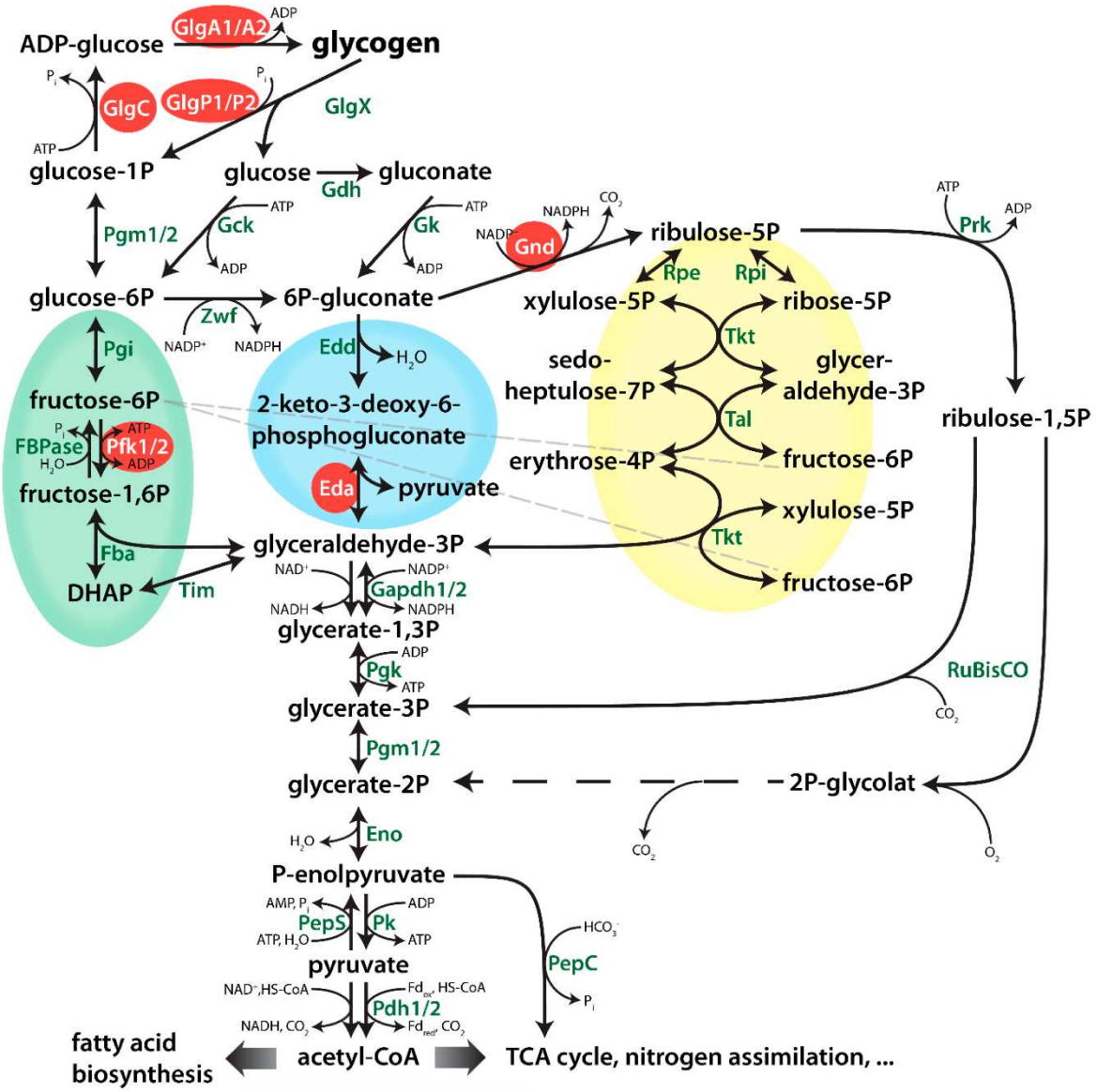

Figure 2: Overview of the main carbon metabolism pathways in *Synechocystis*. Adapted from Koch et al (2019). EMP: Embden-Meyerhof-Parnas (Green), ED: Entner-Doudoroff (Blue), OPP: Oxidative Pentose Phosphate (Yellow)

3.3. The glycogen cycle

In *Synechocystis*, the glycogen cycle—encompassing glycogen synthesis, storage, and degradation—represents a central metabolic mechanism that allows the cell to balance carbon assimilation with fluctuating energy demands and environmental cues **(Figure 2)**. Unlike a passive carbon-storage process, the glycogen cycle in *Synechocystis* is an active, regulatory network that integrates photosynthetic carbon fixation, redox homeostasis, and cellular adaptation to light–dark and nutrient transitions [43].

3.3.1. Glycogen Synthesis

Glycogen synthesis begins with the interconversion of glucose-6-phosphate (Glc-6P) and glucose-1-phosphate (Glc-1P) via phosphoglucomutase (PGM), linking the central carbon metabolism to glycogen biosynthesis [44,45]. The first committed step of the pathway is catalyzed by GlgC (*slr1176*, Glucose-1-phosphate adenylyltransferase), which converts Glc-1P and ATP into ADP-glucose (ADP-Glc) and pyrophosphate (PPi). This reaction commits carbon from central metabolism into glycogen biosynthesis and serves as a primary regulatory node balancing carbon partitioning between anabolic and storage pathways [46].

The regulation of GlgC in *Synechocystis* is characterized by a dual allosteric control system that tightly integrates the cell's photosynthetic and energetic states through two key metabolites: 3-PGA and inorganic phosphate (Pi). During active photosynthesis, when the CBB cycle operates at high flux, 3-PGA accumulates and acts as a potent allosteric activator of GlgC. Binding of 3-PGA induces a conformational change that enhances the enzyme's catalytic efficiency, effectively coupling glycogen synthesis to photosynthetic carbon fixation [47–49]. This ensures that when photosynthetic ATP and NADPH are abundant, excess fixed carbon can be transiently stored in glycogen rather than overloading the reductive metabolism. Conversely, Pi serves as a competitive inhibitor that antagonizes 3-PGA activation [47,48]. During darkness or metabolic limitation, when ATP consumption declines, intracellular Pi concentrations rise and suppress GlgC activity, thereby reducing glycogen synthesis when energy conservation is essential [47,48]. The opposing effects of 3-PGA and Pi create a sensitive metabolic switch: a high 3-PGA/Pi ratio favours glycogen synthesis under light and carbon-replete conditions, whereas a low ratio inhibits it under dark or energy-limited states.

Beyond allosteric regulation, GlgC is also modulated by redox control through reversible thiol–disulfide exchange in cysteine residues. Under reducing conditions—typically during the light phase—thioredoxin-dependent reduction activates GlgC, while oxidative conditions in the dark suppress its activity [46]. This redox regulation adds a further layer of control that synchronizes glycogen synthesis with the photosynthetic electron transport chain and intracellular redox poise. Together, these regulatory features enable GlgC to function as a metabolic integrator, translating dynamic cellular signals of carbon availability, energy status, and redox balance into coordinated control of glycogen synthesis.

Following ADP-Glc formation, two GlgA (glycogen synthase) isoenzymes—GlgA1 (*sll0945*) and GlgA2 (*sll1393*)—elongate the α-1,4-linked glucan chains by transferring glucose residues from ADP-Glc to the growing polymer. Although their functions partially overlap, GlgA2 is believed to be the primary enzyme for glycogen polymerization during photosynthetically active growth, while GlgA1 fine-tunes chain length distribution under specific environmental or stress conditions [50,51]. The branching enzyme GlgB (*sll0158*) introduces α-1,6 linkages to generate a compact and highly branched glycogen granule, improving solubility and enzymatic accessibility during subsequent degradation. During light periods, glycogen serves as a metabolic sink that prevents over-reduction of the photosynthetic apparatus by storing excess carbon and reducing equivalents [52]. Disruption of these enzymes results in severe physiological perturbations, including reduced glycogen accumulation, altered redox homeostasis, and impaired photosynthetic recovery after dark phases [53].

3.3.2. Glycogen Degradation

During darkness, nutrient deprivation or changing environmental conditions, glycogen degradation ensures the supply of carbon skeletons and energy for maintenance metabolism [11,54,55]. Glycogen breakdown begins with glycogen phosphorylase (GlgP), which catalyses phosphorolytic cleavage of α-1,4-glycosidic bonds, releasing Glc-1P. GlgP is present as two isoforms in *Synechocystis*, GlgP1 (*sll1356*) and GlgP2 (*slr1367*), with GlgP2 thought to be the isoform responsible bulk glycogen degradation under normal conditions or nutrient limitation, whereas GlgP1 is involved in adaptation to physical environmental cues [56,57]. The glycogen debranching enzymes GlgX1 (*slr0237*) and GlgX2 (*slr1857*) concurrently hydrolyses the α-1,6 linkages in the glycogen granule, enabling complete polymer degradation [56,58]. The resulting Glc-1P is converted to Glc-6P via PGM and enters glycolysis or the OPP pathway, generating ATP and NADPH during dark or stress conditions. Mutants lacking GlgP exhibit delayed glycogen mobilization, altered day–night glycogen cycling, and compromised dark survival [59,60]

At the transcriptional level, glycogen metabolism is influenced by nutrient-sensing and stress-response regulators. The nitrogen-responsive regulator NrrA, for example, activates GlgP and GlgX expression under nitrogen starvation, promoting glycogen catabolism and redirecting carbon toward polyhydroxybutyrate (PHB) synthesis [15,61]. This metabolic reallocation demonstrates the coupling between glycogen turnover and broader carbon management strategies in *Synechocystis*. Interestingly, glycogen synthesis and degradation can operate concurrently, forming a controlled futile cycle that helps dissipate excess ATP and stabilize redox balance under fluctuating light or nutrient regimes [52,62]. The fine-tuned balance among GlgC, GlgA1/GlgA2, GlgB, and GlgP activities allows the cell to dynamically adjust glycogen turnover to the prevailing environmental and metabolic state.

In summary, the glycogen cycle in *Synechocystis* constitutes a highly regulated network that coordinates carbon storage and mobilization with cellular energy and redox status. Through the coordinated actions of glycogen synthesis and degradation enzymes, *Synechocystis* achieves metabolic flexibility across Diel and nutrient cycles, ensuring survival and physiological stability under environmental fluctuations. Understanding this regulatory framework provides critical insight into how cyanobacteria achieve homeostasis and offers strategies for optimizing carbon flux in biotechnological applications.

4. Nitrogen metabolism

In *Synechocystis*, combined nitrogen (NH_4^+, NO_3^-, urea) is taken up by dedicated permeases, reduced and assimilated via the GS–GOGAT cycle to yield glutamate, the universal nitrogen-donor. The assimilation node 2-oxoglutarate (2-OG) provides the carbon skeleton for GOGAT and simultaneously reports the cellular C/N status, thereby coupling nitrogen flux to central carbon metabolism and transcriptional control by the PII–PipX–NtcA system [63–66].

4.1. Regulation of nitrogen metabolism

PII senses the cellular energy state (ATP/ADP) and binds to 2-OG in its ATP-bound state, thus acting as a sensor for both energy and C/N balance. In cyanobacteria, PII is additionally regulated by T-loop phosphorylation in response to nitrogen status. When 2-OG is low (nitrogen-replete), PII sequesters PipX and prevents NtcA activation; rising 2-OG causes the

release of PipX to co-activate NtcA and induce the low-nitrogen regulon, consisting of around 80 genes, including uptake systems and *glnA* glutamine synthetase (GS) [64–66].

NtcA not only activates assimilation and transport genes but also represses *gifA*/*gifB*, which encode the GS inactivators IF7/IF17, thereby reinforcing GS activity under nitrogen demand. Post-transcriptional layers sharpen this control: the NtcA-induced sRNA NsiR4 represses *gifA* translation (feed-forward), while a glutamine-sensing riboswitch upstream of *gifB* couples IF17 synthesis to intracellular glutamine, allowing rapid, metabolite-level tuning of GS activity [65].

C/N control can also feed directly into carbon partitioning at the 3-PGA node **(Figure 3)**. Under nitrogen sufficiency (low 2-OG), PII forms a complex with PirC (*sll0944*), relieving inhibition of the 2,3-bisphosphoglycerate-independent phosphoglycerate mutase (PGAM) and favouring lower glycolysis. Under N limitation (high 2-OG), PirC dissociates from PII and inhibits PGAM, diverting newly fixed carbon to glycogen. This PirC→PGAM gate provides an immediate, metabolite-driven rerouting of carbon in step with nitrogen status [67].

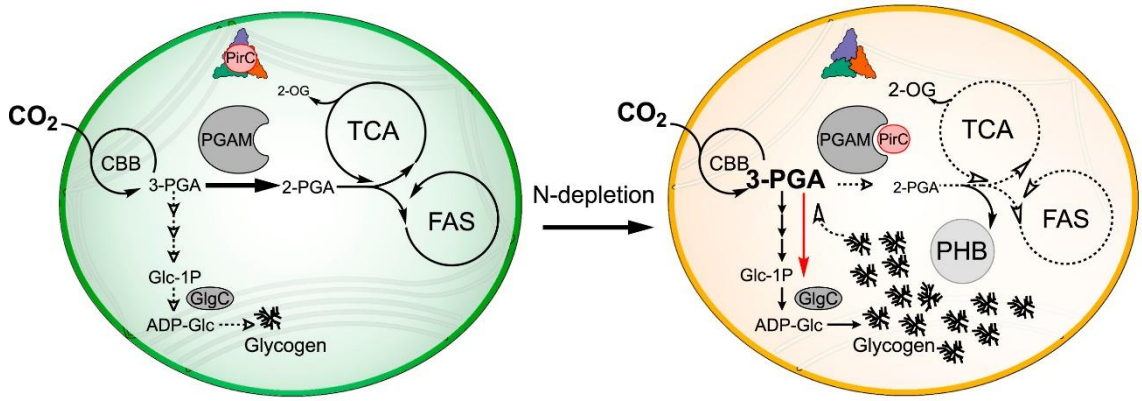

Figure 3: Model of PirC–PII–PGAM control of central carbon flux. Under low 2-oxoglutarate (2-OG; vegetative growth), trimeric PII sequesters PirC, keeping PGAM active so 3-phosphoglycerate (3-PGA) feeds fatty acid synthesis and amino acid biosynthesis via the TCA cycle. Under nitrogen depletion (high 2-OG), PirC is released, inhibits PGAM, elevates 3-PGA, activates GlgC, and redirects carbon to glycogen. CBB: Calvin–Benson–Bassham cycle, FAS: Fatty acid synthesis, TCA: Tricarboxylic acid cycle. Adapted from Orthwein et al (2021).

4.2. Adaptation to nitrogen limitation

Loss of combined nitrogen triggers a rapid 2-OG spike and NtcA-dependent activation of the non-bleaching (nbl) program. NblA-driven phycobilisome dismantling alleviates over-reduction pressure, liberates amino acids, and yields the characteristic chlorosis phenotype (blue-green→yellow-orange) [11,65,68]. Concurrently, essentially all newly fixed carbon is channelled to glycogen; PirC-mediated PGAM inhibition is central to this switch, and glycogen accumulation is essential for successful chlorosis and survival [11,67,68].

Prolonged nitrogen starvation establishes a quiescent state with growth arrest after DNA replication, massive reduction of thylakoid membranes, and a set-point drop of ATP to ~25% of vegetative levels. Bioenergetics pivot to a sodium-motive strategy: residual photosystems and an alternative respiratory chain energize the plasma membrane, and cytoplasmic-membrane ATP synthases use Na^+ to sustain minimal ATP homeostasis—critical both for long-term viability and for rapid ATP upshifts upon the re-availability of nitrogen [34,69].

5. Research goals

Glycogen serves as the principal carbon and energy reserve in cyanobacteria such as *Synechocystis*, buffering fluctuations in photosynthetic input across diurnal cycles and enabling survival under stress (e.g., nutrient limitation or darkness). Although the canonical pathway is established, the regulatory logic and division of labor among enzyme isoforms are not fully resolved. Clarifying how synthesis and degradation are coordinated will illuminate broader principles of bacterial metabolic control and stress acclimation. Guided by this motivation, we aim to answer the following questions:

1. How is GlgC regulated in *Synechocystis*, such as control by the main allosteric effectors and how do these molecules effectively modulate under physiologically relevant conditions?
2. Do the GlgA isoenzymes differ in catalytic properties and substrate/primer preferences, and do they generate distinct product profiles?
3. What is the specific contribution of GlgB to glycogen, and does its activity or functional interplay vary with individual GlgA isoenzymes beyond simply introducing α-1,6 linkages?
4. How do the GlgP and GlgX isoforms contribute to glycogen mobilization and remodelling during prolonged darkness and nitrogen starvation, and by what mechanisms are these activities modulated in response to environmental cues?

Chapter II. Results

This chapter summarises the findings of the respective publications relevant to this thesis. Relevant material from additional research is presented in a separate section unless indicated.

Publication 1: Research Article

Lee K, Doello S, Hagemann M & Forchhammer K (2025) Deciphering the tight metabolite-level regulation of glucose-1-phosphate adenylyltransferase (GlgC) for glycogen synthesis in cyanobacteria. The FEBS Journal 292, 759–775.

Publication 2: Research Article

Lee K, Bekiari D, Doello S & Forchhammer K (2026) The (Glg)ABCs of cyanobacteria--modelling of glycogen synthesis and functional divergence of glycogen synthases in *Synechocystis* sp. PCC 6803. FEBS Letters.

Publication 3: Research Article

Neumann N, Doello S, **Lee K**, Kauderer B & Forchhammer K (2025) Redox control and substrate specificity of the glycogen catabolic isoenzymes in *Synechocystis* sp. PCC 6803.

1. The Regulation of GlgC

Publication 1: Research Article (Published)

Kenric Lee, Sofia Doello, Martin Hagemann & Karl Forchhammer (2025)

Deciphering the tight metabolite-level regulation of glucose-1-phosphate adenylyltransferase (GlgC) for glycogen synthesis in cyanobacteria.

The FEBS Journal 292, 759–775.

1.1. Re-annotation of GlgC and establishment of a continuous glycogen-coupled assay.

Re-examination of the GlgC locus identified a mis-annotated N-terminal extension, and a shorter GlgC variant lacking the extra 10 amino acids was cloned and purified. The truncated GlgC displayed ~10-fold higher specific activity than the long form in a malachite green assay, establishing it as the physiologically relevant isoform **(Publication 1, Fig. 1A–B)**. To overcome the limitations of discontinuous phosphate-release readouts, GlgC was then coupled to GlgA1 and an ADP/NADH system, allowing continuous monitoring of ADP-Glc production via NADH oxidation **(Publication 1, Fig. 2A)**. Compatibility tests confirmed that coupling components did not interfere with either GlgC or GlgA1, and vice versa **(Publication 1, Fig. 2B–D)**. Titration of GlgC against fixed GlgA1 revealed a regime where the coupled velocity scaled linearly with GlgC concentration, and optimisation of enzyme ratios and substrate levels defined a robust operating window for regulation studies **(Publication 1, Fig. 3A–B)**. PPi accumulation remained in the low-µM range and omission of PPiase did not affect GlgC activity, excluding feedback by PPi under assay conditions **(Publication 1, Fig. 3C–D)**. Comparison with the malachite green assay showed that kinetic parameters obtained in the coupled format are quantitatively consistent, validating the continuous assay as a reliable proxy for the native GlgC–GlgA flux **(Publication 1, Fig. 1B; Fig. 4A)**.

1.2. 3-PGA and Fru-6P define the activation landscape of GlgC.

Effector screening using central carbon metabolites identified 3-PGA and fructose-6-phosphate (Fru-6P) as the dominant activators of GlgC, whereas several glycolytic intermediates exerted inhibitory or negligible effects **(Publication 1, Fig. 4B)**. Quantitative titrations revealed that 3-PGA is a high-potency activator, yielding ~8-fold activation with an EC_{50} of ~0.43 mM **(Publication 1, Fig. 5A)**. Fru-6P activated GlgC weakly ($EC_{50} \approx 2.3$ mM) and achieved only ~3-fold maximal stimulation **(Publication 1, Fig. 5B)**. Under low 3-PGA, Fru-6P further increased GlgC activity, but at saturating 3-PGA, the effects of additional Fru-6P were not detectable, indicating an activation ceiling set by 3-PGA **(Publication 1, Fig. 5C–D)**. Equivalence analysis showed that even high Fru-6P concentrations only recapitulate the effect of ~0.35 mM 3-PGA, underscoring 3-PGA as the primary activating signal *in vivo* **(Publication 1, Fig. 5D)**. Together, these data define an activation landscape where GlgC is tuned to respond sensitively to 3-PGA over a physiological range, with Fru-6-P acting as a secondary amplifier that cannot override maximal 3-PGA-driven activation.

1.3. Antagonistic inhibition by Pi, PPi and 2-PGA tunes ADP-Glc supply.

The effector screen also identified Pi and 2-phosphoglycerate (2-PGA) as inhibitors of GlgC activity, with additional mild inhibition by Glc-6P and fructose-1,6-bisphosphate (Fru-1,6P) **(Publication 1, Fig. 4B)**. Detailed 2-PGA titrations across different 3-PGA backgrounds revealed a monotonic, approximately linear inhibition without detectable cooperativity, and

incomplete suppression even at high 2-PGA, indicating the modulatory but not fully inhibitory role of 2-PGA **(Publication 1, Fig. 6A–B)**. In contrast, Pi emerged as a strong inhibitor whose potency is acutely modulated by 3-PGA: increasing 3-PGA shifted the Pi IC_{50} to higher concentrations and increased Hill coefficients, revealing cooperative antagonism between activation and inhibition **(Publication 1, Fig. 7A–B)**. Reciprocally, increasing Pi elevated the apparent EC_{50} for 3-PGA, demonstrating a bidirectional 3-PGA↔Pi toggle at the GlgC node **(Publication 1, Fig. 7C)**. PPi inhibited GlgC with roughly twice the potency of Pi ($IC_{50} \approx 0.39$ mM at 2 mM 3-PGA), but the PPi generated by GlgC under turnover conditions remained far below inhibitory levels, implying that direct PPi feedback is unlikely *in vivo* where pyrophosphatases (PPiases) are active **(Publication 1, Fig. 3C; Fig. 7D)**. Collectively, these results establish a regulatory logic in which 3-PGA drives activation while Pi and 2-PGA oppose flux, with Pi providing a highly sensitive, cooperative brake on ADP-Glc production.

1.4. Effector-driven tetramerisation and structural basis for antagonism.

Mass photometry measurements showed that GlgC is predominantly monomeric in the absence of effectors, with smaller fractions of dimers and tetramers **(Publication 1, Fig. 8A)**. Addition of either 3-PGA or Pi shifted the oligomer distribution toward the tetramer form, and combined 3-PGA plus Pi did not further alter the tetramer abundance **(Publication 1, Fig. 8B–D)**. Thus, both activator and inhibitor stabilise the tetrameric assembly, implying that the sign of regulation is encoded in conformational differences within a common tetrameric state rather than in gross oligomerisation. Multiple sequence alignment highlighted conserved N-terminal arginines corresponding to known Pi/Fru-1,6P binding residues, and conserved C-terminal lysines previously implicated in 3-PGA binding in related systems **(Publication 1, Fig. 9A–B)**. AlphaFold2 modelling of tetrameric GlgC positioned these effector-binding residues in close spatial proximity at the subunit interfaces, with a conserved arginine (R294) lying between the putative 3-PGA and Pi sites **(Publication 1, Fig. 10)**. This architecture provides a structural explanation for the observed antagonism, in which binding of either 3-PGA or Pi influences occupancy and conformation at the neighbouring site without preventing tetramer assembly, enabling mutually opposing allosteric states within the same quaternary structure.

1.5. GlgC as a 3-PGA/Pi sensor for Diel control of glycogen synthesis.

By integrating quantitative EC_{50} and IC_{50} values with known metabolite ranges, the data position GlgC as a sensitive sensor–control point converting the balance of 3-PGA and Pi into ADP-Glc flux. The 3-PGA EC_{50} (~0.43 mM) and the Pi inhibition regime overlap with concentrations reported for *Synechocystis* in light and dark growth conditions, respectively, suggesting that light-driven accumulation of 3-PGA and concurrent reduction in free Pi fully activate GlgC, whereas in the dark or under energy limitation, Pi (and possibly PPi) accumulation suppresses flux **(Publication 1, Fig. 5A; Fig. 7A–C)**. 2-PGA inhibition becomes relevant under conditions of enhanced lower glycolysis or photorespiration, where 2-PGA accumulates in the millimolar range and can fine-tune glycogen synthesis against competing biosynthetic demands **(Publication 1, Fig. 6A–B)**. In this framework, Fru-6P provides only modest additional activation and mainly augments GlgC activity when 3-PGA is sub-saturating, reinforcing the primacy of 3-PGA as the light-linked activator **(Publication 1, Fig. 5B–D)**. Together, these observations support a model in which GlgC integrates signals from the Calvin–Benson–Bassham cycle (3-PGA, Fru-6P), glycolysis (2-PGA) and cellular phosphate/energy status (Pi, PPi) to impose tight Diel control over glycogen synthesis in cyanobacteria.

2. Functional Divergence of GlgA Isoenzymes

Publication 2: Research Article (Published)

Kenric Lee, Dimitrios Bekiari, Sofia Doello & Karl Forchhammer (2026)

The (Glg)ABCs of cyanobacteria--modelling of glycogen synthesis and functional divergence of glycogen synthases in Synechocystis sp. PCC 6803.

FEBS Letters

2.1. Comparable catalytic efficiencies but distinct operating regimes of GlgA1 and GlgA2.

Using an ADP/NADH-coupled assay with bovine glycogen as primer, the catalytic properties of GlgA1 and GlgA2 were quantified under identical conditions. GlgA2 exhibited ~50% higher specific activity than GlgA1 (0.77 vs. 0.51 U/mg) but with a slightly higher K_m for ADP-Glc, resulting in very similar catalytic efficiencies ($k_{cat}/K_m \approx 3.2–3.4$/mM/s) **(Publication 2, Fig. 2A)**. An *E.coli* GlgA control showed ~10^3-fold higher activity under the same conditions, validating assay robustness and highlighting the comparatively slow turnover of cyanobacterial synthases **(Publication 2, Fig. 2B)**. A strict primer requirement was also observed for both GlgA isoenzymes, with no glycogen synthesis activity detected in its absence **(Publication 2, Fig. 2C)**. In addition to that, primer titrations showed steep activation with increasing glycogen concentration but substantially weaker responses to soluble starch, with higher EC_{50} values and reduced V_{max} for starch in both enzymes **(Publication 2, Fig. 2C–D)**. These data indicate that GlgA1 and GlgA2 are kinetically similar catalysts tuned to different substrate regimes: GlgA2 favours high-flux elongation at abundant ADP-Glc, whereas GlgA1 operates effectively at lower substrate and primer availability, hinting at distinct roles *in vivo*.

2.2. Primer architecture dictates GlgA activity profiles.

Systematic variation of primer structure revealed strong preferences for branched glucans. Both GlgA1 and GlgA2 utilised short, linear primers (maltose, maltotetraose) but with markedly reduced activity relative to glycogen, and both showed significantly improved performance with branched glycogen compared to linear starch **(Publication 2, Fig. 2C–D)**. The low EC_{50} values for glycogen, contrasted with much higher EC_{50} for starch, demonstrated that branched substrates with many accessible non-reducing ends optimally support GlgA turnover **(Publication 2, Fig. 2D)**. These observations reinforce a strictly primer-dependent mechanism of α-1,4-glycosidic bond formation and imply that primer architecture—chain length, branching density and surface accessibility—acts as a primary determinant of GlgA activity. In physiological terms, this suggests that additional, as yet unidentified, factors likely initiate *de novo* primer formation, while GlgA1 and GlgA2 are specialised for elongation of pre-existing branched glycogen particles rather than for true initiation.

2.3. GlgB-driven branching preferentially potentiates GlgA2.

Inclusion of the branching enzyme GlgB strongly modulated GlgA activity. When GlgB was titrated into reactions using starch as primer, both GlgA isoenzymes showed pronounced activation, with maximal stimulation at ~20 nM GlgB and at least a twofold net activity increase **(Publication 2, Fig. 3A–B)**. However, GlgA2 responded substantially more strongly, achieving a larger absolute activity gain and a lower EC_{50} for GlgB than GlgA1 (4.4 vs. 7.8 μM), and exhibited a Hill coefficient close to 2, indicative of positive cooperativity between GlgB and GlgA2 **(Publication 2, Fig. 3B–C)**. Starch titrations in the presence of GlgB showed

that branching dramatically lowered the primer EC_{50} (≥70-fold for GlgA1 and ≥330-fold for GlgA2) and increased the catalytic efficiencies of both enzymes by at least two orders of magnitude, with GlgA2 again benefitting most **(Publication 2, Fig. 4A–B)**. Notably, GlgA1's maximal activity at saturating starch remained essentially unchanged by GlgB, whereas GlgA2's V_{max} increased by ~22%, highlighting that GlgB not only relieves steric limitation but also enhances the effective throughput of GlgA2 **(Publication 2, Fig. 4A–B)**. These findings indicate that GlgB cooperates more intimately with GlgA2, partitioning elongation labour such that GlgA2 dominates under highly branched, enzyme-crowded conditions, while GlgA1 plays a more modest and less GlgB-dependent role.

2.4. Distinct polymer architectures produced by GlgA isoenzymes and GlgB cooperation.

To connect enzyme mechanics to polymer structure, an extended pathway was assembled by integrating GlgC upstream of GlgA and GlgB, allowing ADP-Glc generation from Glc-1P and subsequent glycogen synthesis from starch primers **(Publication 2, Fig. 5A–B)**. Product quantification showed that GlgA2, particularly in combination with GlgB, yielded higher total glycogen than GlgA1, whereas in the absence of GlgB both enzymes produced considerably less polymer, underscoring the necessity of branching for sustained synthesis **(Publication 2, Fig. 5A–B)**. Iodine–iodide spectra revealed that GlgA1 plus GlgB produced glycogen with lower λ^{max} values, indicative of higher branching density, whereas GlgA2 plus GlgB generated polymers with higher λ^{max} consistent with more linear architecture **(Publication 2, Fig. 5C–D)**. In reactions lacking GlgB, both isoenzymes produced amylose-like, largely linear glucans with λ^{max} comparable to amylose-starch, and yields were strongly reduced, indicating that elongation in the absence of branching is self-limiting **(Publication 2, Fig. 5B–D)**. Comparison with glycogen isolated from Δ*glgA1* and Δ*glgA2* mutants showed that *in vitro* products recapitulate key features of the *in vivo* polymers: GlgA1-associated glycogen is more highly branched, whereas GlgA2-associated glycogen is more linear **(Publication 2, Fig. 6A–C)**. These structural signatures support a division of labour in which GlgA1 favours dense, highly branched glycogen, potentially advantageous for stress resilience, while GlgA2 supports more extended, less-branched particles optimised for rapid accumulation and mobilisation.

2.5. Flux control and integration with upstream ADP-Glc supply.

To place the GlgA module into the broader glycogen-synthesis pathway, we compared intrinsic catalytic capacities of GlgC (from **Publication 1**) and GlgA isoenzymes on a common flux scale. Calculations based on specific activities indicated that physiologically reasonable GlgC:GlgA ratios still leave GlgA as the bottleneck, whereas an *E. coli*-type GlgA would become strongly supply-limited by GlgC **(Publication 2, Table 2)**. Thus, in *Synechocystis*, glycogen synthesis capacity is dictated not by maximal upstream ADP-Glc production but by modest GlgA catalysis modulated by primer architecture and GlgB-driven branching. Integrating these findings with structural analyses and mutant phenotypes suggests that flux partitioning and polymer architecture are jointly governed by (i) the stoichiometry of GlgC, GlgA1, GlgA2 and GlgB, (ii) primer availability and branching, and (iii) the intrinsic kinetic ceiling of the GlgA isoenzymes.

3. Role of GlgP and GlgX in environmental stress

Publication 3: Research Article (Preprint)

Niels Neumann, Sofia Doello, **Kenric Lee**, Bill Kauderer & Karl Forchhammer (2025)

Redox control and substrate specificity of the glycogen catabolic isoenzymes in Synechocystis sp. PCC 6803.

This section also presents unpublished results relevant to the topic of the article.

3.1. Redox-dependent regulation of GlgP1 and its interplay with GlgP2.

The study demonstrated that GlgP1 is a redox-regulated glycogen phosphorylase whose activity is strongly inhibited under reducing conditions (e.g. by DTT or reduced TrxA), whereas GlgP2 remained essentially insensitive to redox changes **(Publication 3, Fig. 2A–B)**. Mutations in the C-terminal cysteine pair or deletion of the C-terminal extension locked GlgP1 in a low-activity state comparable to the fully reduced wild type, establishing this region as a disulfide-based regulatory switch rather than a structural element **(Publication 3, Fig. 4A–C)**. Diurnal survival assays showed that single Δ*glgP1* or Δ*glgP2* mutants displayed only mild defects, but the Δ*glgP1*Δ*glgP2* double mutant was severely compromised **(Publication 3, Fig. 5)**. Under prolonged darkness, Δ*glgP1* mutants exhibited growth defects and survival of Δ*glgP1*Δ*glgP2* was almost abolished, whereas Δ*glgP2* mutants resembled wild type **(Figure 4A)**. Collectively, these findings indicate that both isoforms contribute to nocturnal glycogen phosphorolysis, with GlgP1 acting as a redox-controlled reserve preferentially engaged under oxidising, stress-associated conditions and playing a key role in glycogen mobilisation during both short and extended dark periods.

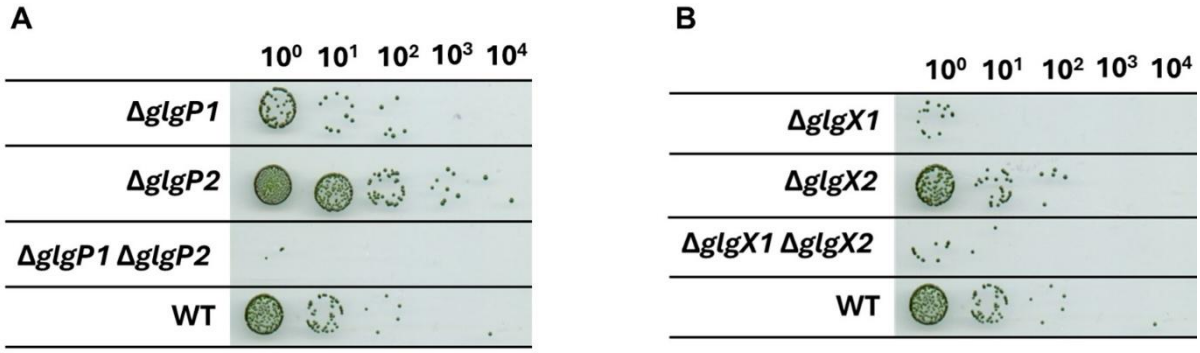

Figure 4: GlgP and GlgX are required for long-term survival during prolonged darkness. [Unpublished results] Spot-viability assay following 14 days of continuous darkness. (A) Δ*glgP* mutants versus wild type (WT). (B) Δ*glgX* mutants versus WT. Strains were first incubated for 14 days in darkness in liquid BG11, then spotted on BG11 agar and placed under constant illumination for 5 days to assess growth.

3.2. GlgX1-dependent debranching as the main route for deep glycogen mobilisation.

While both mutants grew similarly to wild type under standard light and diurnal regimes **(Publication 3, Fig. 6A–B)**, deletion analysis revealed that GlgX1, but not GlgX2, is required for efficient glycogen utilisation during resuscitation from extended chlorosis and prolonged darkness **(Publication 3, Fig. 6C–E; Figure 4B)**. Biochemical assays showed that GlgX1 markedly stimulated GlgP1 and especially GlgP2 on native *Synechocystis* glycogen, whereas GlgX2 lacked detectable debranching activity **(Publication 3, Fig. 7A–B)**. These results

indicate that GlgX1-dependent debranching is essential for complete mobilisation of glycogen stores when carbon reserves must be heavily utilised. Together, the data support a model in which a GlgP2–GlgX1 axis constitutes the principal pathway for deep glycogen degradation, with redox-regulated GlgP1 providing an auxiliary, stress-responsive entry point into the same catabolic module.

4. Additional Results

This section presents additional unpublished results not found in the above publications, but relevant to the topics of this work.

4.1. Effects of Pi inhibition of GlgC on glycogen synthesis

To mechanistically illustrate Pi-dependent control of GlgC on downstream GlgA activity, a minimal kinetic model was constructed that explicitly couples GlgC-mediated ADP-Glc supply to GlgA1 or GlgA2 consumption via a shared ADP-Glc pool, using the kinetic parameters determined in **Publications 1 and 2** and assuming equimolar GlgC:GlgA (1:1) enzyme concentrations **(Figure 5)**.

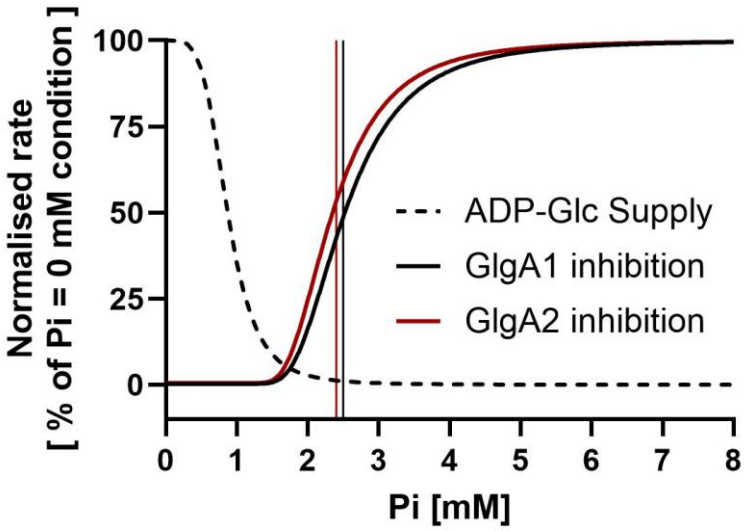

Figure 5: Simulated GlgC–GlgA glycogen-synthesis flux through GlgA1 and GlgA2 at 2 mM 3-PGA as a function of Pi concentration. Solid curves show glycogen-synthesis flux via GlgA1 or GlgA2, normalized to the respective flux at 0 mM Pi and plotted on the y-axis as % of the 0 mM Pi control. The black (GlgA1) and red (GlgA2) vertical lines mark ~2.4–2.5 mM Pi, at which 50% inhibition of GlgC–GlgA glycogen-synthesis flux occurs. The dotted curve shows the predicted GlgC activity (ADP-Glc supply) at 2 mM 3-PGA, likewise expressed as % of the activity at 0 mM Pi. The close overlap of the GlgA1 and GlgA2 curves indicates that, at elevated Pi, flux control resides upstream at GlgC (supply control) rather than downstream at GlgA.

Fluxes are expressed as a percentage of the corresponding 0 mM Pi value to facilitate comparison. Increasing Pi in the low-millimolar range causes a steep decline in ADP-Glc supply and a concomitant reduction in GlgA flux, with ~50% inhibition of glycogen synthesis reached at ~2.4–2.5 mM Pi. Beyond ~4-5 mM Pi, simulated GlgA flux drops to near-zero, indicating an effective inhibition of glycogen synthesis when GlgC is almost fully inhibited. Thus, the model predicts a narrow Pi window in which small changes in inhibitor concentration can produce large changes in net glycogen synthesis, consistent with GlgC acting as a Pi-gated supply node upstream of GlgA.

The inhibition curves for GlgA1- and GlgA2-containing systems are nearly superimposable, with only a modest leftward shift for GlgA2, indicating that both isoforms lose flux capacity

over essentially the same narrow Pi window. Additionally, this behaviour reflects the fact that, in the model, GlgA1 and GlgA2 differ only in their intrinsic catalytic constants, and branching or explicit interactions with GlgB are not represented. *In vivo*, where GlgA1 and GlgA2 form complexes with GlgB and operate on distinct primer landscapes within glycogen particles, these additional layers of organisation are likely to amplify functional divergence between the isoforms and could therefore generate more pronounced differences in Pi-dependent glycogen synthesis behaviour than are captured by this minimal model.

4.2. His-tag pulldown

To probe the protein environment of the glycogen pathway, we performed His-tag pulldowns from chlorotic wild type lysates using bead-immobilised GlgA1, GlgA2 or GlgC as bait (biological triplicates). Enrichment plots display log2 (enrichment vs. empty-bead control) against log10 abundance of the total enrichment; proteins of interest (POIs) were defined by log2FC > 2 and $p < 0.05$.

4.2.1. GlgA1 pulldown co-enriches GlgB and GlgP2 around the glycogen granule.

GlgA1 pulldowns yielded a strong self-recovery of the bait (log2FC = 10.15), validating assay performance. Within the glycogen metabolism module, GlgP2 (sll1367; log2FC = 4.09), GlgB (sll0158; 3.35) and GlgA2 (sll1393; 3.20) were significantly co-enriched, indicating proximity of glycogen phosphorylase and branching activities to the GlgA1-associated glycogen granule during chlorosis **(Figure 6)**. Additional recurrent POIs included an FAD-dependent oxidoreductase (sll1025; 5.70), glutathione S-transferase (slr0605; 3.72) and pterin

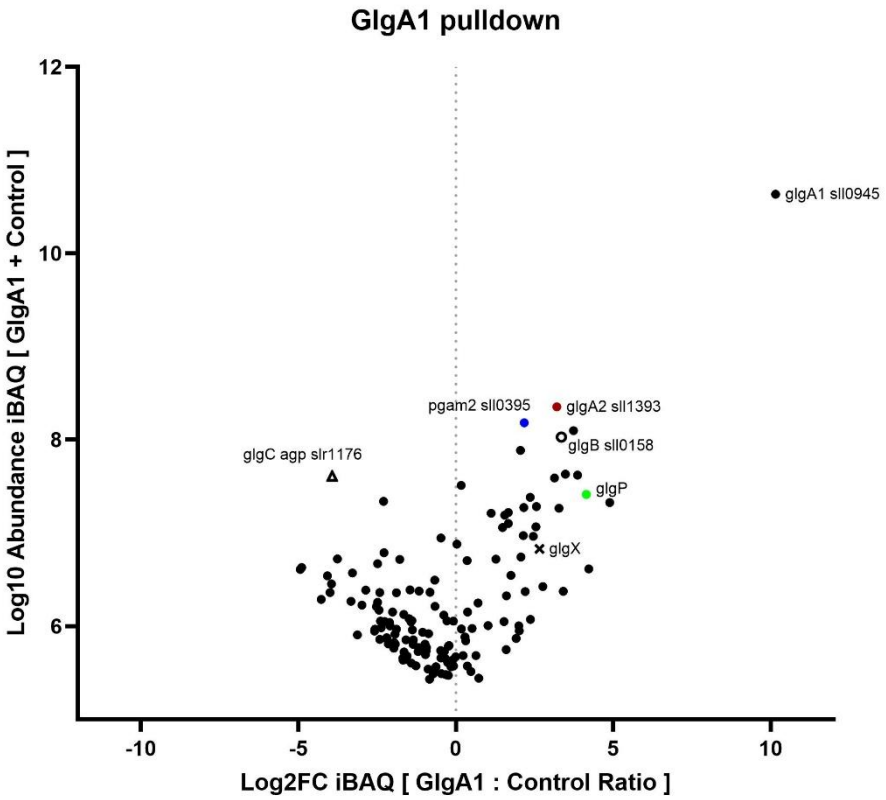

Figure 6: Pulldown of 2-day chlorotic wild type cell lysate using bead-immobilised His-tagged GlgA1 as the bait protein. Each point represents the log2 ratio of protein enrichment in the GlgA1 sample to the control (empty beads) against the log10 abundance of the total enrichment. Each point depicts the mean of biological triplicates (n = 3).

carbinolamine dehydratase (ssl2296; 3.84), alongside other carbon metabolic enzymes such as phosphoglycerate mutase (pgam2, sll0395; 2.17), a phosphoketolase (sll0529; 2.14), and the carboxysome component CcmA (2.34) **(Table 1)**.

Table 1: GlgA1 pulldown POI

	log2FC >2	***P* value < 0.05**
sll0945 Glycogen synthase 1 (GlgA1)	10.15	0.00
sll1025 FAD dependent oxidoreductase	5.70	0.01
sll1367 Alpha-1,4 glucan phosphorylase (GlgP2)	4.09	0.02
sll1524 Haloacid dehalogenase-like hydrolase	3.88	0.00
ssl2296 Pterin carbinolamine dehydratase	3.84	0.00
slr0605 Glutathione S-transferase	3.72	0.01
sll0158 1,4-alpha-glucan branching enzyme (GlgB)	3.35	0.01
sll1393 Glycogen synthase 1 (GlgA2)	3.20	0.00
sll0601 Deaminated glutathione amidase (dGSH amidase)	2.53	0.01
sll0373 Gamma-glutamyl phosphate reductase 1 (GPR 1)	2.51	0.03
ccmA Carboxysome formation protein	2.34	0.03
sll0395 Phosphoglycerate mutase (pgam2)	2.17	0.02
sll0529 D-xylulose 5-phosphate/D-fructose 6-phosphate phosphoketolase	2.14	0.02
folC Tetrahydrofolate synthase	2.11	0.03
slr1619 Rhamnosyl O-methyltransferase (CmcI)	2.04	0.02

4.2.2. GlgA2 pulldown similarly co-enriches GlgB and GlgP2 in addition to GlgX2.

GlgA2 pulldowns likewise showed robust bait enrichment (log2FC = 9.93) and reproducibly captured GlgB (3.46) and GlgP2 (3.33) **(Figure 7)**. Notably, GlgX2 (slr1857; 3.26) surpassed threshold in the GlgA2 dataset, whereas it did not in GlgA1, suggesting a condition-dependent or indirect association between GlgA2-associated glycogen molecules and debranching capacity under chlorosis, even though GlgX2 failed to show any debranching activity in biochemical assays **(Publication 3, Fig. 7)**. GlgA1 co-enriched modestly (2.36), possibly indicating transient or indirect synthase–synthase associations. As in the GlgA1 pulldown, redox-linked proteins (sll1025; slr0605) and ssl2296 were recurrent, and CcmA (2.94) and pgam2 (2.25) were present above cut-off **(Table 2)**.

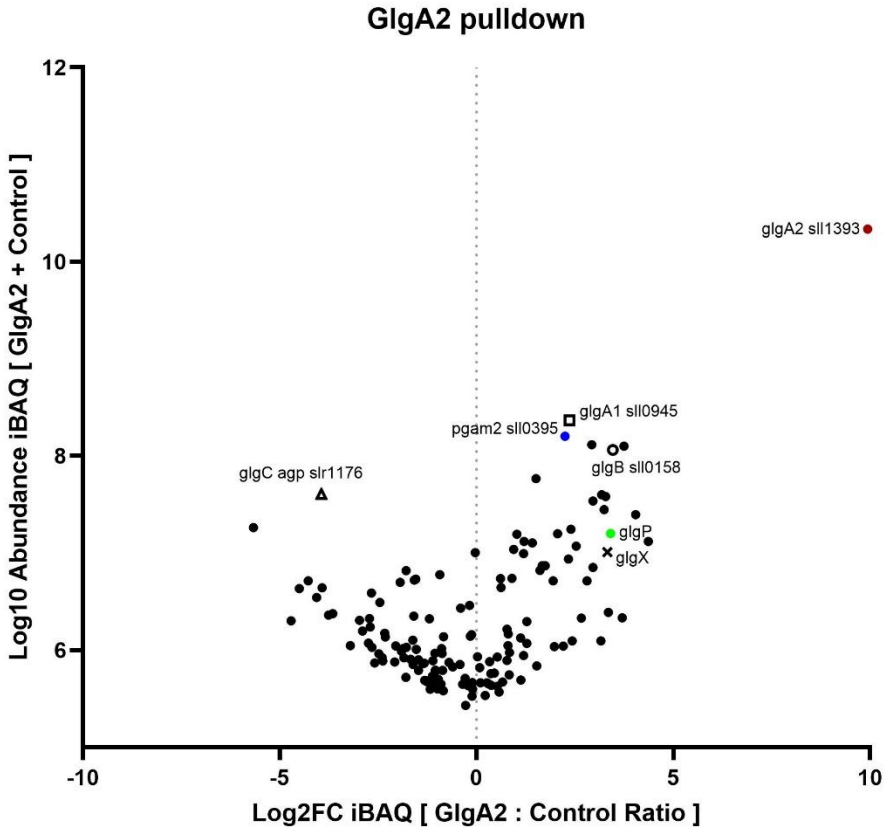

Figure 7: Pulldown of 2-day chlorotic wild type cell lysate using bead-immobilised His-tagged GlgA2 as the bait protein. Each point represents the log2 ratio of protein enrichment in the GlgA2 sample to the control (empty beads) against the log10 abundance of the total enrichment. Each point depicts the mean of biological triplicates (n = 3).

Table 2: GlgA2 pulldown POI

	log2FC >2	***P* value < 0.05**
sll1393 Probable glycogen synthase 2 (GlgA2)	9.93	0.00
sll1025 FAD dependent oxidoreductase	5.60	0.00
slr0605 Glutathione S-transferase	3.72	0.01
sll0158 1,4-alpha-glucan branching enzyme (GlgB)	3.46	0.00
sll1367 Alpha-1,4 glucan phosphorylase (GlgP2)	3.33	0.03
slr1857 Glycogen debranching enzyme (GlgX2)	3.26	0.03
ssl2296 Pterin carbinolamine dehydratase	3.21	0.00
ccmA Carboxysome formation protein	2.94	0.01
sll0945 Glycogen synthase 1 (GlgA1)	2.36	0.00
sll0395 Phosphoglycerate mutase (pgam2)	2.25	0.02

4.2.3. GlgC pulldown indicates a GlgC–GlgA2–GlgB core with proximal GlgP2.

GlgC pulldowns recovered the bait strongly (log2FC = 9.46) and selectively co-enriched GlgA2 (3.22), GlgB (3.29) and GlgP2 (3.66). In contrast, GlgA1 did not exceed the POI threshold in this dataset, pointing to a preferential association of GlgC with GlgA2 under the

tested conditions **(Figure 8)**. Additional recurring POIs included sll1025 (5.45), slr0605 (3.05) and ssl2296 (3.90), together with an uncharacterised UPF0047/YjbQ-like protein (sll1880; 2.36) **(**

Table 3**)**.

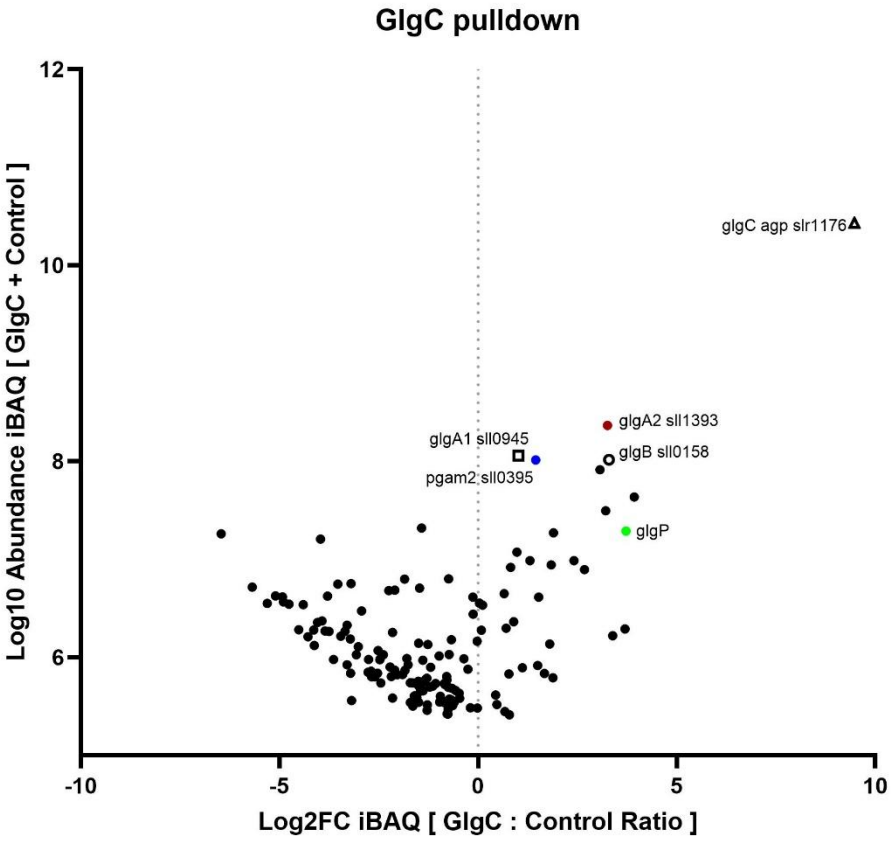

Figure 8: Pulldown of 2-day chlorotic wild type cell lysate using bead-immobilised His-tagged GlgC as the bait protein. Each point represents the log2 ratio of protein enrichment in the GlgC sample to the control (empty beads) against the log10 abundance of the total enrichment. Each point depicts the mean of biological triplicates (n = 3).

Table 3: GlgC pulldown POI

	log2FC >2	***P* value < 0.05**
slr1176 Glucose-1-phosphate adenylyltransferase (GlgC)	9.46	0.00
sll1025 FAD dependent oxidoreductase	5.45	0.02
ssl2296 Pterin carbinolamine dehydratase	3.90	0.00
sll1367 Alpha-1,4 glucan phosphorylase (GlgP2)	3.66	0.02
sll0158 1,4-alpha-glucan branching enzyme (GlgB)	3.29	0.01
sll1393 Glycogen synthase 1 (GlgA2)	3.22	0.00
slr0605 Glutathione S-transferase	3.05	0.01
sll1880 UPF0047 protein YjbQ-like	2.36	0.04

Across all three His-tag pulldowns, the datasets appear to suggest a core glycogen-associated interactome comprising GlgC–GlgA2–GlgB with proximal GlgP2, consistent with co-localisation of ADP-Glc supply, elongation and branching on the glycogen particle, and with dynamic presence of the phosphorolysis machinery during chlorosis. The repeated CcmA enrichment in GlgA pulldowns could also hint at a spatial linkage between glycogen and carboxysomes that warrants additional validation.

4.3. Co-Immunoprecipitation using anti-GlgB and anti-GlgC antibodies.

To detect additional potential binding partners, we performed co-immunoprecipitation (coIP) experiments using 2-day chlorotic wild type lysates with chlorotic GlgC (Δ*glgC*) or GlgB (Δ*glgB*)-deficient mutant lysates as controls. Anti-GlgB and anti-GlgC Ab were used to trap the respective native proteins and detect potential binding partners. Proteins of interest (POIs) were defined by log2FC > 3 and $p < 0.05$.

4.3.1. GlgC CoIP recovers membrane/stress-linked candidates.

The enrichment plot **(Figure 9)** shows that GlgC itself was strongly detected (slr1176; log2FC = 9.21), together with several co-enrichments listed in **(Table 4)**. These include IsiA (sll0247; 8.17), HglK (slr1519; 6.61) and slr7096 (6.57), as well as candidates such as an OprB-family porin (sll0772; 3.79) and a DJ-1/PfpI-family protein (slr1854; 3.70). Overall, these recoveries point to a set of membrane-associated and stress-linked proteins that may be proximal to GlgC during chlorosis, although additional experiments would be needed to determine whether these reflect any real biological significance.

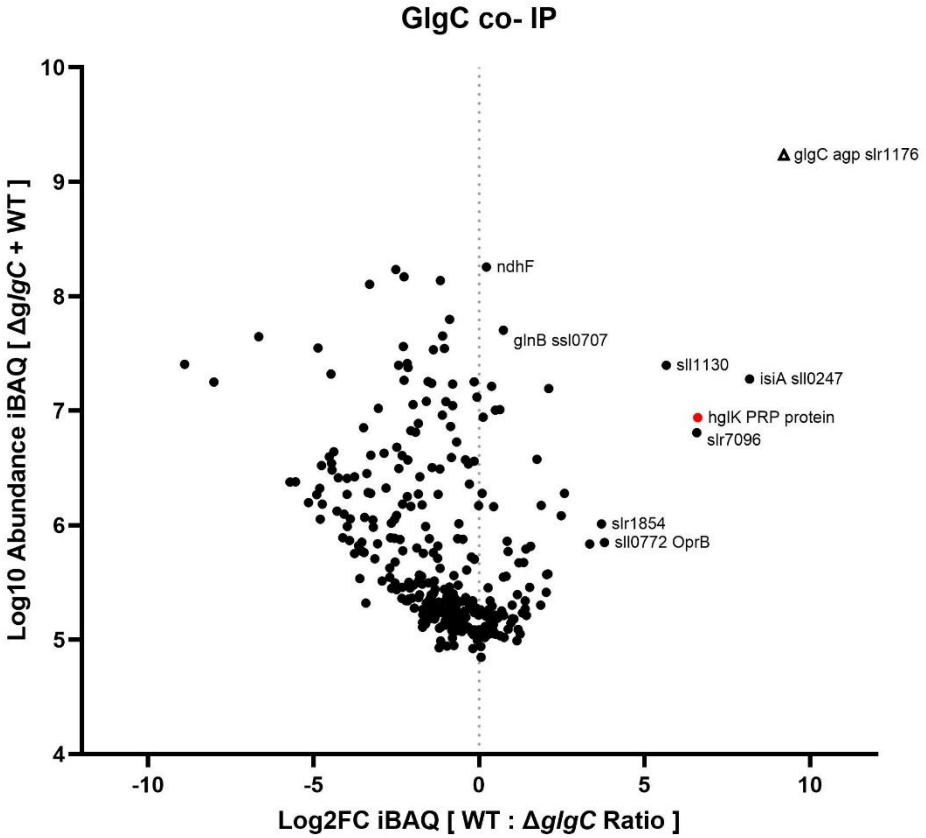

Figure 9: coIP of 2-day chlorotic wild type and Δ*glgC* cell lysates using GlgC as the bait protein. Each point represents the log2 ratio of protein enrichment in the WT sample to the Δ*glgC* sample against the log10 abundance of the total enrichment. Each point depicts the mean of biological triplicates (n = 3).

Table 4: GlgC coIP POI

	log2FC >3	*P* value < 0.05
slr1176 Glucose-1-phosphate adenylyltransferase (GlgC)	9.21	0.00
sll0247 Iron stress-induced chlorophyll-binding protein (isiA)	8.17	0.01
slr1519 Pentapeptide repeats PRP (hglK)	6.61	0.00
slr7096 Unknown protein	6.57	0.02
sll0772 Carbohydrate-selective porin, OprB family	3.79	0.00
slr1854 DJ-1/PfpI family	3.70	0.00

Notably, none of the key glycogen enzymes recovered in the GlgC His-tag pulldown (GlgA2, GlgB, GlgP2) **(Table 3)** exceeded the POI threshold in the GlgC coIP under these conditions, indicating that the glycogen-proximal and membrane/stress-associated GlgC neighbourhoods are either mutually exclusive, differently stabilised by the assays, or present at levels below the detection cut-off in coIP.

4.3.2. GlgB CoIP highlights central-carbon factors and a GlgB-like paralogue.

We next assessed proteins co-immunoprecipitating with GlgB. The enrichment plot shows that GlgB was recovered as expected (sll0158; log2FC = 7.94), and several proteins exceeded the POI threshold, including a GlgB-like paralogue (sll0735; 4.22) and other proteins spanning nucleotide and central carbon metabolism (e.g. PyrG/CTP synthase, sll1443; 4.33; Pgm1,

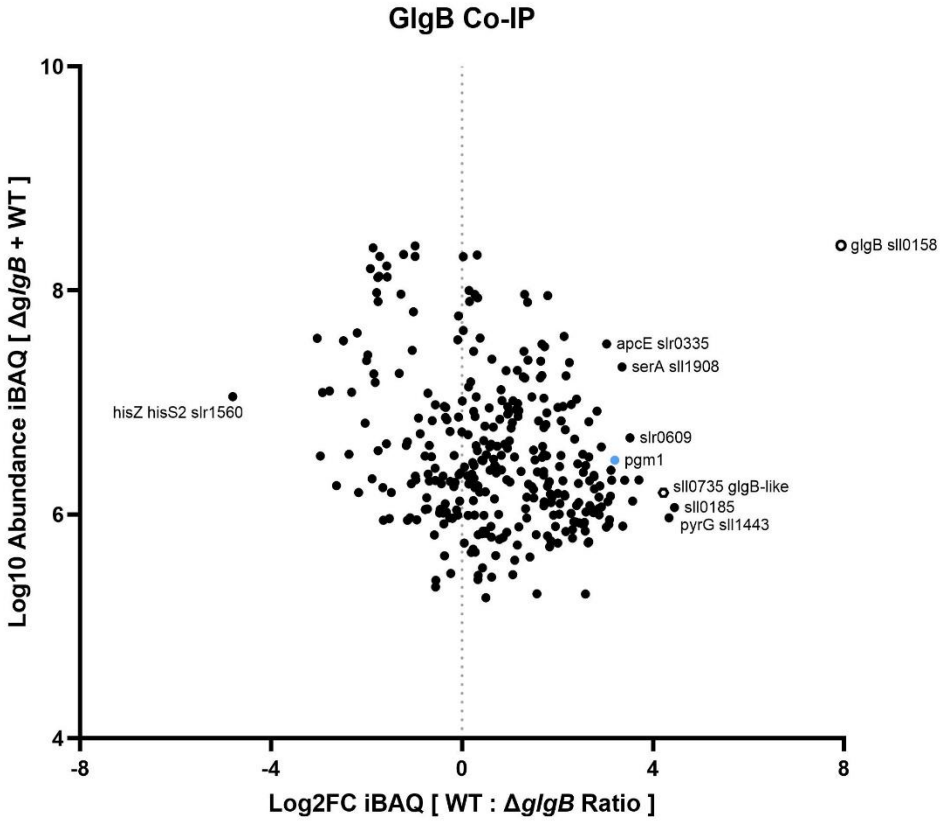

Figure 10: coIP of 2-day chlorotic wild type and Δ*glgB* cell lysates using GlgB as the bait protein. Each point represents the log2 ratio of protein enrichment in the WT sample to the Δ*glgB* sample against the log10 abundance of the total enrichment. Each point depicts the mean of biological triplicates (n = 3).

sll0726; 3.20) **(Figure 10)**. Proteostasis- and thylakoid-associated proteins such as DnaK1 (sll0058; 3.08), ClpR (slr0164; 3.12), and ApcE (slr0335; 3.03) were also present in the POI list **(Table 5)**. Notably, the lack of reciprocal enrichment of GlgA1 or GlgA2 when compared to the consistent GlgB enrichment in the His-tagged pulldowns discussed previously could indicate some conditionality for GlgA association or co-localisation.

Table 5: GlgB coIP POI

	log2FC >3	***P* value < 0.05**
sll0158 1,4-alpha-glucan branching enzyme (GlgB)	7.94	0.01
sll0185 Rho termination factor-like	4.45	0.00
sll1443 CTP synthase (pyrG)	4.33	0.01
sll0735 1,4-alpha-glucan branching enzyme (GlgB-like)	4.22	0.02
SqdB Sulfolipid biosynthesis protein	3.70	0.02
slr0609 47 kD protein	3.52	0.01
sll1553 Phenylalanine--tRNA ligase beta subunit (pheT)	3.41	0.00
sll1435 Glutamyl-tRNA(Gln) amidotransferase subunit B (gatB)	3.37	0.02
sll1908 D-3-phosphoglycerate dehydrogenase (serA)	3.35	0.00
sll0726 Phosphoglucomutase (pgm1)	3.20	0.00
slr0164 ATP-dependent Clp protease (clpR)	3.12	0.02
slr0118 Phosphomethylpyrimidine synthase (thiC)	3.11	0.02
sll0058 Chaperone protein dnaK1	3.08	0.02
slr0335 Phycobiliprotein ApcE	3.03	0.01
sll1234 Adenosylhomocysteinase (ahcY)	3.02	0.02

5. Materials and Methods of the Unpublished Results

5.1. Kinetic modelling of Pi-dependent GlgC regulation

A minimal kinetic model was constructed to describe how inorganic phosphate (Pi) affects ADP-Glc production by GlgC at fixed 3-PGA. Suggestions for the initial equations for this model were drafted with assistance from an AI tool (ChatGPT, GPT-5 Thinking) and the model calculations were independently modified and implemented using python. The simulated data was visualised using GraphPad Prism 10 (GraphPad, CA, USA). In this model, only GlgC is represented explicitly; GlgA, GlgB and downstream enzymes are not included. The enzyme is assumed to operate at 2 mM 3-PGA with saturating ATP and Glc-1P. For each Pi concentration, the model outputs the predicted ADP-Glc production rate as a volumetric flux in µM/s, and this flux can optionally be normalised or converted to percentage inhibition or total ADP-Glc supply.

5.1.1. Enzyme concentration and mass conversion

GlgC is represented as a tetrameric enzyme present at a nominal total concentration: C_{nM} = 200 nM (tetramer).

To convert this to a mass concentration $E_{C,mg/mL}$ (in mg/mL), the molecular weight of GlgC, MW_{GlgC} = 200 856.64 g/mol, is used. As such, $E_{C,mg/mL}$= 200 nM × 200 856.64 g/mol × 10^{-9} ≈ 0.0402 mg/mL.

5.1.2. Pi-free specific activity and ADP Glc supply flux

The intrinsic specific activity of GlgC at 2 mM 3-PGA and saturating ATP and Glc-1P was taken from the malachite green assay in **Publication 1** as:

$V_{C,MG}$ = 8.90 U/mg, where 1 U (unit) is defined as conversion of 1 µmol substrate per min.

At a GlgC mass concentration $E_{C,mg/mL}$, the volumetric activity in U/mL is: $A_C^{U/mL} = V_{C,MG} \times E_{C,mg/mL}$

To convert this activity into an ADP Glc production flux in µM/s, the identity 1 U/mL = 1 µmol/min/mL = 1000 µM/min is used. The Pi-free ADP Glc supply flux v_{C^o} (µM/s) is therefore: $v_{C^o} = A_C^{U/mL} \times (1000 / 60) = V_{C,MG} \times E_{C,mg/mL} \times (1000 / 60)$

With the numerical values above: v_{C^o} = 8.90 U/mg × 0.0402 mg/mL × (1000 / 60) ≈ 5.96 µM/s.

This value defines the maximum ADP Glc supply from GlgC in the absence of Pi inhibition under the chosen conditions.

5.1.3. Pi-dependent allosteric inhibition term A(Pi)

The effect of Pi on GlgC activity at 2 mM 3-PGA is represented by an empirical Hill-type inhibition term A(Pi). This term is dimensionless, ranges between 0 and 1, and was fitted to the experimental Pi inhibition curve for GlgC at 2 mM 3-PGA based on the data drawn from **Publication 1, Table 1**.

A(Pi) is defined as: $A(Pi) = 1 / \{ 1 + [Pi / IC_{50}^{Pi}]^{nH} \}$, where Pi is the free inorganic phosphate concentration (mM), IC_{50}^{Pi} is the Pi concentration giving 50 % inhibition (mM), n^H is the Hill coefficient describing the steepness of inhibition. The parameters used were IC_{50}^{Pi} = 0.87 mM,

$n^H = 4.3$. By construction, A(Pi) → 1 as Pi → 0 (little or no inhibition) and A(Pi) → 0 at high Pi (strong inhibition).

5.1.4. ADP Glc supply as a function of Pi

In the supply-only GlgC model, Pi is assumed to act solely through A(Pi).

The effective GlgC concentration at a given Pi is: $C_{eff}(Pi) = C_{nM} \times A(Pi)$, and the corresponding mass concentration: $E_{C,mg/mL}(Pi) = C_{eff}(Pi) \times MW_{GlgC} \times 10^{-9} = A(Pi) \times E_{C,mg/mL}$.

The ADP Glc supply flux at that Pi value is then: $v_C(Pi) = V_{C,MG} \times E_{C,mg/mL}(Pi) \times (1000 / 60)$. Substituting $E_{C,mg/mL}(Pi) = A(Pi) \times E_{C,mg/mL}$ gives a compact form: $v_C(Pi) = v_{C^o} \times A(Pi)$.

All Pi dependence of ADP Glc production by GlgC in this model is therefore captured by A(Pi).

5.1.5. Generation of the GlgC Pi titration curve

To generate the GlgC supply-only Pi titration curve, $v_C(Pi)$ was evaluated over a series of Pi concentrations spanning the low-millimolar range (0–10 mM, step 0.1 mM).

For each Pi value: A(Pi) was computed from the Hill equation above and $v_C(Pi)$ was calculated as: $v_{C^o} \times A(Pi)$ in µM/s.

These $v_C(Pi)$ values were plotted directly as a function of Pi to give the GlgC supply-only curve with a µM/s ADP Glc readout.

5.1.6. Calculation of GlgA percent inhibition.

The model was then expanded to estimate how Pi-dependent gating of GlgC transfers to GlgA1 and GlgA2 flux. In this approximation, ADP-Glc is not represented as an explicit pool and reverse reactions (e.g. PPi-driven back-reaction) are ignored. For each Pi concentration, GlgA flux is taken as the minimum between the Pi-modulated ADP-Glc supply provided by GlgC and the maximal elongation capacity of the relevant GlgA isoform. Percent inhibition is then defined relative to the Pi-free GlgA flux for each isoform.

5.1.7. Enzyme concentrations and GlgA maximal capacities

GlgA1 and GlgA2 are each represented at a nominal concentration: $A_{nM} = 200$ nM (monomer).

For each isoform, the corresponding mass concentration $E_{Ai,mg/mL}$ (mg/mL) is calculated from its molecular weight MW_{Ai} (g/mol): $E_{Ai,mg/mL} = A_{nM} \times MW_{Ai} \times 10^{-9}$, where *i* denotes GlgA1 or GlgA2.

The intrinsic specific activities of GlgA1 and GlgA2 at saturating ADP-Glc and under the assay conditions used in **Publication 2,** are denoted as: $V_{A1} = 0.510$ U/mg and $V_{A2} = 0.770$ U/mg.

For each isoform, the maximal volumetric elongation flux $V_{max,A}{}^{i}$ (in µM/s) is then: $A_{Ai,}{}^{UmL} = V_{Ai} \times E_{Ai,mg/mL}$. Because the MW of the isoforms differ, $V_{max,A}{}^{A1}$ and $V_{max,A}{}^{A2}$ are not identical, even though the nominal enzyme concentration (200 nM) is the same. For the parameter set used, both $V_{max,A}{}^{A1}$ and $V_{max,A}{}^{A2}$ are smaller than the Pi-free GlgC supply flux : v_{C^o}, such that under Pi-free conditions the pathway is capped at the GlgA step.

5.1.8. Definition of GlgA flux

The steady-state GlgA elongation flux for each isoform at a given Pi is defined algebraically as: $v_{Ai}(Pi) = \min\{ V_{max,A}{}^{i}, v_C(Pi) \}$. This expression captures two regimes: A capacity-limited

regime at low Pi, where GlgC operates close to its Pi-free capacity and $v_C(Pi) \geq V_{max,A}^i$. In this regime, GlgA is saturated and the pathway is capped at the GlgA step: $v_{Ai}(Pi) = V_{max,A}^i$. the second regime is supply-limited at higher Pi. When Pi increases, A(Pi) declines, reducing GlgC supply such that $v_C(Pi) < V_{max,A}^i$. In this regime, GlgA has spare capacity and the flux is limited upstream by GlgC: $v_{Ai}(Pi) = v_C(Pi) = v_{C^o} \times A(Pi)$. The transition between regimes occurs at the Pi value Pi* that satisfies: $v_C(Pi^*) = V_{max,A}^i$.

5.1.9. Reference flux and calculation of percent inhibition

For each GlgA isoform, a Pi-free reference flux is defined at Pi = 0 mM (A(Pi) = 1): $v_{Ai}(0) = \min\{ V_{max,A}^i, v_{C^o} \}$. Given the parameter values used here ($v_{C^o} > V_{max,A}^i$), this reduces to: $v_{Ai}(0) = V_{max,A}^i$. The percent inhibition of GlgA for a given isoform at Pi is then defined as the fractional loss of flux relative to this Pi-free reference: % inhibition of $GlgA^i = 100 \times [1 - v_{Ai}(Pi) / v_{Ai}(0)]$.

Using the piecewise definition of $v_{Ai}(Pi)$:

In the capacity-limited regime: ($v_C(Pi) \geq V_{max,A}^i$), $v_{Ai}(Pi) = V_{max,A}^i$, so: % inhibition of $GlgA^i = 0$ %.

In the supply-limited regime: ($v_C(Pi) < V_{max,A}^i$), $v_{Ai}(Pi) = v_{C^o} \times A(Pi)$, and since $v_{Ai}(0) = V_{max,A}^i$, we can define the % inhibition of $GlgA^i$ as: $100 \times [1 - v_{C^o} \times A(Pi)/ V_{max,A}^i]$.

Operationally, the GlgA Pi titration curves in the supply-only model are obtained by evaluating $v_C(Pi)$ over the chosen Pi range using the GlgC supply-only model. Then computing $v_{A1}(Pi)$ and $v_{A2}(Pi)$ via $v_{Ai}(Pi) = \min\{ V_{max,A}^i, v_C(Pi) \}$, and converting each $v_{Ai}(Pi)$ to % $GlgA^i$ inhibition using the definition above. This yields the GlgA1 and GlgA2 percent inhibition curves plotted in the Pi titration figure, which are directly comparable to the GlgC supply-only ADP-Glc flux curve.

5.2. Cultivation of Synechocystis

All *Synechocystis* strains were cultivated as previously described in **Publication 1-3**. The nitrogen starvation (N-Shifting) of strains was performed as described in **Publication 3**. Details of all *Synechocystis* strains used can be found listed in **Publication 2-3**.

5.3. Spot viability assays after 14-days incubation in darkness

Liquid cultures cultivated in BG11 (supplemented with 5 mM $NaHCO_3$) were adjusted to OD_{750} 0.4 and incubated for 14 days in total darkness at 30ºC with constant shaking (130–140 rpm). Serial dilutions of the cultures were then prepared (undiluted, 10^1, 10^2, 10^4, 10^5), and 5 µL of each dilution was spotted on BG11 agar plates. The plates were cultivated with constant illumination of 50 µmol photons /m^2/s (µE) at 30°C for 5 days.

5.4. His-Tag pulldown / CoIP

Table 6: Pulldown/Co-IP Buffer compositions

Buffer A	50 mM HEPES-NaOH, pH 8.0, 12 mM $MgCl_2$, 0.3 mM NaCl, 0.01 % Tween-20
Buffer B	50 mM HEPES-NaOH, pH 8.0, 12 mM $MgCl_2$
Buffer C	50 mM Tris-HCl, pH 7.4, 0.15 mM NaCl, 0.02 % Tween-20
Buffer D	50 mM HEPES-NaOH, pH 8.0, 12 mM $MgCl_2$, 0.3 mM NaCl

5.4.1. Preparation of crude lysates for pulldown/CoIP

Synechocystis cultures in early chlorosis (2 days/48 hours of nitrogen starvation) were harvested and pelleted via centrifugation before being washed twice with MilliQ water, followed by a final centrifugation step to pellet the washed cells. The washed pellet was then resuspended in at least 10x volume of Buffer B **(Table 6)**, supplemented with Benzonase® (Merck, Darmstadt, Germany), lysozyme and one tablet of cOmplete™ protein inhibitor cocktail (Roche, Mannheim, Germany). The cell suspension was then split into 1.5 mL screw-top vials containing a sufficient amount of acid-washed glass beads. Mechanical lysis was performed at 4°C using the FastPrep®-24 5G bead beating grinder and lysis system (MP Biomedicals, Irvine, USA). The lysis procedure was performed five times for 20 s at 6.5 m/s with 5-min rest intervals, after which the suspension was centrifuged at 16000 x *g* for 30 min 4°C to separate the glass beads from the supernatant. Taking care to avoid the glass beads, the supernatant was carefully decanted and kept on ice until use.

All pulldown and coIP experiments were performed using 2-day chlorotic cultures grown under standardised conditions, such that differences in recovered proteins should primarily reflect the capture method and bait configuration rather than grossly different physiological states.

5.4.2. Pulldown of His-tagged proteins

His-tagged proteins were captured using Dynabeads™ His-Tag magnetic beads (Thermo Fisher Scientific, MA, USA) following the manufacturer's recommendations with minor adjustments described below. All buffers were prepared according to **(Table 6)**. Unless otherwise stated, incubations were carried out at room temperature.

Beads were thoroughly resuspended in the original vial by vortexing for >30 s (or by tilting/rotating for 5 min). An aliquot of 50 µL beads (corresponding to 2 mg) was transferred to a 1.5 mL microcentrifuge tube and placed on a magnetic rack for 2 min to collect the beads. The supernatant was removed, and the beads were combined with ~50 µg of His-tagged protein prepared in Buffer A to a total volume of 800 µL). The bead–sample suspension was mixed thoroughly and incubated on a roller for 10 min. Beads were then magnetically separated for 2 min and the supernatant was discarded. The bead-bound bait proteins were washed five times with 300 µL Buffer A; for each wash, beads were collected on the magnet for 2 min, the supernatant was removed, and beads were fully resuspended before the next wash.

For pull-down experiments, the washed bead–bait complex was incubated with the crude lysates prepared in Buffer B (final volume up to 700 µL). The suspension was mixed thoroughly and incubated on a roller for 30 min. Beads were collected on the magnet for 2 min and the supernatant was discarded. The complex was washed five times with 300 µL Buffer A, ensuring complete resuspension between washes.

5.4.3. Protein co-immunoprecipitation (coIP)

The protein coIP experiment was performed with Dynabeads™-Protein A (Thermo Fisher Scientific, MA, USA) following the manufacturer's recommendations with slight modifications to the buffers used (listed in **Table 6**). Unless otherwise stated, incubations were carried out at room temperature.

The beads were thoroughly resuspended in the original vial by vortexing for >30 s (or by tilting/rotating for 5 min). An aliquot of 50 µL beads (1.5 mg) was transferred to a

microcentrifuge tube. Beads were collected on a magnetic rack, the supernatant was removed, and the tube was taken off the magnet for subsequent antibody coupling.

Custom polyclonal rabbit Ab against recombinant proteins used in this work (His-tagged GlgC or Strep-tagged GlgB) were purchased from ProteoGenix (Schiltigheim, France). 10 µg of Ab in 200 µL Buffer C was added to the prepared beads. The suspension was incubated with rotation for 10 min, after which the beads were collected on the magnet and the supernatant was removed. The bead–antibody (bead–Ab) complex was removed from the magnet and washed twice with 200 µL Buffer C.

Immediately prior to immunoprecipitation, the bead–Ab complex was placed on the magnet and any residual supernatant was removed. 500 µL of the sample containing the target antigen in Buffer B was added, and the beads were gently resuspended. Binding was allowed for 10 min with rotation. Beads were collected on the magnet and the bead–Ab–antigen (bead–Ab–Ag) complex was washed three times with 200 µL Buffer D, using magnetic separation between washes and gentle pipetting to fully resuspend the beads. After the final wash, the complex was resuspended in 100 µL Buffer D and the bead suspension was transferred to a clean tube to minimize co-elution of proteins that might adhere to the original tube wall.

5.4.4. Proteomic analysis

5.4.4.1. In-gel digestion of proteins

Proteins were briefly separated by SDS–PAGE on a NuPAGE 12% Bis-Tris gel (Thermo Fisher Scientific, MA, USA) and stained with colloidal Coomassie (ReadyBlue Protein Gel Stain, Merck, Darmstadt, Germany). Protein-containing bands were excised and diced. Gel pieces were destained three times with 5 mM ammonium bicarbonate (ABC) in acetonitrile (ACN) (1:1, v/v; 20 min each), dehydrated with 100% ACN (10 min), and reduced in 10 mM dithiothreitol (DTT) in 20 mM ABC (45 min, 56 °C). Free thiols were alkylated with 55 mM iodoacetamide (IAA) in 20 mM ABC (45 min, dark). After two washes with 5 mM ABC/ACN (1:1, v/v; 20 min each) and a final dehydration in 100% ACN (15 min), solvent was removed in a vacuum concentrator (10 min). Gel pieces were re-swollen in sequencing-grade trypsin (12.5 ng μL^{-1}, Promega) in 20 mM ABC (pH 8.0; 10 min, RT) and covered with 20 mM ABC for overnight digestion at 37 °C. Peptides were extracted sequentially for 30 min each with (i) 3% (v/v) trifluoroacetic acid (TFA) in 30% (v/v) ACN, (ii) 0.5% (v/v) formic acid (FA) in 80% (v/v) ACN, and (iii) 100% ACN. Pooled extracts were dried by vacuum centrifugation. All incubations were performed with gentle agitation.

5.4.4.2. LC–MS/MS

Desalting was performed using C18 StageTips as previously described [70]. Peptides were analysed on an EASY-nLC 1200 UHPLC coupled to a Q Exactive HF mass spectrometer (both from Thermo Fisher Scientific, MA, USA) essentially as previously described with minor modifications: peptides were separated on the analytical column using a 60-min segmented gradient of 10–33–50% solvent B (80% ACN, 0.1% FA) at 200 nL/min [71]. In the mass spectrometer, full MS and MS/MS spectra were acquired at 60k resolution. The full MS AGC target and maximum injection time were 3×10^6 and 25 ms, respectively. In each duty cycle, the top 7 precursors were selected for HCD MS/MS with an AGC target of 1×10^5 and a maximum IT of 220 ms.

5.4.4.3. Data processing

Raw files from all biological replicates were processed jointly in MaxQuant v2.2.0.0 [72]. MS/MS spectra were searched with the integrated Andromeda engine [73] against a target–decoy *Synechocystis sp*. (strain ATCC 27184 / PCC 6803 / Kazusa) protein database (3507 entries; UniProt), supplemented with 245 common contaminants. Enzyme specificity was set to trypsin with up to two missed cleavages. Carbamidomethyl (Cys) was specified as a fixed modification; Met oxidation and protein N-terminal acetylation were set as variable modifications. Mass tolerances were 4.5 ppm for precursor ions and 0.5 Da for fragment ions. Peptide, protein and site identifications were controlled at 1% FDR using the target–decoy strategy [74]. The proteomics results were subsequently analysed with Perseus v2.0.11 and visualized using GraphPad Prism 10 [75].

Chapter III. Discussion

Glycogen metabolism in *Synechocystis* emerges from our data as a glycogen-centred, metabolite-gated system that couples photosynthetic carbon acquisition to storage and mobilisation. Rather than a linear pathway, the evidence supports a multi-level organisation in which (i) an effector-sensitive GlgC node converts the cellular 3-PGA/Pi balance into ADP-Glc supply, (ii) elongation and branching are apportioned between GlgA1/GlgA2 and GlgB to tune polymer architecture and throughput, and (iii) a GlgP2–GlgX1 axis executes deep degradation, with GlgP1 adding an oxidation-sensitive reserve. Below, we interpret these findings in the context of Diel physiology, spatial organisation, and carbon-allocation logic.

1. GlgC as a metabolite-gated ADP-Glc supply node

1.1. 3-PGA/Pi ratio sensing and Diel control of glycogen synthesis

The combined kinetic and effector analyses position GlgC as a sensitive interpreter of the 3-PGA:Pi balance established by photosynthetic and respiratory fluxes. The steep, bidirectional antagonism between 3-PGA-dependent activation and Pi-dependent inhibition, together with more modest contributions from Fru-6P (activation) and 2-PGA (inhibition), generates a response surface in which relatively small shifts in metabolite ratios can produce large changes in ADP-Glc supply. The finding that both 3-PGA and Pi stabilise a common tetrameric GlgC assembly further indicates that regulation is mediated primarily through alternative allosteric

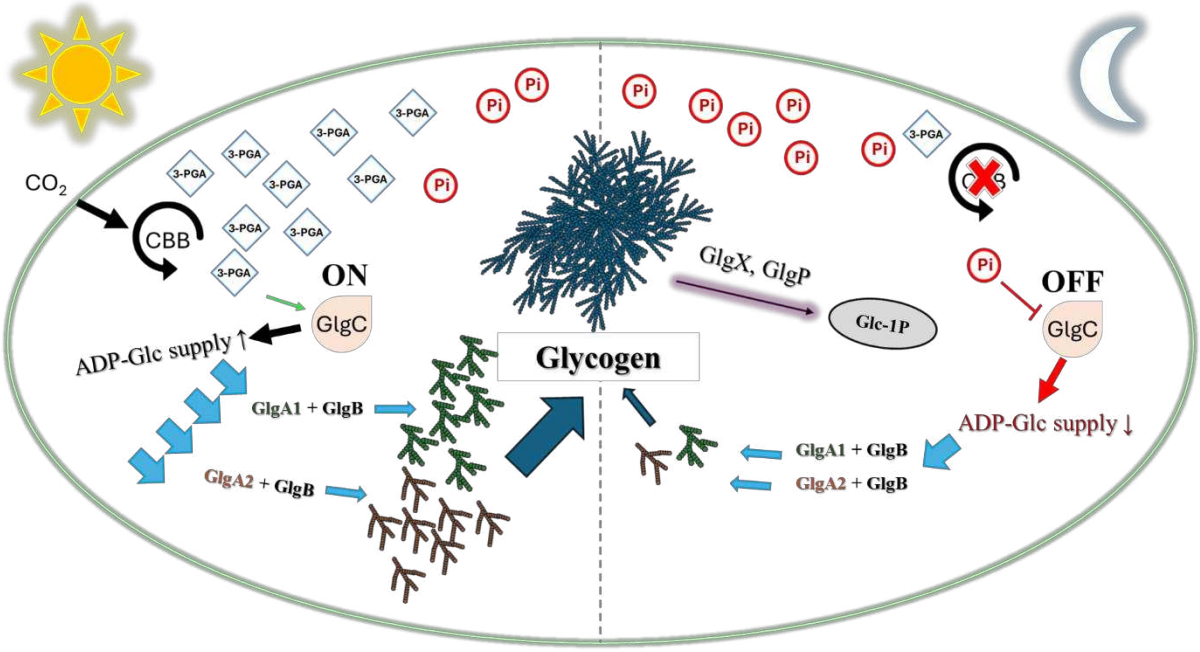

Figure 11: Schematic model of Diel 3-PGA/Pi ratio-sensing at GlgC coordinates ADP-Glc supply with glycogen synthesis and mobilization. Schematic of a cyanobacterial cell with light (left) and dark (right) halves separated by the dashed midline. In the light, high 3-PGA activate GlgC, ADP-Glc production; the number of blue arrows reflects flux magnitude. ADP-Glc is channelled to a synthesis cohort containing GlgA1, GlgA2 and GlgB: GlgA1 preferentially yields highly branched, short-chain glycogen (green), whereas GlgA2 favours longer chains (orange), together shaping particle architecture. The number of glycogen cartoons approximates relative net synthesis. In the dark, rising Pi inhibits GlgC, reducing ADP-Glc supply and shifting the balance toward glycogen debranching and degradation to Glc-1P (magenta arrow). Schematic is qualitative and not to scale.

conformations of the same oligomeric state, rather than through shifts in quaternary structure, originally thought to underlie GlgC regulation.

At the physiological level, this control architecture implements a simple Diel rule. In the light, high 3-PGA derived from the CBB cycle and low free Pi favour an ON state of GlgC and thereby promote glycogen synthesis. In darkness or under energy limitation, Pi concentrations rise as ATP turnover slows and phosphorylated intermediates are dephosphorylated, progressively shifting the gate towards an OFF state even when 3-PGA is not fully depleted. This ratio-sensing scheme provides a mechanistic basis for rapid day–night switching of glycogen synthesis without the need for *de novo* transcriptional responses, enabling fast adaptation to changing environmental conditions **(Figure 11)**.

Simulating this control architecture *in silico* illustrated how this rapid Pi-coupled switch directly impacts GlgA **(Figure 5)**. Once Pi rises above the threshold imposed by GlgC, the locus of control shifts upstream: flux becomes supply-limited by the GlgC gate rather than capacity-limited at GlgA, indicating how a relatively small biochemical adjustment in GlgC activity can translate into a steep reduction in glycogen synthesis at the pathway level. Thus, at the level of bulk flux, Pi-dependent gating by GlgC can largely override isoenzyme-specific properties of GlgA, especially at higher Pi concentrations.

Although the 3-PGA/Pi antagonism constitutes the primary gate at GlgC, Fru-6P and 2-PGA provide secondary control that modulates ADP-Glc supply toward competing metabolic needs without overriding the primary switch discussed previously. Fru-6P, while markedly weaker than 3-PGA, can amplify activation when 3-PGA is sub-saturating, whereas 2-PGA imposes a shallow, incomplete inhibition. We propose that this fine-tuning buffers carbon allocation when ADP-Glc or Glc-1P are required for other metabolic pathways, for example during glucosylglycerol (GG) biosynthesis or to replenish CBB intermediates [42,76,77].

In the initial phase of recovery from nitrogen chlorosis, glycogen is rapidly degraded via phosphorolysis to Glc-1P; with Pi engaged in the GlgP reaction and cellular energy scarce, millimolar 2-PGA accumulating under these conditions could act as a gentle brake on GlgC, preventing futile re-incorporation of recently liberated reserves [11,69,78]. As the second, mixotrophic phase ensues and PirC sequesters PGAM, rising 3-PGA should readily relieve this inhibition, thus allowing for the rapid re-activation of GlgC and once a 3-PGA threshold is exceeded **(Figure 3)** [67]. All the while Pi remains a more effective, antagonistic inhibitor that enforces the dark-state OFF position of the gate under normal conditions.

1.2. Primer-dependent elongation and branching: division of labour between GlgA1, GlgA2 and GlgB

GlgA1 and GlgA2 exhibit comparable catalytic efficiencies under ideal substrate conditions but diverge sharply as primer context and branching vary. Flux benchmarking further indicates that, at realistic approximate equimolar GlgC:GlgA stoichiometries [79], control resides predominantly in the elongation/branching module; once the GlgC gate is ON, ADP-Glc supply is generally permissive. Two conclusions follow. First, strict primer dependence and the marked preference for branched glycogen over linear starch indicate that the number and accessibility of non-reducing ends—not maximal synthase turnover—govern effective flux through chain extension. Second, GlgB increases throughput by lowering the primer requirement for both isoforms, while selectively and cooperatively enhancing GlgA2 efficiency **(Figure 12)**.

Beyond glycogen synthesis, ADP-Glc is also diverted into alternative sinks, including sucrose and glucosylglycerol (GG), and can even support a GlgA-independent glycogen route during salt acclimation [77,80]. Because ADP-Glc is a high-energy sugar nucleotide and excess accumulation is cytotoxic, its intracellular pool is tightly constrained [81]. Multiple safeguards are evident: antagonistic 3-PGA/Pi control at GlgC attenuates ADP-Glc formation as energetic or carbon status declines, and the GlgC reaction is thermodynamically reversible such that PPi imposes mass-action backpressure and product inhibition, shifting the equilibrium toward conversion to Glc-1P when PPi is elevated [82,83]. Together, these layers prevent toxic build-up while maintaining sufficient donor supply for GG formation, sucrose synthesis, and other ADP-Glc-dependent processes [80,81,84].

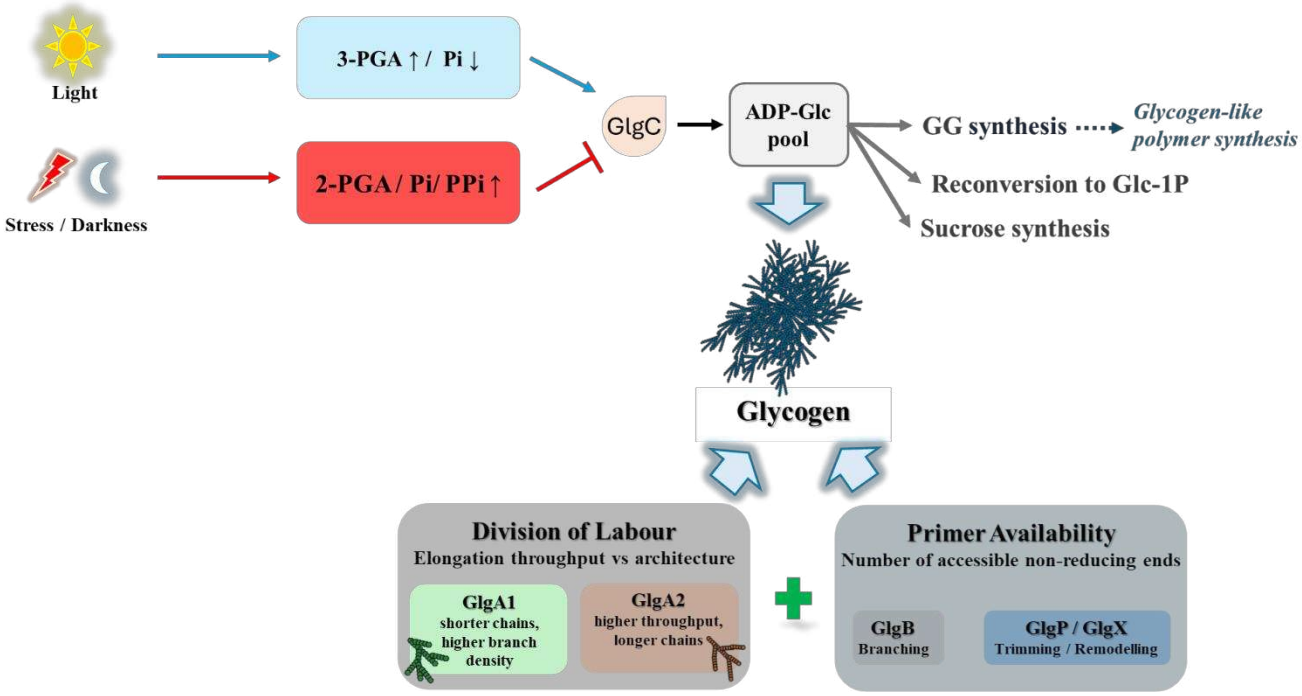

Figure 12: Light (3-PGA↑/Pi↓) activates GlgC to raise ADP-Glc, whereas dark/stress (2-PGA/Pi/PPi↑) inhibit GlgC and favour reconversion to Glc-1P. ADP-Glc is allocated to glycogen, sucrose and glucosylglycerol, with a salt-induced glycogen-like route possible. Glycogen flux is primer-centred—set by GlgB and GlgP/GlgX—rather than synthase-limited, with a division of labour: GlgA2 (higher throughput, longer chains) versus GlgA1 (shorter, more branched). In the coupled-constraints model: flux requires BOTH adequate ADP-Glc supply (GlgC gate) and abundant, accessible primers; neither alone suffices.

Product characterization indicates that GlgA1+GlgB produces more highly branched glycogen, whereas GlgA2+GlgB favours longer chains at a lower branch density. These patterns support complementary operating regimes rather than redundancy: GlgA2 functions as a high-throughput isoform under abundant ADP-Glc and active branching—facilitating rapid daytime accumulation—whereas GlgA1 sculpts a denser subpopulation that may trade maximal rate for resilience, with consequences for subsequent mobilization [51,85]. *In vivo*, further architectural and spatial factors likely amplify these differences, as both isoforms operate within glycogen granules and encounter locally variable primer environments shaped by GlgB, GlgP, and possibly also GlgX.

Viewed at the systems level, phototrophic glycogen synthesis is organized around primer availability rather than maximal elongation velocity. This primer-centered architecture—emergent from cooperation with branching activity—contrasts with the primer-rich, high-

throughput configuration typical of heterotrophs such as *E. coli* [83,86]. The dichotomy helps explain why cyanobacteria position primary control upstream and diversify elongation functions: the network prioritizes managing the number and accessibility of non-reducing ends over accelerating chain extension per se.

A second integrative principle is the preservation of ADP-Glc for competing demands. The 3-PGA/Pi-regulated GlgC "gate" translates photosynthetic and phosphate cues into ADP-Glc supply in a manner that avoids over-committing the ADP-Glc pool, which can be requisitioned for condition-dependent sinks such as GG and sucrose [77]. We therefore propose a coupled-constraints model: primer availability (granule remodelling/branching) and ADP-Glc availability (GlgC regulation) jointly delimit flux—neither abundant ADP-Glc without primers nor abundant primers without sufficient ADP-Glc will drive runaway glycogen synthesis. This coupling provides a mechanistic rationale for flexible allocation between glycogen accumulation and alternative ADP-Glc–dependent processes while preserving metabolic homeostasis **(Figure 12)**.

2. Spatial organisation of the glycogen machinery

2.1. Glycogen particle–associated protein cohort

His-tag pulldowns from chlorotic lysates consistently recover a glycogen synthesis-centred cohort—GlgC, GlgA2 and GlgB, with frequent GlgP2 and carboxysome proteins—suggesting co-residency on the particle surface during high-flux periods (e.g. early chlorosis). These associations appear state-dependent, consistent with dynamic assembly at sites of active elongation/branching [15]. In contrast, GlgC coIP under similar conditions instead emphasises the existence of another cohort of membrane- and stress-associated proteins and did not detect the glycogen synthesis-centred cohort above our POI threshold. Similarly, GlgB coIP did not reciprocally detect GlgA nor GlgC, even though GlgB was consistently enriched in His-tagged pulldowns.

The notable recovery of a GlgB paralogue (*sll0735*) together with the canonical GlgB (*sll0158*) indicates that more than one branching activity is positioned at the glycogen particle during synthesis. Previous studies have indicated the presence of low-level branching in the absence of canonical GlgB [87]. Two non-exclusive arrangements can account for this observation: (i) oligomeric branching assemblies with two GlgB isoforms; or (ii) juxtaposed paralogues with distinct acceptor- and chain-length preferences branching the same glycogen pool. Either arrangement provides a mechanism to adjust the density and placement of branches independently of total elongation rate, thereby tuning the number of non-reducing ends available to GlgA.

Interestingly, neither GlgA nor GlgC is strongly enriched in the GlgB coIP, despite GlgB being reproducibly recovered in the His-GlgA and His-GlgC pulldowns. This asymmetry is difficult to reconcile with a simple, rigid GlgC–GlgA–GlgB complex, but is readily compatible with a model in which glycogen itself acts as the primary scaffold: immobilisation of His-tagged GlgA on the Ni–NTA resin may leave their binding surfaces accessible, allowing intact particles to bridge in additional glycogen-binding enzymes (GlgB, GlgP2). In contrast, the binding of antibodies to GlgB in the coIP may partially occlude its glycogen-binding region or alter its conformation, thereby destabilising particle association and preventing efficient co-recovery of other glycogen enzymes. Under this view, one alternative interpretation is that the His-tag

pulldowns preferentially report glycogen-mediated co-residency on particles, whereas coIPs are biased toward glycogen-independent, protein–protein or membrane-proximal contacts that would be obfuscated by signals from the glycogen-proximal cohort. Given that our data is unable to resolve the molecular nature of these interactions, these interpretations remain limited as hypotheses pending direct structural and kinetic evidence in addition to sensible controls which consider the possibility of Ab-screening effects.

In GlgC coIPs, HglK, a pentapeptide-repeat protein (PRP) implicated in glycolipid localisation, was enriched [88]. Together with preliminary evidence that a carboxysome-associated PRP binds GlgC in *Synechococcus elongatus* (Personal communication with Drs. Joshua MacCready and Daniel Ducat), these data support a model in which PRPs scaffold the GlgC 3-PGA/Pi gate at carboxysome- or thylakoid-adjacent glycolipid microdomains. Consistent with this placement, CcmA and PGAM2 co-enrich in GlgA1/GlgA2 pulldowns, suggesting that a fraction of GlgA is likewise positioned at carboxysomes and that PGAM2 might operate locally to tune the 3-PGA↔2-PGA ratio in the immediate vicinity of GlgC at the site of 3-PGA production. Because 3-PGA activates—and 2-PGA inhibits—GlgC, a carboxysome-proximal PGAM2 would additionally provide a direct means to shape gate output and hence ADP-glucose supply to nearby elongation/branching machinery.

Despite these possible associations, it is also important to note that the GlgC His-tag pulldown and the GlgC coIP recovered largely distinct candidate partners. Whereas the Ni–NTA pulldown of bead-immobilised His-GlgC from chlorotic lysates enriched glycogen enzymes (GlgA2, GlgB, GlgP2), the anti-GlgC coIP of the native enzyme under similar conditions predominantly yielded membrane- and stress-associated proteins (IsiA, HglK) and did not recover GlgA2, GlgB or GlgP2 above the applied significance threshold. This divergence likely reflects a combination of factors—bait configuration (His-tagged vs. native GlgC), resin/antibody chemistry as discussed above, buffer and wash stringency, and the distinct negative controls (empty beads vs. Δ*glgC*)—each of which can selectively stabilise or eliminate subsets of transient or low-affinity interactions. We therefore regard both datasets as method-shaped biased snapshots rather than as mutually confirming evidence for a single, well-defined GlgC complex. Accordingly, we infer that GlgC likely participates in at least two partially segregated, condition-dependent neighbourhoods: one glycogen-proximal and one membrane-/carboxysome-associated. Our current datasets are insufficient to determine whether these reflect stable subpopulations of GlgC or dynamic re-localisation between compartments. At present, both should be treated as working models that require independent validation (e.g. reciprocal pulldowns, GFP localisation experiments, or cross-linking) rather than as definitive maps of a stable GlgC interactome.

2.2. Local granule remodelling by catabolic enzymes

The repeated enrichment of glycogen-catabolic enzymes in synthesis-side pulldowns is consistent with, and lends support to, the working hypothesis that these enzymes co-localise with the glycogen granule even during phases of net glycogen synthesis **(Figure 6 and Figure 7)**. In line with this idea, granule-bound debranching and phosphorolytic activities have been detected during net synthesis in plants, supporting a model in which local trimming and phosphorolysis tune primer quality and chain-end availability while largely preserving elongation flux, rather than invoking bulk polymer degradation [89,90]. Nevertheless, in the absence of direct evidence of these activities in *Synechocystis*, this co-localisation model should still be regarded as a supported but unproven hypothesis.

Nonetheless, this hypothesis offers a mechanistic explanation for the observed divergence between *in vitro*-synthesized and *in vivo*-purified glycogen architectures: polymers assembled *in vivo* display branching patterns of marginally longer chains not fully reproduced in minimal reconstitutions. The presence of GlgX/GlgP would be expected to lower branch density and could explain this observed difference. This also indicates that GlgX and GlgP might be responsible for local debranching and phosphorolysis during glycogen granule assembly, to remove very short, non-productive B-chains and to regulate end availability for optimal access and extension by GlgA. As such, the selective co-enrichment of GlgX2 with GlgA2 **(Figure 7)** merits specific consideration.

Although GlgX1 was established as the dominant debranching isoform in **Publication 3**, the particle-level proximity of GlgX2 to the GlgA2–GlgB elongation/branching module during active synthesis argues for functions distinct from bulk mobilisation. Data on chain length distribution in GlgX deficient *S. elongatus* complemented with either *Synechocystis* GlgX showed comparable function of both isoforms, suggesting that GlgX2's primary role may lie outside bulk glycogen degradation [58]. In line with work on bacterial glycogen and plant debranching, we favour a "pruning-during-synthesis" model in which GlgX2 preferentially hydrolyses very short B-chains generated stochastically by GlgB (i.e. chains below the critical length for productive elongation), thereby preventing over-branching and maintaining chain-length distributions that support high GlgA2 throughput; analogous isoamylase-like proofreading is recognised in starch biosynthesis and has been posited for bacterial glycogen to avoid limit-dextrin-like structures [58,91].

Another point of note is that GlgX2 enrichment is only specific to the GlgA2 pulldown and otherwise not significantly enriched in GlgC or GlgA1 pulldowns. Given that GlgA2 results in longer chain extensions and is more sensitive to steric hindrance than GlgA1 [92], the GlgA2 affinity matrix may select for granules with particular surface characteristics—"cleared" substrates on which GlgX2 has already trimmed abortive branches or to which it remains bound—thereby enriching GlgX2–granule–GlgA2 assemblies. By contrast, the more sterically tolerant GlgA1 may bind a broader glycogen ensemble lacking this bias. Nonetheless, we acknowledge the following limitations: pulldowns can reflect selection effects (epitope exposure, avidity, chain-length/branching density) as much as true coupling, and association does not prove direct binding. Verifications with GlgX2 active-site mutants that retain binding but lose catalysis will be required to definitively determine catalytic pruning and to test whether GlgX2's specific localisation is cause or consequence of GlgA2-centred synthesis to cement this hypothesis.

3. The regulation of glycogen synthesis and degradation

Collectively, this work shows that glycogen metabolism in *Synechocystis* is organised as a multi-layered control system rather than a simple on/off switch between synthesis and degradation. On the synthesis side, the first committed step catalysed by GlgC functions as a metabolite-level gate that converts the cellular 3-PGA/Pi balance into ADP-Glc supply. High 3-PGA and low Pi during active photosynthesis favour an "ON" state and promote glycogen accumulation, whereas rising Pi in the dark or during energy limitation switches the gate "OFF", sharply reducing flux into glycogen even if downstream capacity remains. Secondary control by metabolites such as 2-PGA and Fru-6P, together with the upstream PGAM–PII–PirC

module, further links GlgC activity to nitrogen status and to the partitioning of carbon between the CBB cycle, glycolysis, compatible solute synthesis and storage.

Downstream of GlgC, regulation is dominated by primer availability and polymer architecture rather than by the maximal catalytic capacity of GlgA1 and GlgA2. Both GlgA isoforms are strictly primer-dependent and strongly favour branched substrates, and GlgB lowers primer requirements while differentially tuning the throughput and architecture of GlgA1- and GlgA2-derived glycogen. As a result, effective synthesis requires both sufficient ADP-Glc supply (GlgC gate "ON") and a favourable landscape of accessible non-reducing ends generated by branching and local granule remodelling. Proteomic and biochemical data suggest a model in which catabolic enzymes (GlgP and GlgX) are co-localised with GlgA/GlgB on glycogen particles even during net synthesis, allowing local "trimming during synthesis" that removes non-productive branches and optimises primer quality without triggering bulk degradation.

Glycogen degradation is organised along a complementary hierarchy. The GlgP1/GlgP2 pair provides a dual entry point into catabolism: GlgP2 acts as the main phosphorylase during normal metabolism and resuscitation from chlorosis, whereas GlgP1 is a redox-regulated reserve that is preferentially engaged under oxidising, stress-associated states, as well as under prolonged darkness. Complete mobilisation of glycogen further depends on GlgX1-mediated debranching, which is specifically required for recovery from prolonged darkness and extended chlorosis. Although GlgX2 showed no detectable debranching activity in the assay conditions used in **Publication 3**, its selective co-enrichment with GlgA2 in our pulldowns, together with cross-complementation data in *S. elongatus*, is consistent with a specialised pruning-during-synthesis role rather than bulk glycogen mobilisation [58,89,91].

Embedded in transcriptional control (e.g. nitrogen-responsive regulation of glycogen genes) and the developmental chlorosis–resuscitation programme, these enzymatic modules together implement an integrated control logic: glycogen reserves are filled when conditions (light and nitrogen) permit, preserved against premature loss, and then rapidly and deeply mobilised when carbon reserves are needed to support survival and regrowth.

4. Limitations and outlook

This work combines a wide range of methods to build a mechanistic picture of glycogen regulation in *Synechocystis*. Inevitably, each approach introduces constraints. Most biochemical characterisations rely on purified proteins overexpressed in *E. coli* and assayed in dilute, well-buffered systems with defined pH, ion and metabolite ranges. These conditions enable precise parameter estimation for proteins of interests, but they neglect macromolecular crowding, native ionic composition, post-translational modification and localised metabolite channelling present *in vivo*. Effector concentrations were chosen to span or mimic plausible physiological ranges, yet *in vivo* metabolite pools and redox couples are highly dynamic and compartmentalised, and direct measurements for key concentrations of metabolites such as ADP-Glc and Glc-1P are still sparse.

Similarly, the pulldown and coIP datasets define a general interactome, but cannot definitively discriminate direct from indirect contacts via glycogen association and resolve stoichiometries using the current experimental design. A further limitation concerns the interactome data: His-tag pulldown and coIP experiments enrich largely non-overlapping sets of candidate partners,

underscoring the strong method dependence of protein-interaction datasets and our inability at present to define a single, stable Glycogen synthesis complex.

Finally, the simulated mathematical models of Pi- and 3-PGA-gated control are intentionally minimal: they treat central metabolites as external parameters and ignore broader network feedback and spatial organisation, so they should be seen as conceptual rather than predictive pending experimental verification, such as with a well calibrated GlgC-GlgA-GlgB spectrophotometric assay for this purpose.

These caveats point directly to productive next steps. A logical extension is to move from minimal towards progressively more complete reconstitutions that sequentially incorporate additional enzymatic players. Systematically probing the effects of GlgP (±GlgX) on GlgA + GlgB activity would clarify how glycogen is remodelled during net synthesis, and whether local trimming and elongation are mechanistically coupled. The GlgB paralogue recovered in GlgB coIP experiments likewise warrants dedicated analysis: applying the same characterisation pipeline used for canonical GlgB, combined with capillary electrophoresis of synthesis products, should reveal its interaction with GlgA and its specific impact on branch density and placement.

In parallel, the role of GlgC in completing the glycogen synthesis pathway remains underexplored. Reconstitutions employing sufficiently pure GlgC preparations will be essential to capture critical modulations in ADP-Glc supply and their downstream consequences for elongation and branching. In this manner, additional explorations into GlgC-PRP interactions should also provide indications of GlgC-carboxysome localisations.

Complementary approaches could refine the spatial and organisational model of the glycogen machinery. Additional pulldown strategies and/or biophysical methods employing glycogen itself as bait—either commercial or generated *in vitro* by GlgA—may resolve the association of individual enzymes and regulatory factors with the granule surface. High-resolution imaging, such as correlative light–electron microscopy or cryo-ET of glycogen granules decorated with defined enzyme subsets, could directly test the proposed glycogen-centred microdomain linking carboxysomes, granule architecture and local GlgP/GlgX trimming. Finally, extending this framework beyond Synechocystis to diverse cyanobacteria and, ultimately, plant starch metabolism would enable systematic comparison of 3-PGA/Pi gating and primer-based control. In this way, the present work can serve as a blueprint for engineering programmable storage polysaccharides to optimise stress resilience, carbon allocation and bioproduct formation in phototrophs.

References

1 Schirrmeister BE, Sanchez-Baracaldo P & Wacey D (2016) Cyanobacterial evolution during the Precambrian. *Int J Astrobiol* **15**, 187–204.

2 Demoulin CF, Lara YJ, Cornet L, François C, Baurain D, Wilmotte A & Javaux EJ (2019) Cyanobacteria evolution: Insight from the fossil record. *Free Radic Biol Med* **140**, 206–223.

3 Blankenship RE (2017) How Cyanobacteria went green. *Science* **355**, 1372–1373.

4 Houmard J (1995) How Do Cyanobacteria Perceive and Adjust to Their Environment? In *Molecular Ecology of Aquatic Microbes* (Joint I, ed), pp. 153–170. Springer, Berlin, Heidelberg.

5 Durall C & Lindblad P (2015) Mechanisms of carbon fixation and engineering for increased carbon fixation in cyanobacteria. *Algal Res* **11**, 263–270.

6 Komrek, J., Kastovsksy, J., Mares, J. and Johnsen, J. (2014) Taxonomic Classification of Cyanoprokaryotes (Cyanobacterial Genera) 2014, Using a Polyphasic Approach. Preslia, 86, 295-335. - References - Scientific Research Publishing

7 Rippka R, Deruelles J, Waterbury JB, Herdman M & Stanier RY (1979) Generic Assignments, Strain Histories and Properties of Pure Cultures of Cyanobacteria. *Microbiology* **111**, 1–61.

8 Zavřel T, Očenášová P & Červený J (2017) Phenotypic characterization of Synechocystis sp. PCC 6803 substrains reveals differences in sensitivity to abiotic stress. *PloS One* **12**, e0189130.

9 Ikeuchi M & Tabata S (2001) Synechocystis sp. PCC 6803 - a useful tool in the study of the genetics of cyanobacteria. *Photosynth Res* **70**, 73–83.

10 Iijima H, Nakaya Y, Kuwahara A, Hirai MY & Osanai T (2015) Seawater cultivation of freshwater cyanobacterium Synechocystis sp. PCC 6803 drastically alters amino acid composition and glycogen metabolism. *Front Microbiol* **6**, 326.

11 Klotz A, Georg J, Bučinská L, Watanabe S, Reimann V, Januszewski W, Sobotka R, Jendrossek D, Hess WR & Forchhammer K (2016) Awakening of a Dormant Cyanobacterium from Nitrogen Chlorosis Reveals a Genetically Determined Program. *Curr Biol CB* **26**, 2862–2872.

12 Koch M, Berendzen KW & Forchhammer AK (2020) On the Role and Production of Polyhydroxybutyrate (PHB) in the Cyanobacterium Synechocystis sp. PCC 6803. *Life Basel Switz* **10**, 47.

13 Voronkov A & Sinetova M (2019) Polyphosphate accumulation dynamics in a population of Synechocystis sp. PCC 6803 cells under phosphate overplus. *Protoplasma* **256**, 1153–1164.

14 Watzer B & Forchhammer K (2018) Cyanophycin Synthesis Optimizes Nitrogen Utilization in the Unicellular Cyanobacterium Synechocystis sp. Strain PCC 6803. *Appl Environ Microbiol* **84**, e01298-18.

15 Koch M, Doello S, Gutekunst K & Forchhammer K (2019) PHB is Produced from Glycogen Turn-over during Nitrogen Starvation in Synechocystis sp. PCC 6803. *Int J Mol Sci* **20**, 1942.

16 Chen X, Schreiber K, Appel J, Makowka A, Fähnrich B, Roettger M, Hajirezaei MR, Sönnichsen FD, Schönheit P, Martin WF & Gutekunst K (2016) The Entner-Doudoroff pathway is an overlooked glycolytic route in cyanobacteria and plants. *Proc Natl Acad Sci U S A* **113**, 5441–5446.

17 Baers LL, Breckels LM, Mills LA, Gatto L, Deery MJ, Stevens TJ, Howe CJ, Lilley KS & Lea-Smith DJ (2019) Proteome Mapping of a Cyanobacterium Reveals Distinct

Compartment Organization and Cell-Dispersed Metabolism. *Plant Physiol* **181**, 1721–1738.
18 Westermark S & Steuer R (2016) Toward Multiscale Models of Cyanobacterial Growth: A Modular Approach. *Front Bioeng Biotechnol* **4**, 95.
19 Mullineaux CW (2014) Co-existence of photosynthetic and respiratory activities in cyanobacterial thylakoid membranes. *Biochim Biophys Acta BBA - Bioenerg* **1837**, 503–511.
20 Pagels F, Guedes AC, Amaro HM, Kijjoa A & Vasconcelos V (2019) Phycobiliproteins from cyanobacteria: Chemistry and biotechnological applications. *Biotechnol Adv* **37**, 422–443.
21 Björn LO, Shevela D & Govindjee G (2018) *Photosynthesis: Solar energy for life* World Scientific Publishing, Singapore.
22 Schneider H, Lai B & Krömer JO (2025) Understanding the electron pathway fluidity of Synechocystis in biophotovoltaics. *Plant J Cell Mol Biol* **121**, e17225.
23 Shen J-R (2015) The Structure of Photosystem II and the Mechanism of Water Oxidation in Photosynthesis. *Annu Rev Plant Biol* **66**, 23–48.
24 Lea-Smith DJ, Bombelli P, Vasudevan R & Howe CJ (2016) Photosynthetic, respiratory and extracellular electron transport pathways in cyanobacteria. *Biochim Biophys Acta* **1857**, 247–255.
25 Yamori W, Makino A & Shikanai T (2016) A physiological role of cyclic electron transport around photosystem I in sustaining photosynthesis under fluctuating light in rice. *Sci Rep* **6**, 20147.
26 Watzer B, Engelbrecht A, Hauf W, Stahl M, Maldener I & Forchhammer K (2015) Metabolic pathway engineering using the central signal processor PII. *Microb Cell Factories* **14**, 192.
27 Nelson N & Ben-Shem A (2004) The complex architecture of oxygenic photosynthesis. *Nat Rev Mol Cell Biol* **5**, 971–982.
28 Deckers-Hebestreit G & Altendorf K (1996) The F0F1-type ATP synthases of bacteria: structure and function of the F0 complex. *Annu Rev Microbiol* **50**, 791–824.
29 Westermark S & Steuer R (2016) Toward Multiscale Models of Cyanobacterial Growth: A Modular Approach. *Front Bioeng Biotechnol* **4**, 95.
30 Pils D & Schmetterer G (2001) Characterization of three bioenergetically active respiratory terminal oxidases in the cyanobacterium *Synechocystis* sp. strain PCC 6803. *FEMS Microbiol Lett* **203**, 217–222.
31 Kok B (1949) On the interrelation of respiration and photosynthesis in green plants. *Biochim Biophys Acta* **3**, 625–631.
32 Yin X, Niu Y, van der Putten PEL & Struik PC (2020) The Kok effect revisited. *New Phytol* **227**, 1764–1775.
33 Huang F, Parmryd I, Nilsson F, Persson AL, Pakrasi HB, Andersson B & Norling B (2002) Proteomics of *Synechocystis* sp. Strain PCC 6803. *Mol Cell Proteomics* **1**, 956–966.
34 Doello S, Burkhardt M & Forchhammer K (2021) The essential role of sodium bioenergetics and ATP homeostasis in the developmental transitions of a cyanobacterium. *Curr Biol* **31**, 1606-1615.e2.
35 Hagemann M, Eisenhut M, Hackenberg C & Bauwe H (2010) Pathway and importance of photorespiratory 2-phosphoglycolate metabolism in cyanobacteria. *Adv Exp Med Biol* **675**, 91–108.
36 Badger MR & Price GD (2003) CO2 concentrating mechanisms in cyanobacteria: molecular components, their diversity and evolution. *J Exp Bot* **54**, 609–622.
37 Lucius S & Hagemann M (2024) The primary carbon metabolism in cyanobacteria and its regulation. *Front Plant Sci* **15**.

38 Scholl J, Dengler L, Bader L & Forchhammer K (2020) Phosphoenolpyruvate carboxylase from the cyanobacterium Synechocystis sp. PCC 6803 is under global metabolic control by PII signaling. *Mol Microbiol* **114**, 292–307.
39 Scheurer NM, Rajarathinam Y, Timm S, Köbler C, Kopka J, Hagemann M & Wilde A (2021) Homologs of Circadian Clock Proteins Impact the Metabolic Switch Between Light and Dark Growth in the Cyanobacterium Synechocystis sp. PCC 6803. *Front Plant Sci* **12**, 675227.
40 Saha R, Liu D, Hoynes-O'Connor A, Liberton M, Yu J, Bhattacharyya-Pakrasi M, Balassy A, Zhang F, Moon TS, Maranas CD & Pakrasi HB (2016) Diurnal Regulation of Cellular Processes in the Cyanobacterium Synechocystis sp. Strain PCC 6803: Insights from Transcriptomic, Fluxomic, and Physiological Analyses. *mBio* **7**, e00464-16.
41 Mills LA, McCormick AJ & Lea-Smith DJ (2020) Current knowledge and recent advances in understanding metabolism of the model cyanobacterium Synechocystis sp. PCC 6803. *Biosci Rep* **40**, BSR20193325.
42 Makowka A, Nichelmann L, Schulze D, Spengler K, Wittmann C, Forchhammer K & Gutekunst K (2020) Glycolytic Shunts Replenish the Calvin-Benson-Bassham Cycle as Anaplerotic Reactions in Cyanobacteria. *Mol Plant* **13**, 471–482.
43 Kugler A & Stensjö K (2023) Optimal energy and redox metabolism in the cyanobacterium Synechocystis sp. PCC 6803. *Npj Syst Biol Appl* **9**, 47.
44 Doello S, Neumann N & Forchhammer K (2022) Regulatory phosphorylation event of phosphoglucomutase 1 tunes its activity to regulate glycogen metabolism. *FEBS J* **289**, 6005–6020.
45 Ortega-Martínez P, Roldán M, Díaz-Troya S & Florencio FJ (2023) Stress response requires an efficient connection between glycogen and central carbon metabolism by phosphoglucomutases in cyanobacteria. *J Exp Bot* **74**, 1532–1550.
46 Díaz-Troya S, López-Maury L, Sánchez-Riego AM, Roldán M & Florencio FJ (2014) Redox Regulation of Glycogen Biosynthesis in the Cyanobacterium Synechocystis sp. PCC 6803: Analysis of the AGP and Glycogen Synthases. *Mol Plant* **7**, 87–100.
47 Lee K, Doello S, Hagemann M & Forchhammer K (2025) Deciphering the tight metabolite-level regulation of glucose-1-phosphate adenylyltransferase (GlgC) for glycogen synthesis in cyanobacteria. *FEBS J* **292**, 759–775.
48 Ballicora MA, Iglesias AA & Preiss J (2004) ADP-Glucose Pyrophosphorylase: A Regulatory Enzyme for Plant Starch Synthesis. *Photosynth Res* **79**, 1–24.
49 Ball K & Preiss J (1994) Allosteric sites of the large subunit of the spinach leaf ADPglucose pyrophosphorylase. *J Biol Chem* **269**, 24706–24711.
50 Kadouche D, Ducatez M, Cenci U, Tirtiaux C, Suzuki E, Nakamura Y, Putaux J-L, Terrasson AD, Diaz-Troya S, Florencio FJ, Arias MC, Striebeck A, Palcic M, Ball SG & Colleoni C (2016) Characterization of Function of the GlgA2 Glycogen/Starch Synthase in Cyanobacterium sp. Clg1 Highlights Convergent Evolution of Glycogen Metabolism into Starch Granule Aggregation1. *Plant Physiol* **171**, 1879–1892.
51 Yoo S-H, Lee B-H, Moon Y, Spalding MH & Jane J (2014) Glycogen Synthase Isoforms in Synechocystis sp. PCC6803: Identification of Different Roles to Produce Glycogen by Targeted Mutagenesis. *PLOS ONE* **9**, e91524.
52 Ortega-Martínez P, Nikkanen L, Wey LT, Florencio FJ, Allahverdiyeva Y & Díaz-Troya S (2024) Glycogen synthesis prevents metabolic imbalance and disruption of photosynthetic electron transport from photosystem II during transition to photomixotrophy in Synechocystis sp. PCC 6803. *New Phytol* **243**, 162–179.
53 Cano M, Holland SC, Artier J, Burnap RL, Ghirardi M, Morgan JA & Yu J (2018) Glycogen Synthesis and Metabolite Overflow Contribute to Energy Balancing in Cyanobacteria. *Cell Rep* **23**, 667–672.

54 Kato Y, Hidese R, Matsuda M, Ohbayashi R, Ashida H, Kondo A & Hasunuma T (2024) Glycogen deficiency enhances carbon partitioning into glutamate for an alternative extracellular metabolic sink in cyanobacteria. *Commun Biol* **7**, 233.
55 Lucius S, Makowka A, Michl K, Gutekunst K & Hagemann M (2021) The Entner-Doudoroff Pathway Contributes to Glycogen Breakdown During High to Low CO2 Shifts in the Cyanobacterium Synechocystis sp. PCC 6803. *Front Plant Sci* **12**.
56 Fu J & Xu X (2006) The functional divergence of two glgP homologues in Synechocystis sp. PCC 6803. *FEMS Microbiol Lett* **260**, 201–209.
57 Doello S, Klotz A, Makowka A, Gutekunst K & Forchhammer K (2018) A Specific Glycogen Mobilization Strategy Enables Rapid Awakening of Dormant Cyanobacteria from Chlorosis. *Plant Physiol* **177**, 594–603.
58 Suzuki E, Umeda K, Nihei S, Moriya K, Ohkawa H, Fujiwara S, Tsuzuki M & Nakamura Y (2007) Role of the GlgX protein in glycogen metabolism of the cyanobacterium, *Synechococcus elongatus* PCC 7942. *Biochim Biophys Acta BBA - Gen Subj* **1770**, 763–773.
59 Shinde S, Zhang X, Singapuri SP, Kalra I, Liu X, Morgan-Kiss RM & Wang X (2020) Glycogen Metabolism Supports Photosynthesis Start through the Oxidative Pentose Phosphate Pathway in Cyanobacteria1[OPEN]. *Plant Physiol* **182**, 507–517.
60 Shimakawa G, Hasunuma T, Kondo A, Matsuda M, Makino A & Miyake C (2014) Respiration accumulates Calvin cycle intermediates for the rapid start of photosynthesis in Synechocystis sp. PCC 6803. *Biosci Biotechnol Biochem* **78**, 1997–2007.
61 Ehira S, Shimmori Y, Watanabe S, Kato H, Yoshikawa H & Ohmori M (2017) The nitrogen-regulated response regulator NrrA is a conserved regulator of glycogen catabolism in β-cyanobacteria. *Microbiol Read Engl* **163**, 1711–1719.
62 Cantrell M, Cano M, Sebesta J, Paddock T, Xiong W, Chou KJ & Yu J (2023) Manipulation of glycogen and sucrose synthesis increases photosynthetic productivity in cyanobacteria. *Front Microbiol* **14**, 1124274.
63 Watzer B, Spät P, Neumann N, Koch M, Sobotka R, Macek B, Hennrich O & Forchhammer K (2019) The Signal Transduction Protein PII Controls Ammonium, Nitrate and Urea Uptake in Cyanobacteria. *Front Microbiol* **10**, 1428.
64 Forcada-Nadal A, Llácer JL, Contreras A, Marco-Marín C & Rubio V (2018) The PII-NAGK-PipX-NtcA Regulatory Axis of Cyanobacteria: A Tale of Changing Partners, Allosteric Effectors and Non-covalent Interactions. *Front Mol Biosci* **5**, 91.
65 Giner-Lamia J, Robles-Rengel R, Hernández-Prieto MA, Muro-Pastor MI, Florencio FJ & Futschik ME (2017) Identification of the direct regulon of NtcA during early acclimation to nitrogen starvation in the cyanobacterium Synechocystis sp. PCC 6803. *Nucleic Acids Res* **45**, 11800–11820.
66 Espinosa J, Forchhammer K, Burillo S & Contreras A (2006) Interaction network in cyanobacterial nitrogen regulation: PipX, a protein that interacts in a 2-oxoglutarate dependent manner with PII and NtcA. *Mol Microbiol* **61**, 457–469.
67 Orthwein T, Scholl J, Spät P, Lucius S, Koch M, Macek B, Hagemann M & Forchhammer K (2021) The novel PII-interactor PirC identifies phosphoglycerate mutase as key control point of carbon storage metabolism in cyanobacteria. *Proc Natl Acad Sci U S A* **118**, e2019988118.
68 Spät P, Klotz A, Rexroth S, Maček B & Forchhammer K (2018) Chlorosis as a Developmental Program in Cyanobacteria: The Proteomic Fundament for Survival and Awakening*. *Mol Cell Proteomics* **17**, 1650–1669.
69 Neumann N, Doello S & Forchhammer K (2021) Recovery of Unicellular Cyanobacteria from Nitrogen Chlorosis: A Model for Resuscitation of Dormant Bacteria. *Microb Physiol* **31**, 78–87.

70 Rappsilber J, Mann M & Ishihama Y (2007) Protocol for micro-purification, enrichment, pre-fractionation and storage of peptides for proteomics using StageTips. *Nat Protoc* **2**, 1896–1906.
71 Semanjski M, Germain E, Bratl K, Kiessling A, Gerdes K & Macek B (2018) The kinases HipA and HipA7 phosphorylate different substrate pools in Escherichia coli to promote multidrug tolerance. *Sci Signal* **11**, eaat5750.
72 Tyanova S, Temu T & Cox J (2016) The MaxQuant computational platform for mass spectrometry-based shotgun proteomics. *Nat Protoc* **11**, 2301–2319.
73 Cox J, Neuhauser N, Michalski A, Scheltema RA, Olsen JV & Mann M (2011) Andromeda: a peptide search engine integrated into the MaxQuant environment. *J Proteome Res* **10**, 1794–1805.
74 Elias JE & Gygi SP (2007) Target-decoy search strategy for increased confidence in large-scale protein identifications by mass spectrometry. *Nat Methods* **4**, 207–214.
75 Tyanova S, Temu T, Sinitcyn P, Carlson A, Hein MY, Geiger T, Mann M & Cox J (2016) The Perseus computational platform for comprehensive analysis of (prote)omics data. *Nat Methods* **13**, 731–740.
76 Klähn S & Hagemann M (2011) Compatible solute biosynthesis in cyanobacteria. *Environ Microbiol* **13**, 551–562.
77 Kirsch F, Klähn S & Hagemann M (2019) Salt-Regulated Accumulation of the Compatible Solutes Sucrose and Glucosylglycerol in Cyanobacteria and Its Biotechnological Potential. *Front Microbiol* **10**.
78 Eisenhut M, Huege J, Schwarz D, Bauwe H, Kopka J & Hagemann M (2008) Metabolome Phenotyping of Inorganic Carbon Limitation in Cells of the Wild Type and Photorespiratory Mutants of the Cyanobacterium Synechocystis sp. Strain PCC 6803. *Plant Physiol* **148**, 2109–2120.
79 Plohnke N, Seidel T, Kahmann U, Rögner M, Schneider D & Rexroth S (2015) The Proteome and Lipidome of *Synechocystis* sp. PCC 6803 Cells Grown under Light-Activated Heterotrophic Conditions*,. *Mol Cell Proteomics* **14**, 572–584.
80 Ortega-Martínez P, Giner-Lamia J, Roldán M, Florencio FJ & Díaz-Troya S (2025) Identification of an alternative glycogen synthesis pathway independent of glycogen synthases in the cyanobacterium *Synechocystis* sp. PCC 6803. *Plant Physiol Biochem* **229**, 110519.
81 Díaz-Troya S, Roldán M, Mallén-Ponce MJ, Ortega-Martínez P & Florencio FJ (2020) Lethality caused by ADP-glucose accumulation is suppressed by salt-induced carbon flux redirection in cyanobacteria. *J Exp Bot* **71**, 2005–2017.
82 Ballicora MA, Frueauf JB, Fu Y, Schürmann P & Preiss J (2000) Activation of the Potato Tuber ADP-glucose Pyrophosphorylase by Thioredoxin*. *J Biol Chem* **275**, 1315–1320.
83 Ballicora MA, Iglesias AA & Preiss J (2003) ADP-Glucose Pyrophosphorylase, a Regulatory Enzyme for Bacterial Glycogen Synthesis. *Microbiol Mol Biol Rev* **67**, 213–225.
84 Curatti L, Folco E, Desplats P, Abratti G, Limones V, Herrera-Estrella L & Salerno G (1998) Sucrose-phosphate synthase from Synechocystis sp. strain PCC 6803: identification of the spsA gene and characterization of the enzyme expressed in Escherichia coli. *J Bacteriol* **180**, 6776–6779.
85 Wang L & Wise MJ (2011) Glycogen with short average chain length enhances bacterial durability. *Naturwissenschaften* **98**, 719–729.
86 Fox J, Kawaguchi K, Greenberg E & Preiss J (1976) Biosynthesis of bacterial glycogen. Purification and properties of the Escherichia coli B ADPglucose:1,4-alpha-D-glucan 4-alpha-glucosyltransferase. *Biochemistry* **15**, 849–857.

87 Yoo S-H, Spalding MH & Jane J (2002) Characterization of cyanobacterial glycogen isolated from the wild type and from a mutant lacking of branching enzyme. *Carbohydr Res* **337**, 2195–2203.
88 Black K, Buikema WJ & Haselkorn R (1995) The hglK gene is required for localization of heterocyst-specific glycolipids in the cyanobacterium Anabaena sp. strain PCC 7120. *J Bacteriol* **177**, 6440–6448.
89 Delatte T, Umhang M, Trevisan M, Eicke S, Thorneycroft D, Smith SM & Zeeman SC (2006) Evidence for distinct mechanisms of starch granule breakdown in plants. *J Biol Chem* **281**, 12050–12059.
90 Grimaud F, Rogniaux H, James MG, Myers AM & Planchot V (2008) Proteome and phosphoproteome analysis of starch granule-associated proteins from normal maize and mutants affected in starch biosynthesis. *J Exp Bot* **59**, 3395–3406.
91 Myers AM, Morell MK, James MG & Ball SG (2000) Recent progress toward understanding biosynthesis of the amylopectin crystal. *Plant Physiol* **122**, 989–997.
92 Fermont L, Szydlowski N & Colleoni C (2022) Determination of Glucan Chain Length Distribution of Glycogen Using the Fluorophore-Assisted Carbohydrate Electrophoresis (FACE) Method. *J Vis Exp JoVE*, e63392.

Acknowledgements

Completing this doctoral thesis has been a long and intensive journey, marked by challenges, growth, and many memorable moments. I am deeply grateful to all those who have accompanied and supported me along the way.

I warmly thank my supervisor, Prof. Dr. Forchhammer, for the opportunity to work on this project and for his excellent guidance and support, and my second supervisor Prof. Dr. Hannes Link for kindly evaluating this work. My sincere thanks also go to all past and present members of AG Forchhammer, Maldener and Mayer, especially the colleagues and mentors who helped me settle into the lab, introduced me to new methods, and laid important groundwork for this thesis.

I am also very thankful for the many moments outside the lab that made these years special. My friends on two continents have provided much-needed balance, laughter, and perspective through shared meals, activities, and long conversations through the years. The various communities and groups I have been part of have offered a sense of belonging and support that extended far beyond academic life and brought me the very point where I stand now. Special shoutout to the guys at Sportschützen Hagelloch e.V. for the fun times, especially during the most difficult last phases of my PhD.

My deepest gratitude goes to my family for their unconditional love and encouragement. To my Mom, for nurturing my curiosity, supporting my education, and standing by my decisions even when they meant distance and uncertainty. This milestone achievement is also yours. I am also thankful for my extended family, Heike and Opa Albert, for welcoming me warmly and for their kindness and support, and ensuring that I always take a little piece of home with me back to Tübingen.

Finally and most importantly, I would like to thank my wonderful partner in all grand thefts; the divine and endearing Chiara, as her patience, understanding, and continuous encouragement have carried me through both the everyday routines and the most demanding periods of this work, and whose winsome ability to offer comfort and joy in difficult moments has been invaluable. This would not have been possible without you, and I am endlessly grateful for your loving presence in my life.

The world is a tavern,
and time an old, familiar guest.
We walk a long road through bitter wind and snow,
good friends laughing and singing at our side.
At last, returning to the warmth of homely lamplight,
and in that moment, all is well.

Appendix

The publications referenced in this thesis appear in the following sequence:

Publication 1: *Deciphering the tight metabolite-level regulation of glucose-1-phosphate adenylyltransferase (GlgC).*

Publication 2: *The (Glg)ABCs of cyanobacteria--modelling of glycogen synthesis and functional divergence of glycogen synthases in Synechocystis sp. PCC 6803.*

Publication 3: *Redox control and substrate specificity of the glycogen catabolic isoenzymes in Synechocystis sp. PCC 6803.*

The FEBS Journal

FEBS PRESS science publishing by scientists

Deciphering the tight metabolite-level regulation of glucose-1-phosphate adenylyltransferase (GlgC) for glycogen synthesis in cyanobacteria

Kenric Lee[1], Sofia Doello[1], Martin Hagemann[2] and Karl Forchhammer[1]

1 Interfaculty Institute of Microbiology and Infection Medicine, University of Tübingen, Germany
2 Department of Plant Physiology, University of Rostock, Germany

Keywords
3-PGA/Pi; biochemical assay; cyanobacteria; GlgC regulation; glycogen synthesis

Correspondence
K. Forchhammer, Interfaculty Institute of Microbiology and Infection Medicine, University of Tübingen, Organismic interactions Auf der Morgenstelle 28, Tübingen 72076, Germany
Tel: +49 7071 2972096
E-mail: karl.forchhammer@uni-tuebingen.de

(Received 9 July 2024, revised 22 October 2024, accepted 27 November 2024)

doi:10.1111/febs.17348

The enzyme glucose-1-phosphate adenylyltransferase (GlgC, EC:2.7.7.27) catalyses the first step in glycogen synthesis by converting glucose-1-phosphate into ADP-glucose, which is added in turn to a growing glycogen chain by glycogen synthases. Thus far, *in vitro* studies of GlgC were mainly performed using colorimetric or radiolabel-based phosphate release assays, limiting the option for analysing this reaction. With this work, we present a novel *in vitro* continuous assay coupling the subsequent glycogen synthase reaction to the GlgC reaction, thus simulating the process of glycogen synthesis *in vivo*. Using this assay, we revisited GlgC catalytic parameters and screened for metabolites that affect GlgC activity in *Synechocystis* sp. PCC 6803. We also describe in further detail the antagonistic interplay between the GlgC activator, 3-PGA and the inhibitor, inorganic phosphate, revealing the intricate mechanism by which glycogen formation responds to fluctuations in carbon and energy supply in cyanobacteria.

Introduction

Cyanobacteria are a large group of photosynthetic prokaryotes present in nearly every biome on the planet. Given their ability to fix atmospheric CO_2 via photosynthesis, glycogen is an important storage molecule for carbon assimilation and plays a distinct role in the ability to respond to changing environmental conditions. In cases where nitrogen sources are exhausted, the cells can enter a dormant state known as chlorosis, where they accumulate glycogen, which is later rapidly degraded, once nitrogen is available for a rapid recovery to normal growth [1]. Glycogen degradation serves to provide metabolites for the oxidative pentose phosphate (OPP) pathway, generating reducing equivalents for respiration in the dark, as well as to replenish Calvin-Benson-Bassham (CBB) cycle intermediates and other glycolytic shunts once photosynthetic activity is unbalanced or resumes [2,3]. Furthermore, glycogen degradation can also serve to refill the pool of ADP-glucose, which is required for the synthesis of the osmoprotectant glucosylglycerol, allowing for better adaptability in changing osmotic conditions [4].

In all cyanobacteria, including the model strain *Synechocystis* sp. PCC 6803 (hereafter *Synechocystis*), the Glucose-1-phosphate adenylyltransferase (GlgC, product of *slr1176*, EC:2.7.7.27) catalyses the first committed step in glycogen synthesis, which is the reversible conversion of glucose-1-phosphate (Glc-1P)

Abbreviations
2-PG, 2-phosphoglycolate; 2-PGA, 2-phosphoglycerate; 3-PGA, 3-phosphoglycerate; ADP-Glc, ADP-Glucose; CBB Cycle, Calvin-Benson-Bassham cycle; Fru-1,6P, fructose-1,6-bisphosphate; Fru-6P, fructose-6-phosphate; Glc-1P, glucose-1-phosphate; Glc-6P, glucose-6-phosphate; GlgA1, glycogen Synthase 1; GlgC, glucose-1-phosphate adenylyltransferase; LDH, lactate dehydrogenase; OPP Cycle, oxidative pentose phosphate cycle; PEP, phosphoenolpyruvate; PGAM, phosphoglycerate mutase; Pi, inorganic orthophosphate; PK, pyruvate kinase; PPi, pyrophosphate; PPiase, pyrophosphatase.

and ATP to pyrophosphate (PPi) and ADP-glucose (ADP-Glc), the immediate precursor for glycogen synthesis. This reaction is rendered irreversible by the action of cellular pyrophosphatases (PPiase), which split the product PPi into two molecules of orthophosphate (Pi). The ADP-Glc produced is added via a 1,4-alpha bond to a growing glycogen molecule by glycogen synthase, present as two isoenzymes in *Synechocystis* (GlgA1/*sll0945*, EC:2.4.1.21 and GlgA2/*sll1393*, EC:2.4.1.21). Finally, the branching enzyme (GlgB/*sll0158*, EC:2.4.1.18) introduces 1,6-branches into the maturating glycogen molecule, increasing the number of potential extension sites for glycogen synthases.

The regulatory and structural properties of cyanobacterial GlgC enzymes have been the subject of extensive study, given their structural and regulatory similarities to those found in plants involved in starch synthesis. The enzyme from cyanobacteria is functionally related to the small subunits of GlgC from photosynthetic eukaryotes, and share a similar sensitivity to changing levels of 3-phosphoglycerate (3-PGA) and Pi, which act as an activator and inhibitor, respectively [5–8]. With that in mind, and given the availability of genetic tools for *Synechocystis*, many efforts were made to improve the productivity of commercially valuable compounds by exploiting and modifying the carbon assimilation pathways present in *Synechocystis* [9–13].

Despite the key role of GlgC in glycogen synthesis, the current methods employed to study GlgC in the direction of ADP-Glc synthesis have been limited to discontinuous phosphate release assays using colorimetric methods such as the malachite green assay or radioactive isotope-based methods, or have other previously reported limitations in terms of sample handling, equipment requirements and cost factor [7,14–18]. In this work, we present a new approach to study the GlgC reaction in the direction of ADP-Glc synthesis. The method combines a continuous spectrophotometric method previously established for GlgA1 with the GlgC reaction [19]. Our method allows for the processing of multiple sets of samples, allowing for the testing of multiple experimental conditions in a single run. Furthermore, the required equipment and reagents for the assay should already be available in most standard research laboratories. As a demonstration, we utilised our assay to further investigate the regulation of GlgC by its allosteric regulators, providing deeper insight into the fine-tuned regulation of the key reaction in carbon metabolism. We propose that our method could be a useful and easily accessible tool for the study of glycogen synthesis enzymes, and for the modelling of glycogen metabolism *in vitro*.

Results

GlgC (Slr1176) gene cloning and sequence analysis

The sequence coding for the *Synechocystis* GlgC was retrieved from Uniprot database (P52414). However, using this amino acid sequence in multiple alignment analyses with GlgC proteins from several other cyanobacteria revealed an extension of 10 amino acids at the N-terminus with a second downstream start codon congruent with those of the other reference organisms (Fig. 1A). The additional 10 amino acids could thus be a result of mis-annotation, similar to what we experienced with other enzymes from *Synechocystis* [20,21]. With that in mind, we prepared another pET28a expression construct without the extension and purified both proteins, naming them GlgC and GlgC-Long, according to their lengths.

GlgC activity measurements

Figure 1B shows the activity of both GlgC variants in a malachite green assay, where the release of pyrophosphate and its subsequent conversion to orthophosphate from Glc-1P is colorimetrically quantified after stopping the reaction. GlgC was observed to be more active than GlgC-long, with specific activities (V_{max}) of 8.9 ± 0.61 U·mg^{-1} and 1.5 ± 0.14 U·mg^{-1} respectively, when assayed with the substrate Glc-1P in the presence of the activator 3-PGA. It is clearly seen that the shorter variant of GlgC is almost 10-times more active, reinforcing the biological relevance of the shorter variant. Based on this observation we adopted the use of the shorter variant as our standard GlgC.

Coupling GlgC to the GlgA1 reaction

Assaying the GlgC reaction by the malachite green method has several limitations: the method does not allow real-time detection of the reaction but requires end-point measurements, making kinetic analyses less precise than assays with continuous read-outs. Furthermore, this method prevents the use of phosphate-containing buffers. To overcome these limitations, we attempted to establish a coupled assay, where the GlgC reaction is subsequently coupled to glycogen synthesis. The concomitant release of ADP from glycogen synthesis can be detected by a standard coupled assay with photometric read-out (ADP/NADH coupling). Figure 2A presents the design of our entire coupled assay, where Glc-1P was used as the substrate for the GlgC reaction producing ADP-

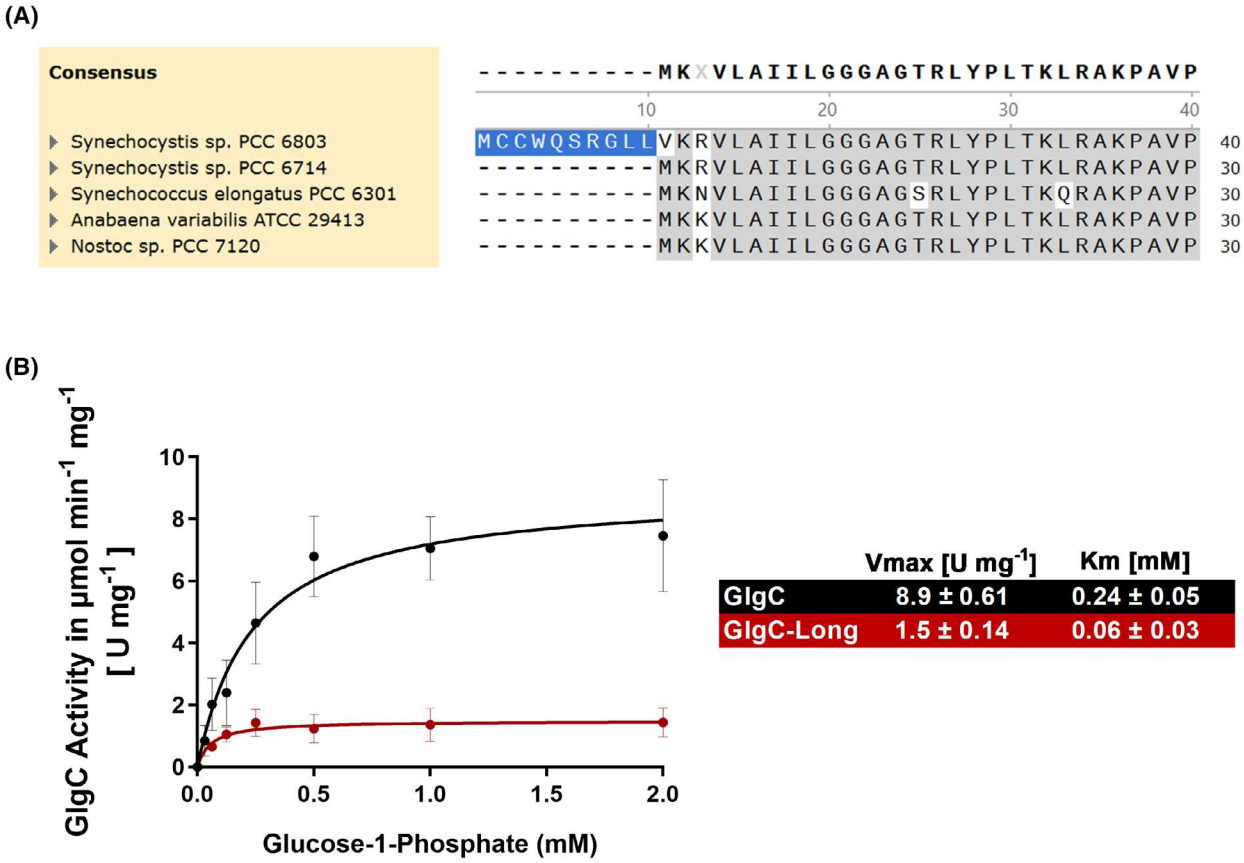

Fig. 1. Reannotation of GlgC in *Synechocystis* sp. PCC 6803 with a shorter protein exhibiting higher activity. (A) ClustalW multiple sequence alignment of cyanobacterial GlgC with the first 40 amino acids shown and 10 amino acid N-terminal extension highlighted in blue. (B) Michaelis–Menten kinetics of GlgC (black) and GlgC-Long (red). A malachite green assay for free phosphate was used to assess the activity of both variants with Glc-1P concentrations reflected on the *x*-axis. The reaction was conducted in the presence of 2 mM 3-PGA. Each data point represents the mean of at least 3 experiments ($n = 3$) with error bars representing the standard deviation (SD).

Glc, which was added to a growing glycogen chain via the GlgA1 reaction, releasing ADP. The released ADP was quantified, as described previously by Wayllace *et al.* [19], by coupling to pyruvate kinase and lactate dehydrogenase. The entire reaction was spectrophotometrically tracked for absorbance at 340 nm, from which the change in A340 is directly proportional to the amount of released ADP (Fig. 2A). As a first step, we assessed the compatibility of the substrates necessary for the downstream coupled enzyme assay with the GlgC reaction. The GlgA1 protein was also assessed for possible compatibility issues, for all of which no significant interference with the GlgC reaction was observed (Fig. 2B,C). Conversely, the components of the GlgC reaction had also no significant impact on the GlgA1 reaction when assayed alone using the ADP/NADH coupled assay, with ADP-Glc as the starting substrate (Fig. 2D).

After excluding possible incompatibility issues, we analysed the raw reaction curve over 30 min, where NADH oxidation can be spectrophotometrically followed by a decreasing absorption at 340 nm (A340). As shown in Fig. 3A, the change in absorbance was not immediately linear upon starting the reaction by the addition of Glc-1P but the reaction velocity gradually increased and reached a stable slope after about 15 min. This result shows that the concentration of the GlgC reaction product ADP-glucose initially increases until an equilibrium between synthesis and consumption is achieved. Next, we needed to identify the appropriate concentration of GlgC in this coupled system to reach a nearly linear relation between GlgC activity and measured velocity of the coupled GlgA1 reaction. Therefore, different amounts of GlgC were titrated in a series of assays containing a fixed concentration of 10 $\mu g \cdot mL^{-1}$ GlgA1 and starting the reaction

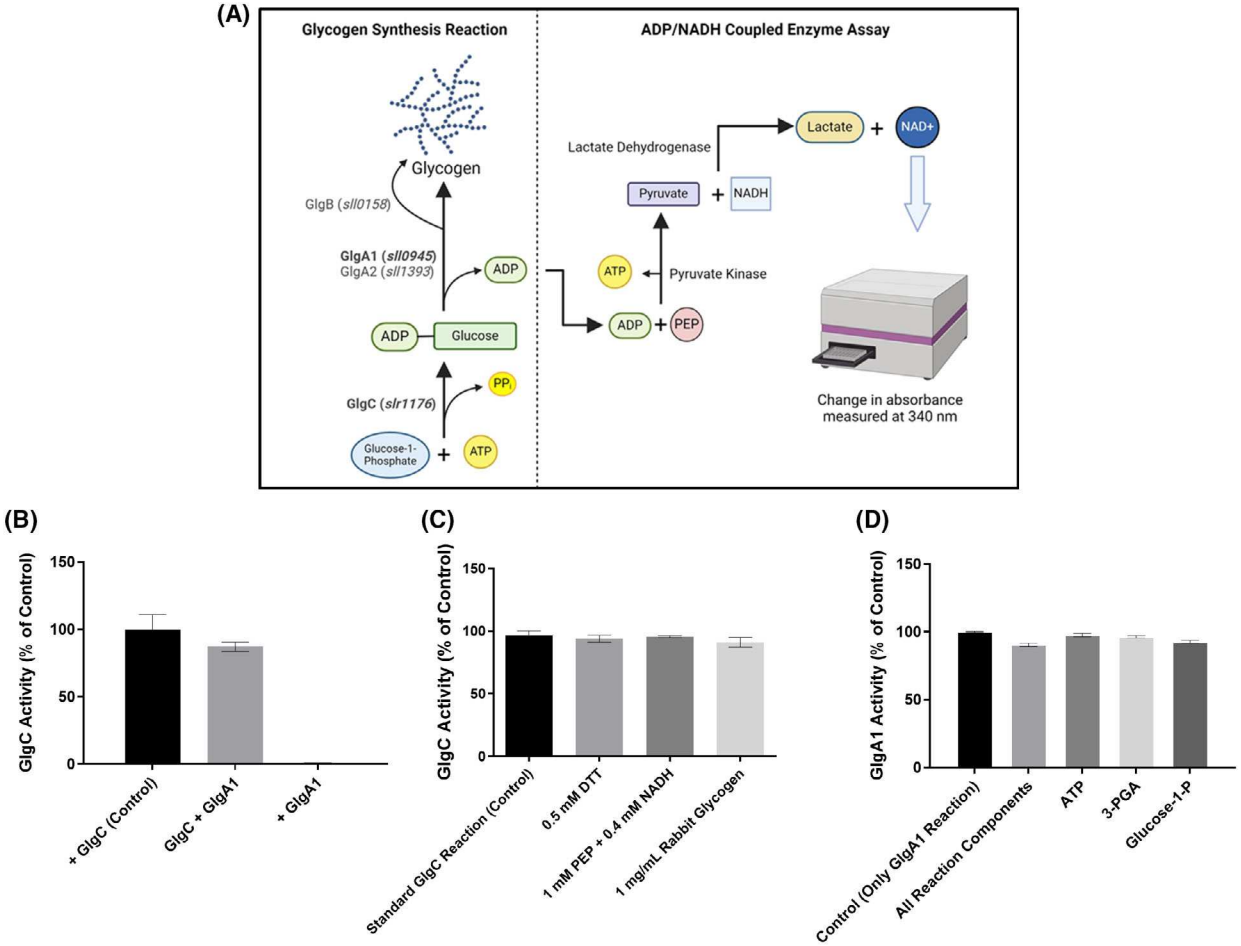

Fig. 2. Assay development and Compatibility Testing. (A) Schematic diagram of the glycogen coupled enzyme assay showing the reactions of both GlgC and GlgA1, as well as those corresponding to pyruvate kinase and lactate dehydrogenase of the NADH coupled enzyme system. The cross compatibility of each component was performed using a malachite green assay to assess the impacts of GlgA1 (B) and the components of the GlgA1 coupling assay on the GlgC reaction (C). (D) GlgA1 assay using the ADP/NADH coupling system performed with 2 mM of each tested component of the GlgC reaction, where the reaction was started with 0.25 mM ADP-Glc. Each data point represents the mean of at least 3 replicate experiments ($n = 3$), with error bars representing the standard deviation (SD).

with 2 mM Glc-1P. Fig. 3B shows that the reaction read-out, in terms of GlgA1 activity, is nearly linear to the amount of added GlgC at low concentration ranges, whereas above 2 $\mu g \cdot mL^{-1}$ GlgC, the reaction velocity begins to approach saturation. With these considerations in mind, we decided to use 1 $\mu g \cdot mL^{-1}$ GlgC for further kinetic assays coupled with 10 $\mu g \cdot mL^{-1}$ GlgA1, which allows sensitive detection of any changes in GlgC activity imposed by substrate and effector molecules. We also investigated the concentration of PPi after a standard 30-min reaction and found that the highest concentration lies within the micromolar range (Fig. 3C), which is below the concentrations that turned out to be inhibitory (see below). Compared to the malachite green assay, we also excluded PPiase from the coupled assay after verifying that the exclusion of PPiase from the coupled assay setup did not have any significant effect (Fig. 3D).

Coupled assay kinetic parameters for GlgC are comparable to those of malachite green assays

With the basic parameters of the assay in hand, we compared GlgC with GlgC-Long in a similar fashion as presented above (Fig. 1C) but using our newly established assay. Figure 4A shows the Michaelis–Menten kinetics of both enzymes. Again, the shorter GlgC protein was observed to be more active than GlgC-Long. We found that the V_{max} of GlgC was

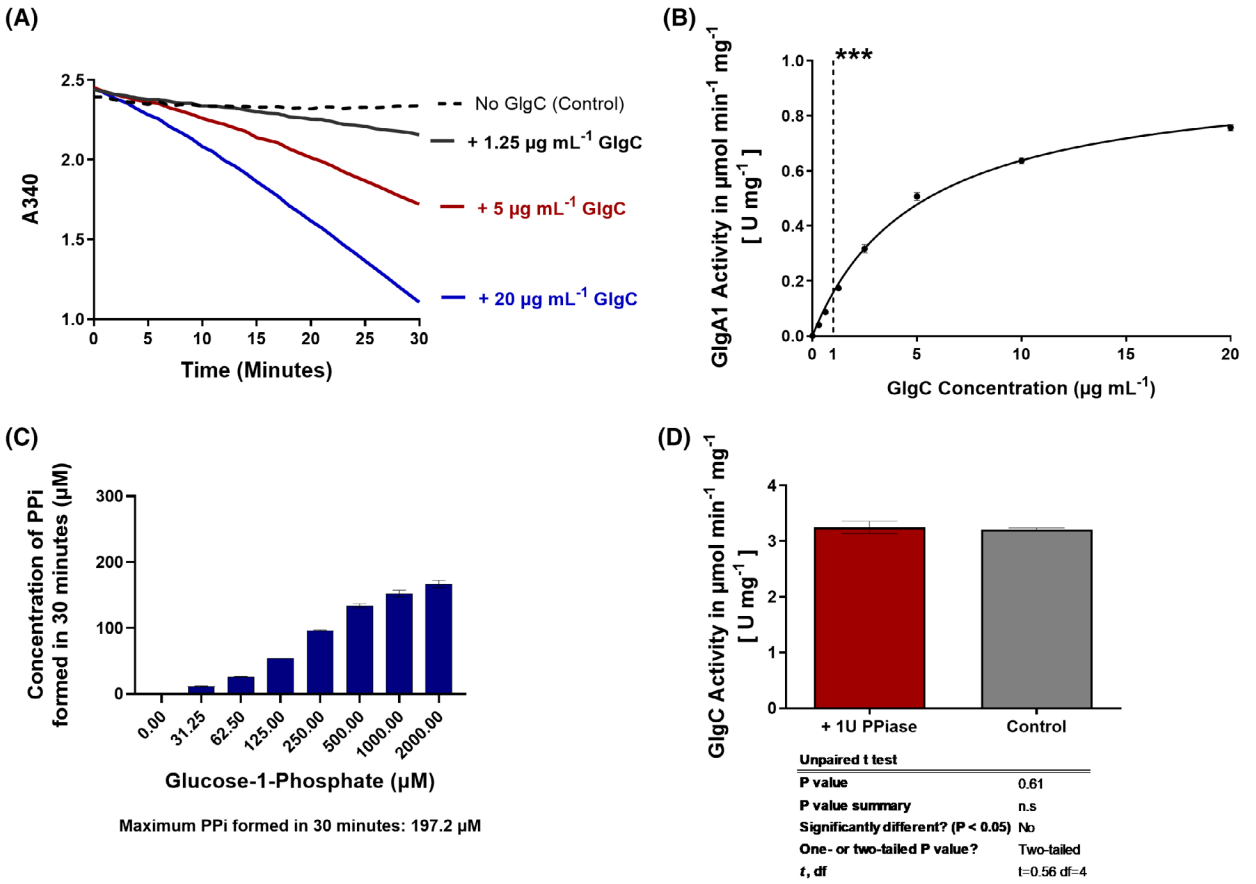

Fig. 3. Optimisation of the assay through testing GlgC-GlgA1 Coupling parameters. (A) Raw reaction curves featuring 3 concentrations of GlgC. GlgC was titrated with 10 µg·mL^{-1} GlgA1 protein. The assay was started with the addition of 2 mM Glc-1P. (B) Curve showing the relationship between GlgC concentration and GlgA1 activity for the aforementioned assay in part A. (C) Calculated concentration of PPi after 30 min. The assay was started in the presence of 2 mM 3-PGA by the addition of Glc-1P at the concentrations on the *x*-axis. (D) Test for possible effects of 1 U PPiase on the GlgC reaction, controls are samples without PPiase. Where applicable, each data point represents the mean of at least 3 replicate experiments ($n = 3$) with error bars showing the SD. ***1 µg·mL^{-1} GlgC and 10 µg·mL^{-1} GlgA1 were taken as standard concentrations for subsequent assays performed in this work.

around 20% lower in the coupled assay as compared to the malachite green assay (6.9 ± 0.16 mM compared to 8.9 ± 0.61 mM), whereas the V_{max} of GlgC-Long was comparable across assays (1.8 ± 0.04 mM compared to 1.5 ± 0.14 mM). The respective Michaelis constant (K_m) value for the substrate Glc-1P was slightly lower in the coupled assay as compared to the malachite green assay, for both GlgC and GlgC-Long variants (GlgC: 0.30 ± 0.02 mM compared to 0.24 ± 0.05 mM, and GlgC-Long: 0.08 ± 0.01 mM compared to 0.06 ± 0.03 mM).

Screening for GlgC effectors

As a first step, we screened for further effector molecules of GlgC activity, by shortlisting a few metabolites that play roles in glycolysis and carbon metabolism in *Synechocystis* (Fig. 4B). To exclude any impacts of these compounds on GlgA1, we also tested the effect of these metabolites, in addition to PPi, on the GlgA1-based coupling reaction (Fig. 4C), confirming that these molecules do not affect the GlgA1 reaction. Accounting for potential additive effects with the activator 3-PGA, we also tested these metabolites in the absence of 3-PGA as well as at a concentration near the calculated EC50 value of 0.5 mM (Fig. 5A). Figure 4B shows that in the presence or absence of 3-PGA, Pi and 2-phosphoglycerate (2-PGA) were observed to be inhibitors whereas fructose-6-phosphate (Fru-6P) activated the reaction. Moreover, glucose-6-phosphate (Glc-6P) and fructose-1,6-biphosphate (Fru-1,6P) were observed to also act as mild inhibitors of

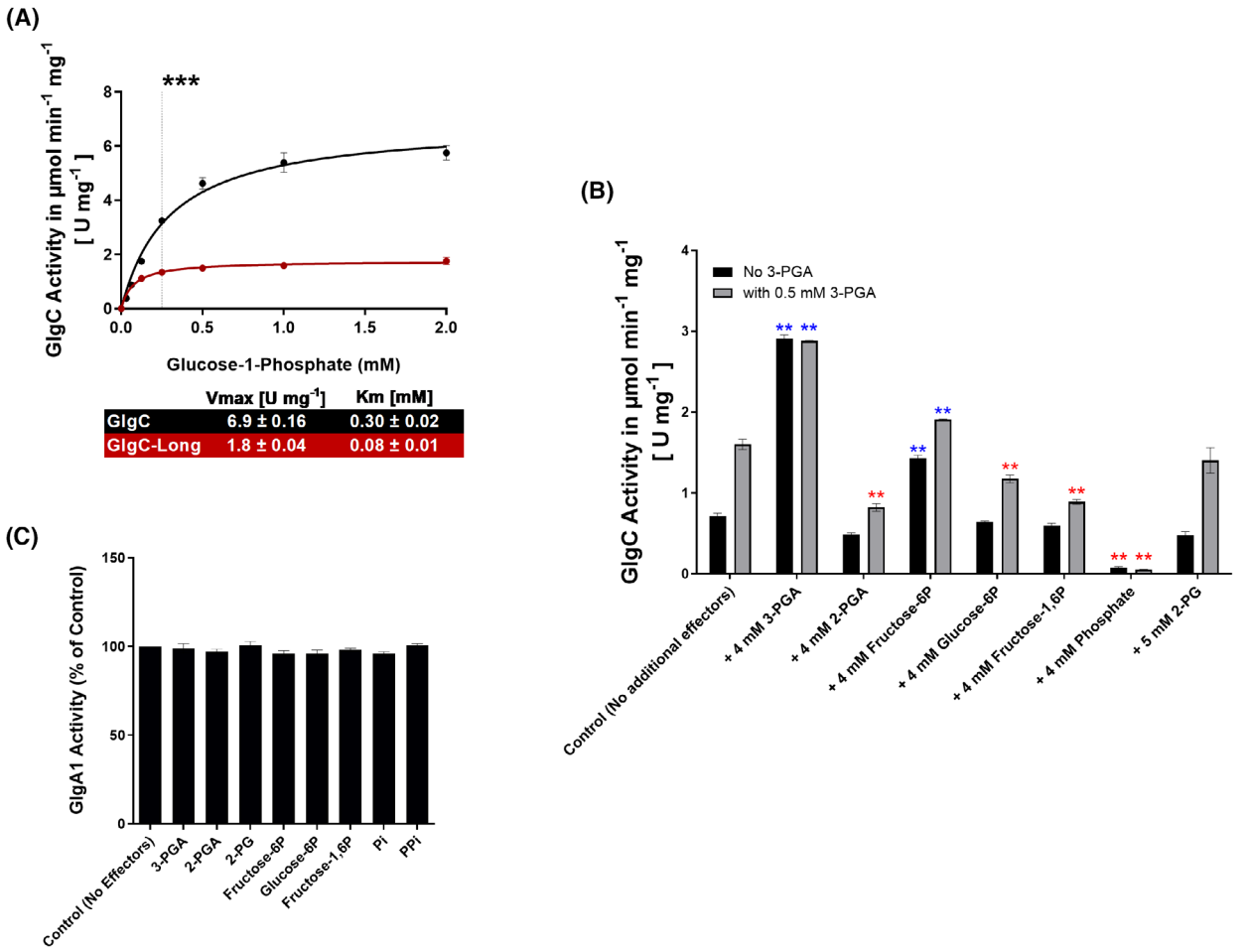

Fig. 4. GlgC coupled assay kinetics and effector screening. (A) Michaelis–Menten kinetics of GlgC (black) and GlgC-Long (red) performed with the coupled assay using the previously determined parameters. The assay was started in the presence of 2 mM 3-PGA by the addition of Glc-1P. ***0.25 mM Glc-1P used for subsequent assays. (B) Screening of potential activators of GlgC, in black are GlgC reactions without activator (3-PGA), reactions with 0.5 mM 3-PGA are shown in grey. Additional effectors were added to both groups to screen for potential regulatory effects. **Blue stars represent significant activation vs controls, while red stars represent inhibition. (C) A similar experiment performed using the ADP/NADH coupled assay using ADP-Glc and GlgA1 to screen for impacts on GlgA1 activity. Where applicable, each data point represents the mean of at least 3 replicate experiments ($n = 3$) with error bars showing the SD.

GlgC in the presence of 3-PGA, in addition to those already mentioned above. The metabolic indicator of carbon limitation, 2-phosphoglycolate (2-PG), was found to have no effect on the GlgC reaction.

To further quantify the activating effect of 3-PGA, we titrated 3-PGA in the GlgC reaction and started the assay with the previously defined concentration of Glc-1P close to K_m (0.25 mM). To determine the EC50 for 3-PGA, the measured GlgC activity was fitted to logarithmic 3-PGA concentrations with variable slopes, yielding an EC50 of 0.43 mM and an eight-fold activation of the GlgC reaction at saturating activator concentrations was determined (Fig. 5A).

Next, to more closely analyse the activating effect of Fru-6P, we first assessed the activation of the GlgC reaction in the absence of 3-PGA. Fitting the data as described above for 3-PGA, revealed an EC50 of 2.3 mM and an approximate three-fold increase in activity at saturating concentrations of Fru-6P (Fig. 5B). In the presence of low levels of 3-PGA, Fru-6P was able to further activate GlgC, but when 3-PGA was present at saturating concentrations, no further activation of GlgC reaction occurred (Fig. 5C). The equivalent concentrations of 3-PGA corresponding to the same degree of activation of GlgC as caused by Fru-6P were estimated by comparing the activation

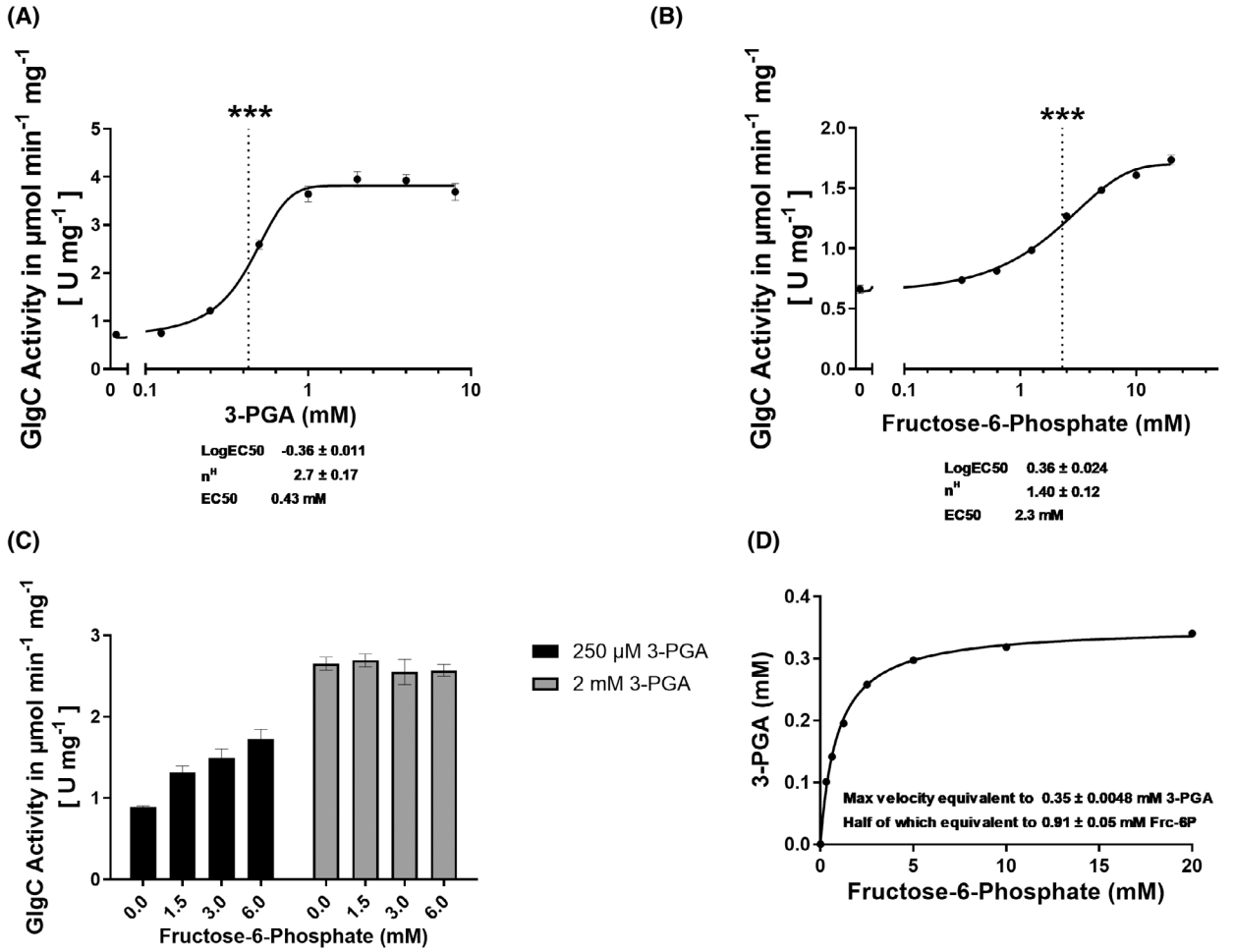

Fig. 5. Effect of the GlgC activators: 3-PGA and Fru-6P. EC50 curves established using the coupled enzyme assay with varying concentrations of (A) 3-PGA and (B) Fru-6P. ***EC50 values of 3-PGA (0.43 mM) and Fru-6P (2.30 mM). (C) GlgC activity with increasing concentrations of Fru-6P in the presence of low and high concentrations of 3-PGA. (D) Curve showing the equivalent concentration of 3-PGA corresponding to the concentration of Fru-6P with regards to GlgC activation. Where applicable, each data point represents the mean of at least 3 replicate experiments ($n = 3$) with error bars showing the SD.

curves of 3-PGA and Fru-6P and fitting the corresponding values as shown in Fig. 5D. It was observed that excess Fru-6P can only achieve as much activation as 0.35 mM 3-PGA, which is slightly under the calculated EC50 value of 3-PGA of 0.43 mM.

2-PGA acts as a negative regulator of GlgC

Contrary to previously reported findings [7], our effector molecule screening showed a negative effect of 2-PGA on GlgC activity (Fig. 6A). 2-PGA substantially inhibited GlgC at higher concentrations. However, when compared to Pi, 2-PGA inhibition appeared significantly weaker, with no complete inhibition of GlgC achievable with the concentration range tested (Fig. 6B). Furthermore, in contrast to the inhibitor Pi, inhibition by 2-PGA did not exhibit any cooperativity with 3-PGA, given by the linear decrease in GlgC activity with increasing 2-PGA concentrations seen in Fig. 6.

3-PGA lifts pi inhibition

The role of Pi in GlgC regulation has previously been described using discontinuous assay methods [5,7]. With our novel continuous assay in hand, we revisited the inhibitory effects of Pi in greater detail. Figure 7 shows the interplay between the key activator 3-PGA and the inhibitor Pi via a series of Pi inhibition curves at increasing 3-PGA concentrations. Immediately

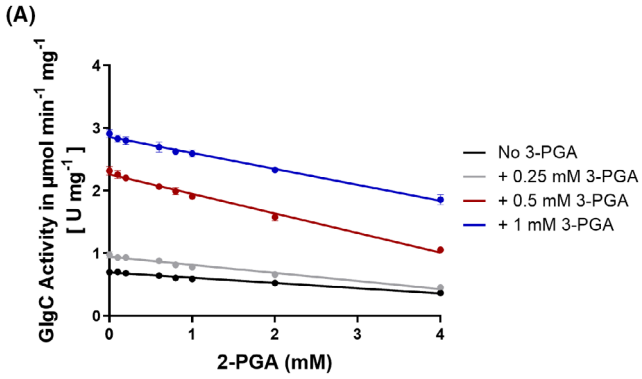

(B)

2-PGA	3-PGA (mM) 0.00	0.25	0.50	1.00
Control (no 2-PGA)	0%	0%	0%	0%
0.1 mM	0%	4%	3%	3%
0.2 mM	3%	4%	5%	4%
0.6 mM	9%	10%	11%	7%
0.8 mM	14%	16%	14%	10%
1 mM	16%	20%	18%	11%
2 mM	25%	32%	32%	20%
4 mM	48%	54%	54%	36%

Fig. 6. 2-PGA inhibition of GlgC. (A) 2-PGA inhibition curves of GlgC in the presence of the listed concentrations of 3-PGA. (B) Accompanying table showing the percentage inhibition of GlgC activity. Samples not treated with 2-PGA were taken as controls. Where applicable, each data point represents the mean of at least 3 replicate experiments (n = 3) with error bars showing the SD.

apparent is that Pi concentrations in the millimolar range led to an almost complete inhibition of GlgC. Furthermore, we observed that the inhibition of GlgC by Pi is strongly modulated by 3-PGA concentrations in a non-linear manner. Plotting the IC50 of phosphate inhibition against the respective 3-PGA concentrations present in the assay revealed a sigmoidal relationship between 3-PGA concentration and the IC50 of Pi, indicating cooperative behaviour in the antagonistic relationship between Pi inhibition and 3-PGA activation of GlgC (Fig. 7B). Conversely, plotting the EC50 for 3-PGA in the presence of varying Pi concentrations also showed a similar sigmoidal relationship (Fig. 7C). Table 1 shows that this relationship also results in greater Hill coefficient (n^H) of the Pi inhibition curves at higher 3-PGA concentrations, indicating that 3-PGA directly affects the cooperativity of GlgC towards Pi inhibition. We also further examined the potential inhibitory effect of PPi, revealing that PPi is a potent inhibitor of GlgC. In the presence of 2 mM 3-PGA, an IC50 of 0.39 mM PPi was determined, compared to 0.87 mM for Pi at the same concentration of 3-PGA (Fig. 7D). This indicates that PPi is inhibiting approximately twice as effective as Pi and that whether PPi is converted into two molecules of Pi or remains unhydrolysed does not impact the assay. Furthermore, we note that the concentration of PPi generated during a given reaction is still well below the IC50 value (Figs 3C and 7D), indicating that PPi produced in this manner has little to no impact on GlgC regulation.

Binding of effector molecules promotes GlgC tetramerisation

Given that *Synechocystis* GlgC is known to be active in its tetrameric form, we analysed the effect of the activator 3-PGA and inhibitor Pi on its oligomeric state using mass photometry [22]. In the absence of effectors, GlgC was found to be mainly present as monomers, with dimers and tetramers being far less prevalent (Fig. 8A). Upon incubation with the effectors 3-PGA or Pi, the distribution of the species shifted to favour the assembly of tetramers (Fig. 8B, C). This indicates that both the inhibitor and the activator promote tetramerisation, where the activator promotes the formation of an active tetramer, whereas the inhibitor Pi promotes the assembly of an inactive tetrameric form. In agreement with this observation, the concurrent presence of Pi and 3-PGA did not further impact oligomerisation, with the tetrameric form of the enzyme being present regardless of which allosteric effector is present (Fig. 8D). Together, it can be assumed that the tetrameric state of GlgC is the physiologically relevant state due to the crowded cellular environment and the constant presence of allosteric effectors stemming from various cellular processes.

Discussion

We constructed an *in vitro* assay by coupling the GlgC reaction with that of GlgA1 and adapting a previously established ADP/NADH-coupling system [19]. Using this assay, we studied in detail the synthesis of ADP-Glc from Glc-1P by GlgC, the first step in glycogen synthesis. We took advantage of the continuous spectrophotometric design of the assay to further study the interactions between selected regulators of GlgC.

The coupled assay detects the formation of ADP-glucose by the subsequent release of ADP via GlgA1 reaction. Compared to the malachite green phosphate release assay, this more precise measurement revealed slightly lower V_{max} values (Malachite green:

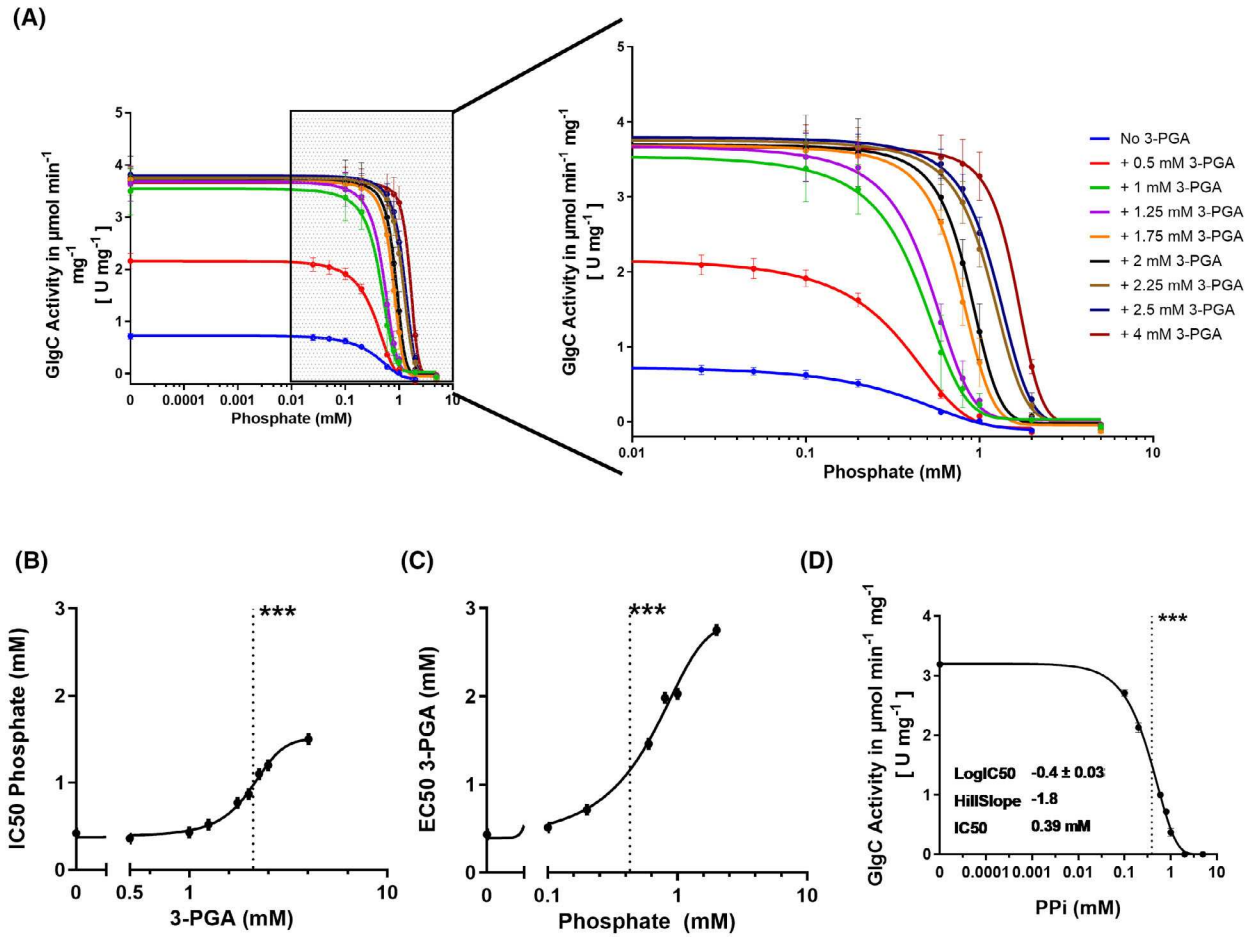

Fig. 7. Modulation of GlgC Inhibition by 3-PGA. (A) Phosphate inhibition curves of GlgC with increasing concentrations of 3-PGA. The coupled assay was used to evaluate the effect of increasing concentrations of phosphate on the GlgC reaction in the presence of increasing 3-PGA concentrations. (B) Pi IC50 in relation to increasing 3-PGA concentration. ***At 2.1 mM 3-PGA, the IC50 of phosphate is increased by half. (C) 3-PGA EC50 in relation to increasing Pi concentration. ***At 0.43 mM Pi, the EC50 of phosphate is increased by half. (D) PPi inhibition curves of GlgC in the presence of 2 mM 3-PGA. ***IC50 of PPi is 0.39 mM at 2 mM 3-PGA. Where applicable, each data point represents the mean of at least 3 replicate experiments ($n = 3$) with error bars showing the SD.

8.9 ± 0.61 U·mg^{-1}, Coupled assay: 6.9 ± 0.16 U·mg^{-1}), resulting from a significant reduction in the standard deviation of the measurements, and in particular, a more precise assessment at low substrate concentrations, when comparing Figs 1B to 4A. Additionally, the assay overcomes several technical disadvantages of the non-continuous, multi-step design of the malachite green assay, where the reaction has to be stopped after selected time points and samples drawn for incubation with the malachite green solution prior to measurement. This presents a technical challenge when studying a reaction over time, where the window between sampling and measurement can be especially small and prone to errors, growing with increasing sample numbers, in addition to disruptions in the assay system itself when samples are drawn. The coupled assay is also a safer and more accessible alternative to radioactive label-based methods, producing comparable results with the aforementioned advantages [18].

Taking advantage of these improvements, we were able to validate the role and fine interplay between key regulators of GlgC, 3-PGA and Pi, as well as screen other previously reported metabolites. The possibility of high-resolution reaction curves without technical interference of Pi when added as an effector molecule allows for the real-time observations of GlgC inhibition by Pi to be made. Interestingly, we found that

Table 1. Percentage inhibition of GlgC by Pi at the given concentrations in the presence of the stated concentrations of 3-PGA. IC50 and hill constant (n^H) values for Pi are also listed at the given concentrations of 3-PGA. Samples without Pi were taken as controls.

	3-PGA (mM)									
Phosphate (pi)	0.00	0.50	1.00	1.25	1.75	2.00	2.25	2.50	3.00	4.00
Control (no Pi)	0%	0%	0%	0%	0%	0%	0%	0%	0%	0%
0.025 mM	3%	3%	–	–	–	–	–	–	–	–
0.05 mM	6%	5%	–	–	–	–	–	–	–	–
0.1 mM	11%	11%	4%	3%	3%	2%	1%	2%	2%	1%
0.2 mM	25%	23%	11%	7%	5%	4%	3%	3%	3%	2%
0.6 mM	71%	78%	72%	63%	28%	19%	11%	10%	8%	5%
0.8 mM	–	–	86%	83%	55%	42%	22%	18%	16%	7%
1 mM	85%	91%	92%	91%	76%	66%	38%	33%	29%	11%
2 mM	100%	100%	97%	98%	96%	95%	93%	91%	93%	79%
5 mM	–	–	100%	100%	100%	100%	100%	100%	100%	100%
Phosphate IC50	0.42	0.36	0.43	0.52	0.77	0.87	1.10	1.20	1.20	1.50
n^H	−1.70	−2.20	−2.90	−3.60	−4.40	−4.30	−4.00	−4.10	−4.70	−5.00

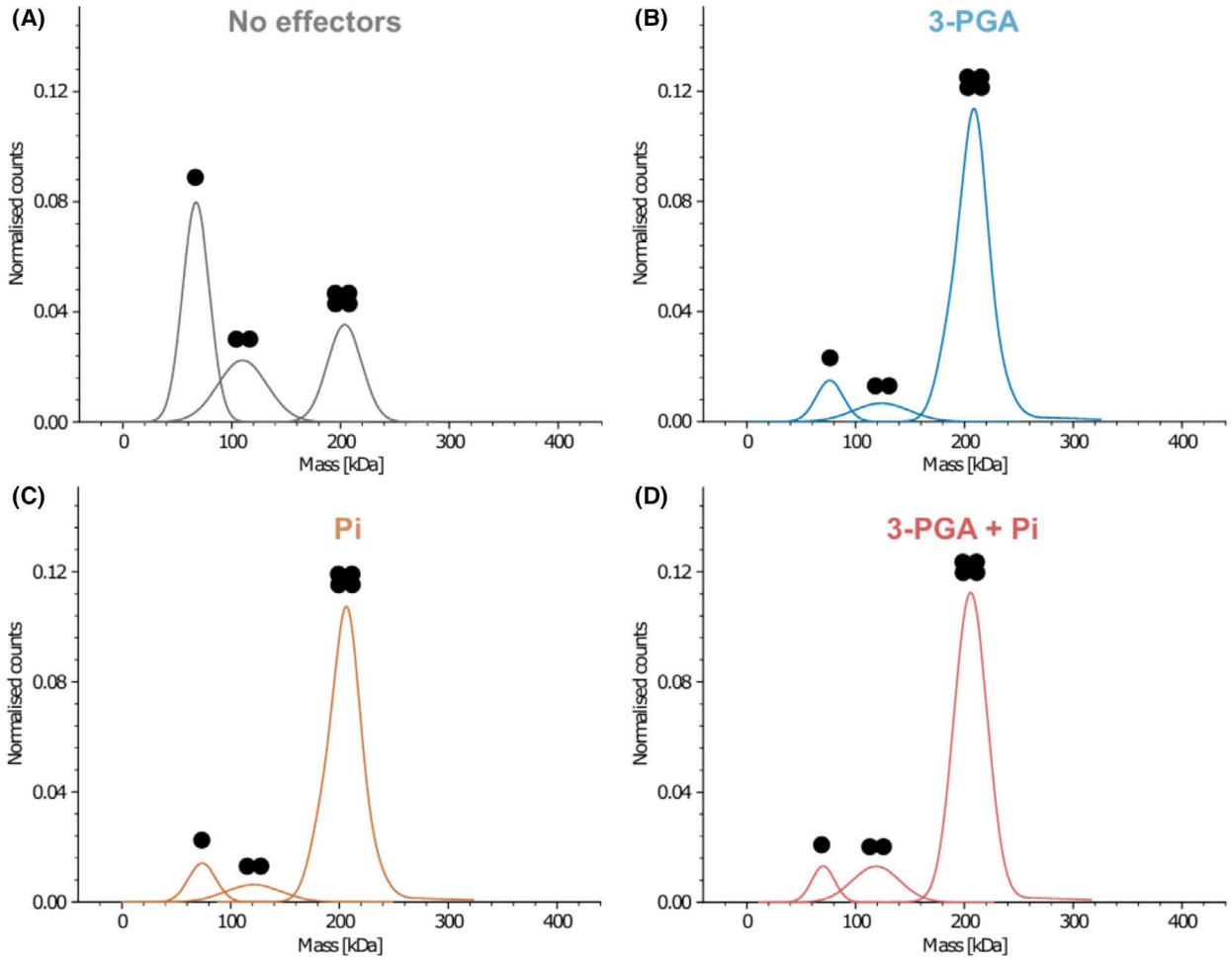

Fig. 8. Mass photometry analysis of the oligomeric state of GlgC. GlgC monomer mass 49.3 kDa. Oligomers are denoted by the respective number of black points above each corresponding peak. (A) Oligomerisation states of GlgC in the absence of effectors. (B) With 2 mM 3-PGA. (C) With 2 mM Pi. (D) With 2 mM 3-PGA and 2 mM Pi.

PEP had no impact on the GlgC at tested concentrations and that 2-PGA acted as a weak inhibitor of GlgC while they were both previously reported to be slight activators of GlgC in *Synechocystis* [7].

GlgC is regulated by 3-PGA and pi antagonism

The role of 3-PGA as a cyanobacterial GlgC activator has been firmly established, in addition to the inhibitory role of Pi [5,7,23]. However, the significance and dynamics of Pi inhibition was not further addressed for cyanobacteria despite the abundance of relevant work on plant GlgC. Using the newly established assay we were able to study Pi in more detail and expand upon its relation to 3-PGA activation of *Synechocystis* GlgC.

As an important first step, we demonstrated that the increase in GlgC activity was observed to be up to a maximum of eight-fold at concentrations of above 1 mM 3-PGA. This activation also corresponds to the increase in GlgC tetramerisation (Fig. 8A) [22]. Previous studies with *Synechocystis* showed that the cellular amount may vary between 1 and 5 mM when cultivated under continuous light and high or ambient CO_2 conditions [24]. Experiments with *Synechocystis* under diurnal conditions revealed that 3-PGA levels were found to be more than two-fold higher during light phases when the CBB cycle is active compared to levels in the dark [25]. These values lie within the ranges at which we observe full activation of GlgC and EC50 value of 3-PGA, respectively. Should these findings be further validated, this could firmly establish the link between light/dark regulation of GlgC via 3-PGA.

With our assay, we revealed a marked antagonism based on cooperative interactions between Pi inhibition and 3-PGA activation (Fig. 7A,B). The sigmoidal increase in the IC50 of Pi caused by 3-PGA, along with increasing Hill coefficient of the cooperative phosphate inhibition (Table 1) indicates a mechanism by which 3-PGA alleviates Pi inhibition by decreasing the affinity of the respective allosteric regulatory sites for Pi. This relationship appears to be reciprocal, such that Pi also increases 3-PGA EC50 in a similar manner (Fig. 7C). These findings agree with the observations from previous work on GlgC from *Anabaena* (*Nostoc*) sp. strain PCC 7120, indicating that this regulatory mechanism might be shared among cyanobacteria. The antagonism between the effectors Pi and 3-PGA also suggests that they act at nearby sites that directly influence each other. Two arginine sites in the N-terminal region (R33 and R45) of GlgC from *Agrobacterium tumefaciens* were previously shown to be the binding sites for the inhibitor Pi [26]. A multiple alignment with GlgC from cyanobacteria showed conservation of the respective residues, corresponding to R24 and R36 in GlgC from *Synechocystis* (Fig. 9A). The binding sites of 3-PGA have also previously been

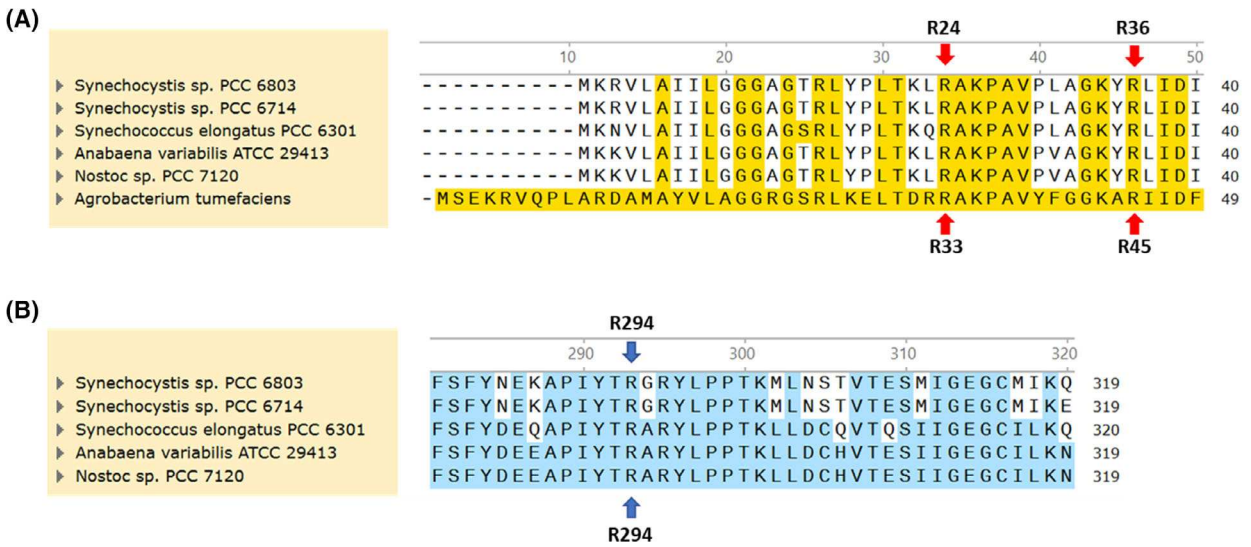

Fig. 9. ClustalW multiple sequence alignment of cyanobacterial GlgC. (A) N-terminal amino acids shown with conserved served sequences highlighted in yellow, compared to *Agrobacterium tumefaciens*. Conserved arginine sites responsible for Fru-6P and Pi binding, R33 (R24) and R45 (R36) are indicated with red arrows. (B) C-Terminal amino acids shown with conserved served sequences highlighted in blue. The conserved arginine residue (R294) responsible for inhibitor selectivity is indicated by blue arrows.

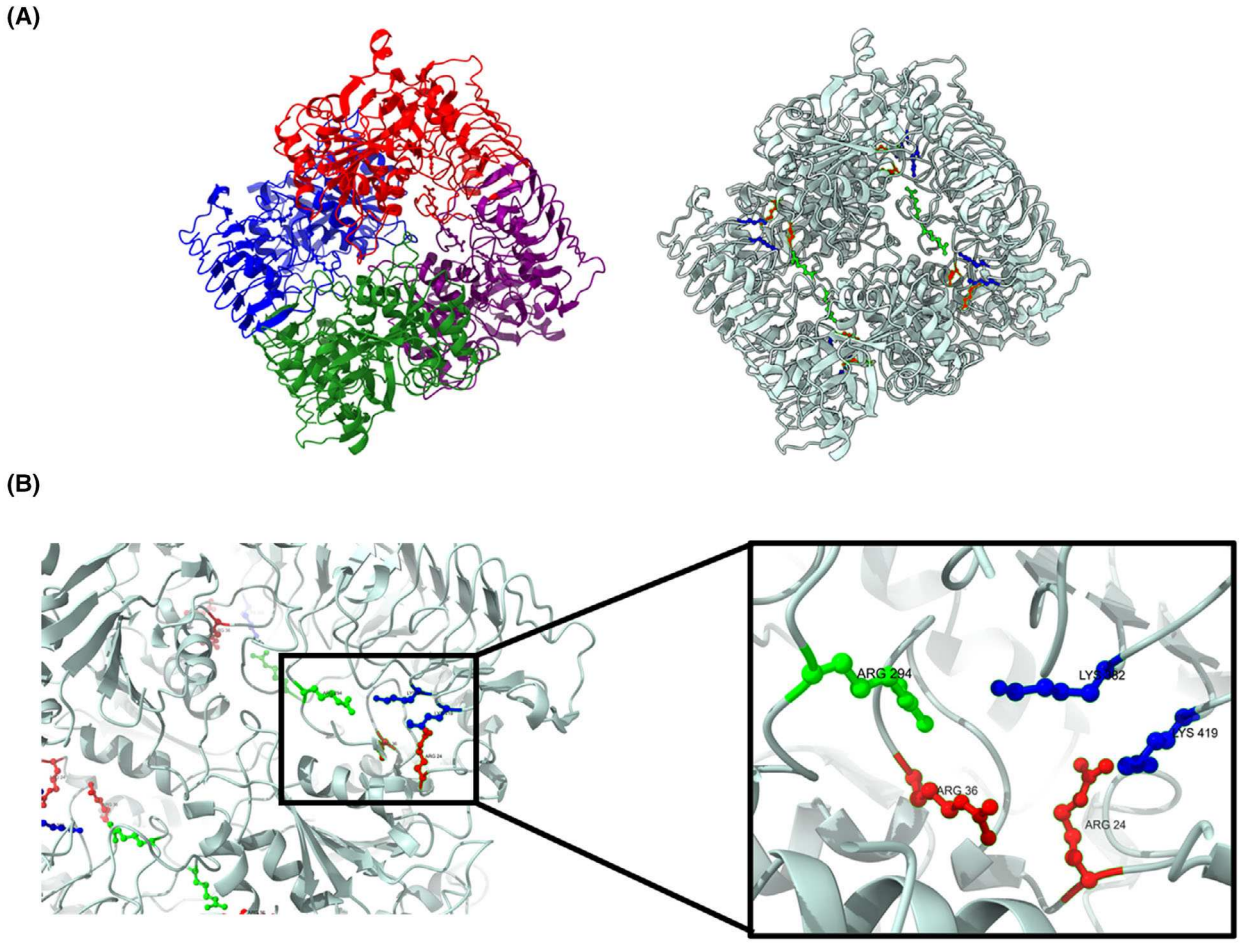

Fig. 10. GlgC tetrameric structure predicted using Alphafold2. (A) Structure predictions of GlgC showing the individual GlgC monomers in different colours (left), and the binding sites of the effectors (right). (B) Expanded view showing the side chains of Lys382, Lys418 responsible for 3-PGA binding (blue), and Arg24, Arg36 for Pi (red) as well as Arg294 responsible for effector selectivity (green).

identified as two lysine residues (K382 and K419) near the C-terminus of the enzyme by the group of Jack Preiss [8,27,28]. Furthermore, these previous studies revealed by site-directed mutagenesis, a conserved arginine residue near the C terminus (R294) in GlgC from *Anabaena* (*Nostoc*) sp. strain PCC 7120 that plays an important role in inhibitor selectivity and also impacted 3-PGA binding and activation (Fig. 9B) [29].

Modelling these conserved effector binding sites with alphafold2 predicted a tetrameric structure of GlgC which revealed the close proximity of these sites to each other (Fig. 10) [8,27,28]. Thus, the model provides straight-forward mechanistic explanation for the experimental findings when assuming that the antagonism between 3-PGA activation and Pi inhibition results from the interference between their binding sites. A similar mechanism is present in the GlgC of *Escherichia coli*, where the allosteric sites of its activator Fru-1,6P and inhibitor AMP were shown to partially overlap, leading to the protection of the opposite binding site when an effector is bound [30]. Given our observation that the presence of Pi did not prevent GlgC tetramerisation, but instead also promoted it, indicates that the inhibitory effect of Pi in GlgC is not a simple reversal or prevention of 3-PGA facilitated tetramerisation. A similar mechanism to that of the *E. coli* GlgC could be conceivable for Synechocystis GlgC, where the binding of either 3-PGA or Pi to their respective could antagonise the binding of the other effector without impacting the assembly of the GlgC homotetramer. Given the location of R294 between the allosteric sites of both effectors, it is reasonable to suggest that R294 could play a role in coordinating the binding of effectors or might facilitate the effects of their binding.

Additionally, we also found that the inhibition of GlgC by PPi is twice that of Pi, although it is unlikely that it plays a direct regulatory role due to the action of cellular pyrophosphatases. With that in mind, while the PPi generated during the formation of ADP-Glc might contribute to GlgC regulation directly or via the release of two molecules of Pi, the concentration of PPi produced in an ongoing reaction is well below inhibitory levels (Figs 3C and 7D). Furthermore, under energy sufficient conditions, the released Pi is immediately reused in other cellular processes such as ATP regeneration, allowing for the uninhibited GlgC reaction to occur. On the contrary, energy limitation or situations that could lead to increased Pi levels would result Pi accumulation arising from ADP-Glc synthesis and GlgC inhibition could occur.

2-PGA and Fru-6P contribute to GlgC regulation in response to changing conditions

In *Synechocystis*, nitrogen deprivation, sensed by the PII signalling protein as increased 2-oxoglutarate levels, results in PirC-mediated phosphoglycerate mutase (PGAM) inhibition and the subsequent accumulation of 3-PGA [20]. This accumulation of 3-PGA drives the carbon flux in the direction of glycogen synthesis. In this situation, elevated 3-PGA concentrations could be essential to balance and maintain the full activation of GlgC in light of the constant regeneration of the Pi pool from ADP-Glc synthesis via cellular PPiases, and those arising from other cellular processes. An increase in 3-PGA levels, caused by an increase in carbon fixation via the CBB cycle, would also result in a shift towards glycogen synthesis by the activation of GlgC.

The product of RubisCO 3-PGA is converted into 2-PGA by the PGAM reaction, which funnels newly fixed carbon into lower glycolysis, where it is directed towards anabolic pathways such as amino acid or fatty acid synthesis. 2-PGA is also generated from the oxygenase reaction of RubisCO, where 2-PGA is the final product of photorespiration in *Synechocystis* [31]. The high concentrations at which 2-PGA exerts a noticeable inhibition of GlgC could therefore be relevant under conditions of photorespiration, given that 2-PGA was found to accumulate in the millimolar concentration range under low carbon conditions [24]. Under these conditions, carbon is lost rather than assimilated and glycogen degradation acts to refill the CBB metabolite pool [3]. The linear relationship observed between GlgC inhibition and 2-PGA concentration, together with the structural similarities with 3-PGA, could indicate that 2-PGA might be binding to the same allosteric sites as 3-PGA. Regulation by 2-PGA could be an additional layer of regulation for fine-tuning glycogen synthesis, with the main inhibitor being Pi.

We also found that Fru-6P is able to activate GlgC, albeit to a lesser extent than 3-PGA, which could indicate that Fru-6P could also occupy the same allosteric sites as 3-PGA and activate GlgC. Supporting this hypothesis was our observation of an additive effect on GlgC activation by Fru-6P at lower 3-PGA concentrations. However, once 3-PGA is present at saturating concentrations, no further activation by Fru-6P occurs. This shows that the preferred activator is still 3-PGA (Fig. 5). An alternative model for this observation could be that Fru-6P binds to a separate allosteric site that only results in a maximum activation of GlgC which less than that of 3-PGA. The *A. tumefaciens* GlgC is regulated by Pi and Fru-6P, instead of 3-PGA. It has been shown that the previously discussed conserved arginine sites in the N-terminal region responsible for Pi binding are also responsible for activation by Fru-6P [26]. This might provide hints that the same regulatory sites could also contribute to the activation of GlgC by Fru-6P in *Synechocystis*. We propose that under certain nutritional conditions, such as photomixotrophic conditions, Fru-6P could act as an alternative activator of GlgC when 3-PGA levels are low adding another layer of regulation for carbon entry into the glycogen cycle. By contrast, under conditions of nitrogen-limitation, the inhibition of PGAM activity by the PII-controlled effector protein PirC results in an increase in 3-PGA, which overrides the effect of other effector molecules, leading to a drastic increase in glycogen synthesis.

Materials and methods

Culture and growth conditions

Unless otherwise specified, liquid cultures were grown at 37 °C with shaking at 125 rpm in Luria-Bertani (Lennox) medium with appropriate antibiotics, where applicable. Plate cultures were grown under similar conditions with the addition of 1.5%$_{(w/v)}$ agar. All *E. coli* strains are listed in Table 2.

Expression and purification of recombinant his-tag proteins

Glycogen synthesis genes from *Synechocystis* sp. PCC 6803 were amplified from genomic DNA via PCR using primers 1–4 specific for GlgA1 or GlgC, with overlap extensions for Gibson assembly (Table 3). The pET28a plasmid backbone

Table 2. *Escherichia coli* strains used for cloning and protein expression.

Strain: *E. coli* NEB10β
Genotype: *Δ(ara-leu) 7697 araD139 fhuA ΔlacX74 galK16 galE15 e14- φ80dlacZΔM15 recA1 relA1 endA1 nupG rpsL (StrR) rph spoT1 Δ(mrr-hsdRMS-mcrBC)*
Strain: *E. coli* Rosetta-gami (DE3)
Genotype: *Δ(ara-leu)7697 ΔlacX74 ΔphoA PvuII phoR araD139 ahpC galE galK rpsL (DE3) F′[lac + lacIq pro] gor522::Tn10 trxB pRARE2 (CamR, StrR, TetR)*

was similarly linearised and amplified using PCR with primers 5–8. Gibson assembly was used to assemble the final expression constructs for GlgA1 and GlgC, which were used to transform electrocompetent *E. coli* NEB10β cells for selection with 50 $\mu g \cdot mL^{-1}$ kanamycin. Positive clones were verified via sequencing and transformed into electrocompetent *E. coli* Rosetta-gami cells for protein expression.

To produce the GlgC-long protein, the coding sequence of *slr1176* was amplified using primers 9 and 10, which contain appropriate extensions for the subsequent cloning (Table 3). The PCR product was cloned into pGEMT (Promega, Walldorf, Germany). DNA from sequence-positive clones was extracted and the gene was cut out by restriction with *Nde*I and *Bam*HI. This fragment was then ligated with *Nde*I/*Bam*HI cut pET28a.

Production cultures of Rosetta-gami cells with expression constructs were grown in batches of 2 L under standard conditions with 50 $\mu g \cdot mL^{-1}$ kanamycin for 4 h to OD_{600} = 0.6, then chilled at 4 °C for 10 min to bring down the culture temperature prior to induction. 1 mM isopropyl-b-D-thiogalactoside (IPTG) was then added to the culture medium followed by incubation for 20 h at 18 °C with shaking at 125 rpm.

Cells were harvested by centrifugation at 6000 ***g*** for 13 min at 4 °C and flash frozen in liquid nitrogen for storage, or allowed to thaw at room temperature before resuspension and lysis in 50 mL of buffer containing 20 mM Tris/HCl pH 7.8, 50 mM NaCl, 5 mM $MgCl_2$, 20 mM imidazole, DNase, RNase, lysozyme and one tablet of cOmplete™ Mini protein inhibitor cocktail (Roche, Mannheim, Germany). The His-tagged proteins were purified using a desktop peristaltic pump with a 1 mL Ni-NTA HisTrap columns (Cytiva, Freiburg, Germany) equilibrated with a buffer containing 20 mM Tris/HCl pH 7.8, 50 mM NaCl, 5 mM $MgCl_2$, 20 mM imidazole. The column was washed with 5 and 3 column volumes (CVs) of buffer W1 (20 mM Tris/HCl pH 7.8, 500 mM NaCl, 40 mM imidazole) and W2 (20 mM Tris/HCl pH 7.8, 1000 mM NaCl, 80 mM imidazole), respectively before the His-Tagged proteins were eluted with elution buffer (20 mM Tris/HCl pH 7.8, 500 mM NaCl, 300 mM imidazole). Positive fractions were selected using a Bradford test, pooled and subjected to a buffer exchange with dialysis buffer (20 mM Tris/HCl pH 7.8, 150 mm KCl, 1 mM EDTA, $50\%_{(v/v)}$ glycerol) and a 3 kDa cut-off regenerated cellulose tube. All purification steps were verified via SDS/PAGE and qualitatively prior to any large-scale purification using a His-SpinTrap kit (Cytiva) and the aforementioned buffers, following the manufacturer's instructions.

Malachite green assay for GlgC activity

The activity of GlgC was assayed in the ADP-Glc synthesis direction using a malachite green assay kit (Sigma-Aldrich, MO, USA) and modification of a previously reported colorimetric method [7,15]. Assays were performed in assay buffer containing 50 mM HEPES-NaOH, pH 8.0, 12 mM $MgCl_2$, and variable metabolite concentrations. The standard concentrations of the following metabolites (for a standard GlgC reaction) in a total reaction volume of 200 µL are, 2 mM 3-PGA, 2 mM ATP, 2 mM Glc-1P, 1 $U \cdot mL^{-1}$ PPiase (Thermo Fisher Scientific, Sindelfingen, Germany) and 5 $\mu g \cdot mL^{-1}$ of GlgC protein. All reactions were performed in 1.5 mL tubes at 30 °C, with shaking for 30 min. Reactions were started with the addition of substrate Glc-1P or GlgC protein, depending on assay design. 8 µL of reaction mix was

Table 3. List of PCR primers used for the construction of His-tagged GlgC, GlgC-Long and GlgA1 expression plasmids.

No.	Label	Sequence
1	GlgA1.FOR	GCCTGGTGCCGCGCGGCAGCATGAAGATTTTATTTGTGGCGGCGGAAGTATCCC
2	GlgA1.REV	TGTCGACGGAGCTCGAATTCTTAGCGATAGGAAGCAGTTAACTCAGCGATTTTTTCCTCT
3	GlgC.FOR	TCATCATCATCACAGCAGCGGCCTGGTGCCGCGCGGCAGCGTGAAACGTGTCTTAGCGATT ATCCT GGGCGG
4	GlgC.REV	CTCGAGTGCGGCCGCAAGCTTGTCGACGGAGCTCGAATTCCTAGATTACCGTGCCGTCGGCGA TCGT
5	pET28a-GlgA1.FOR	GCCACAAATAAAATCTTCATGCTGCCGCGCGGCACC
6	pET28a-GlgA1.REV	TAACTGCTTCCTATCGCTAAGAATTCGAGCTCCGTCGACAAGCTTGC
7	pET28a-GlgC.FOR	GCTGCCGCGCGGCACC
8	pET28a-GlgC.REV	GAATTCGAGCTCCGTCGACAAGCTTGCG
9	slr1176NdeI (fw)	CATATGGTGTGTTGTTGGCAATCG
10	slr1176BamHI (rev)	GGATCCCTAGATTACCGTGCCGTC

removed at specific timepoints for the malachite green assay, following the manufacturer-supplied protocol.

ADP/NADH coupled assay for GlgA1 activity

The activity of GlgA1 was evaluated using a modified spectrophotometric method from that presented by Wayllace *et al.* [19]. Assays were performed in assay buffer (50 mM HEPES-NaOH, pH 8.0, 12 mM $MgCl_2$) with 10 $U \cdot mL^{-1}$ Lactate Dehydrogenase (LDH), 5 $U \cdot mL^{-1}$ Pyruvate Kinase (PK), 1 mM Phosphoenolpyruvate (PEP), 0.4 mM NADH, 1 $mg \cdot mL^{-1}$ Rabbit Glycogen and 10 $\mu g \cdot mL^{-1}$ GlgA1 protein. The reaction was assayed in 96-well clear bottom plates at 30 °C for 60 min. Absorbance was measured using Tecan Spark 10M (Tecan, Männedorf, Switzerland) every minute at 340 nm. Each reaction was started with the addition of 2 mM ADP-Glc to a total assay volume of 200 µL.

GlgC-GlgA1 coupled glycogen synthesis assay

The entire glycogen synthesis reaction couples the synthesis of ADP-Glc by GlgC with the GlgA1 reaction. Assays were performed in assay buffer with the components described above with 2 mM ATP, glycogen synthesis enzymes were added in a concentration ratio of 10 $\mu g \cdot mL^{-1}$ GlgA1 and 1 $\mu g \cdot mL^{-1}$ GlgC. Varying concentrations of test metabolites were according adjusted to reflect each assays design. The reaction was assayed and measured in 96-well clear bottom plates as described above, beginning with the addition of Glc-1P to a total assay volume of 200 µL.

Mass photometry analysis

The procedure for mass photometry analysis was described in our previous work [32]. In brief, microscope coverslips (No. 1.5H, 24 × 5 mm, Marienfeld, Lauda-Königsfeld, Germany) were prepared via immersion in isopropanol and ultrapure water. CultureWell gaskets (3 mm × 1 mm, Grace Bio-Labs, Bend, OR, USA) were then applied to the coverslips. Prior to measurement, samples were diluted to 200 nM in assay buffer. Measurements used a TwoMP mass photometer (Refeyn, Oxford, UK) with AcquireMP v2022 R1 software, preceded by calibration. Focus was established by adding 5 µL buffer to a well, using an autofocus system based on total internal reflection. For acquisition, 5 µL of diluted protein was added, and 60-s movies were recorded. Each sample was measured in triplicate. Images were processed and analysed using the DiscoverMP v2022 R1 software as described in Kofinova *et al.* [33].

Figures, bioinformatics and analyses

All results were analysed and visualised using GRAPHPAD PRISM 10 (GraphPad, Boston, MA, USA). *In silico* design of primers and expression constructs were all performed with Snapgene (GSL Biotech, Boston, MA, USA). Figure 2A was created with Biorender (Biorender.com). GlgC structure prediction was performed with ALPHAFOLD2 and visualised using CHIMERAX [34,35].

Acknowledgements

We thank Paula Alcain Arranz for bench-work assistance and Dr John Weir and Maria Kharlamova for their help with mass photometry experiments. This work was supported by the DFG funded research consortium FOR2816 "The Autotrophy-Heterotrophy Switch in Cyanobacteria: Coherent Decision-Making at Multiple Regulatory Layers", research grant Fo195/16-2. We also acknowledge infrastructural funding by the Cluster of Excellence EXC 2124 (Controlling Microbes to Fight Infections, CMFI, grant 390838134) at the Eberhard Karls Universität Tübingen.

Conflict of interest

The authors declare no conflict of interest.

Author contributions

KL: designed and carried out experiments and wrote paper. SD: mass photometry experiments and drawing MH: construction of GlgC-Long. KF: conceptualisation, supervision and paper writing. All authors contributed at varying stages in the editing and review of the paper.

Peer review

The peer review history for this article is available at https://www.webofscience.com/api/gateway/wos/peer-review/10.1111/febs.17348.

Data availability

Enzymatic data generated during this study have been deposited here (DOI: 10.15490/fairdomhub.1.study.1296.1) on the data and model management platform FAIRDOMHub [36].

References

1 Doello S, Klotz A, Makowka A, Gutekunst K & Forchhammer K (2018) A specific glycogen mobilization strategy enables rapid awakening of

dormant cyanobacteria from chlorosis. *Plant Physiol* **177**, 594–603.
2 Shinde S, Zhang X, Singapuri SP, Kalra I, Liu X, Morgan-Kiss RM & Wang X (2020) Glycogen metabolism supports photosynthesis start through the oxidative pentose phosphate pathway in cyanobacteria. *Plant Physiol* **182**, 507–517.
3 Makowka A, Nichelmann L, Schulze D, Spengler K, Wittmann C, Forchhammer K & Gutekunst K (2020) Glycolytic shunts replenish the Calvin–Benson–Bassham cycle as anaplerotic reactions in cyanobacteria. *Mol Plant* **13**, 471–482.
4 Miao X, Wu Q, Wu G & Zhao N (2003) Sucrose accumulation in salt-stressed cells of agp gene deletion-mutant in cyanobacterium *Synechocystis* sp. PCC 6803. *FEMS Microbiol Lett* **218**, 71–77.
5 Ballicora MA, Iglesias AA & Preiss J (2004) ADP-glucose pyrophosphorylase: a regulatory enzyme for plant starch synthesis. *Photosynth Res* **79**, 1–24.
6 Salamone PR, Kavakli IH, Slattery CJ & Okita TW (2002) Directed molecular evolution of ADP-glucose pyrophosphorylase. *Proc Natl Acad Sci USA* **99**, 1070–1075.
7 Iglesias AA, Kakefuda G & Preiss J (1991) Regulatory and structural properties of the cyanobacterial ADPglucose pyrophosphorylases. *Plant Physiol* **97**, 1187–1195.
8 Ballicora MA, Iglesias AA & Preiss J (2003) ADP-glucose pyrophosphorylase, a regulatory enzyme for bacterial glycogen synthesis. *Microbiol Mol Biol Rev* **67**, 213–225, table of contents.
9 Namakoshi K, Nakajima T, Yoshikawa K, Toya Y & Shimizu H (2016) Combinatorial deletions of glgC and phaCE enhance ethanol production in *Synechocystis* sp. PCC 6803. *J Biotechnol* **239**, 13–19.
10 Mittermair S, Lakatos G, Nicoletti C, Ranglová K, Manoel JC, Grivalský T, Kozhan DM, Masojídek J & Richter J (2021) Impact of *glgA1*, *glgA2* or *glgC* overexpression on growth and glycogen production in *Synechocystis* sp. PCC 6803. *J Biotechnol* **340**, 47–56.
11 Lakatos GE, Ranglová K, Manoel JC, Grivalský T, Kopecký J & Masojídek J (2019) Bioethanol production from microalgae polysaccharides. *Folia Microbiol (Praha)* **64**, 627–644.
12 Koch M & Forchhammer K (2021) Polyhydroxybutyrate: a useful product of chlorotic cyanobacteria. *Microb Physiol* **31**, 67–77.
13 Arisaka S, Terahara N, Oikawa A & Osanai T (2019) Increased polyhydroxybutyrate levels by *ntcA* overexpression in *Synechocystis* sp. PCC 6803. *Algal Res* **41**, 101565.
14 Roberts MW, Preiss J & Okita TW (1995) A capillary zone electrophoresis assay for the nucleoside transfer enzyme adenosine diphosphate-glucose pyrophosphorylase. *Anal Biochem* **225**, 121–126.
15 Fusari C, Demonte AM, Figueroa CM, Aleanzi M & Iglesias AA (2006) A colorimetric method for the assay of ADP-glucose pyrophosphorylase. *Anal Biochem* **352**, 145–147.
16 McCracken DA & Rutherford WM (1980) A rapid, sensitive assay for starch phosphorylase and ADPglucose pyrophosphorylase. *Anal Biochem* **101**, 275–277.
17 Yep A, Bejar CM, Ballicora MA, Dubay JR, Iglesias AA & Preiss J (2004) An assay for adenosine 5′-diphosphate (ADP)-glucose pyrophosphorylase that measures the synthesis of radioactive ADP-glucose with glycogen synthase. *Anal Biochem* **324**, 52–59.
18 Casati DFG, Aon MA & Iglesias AA (2000) Kinetic and structural analysis of the ultrasensitive behaviour of cyanobacterial ADP-glucose pyrophosphorylase. *Biochem J* **350**, 139–147.
19 Wayllace NZ, Valdez HA, Merás A, Ugalde RA, Busi MV & Gomez-Casati DF (2012) An enzyme-coupled continuous spectrophotometric assay for glycogen synthases. *Mol Biol Rep* **39**, 585–591.
20 Orthwein T, Scholl J, Spät P, Lucius S, Koch M, Macek B, Hagemann M & Forchhammer K (2021) The novel PII-interactor PirC identifies phosphoglycerate mutase as key control point of carbon storage metabolism in cyanobacteria. *Proc Natl Acad Sci USA* **118**, e2019988118.
21 Doello S, Neumann N & Forchhammer K (2022) Regulatory phosphorylation event of phosphoglucomutase 1 tunes its activity to regulate glycogen metabolism. *FEBS J* **289**, 6005–6020.
22 Díaz-Troya S, López-Maury L, Sánchez-Riego AM, Roldán M & Florencio FJ (2014) Redox regulation of glycogen biosynthesis in the cyanobacterium *Synechocystis* sp. PCC 6803: analysis of the AGP and glycogen synthases. *Mol Plant* **7**, 87–100.
23 Preiss J (1984) Bacterial glycogen synthesis and its regulation. *Ann Rev Microbiol* **38**, 419–458.
24 Eisenhut M, Huege J, Schwarz D, Bauwe H, Kopka J & Hagemann M (2008) Metabolome phenotyping of inorganic carbon limitation in cells of the wild type and photorespiratory mutants of the cyanobacterium *Synechocystis* sp. strain PCC 6803. *Plant Physiol* **148**, 2109–2120.
25 Scheurer NM, Rajarathinam Y, Timm S, Köbler C, Kopka J, Hagemann M & Wilde A (2021) Homologs of circadian clock proteins impact the metabolic switch between light and dark growth in the cyanobacterium *Synechocystis* sp. PCC 6803. *Front Plant Sci* **12**, 675227.
26 Gómez-Casati DF, Igarashi RY, Berger CN, Brandt ME, Iglesias AA & Meyer CR (2001) Identification of functionally important amino-terminal arginines of agrobacterium tumefaciens ADP-glucose pyrophosphorylase by alanine scanning mutagenesis. *Biochemistry* **40**, 10169–10178.

27 Preiss J & Sivak MN (1998) Biochemistry, molecular biology and regulation of starch synthesis. *Genet Eng (N Y)* **20**, 177–223.
28 Charng YY, Iglesias AA & Preiss J (1994) Structure-function relationships of cyanobacterial ADP-glucose pyrophosphorylase. Site-directed mutagenesis and chemical modification of the activator-binding sites of ADP-glucose pyrophosphorylase from *Anabaena* PCC 7120. *J Biol Chem* **269**, 24107–24113.
29 Frueauf JB, Ballicora MA & Preiss J (2002) Alteration of inhibitor selectivity by site-directed mutagenesis of Arg294 in the ADP-glucose pyrophosphorylase from *Anabaena* PCC 7120. *Arch Biochem Biophys* **400**, 208–214.
30 Cifuente JO, Comino N, Trastoy B, D'Angelo C & Guerin ME (2019) Structural basis of glycogen metabolism in bacteria. *Biochem J* **476**, 2059–2092.
31 Bartsch O, Hagemann M & Bauwe H (2008) Only plant-type (GLYK) glycerate kinases produce d-glycerate 3-phosphate. *FEBS Lett* **582**, 3025–3028.
32 Doello S, Shvarev D, Theune M, Sauerwein J, Klon A, Keskin E, Boehm M, Gutekunst K & Forchhammer K (2024) Structural basis of the allosteric regulation of cyanobacterial glucose-6-phosphate dehydrogenase by the redox sensor OpcA. *bioRxiv* 10.1101/2024.02.29.582749 [PREPRINT]
33 Kofinova Z, Karunanithy G, Ferreira AS & Struwe WB (2024) Measuring protein-protein interactions and quantifying their dissociation constants with mass photometry. *Curr Protoc* **4**, e962.
34 Jumper J, Evans R, Pritzel A, Green T, Figurnov M, Ronneberger O, Tunyasuvunakool K, Bates R, Žídek A, Potapenko A *et al.* (2021) Highly accurate protein structure prediction with AlphaFold. *Nature* **596**, 583–589.
35 Meng EC, Goddard TD, Pettersen EF, Couch GS, Pearson ZJ, Morris JH & Ferrin TE (2023) UCSF ChimeraX: tools for structure building and analysis. *Protein Sci* **32**, e4792.
36 Wolstencroft K, Krebs O, Snoep JL, Stanford NJ, Bacall F, Golebiewski M, Kuzyakiv R, Nguyen Q, Owen S, Soiland-Reyes S *et al.* (2017) FAIRDOMHub: a repository and collaboration environment for sharing systems biology research. *Nucleic Acids Res* **45**, D404–D407.

FEBS Letters

FEBS PRESS science publishing by scientists

RESEARCH ARTICLE

The (Glg)ABCs of cyanobacteria: modelling of glycogen synthesis and functional divergence of glycogen synthases in *Synechocystis* sp. PCC 6803

Kenric Lee, Dimitrios Bekiari, Sofia Doello and Karl Forchhammer

Interfaculty Institute of Microbiology and Infection Medicine, University of Tübingen, Germany

Correspondence
K. Forchhammer, Interfaculty Institute of Microbiology and Infection Medicine, University of Tübingen, Germany
Tel: +49 70712972096
E-mail: karl.forchhammer@uni-tuebingen.de

(Received 27 November 2025, revised 9 January 2026, accepted 13 January 2026)

doi:10.1002/1873-3468.70299

Edited by Peter Brzezinski

Glycogen is the principal carbon reserve in *Synechocystis* sp. PCC 6803. We reconstituted its biosynthetic pathway *in vitro*—GlgC (glucose-1-phosphate adenylyltransferase), two glycogen synthase isoenzymes (GlgA1, GlgA2) and the branching enzyme GlgB—to define how supply, polymerization and branching set flux and product structure. GlgA2 shows higher specific activity and cooperates with GlgB-generated branched primers, whereas GlgA1 has higher substrate affinity and responds more to primer concentration. Product profiling links mechanism to architecture: GlgA1 produces more-branched glycogen, while GlgA2 yields longer, less-branched polymers, with GlgB biasing utilization toward GlgA2. The complementary behaviors of GlgA1 and GlgA2 provide capacity for rapid accumulation versus steady-state maintenance and offer dynamic metabolic levers to tune glycogen content and architecture in cyanobacteria.

Keywords: biochemical assay; cyanobacteria; enzyme coupling; flux control; GlgA regulation; glycogen synthesis model; metabolic engineering; stoichiometry

Cyanobacteria are a large group of photoautotrophic prokaryotes, of which some species are also capable of heterotrophic growth. Owing to their adaptability, representatives of cyanobacteria have been found to be successful in nearly every biome on the planet and are regarded as the precursors to higher plants [1]. Glycogen is the principal carbon storage polysaccharide in cyanobacteria, playing a central role in cellular energy homeostasis and adaptation to fluctuating environmental conditions [2–4].

In *Synechocystis* sp. PCC 6803 (hereafter *Synechocystis*), the pathway for glycogen biosynthesis is orchestrated by a suite of specialized enzymes [5]. Glycogen synthesis begins with the starting molecule, glucose-1-phosphate (Glc-1P) which is interchangeably converted from glucose-6-phosphate (Glc-6P) mainly by phosphoglucomutase (PGM, product of *sll0726*, EC:5.4.2.2). Glc-1P is then utilized in the initial, rate-limiting step catalyzed by glucose-1-phosphate adenylyltransferase (hereafter GlgC, product of *slr1176*, EC:2.7.7.27), which synthesizes ADP-glucose (ADP-Glc) from ATP and Glc-1P—a process subject to intricate allosteric regulation by metabolic effectors such as 3-phosphoglycerate (3-PGA) and inorganic phosphate (Pi) [6–9]. The ADP-Glc generated then serves as the activated glucosyl donor for glycogen synthase (hereafter GlgA) enzymes (EC:2.4.1.21), which directly catalyze the elongation of a growing

Abbreviations
3-PGA, 3-phosphoglycerate; ADP-Glc, ADP-Glucose; Cα RMSD, Cα root-mean-square deviation; Glc-1P, Glucose-1-phosphate; Glc-6P, Glucose-6-phosphate; GlgA, Glycogen Synthase; GlgB, Glycogen branching enzyme; GlgC, Glucose-1-phosphate adenylyltransferase; LDH, Lactate dehydrogenase; MG, Malachite Green (Assay); PEP, Phosphoenolpyruvate; PGM, Phosphoglucomutase; Pi, Inorganic orthophosphate; PK, Pyruvate kinase; PPi, Pyrophosphate; *Synechocystis*, *Synechocystis* sp. PCC 6803.

glycogen chain. These processes mirror the complexity observed in higher plants and shed light on evolutionary parallels in α-glucan metabolism [5].

Synechocystis encodes two distinct GlgA isoenzymes, GlgA1/*sll0945* and GlgA2/*sll1393*. Unlike most bacteria, which typically possess a single GlgA, these isoforms display complementary and, in some contexts, specialized roles in glycogen polymerization and chain elongation [5]. Recent studies indicate that GlgA1 and GlgA2 differ in their chain extension properties—GlgA1 being distributive and GlgA2 more progressive—affecting the fine structure and branching patterns of the resulting glycogen granules [5,10]. These differences suggest isoenzyme divergence for nuanced physiological or metabolic adaptation and underscore the need for a systematic characterization of their respective biochemical properties. The final step in the maturation of glycogen involves the glycogen branching enzyme (product of *sll0158*, EC:2.4.1.18, hereafter GlgB), which inserts α-1,6-glycosidic linkages, increasing the number of non-reducing ends and enhancing the water solubility of the polymer [11,12]. The interplay between GlgA and GlgB is a key determinant of the overall structure, size, and accessibility of glycogen particles, which in turn can influence the cell's capacity for rapid carbon mobilization under stress or during recovery from nutrient deprivation [13,14].

Despite these advances, understanding of how GlgA isoenzymes coordinate with GlgC and GlgB remains incomplete. Questions persist regarding their kinetic properties, primer utilization preferences, differential regulation by allosteric metabolites, and the structural outcomes of their activity under varying enzymatic and substrate conditions. Dissecting these parameters is critical for comprehending not only glycogen metabolism in cyanobacteria but also its parallels with starch biosynthesis in plants and the broader evolutionary context of polysaccharide storage in photoautotrophic organisms.

In this work, we establish an integrated *in vitro* model for *Synechocystis* glycogen synthesis, leveraging precise biochemical assays to dissect the individual and collective roles of GlgA1, GlgA2, and GlgB. Our work aims to clarify substrate selectivity, primer dependency, regulatory mechanisms, and product structure, providing new insights into the functional divergence of GlgA isoenzymes and their physiological significance.

Methods

Culture and growth conditions of *E. coli*

Unless otherwise specified, the cultivation of all strains was performed as previously reported [6]. All strains used in this study are listed in Table 1.

Table 1. *E. coli* and *Synechocystis sp.* PCC 6803 strains used in this work.

Strain	Genotype/references
E. coli NEB10β	Δ(ara-leu) 7697 araD139 fhuA ΔlacX74 galK16 galE15 e14- φ80dlacZΔM15 recA1 relA1 endA1 nupG rpsL (StrR) rph spoT1 Δ(mrr-hsdRMS-mcrBC)
E. coli Rosetta-gami (DE3)	Δ(ara-leu)7697 ΔlacX74 ΔphoA PvuII phoR araD139 ahpC galE galK rpsL (DE3) F′[lac+ lacIq pro] gor522::Tn10 trxB pRARE2 (CamR, StrR, TetR)
Synechocystis sp. 6803 WT-GT	From Chen *et al.* [49], Glucose tolerant wild-type strain
Synechocystis sp. 6803 Δ*glgA1*	From Gründel *et al.* [50], WT-GT Background, *sll0945::km*^{R}
Synechocystis sp. 6803 Δ*glgA2*	From Gründel *et al.* [50], WT-GT Background, *sll1393::cm*^{R}

Culture and growth conditions of *Synechocystis* sp. PCC 6803

The cultivation of all cyanobacterial strains was performed as previously described [14]. All strains used in this study are listed in Table 1.

Expression and purification of recombinant his-tagged glycogen synthesis enzymes

The assembly of the expression constructs of N-terminal His-tagged GlgA1 and GlgC proteins was performed previously as described [6].

The GlgA2 gene was amplified from *Synechocystis* sp. PCC 6803 genomic DNA using the following primers; forward: 5′-GCCTGGTGCCGCGCGGCAGCATGTACATC GTTCAAATTGCCTCAGAATGCGC-3′ and reverse: 5′-TGTCGACGGAGCTCGAATTCTTAAGCCCGGATGTA TTCGTAGGCTTCCACA-3′. The expression plasmid pET28a was similarly linearized and amplified using the following primer pair; forward: 5′-GCAATTTGAACGATGT ACATGCTGCCGCGCGGCACC-3′ and reverse: 5′-ACGA ATACATCCGGGCTTAAGAATTCGAGCTCCGTCGAC AAGCTTGCGGC-3′.

Similarly, the GlgA gene from *E. coli* (GlgA$^{E.coli}$) was amplified from genomic DNA using the following primers; forward: 5′-GCCTGGTGCCGCGCGGCAGCATGCAGG TTTTACATGTATGTTCAGAGATGTTCCCG-3′ and reverse: 5′-TGTCGACGGAGCTCGAATTCCTATTTCA AGCGATAGTAAAGCTCACGGTACGACTTCG-3′. The expression plasmid pET28a was similarly linearized and amplified using the following primer pair; forward: 5′-TT TACTATCGCTTGAAATAGGAATTCGAGCTCCGTCG ACAAGCTTGC-3′ and reverse: 5′-CATACATGTAAAAC CTGCATGCTGCCGCGCGGCACC-3′.

The subsequent assembly of the pET28a expression constructs for GlgA2 and $GlgA^{E.coli}$ was carried out in the same manner as for GlgA1 and GlgC. The subsequent induction and expression of recombinant proteins were performed using IMAC as previously described [6]. Cell lysis was carried out in lysis buffer (20 mM Tris/HCl pH 7.8, 50 mM NaCl, 5 mM $MgCl_2$, 40 mM imidazole) supplemented with CellLytic buffer, Benzonase® (both from Merck, Darmstadt, Germany), lysozyme and one tablet of cOmplete™ protein inhibitor cocktail (Roche, Mannheim, Germany). The lysate was clarified via ultracentrifugation at 16 000 ***g***, 30 min at 4 °C and filtered using a 0.22 µm syringe filter prior to column application.

The recombinant proteins were purified via immobilized metal affinity chromatography (IMAC) followed by a polishing step using anion exchange to yield proteins of a high purity. All purifications steps were performed using the ÄKTA purifier chromatography system (Cytiva, Freiburg, Germany). IMAC was performed with Ni-NTA HisTrap columns (Cytiva) according to the manufacturer's directions. The His-Tagged proteins were eluted with a 30 CV gradient of 40 mM to 500 mM imidazole in a buffer containing 20 mM Tris/HCl pH 7.8, 500 mM NaCl. Peak fractions were identified based on their UV 280 nm signal and pooled.

Buffer exchange of the pooled fractions was performed with the Amicon® Ultra Centrifugal Filter, 30 kDa MWCO (Merck) with two washes with IEX buffer (20 mM Tris/HCl pH 7.8) prior to anion exchange with HiTrap Q High Performance columns (Cytiva) according to the manufacturer's directions. The proteins were eluted with a 30 CV gradient of 0–750 mM NaCl in IEX buffer (20 mM Tris/HCl pH 7.8). As before, fractions from the largest peak were collected and buffer exchange was performed with two washes of concentration buffer (20 mM Tris/HCl pH 7.8, 150 mM KCl, 1 mM EDTA) followed by exchange into storage buffer (20 mM Tris/HCl pH 7.8, 150 mM KCl, 1 mM EDTA, $50\%_{(v/v)}$ glycerol).

Expression and purification of recombinant strep-tagged proteins

The construct for recombinant C-terminal Strep II-tagged GlgB was purified as previously described [15]. PGM was purified as previously described [16].

ADP/NADH coupled assay for GS activity (Assay A)

Glycogen synthase activity was assayed as previously described using a modified spectrophotometric method from that presented by Wayllace *et al.* [6,17]. The following assay parameters were changed to suit the requirements for this study. The components of the assay in a total volume of 100 µL per reaction were; assay buffer (50 mM HEPES-NaOH, pH 8.0, 12 mM $MgCl_2$) with 10 $U{\cdot}mL^{-1}$ Lactate Dehydrogenase (LDH), 9 $U{\cdot}mL^{-1}$ Pyruvate Kinase (PK), 1 mM Phosphoenolpyruvate (PEP), 0.4 mM NADH, 1 $mg\,mL^{-1}$ Bovine Glycogen and 200 nM GlgA1 or GlgA2. The reaction was assayed in 96-well clear bottom plates at 30 °C for variable durations, depending on the experimental design. Absorbance was measured using Tecan Spark 10 M (Tecan, Männedorf, Switzerland) with readings taken every minute at 340 nm. Each standard reaction was started with the addition of the substrate ADP-Glc.

Glycogen synthesis and precipitation (assay B)

The synthesis of glycogen was performed in a similar manner to that of assay A with several modifications. The components of the assay in a total volume of 5 mL per reaction were as follows: assay buffer (50 mM HEPES-NaOH, pH 8.0, 12 mM $MgCl_2$) with 4 mM ATP, 4 mM 3-PGA, 4 mM Glc-1P and 200 $\mu g{\cdot}mL^{-1}$ starch as a primer. About 9 $U{\cdot}mL^{-1}$ PK and 2 mM PEP were also added to maintain ATP concentrations for optimal GlgC activity. Glycogen synthesis enzymes were added in a concentration ratio of 200 nM monomeric GS to 200 nM tetrameric GlgC, with and without 20 nM of GlgB. The reaction was left to run overnight (~20 h) at 30 °C with gentle agitation on a shaker.

The next day, all samples were heated at 90 °C for 10 min to inactivate the protein components of the reaction, followed by centrifugation at 17 000 ***g***, 4 °C for 30 min to separate the insoluble fraction of the reaction. The supernatant was carefully decanted and mixed with 4 volumes of ice-cold absolute ethanol before being stored overnight at −20 °C to precipitate the reaction products. The precipitate was then pelleted via centrifugation at 17 000 ***g***, 4 °C for 15 min and washed twice with 70% ethanol and 100% ethanol before being left to dry completely in a 60 °C oven. The dried products were resuspended in distilled water, and an additional filtration step was performed using Amicon® Ultra Centrifugal Filter, 3 kDa MWCO (Merck) with four washes of distilled water to remove soluble contaminants. The remaining concentrate was resuspended in distilled water for further analysis.

PGM forward reaction assay (Assay C)

The PGM forward reaction assay was adapted from Assay A and the coupled assay described in our previous report [6]. Each reaction (100 µL total volume) contained assay buffer (50 mM HEPES-NaOH, pH 8.0, 12 mM $MgCl_2$), 40 µM Glc-1,6-phosphate, 2 mM ATP, 2 mM 3-PGA, 1 mM PEP, 0.4 mM NADH, and 1 $mg{\cdot}mL^{-1}$ bovine glycogen as primer, together with the coupling enzymes LDH and PK as specified above. Glycogen synthesis was catalyzed by

400 nM monomeric $GlgA^{E.coli}$ and 400 nM tetrameric GlgC in the presence of PGM. Reactions were performed in 96-well clear bottom plates as described previously and initiated by the addition of Glc-6P.

GlgC tetramer concentration ratios required to match GlgA activity under assay conditions

We calculated the theoretical GlgA–GlgC stoichiometries on a flux basis using the intrinsic specific activities from Assay A (GlgA1, GlgA2, $GlgA^{E.\ coli}$ with ADP-Glc) and the previously reported intrinsic GlgC activity from the MG assay [6] (Table 2). For a given enzyme, the flux was expressed in μM min^{-1} per nanomolar enzyme, as $J = V_{max} \cdot MW \cdot 10^{-6}$, where V_{max} was expressed in $U \cdot mg^{-1}$, MW is the molecular weight of GlgA monomers or GlgC tetramers in g mol^{-1}, and 1 U = 1 μmol·min^{-1}. For GlgC, the supply capacity was computed as J_C, while for each GlgA isoform the consumption capacity per nM was computed as J_A. The GlgA: GlgC stoichiometric ratio required to match the GlgA demand was then obtained as $A : C_{\text{ideal ratio}} = \frac{J_C}{J_A}$ and the corresponding ideal concentration of GlgC required was calculated as $[C]_{V_{max_A}} = \frac{[A]}{A:C_{\text{ideal ratio}}}$. These calculations were used to compare the intrinsic supply capacity of GlgC with the utilization capacities of GlgA1, GlgA2, and $GlgA^{E.\ coli}$, and to interpret the minimum GlgC concentration required for a stable supply of ADP-Glc to GlgA under assay conditions. Table 2 summarizes all relevant parameters for this calculation.

Glycogen purification from *Synechocystis* cultures

Exponential *Synechocystis* cultures of 300 mL at ~0.8 OD_{750} were harvested via centrifugation and washed twice with 30%$_{(w/v)}$ KOH. The washed cell pellets were resuspended in 30%$_{(w/v)}$ KOH and heated at 85 °C for 30 min for cell lysis. After lysis, the precipitation of glycogen was carried out as previously described; the lysate was centrifuged at 17 000 ***g***, 4 °C for 30 min to separate cell debris. The supernatant was carefully decanted and mixed with 4 volumes of ice-cold absolute ethanol before being stored overnight at −20 °C to precipitate glycogen. The precipitate was then pelleted via centrifugation at 17 000 ***g***, 4 °C for 15 min and washed twice with 70% ethanol and 100% ethanol before being left to dry completely in a 60 °C oven. The dried products were resuspended in distilled water and an additional filtration step was performed using Amicon® Ultra Centrifugal Filter, 3 kDa MWCO (Merck) with four washes of distilled water to remove soluble contaminants. The remaining concentrate was resuspended in distilled water for further analysis.

GS reaction product quantification and analysis (spectrophotometric quantification: Iodine-iodide assay)

The quantification of the *in vitro* reaction products was performed by mixing the reaction products with 70 μL of iodine solution (2 mM I_2, 30 mM KI) in a total volume of 150 μL. The reaction products were compared to glycogen or starch standard solutions in the concentration range of 0–2 mg·mL^{-1} based on their absorbances at wavelengths of 490 nm or 560 nm for glycogen and starch, respectively. For the measurement of the reaction product absorbance spectra, the concentration of the reaction products was adjusted to 0.5 mg·mL^{-1}, and the absorbance was measured from 400 nm to 700 nm. Measurements were performed using the Tecan Spark 10 M (Tecan).

Fast glycogen measurement assay (enzymatic quantification)

The enzymatic determination of glycogen was performed with the method presented by Vidal et al. with some minor modifications and was used to validate our Iodine-Iodide assay described above [18]. The total assay volume was modified to 100 μL, consisting of 30 μL enzymatic mix and 70 μL of glycogen sample from Assay B. The concentration of the glycogen sample was previously determined using the Iodine-Iodide assay and was used for comparisons. All measurements were done using the Tecan Spark 10 M (Tecan).

Figures, bioinformatics, and analyses

All data were analyzed and visualized using GraphPad Prism 10 (GraphPad, Boston, MA, USA). Primer and expression construct designs were carried out *in silico* using SnapGene (GSL Biotech, San Diego, CA, USA). Multiple

Table 2. Experimental assay parameters and enzyme concentrations with molecular weights.

Enzyme	Molecular weight [g mol^{-1}]	Substrate	Spec. activity [U·mg^{-1}]	Flux capacity [μM·min^{-1} per nM]	K_m [μM]	Optimal GlgA: GlgC ratio
GlgC Tetramer	200 856.64	Glc-1P	8.90	1.79	240 ± 50	—
GlgA1	56 372.5	ADP-Glc	0.51	2.86×10^{-2}	152 ± 3.6	62 : 1
GlgA2	58 251.0	ADP-Glc	0.77	4.49×10^{-2}	219 ± 9.9	40 : 1
$GlgA^{E.coli}$	54 848.6	ADP-Glc	538	2.95×10^{1}	275 ± 17	0.06 : 1

sequence alignment was generated in ClustalW using the UniProt GlgA sequences, and structure-guided motif mapping was performed in UCSF ChimeraX by superposing AlphaFold3 GlgA models with Matchmaker and extracting alignment-equivalent residues from the resulting structure-informed sequence alignment. Cα RMSD (Cα–root-mean-square deviation) analysis of superimposed models was also performed in UCSF ChimeraX [19–21].

Results

Comparable catalytic efficiencies of GlgA1 and GlgA2

Recombinant His-tagged GlgA1, GlgA2 and GlgC, and Strep-tagged GlgB were expressed in *E. coli* and purified to near-homogeneity by affinity chromatography followed by anion exchange. Purified proteins were recovered at the expected molecular weights and were used for kinetic assays. We first revisited the kinetic properties of the GlgA isoenzymes by initiating glycogen synthesis with direct addition of ADP-Glc and using bovine glycogen as the primer (Assay A) GlgA activity was monitored via a well-documented coupled spectrophotometric assay detecting ADP release through pyruvate kinase (PK) and lactate dehydrogenase (LDH) activities in the presence of phosphoenolpyruvate (PEP) and NADH (Fig. 1) [6,17]. As shown in Fig. 2A, GlgA2 (0.77 ± 0.02 U·mg^{-1}) exhibited approximately 50% higher activity than GlgA1 (0.51 ± 0.01 U·mg^{-1}), albeit with a slightly higher K_m for ADP-Glc (GlgA2 K_m: 219 ± 9.9 μM; GlgA1 K_m: 152 ± 3.6 μM). The resulting catalytic efficiency (K_{cat}/K_m) of GlgA1 was calculated to be 3.2 mM^{-1} s^{-1} which is comparable to GlgA2 at 3.4 mM^{-1} s^{-1}. To further validate our assay method, we performed parallel ADP-Glc titration replacing the *Synechocystis* GlgA isoenzymes with *E. coli* GlgA (GlgA$^{E.coli}$) under identical reaction conditions (Fig. 2B). Notably, GlgA$^{E.coli}$ exhibited enzymatic activity approximately 10^3-fold higher than *Synechocystis* GlgA1 and GlgA2, consistent with previous reports [22]. These results confirm the assay's reliability across different GlgA enzymes, while highlighting the substantially slower catalytic rates of *Synechocystis* isoenzymes relative to *E. coli*.

Primer architecture dictates GlgA activity profiles

Next, we assessed the impact of primer structure on glycogen synthesis by testing maltose and maltotetraose as alternative short and unbranched primers, alongside comparisons with soluble potato starch (hereafter starch) and bovine glycogen to evaluate the effect of primer branching. Both GlgA1 and GlgA2 utilized the shorter, less-branched primers, albeit with reduced activity compared to glycogen (Fig. 2C). No GlgA activity was observed in the absence of a primer. These results indicate that α-1,4-glycosidic bond formation by GlgA at non-reducing ends strictly requires priming, with a preference for longer, branched glycan primers.

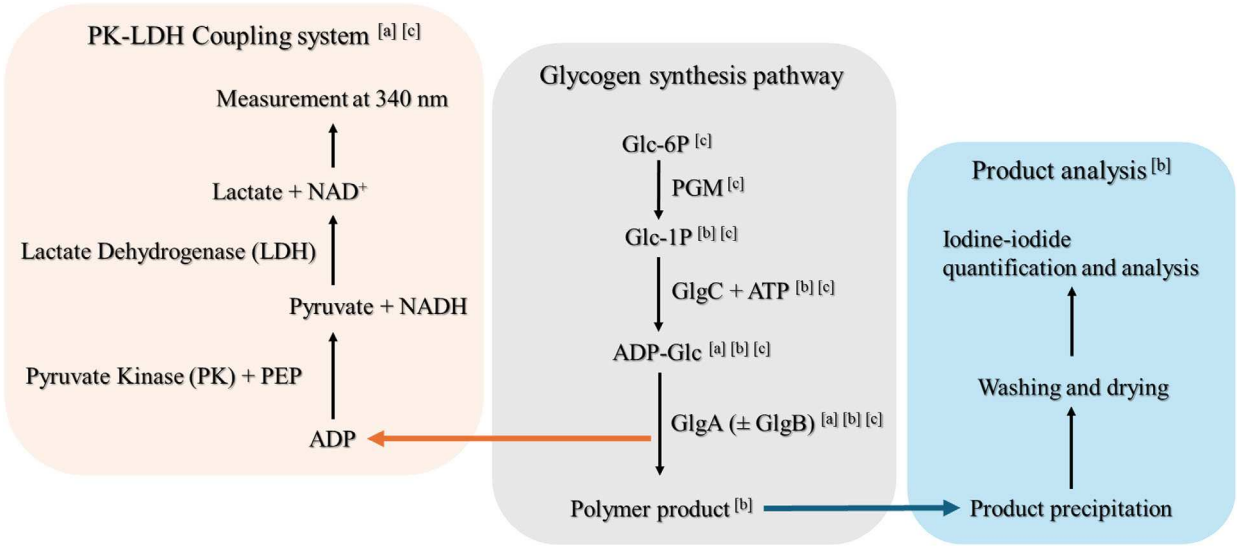

Fig. 1. Schematic overview of the glycogen synthesis pathway in *Synechocystis*, and methods used in this study to assay different components of the pathway. Indicated are components [a] involved in Assay A [b] involved in Assay B [c] involved in Assay C. The details of each assay are given in their respective sections in the methods.

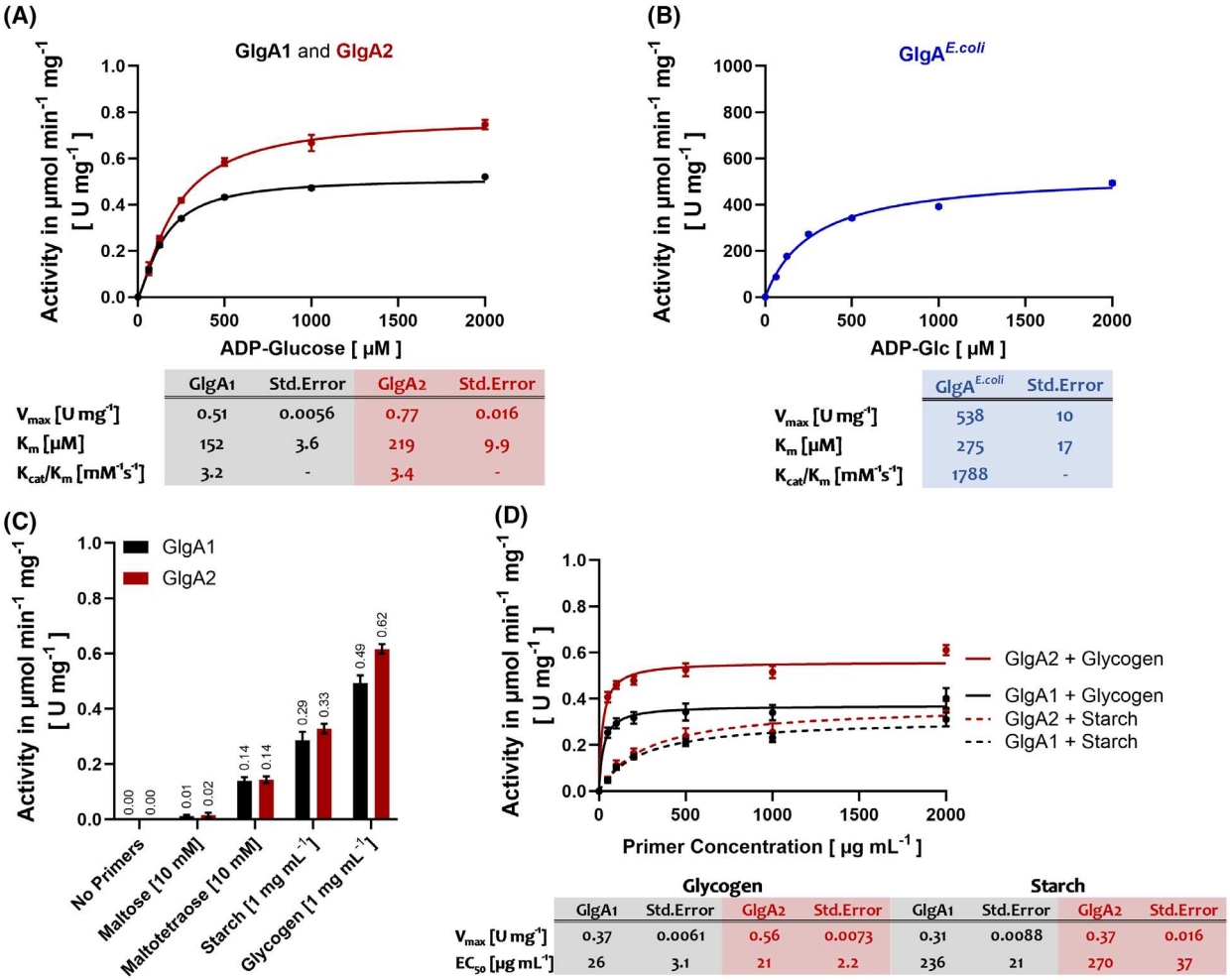

	GlgA1	Std.Error	GlgA2	Std.Error
V_{max} [U mg^{-1}]	0.51	0.0056	0.77	0.016
K_m [µM]	152	3.6	219	9.9
K_{cat}/K_m [mM^{-1}s^{-1}]	3.2	-	3.4	-

	GlgA$^{E.coli}$	Std.Error
V_{max} [U mg^{-1}]	538	10
K_m [µM]	275	17
K_{cat}/K_m [mM^{-1}s^{-1}]	1788	-

	Glycogen				Starch			
	GlgA1	Std.Error	GlgA2	Std.Error	GlgA1	Std.Error	GlgA2	Std.Error
V_{max} [U mg^{-1}]	0.37	0.0061	0.56	0.0073	0.31	0.0088	0.37	0.016
EC_{50} [µg mL^{-1}]	26	3.1	21	2.2	236	21	270	37

Fig. 2. GlgA Kinetics assayed using the ADP/NADH Coupled Assay for glycogen synthesis Activity (Assay A). (A) ADP-Glc titration with 200 nM GlgA1 or GlgA2. About 1 mg·mL^{-1} glycogen was used as a primer. (B) ADP-Glc titration with 1 nM GlgA$^{E.coli}$. 1 mg·mL^{-1} glycogen was used as a primer. (C) Comparison between synthesis primers. The reaction was started with 1 mM ADP-Glc. (D) Titration curves for glycogen and starch. As above, the reaction was started with the addition of 1 mM ADP-Glc. Where applicable, each data point represents the mean of replicates with the SD shown as error bars ($n = 3$–12).

To further evaluate primer-dependent modulation, starch and glycogen concentrations were titrated at near saturating ADP-Glc levels (1 mM) (Fig. 2D). Both isoenzymes exhibited a rapid increase in activity with rising glycogen concentrations (EC_{50}: GlgA1 = 26 ± 3.1 µg·mL^{-1}; GlgA2 = 21 ± 2.2 µg·mL^{-1}), whereas responses to starch were significantly weaker (EC_{50}: GlgA1 = 236 ± 21 µg·mL^{-1}; GlgA2 = 270 ± 37 µg·mL^{-1}). Comparing maximal activities (V_{max}), reactions using starch as a primer resulted in a reduction in GlgA1 activity by 16% and GlgA2 activity by 34% compared to glycogen. These data suggest that, despite comparable catalytic efficiencies, the isoenzymes differ in their primer interactions, potentially reflecting variant preferences for primer structure or branching.

GlgB-driven branching preferentially enhances GlgA2 activity

Next, we introduced the branching enzyme GlgB into the glycogen synthesis reaction to promote primer branching and examined its effects on GlgA activity. Both GlgA isoenzymes exhibited noticeable activation with increasing GlgB concentrations up to around 20 nM GlgB or a molar ratio of one GlgB to ten GlgA monomers (Fig. 3A). Fig. 3B illustrates the net activation (activity normalized against a control without GlgB) of both GlgA isoenzymes with increasing concentrations of GlgB, using starch as a representative of an unbranched primer, demonstrating at least a two-fold enhancement in their activity. However, the

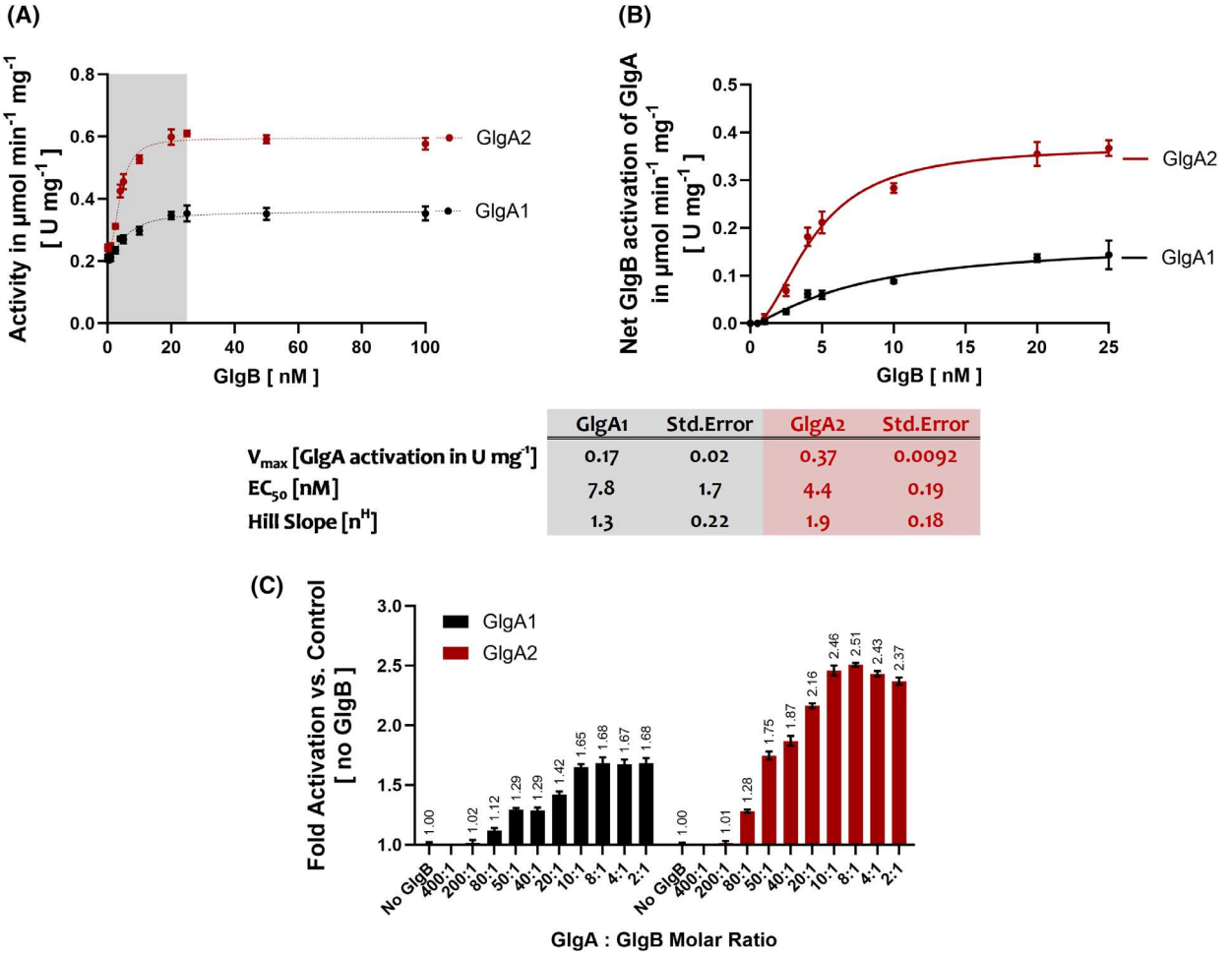

	GlgA1	Std.Error	GlgA2	Std.Error
V_{max} [GlgA activation in U mg^{-1}]	0.17	0.02	0.37	0.0092
EC_{50} [nM]	7.8	1.7	4.4	0.19
Hill Slope [n^H]	1.3	0.22	1.9	0.18

Fig. 3. Activation of GlgA isoenzymes by GlgB. (A) GlgA enzymatic activity with GlgB. The assay was performed using increasing concentrations of GlgB with 200 µg·mL^{-1} soluble starch as the synthesis primer. Reactions were initiated by adding 1 mM ADP-Glc. The area shaded in gray is represented in panel (B). (B) Net activation of both GlgA isoenzymes (200 nM GlgA) was assessed with increasing GlgB concentrations in the presence of 200 µg·mL^{-1} soluble starch as the synthesis primer. Reactions were initiated by adding 1 mM ADP-Glc. Net activity values on the *y*-axis represent GlgA activity after subtracting the baseline activity measured without GlgB from each corresponding data point on the *x*-axis. (C) The fold change in GlgA activity was calculated relative to a control reaction without GlgB. GlgB concentrations are expressed as molar ratios to 200 nM GlgA isoenzyme, with the optimal GlgA: GlgB ratio determined to be 10 : 1. Raw activity values are presented in panel (A). Where applicable, each data point represents the mean of replicates with the SD shown as error bars ($n = 3$–6).

maximum activation of GlgA1 (increase of 0.17 ± 0.02 U·mg^{-1}) was substantially lower than that of GlgA2 (increase of 0.37 ± 0.01 U·mg^{-1}). Furthermore, GlgA1 required almost twice the amount of GlgB for half-maximal activation (EC_{50}: 7.8 ± 1.7 µM) compared to GlgA2 (EC_{50}: 4.4 ± 0.19 µM). These results suggest that GlgB activation of GlgA2 is slightly more efficient than that of GlgA1, which is further supported by the Hill coefficient for GlgA2 (n^H: 1.9 ± 0.18) compared to GlgA1 (n^H: 1.3 ± 0.22), indicating positive cooperativity between GlgB and GlgA2 (Fig. 3C).

To elucidate the modulatory effects of GlgB on GlgA isoenzyme activity, we tested increasing concentrations of starch in the presence of both enzymes to identify the primer concentration at which GlgB-mediated branching most effectively potentiates GlgA catalytic performance. In the presence of GlgB, the EC_{50} for starch was approximately fourfold lower for GlgA2 than GlgA1, accompanied by a higher V_{max} for GlgA2 (Fig. 4A). More strikingly, when GlgB cooperates with either GlgA isoenzyme, the EC_{50} for starch decreased by at least 70-fold for GlgA1 and 330-fold for GlgA2 compared to reactions without GlgB

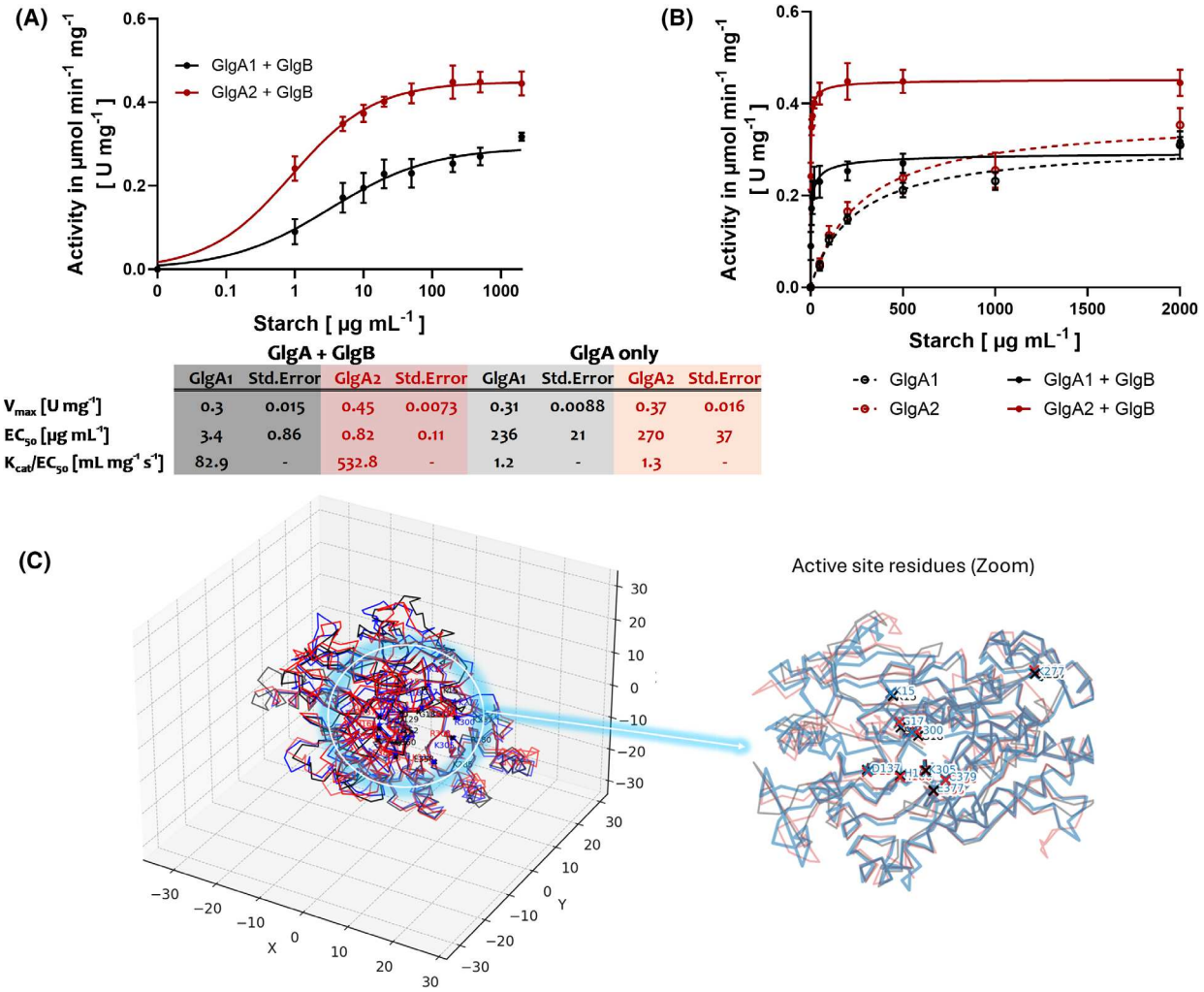

	GlgA + GlgB				GlgA only			
	GlgA1	Std.Error	GlgA2	Std.Error	GlgA1	Std.Error	GlgA2	Std.Error
V_{max} [U mg^{-1}]	0.3	0.015	0.45	0.0073	0.31	0.0088	0.37	0.016
EC_{50} [µg mL^{-1}]	3.4	0.86	0.82	0.11	236	21	270	37
K_{cat}/EC_{50} [mL mg^{-1} s^{-1}]	82.9	-	532.8	-	1.2	-	1.3	-

Fig. 4. Effect of branching on GlgA primer sensitivity and structure-guided motif mapping of GlgA. (A) Starch titration in the presence of 20 nM GlgB and 200 nM GlgA (1 : 10 molar ratio of GlgB to GlgA) with 1 mM ADP-Glc, showing the effect of primer concentration on GlgA activity. (B) Overlay of starch titration curves with GlgB (solid lines) and corresponding starch titration data from Fig. 2C (dashed lines) for direct comparison. (C) Structure-based superposition of GlgA1 and GlgA2 onto $GlgA^{E.coli}$ shown as Cα traces ($GlgA^{E.coli}$, blue; GlgA1, gray; GlgA2, red). Positions of key catalytic/substrate-binding residues (K15, G17, G18, D137, H161, K277, R300, K305, E377, C379; $GlgA^{E.coli}$ numbering) are indicated by crosses at the corresponding Cα atoms, with residue labels color-coded by protein (blue/gray/red). The active site pocket is highlighted (circle) and shown as a magnified view on the right to emphasize local structural conservation. Where applicable, each data point represents the mean of replicates with the SD shown as error bars ($n = 3$–12).

(Fig. 4B). Interestingly, the maximum activity of GlgA1 at saturating starch concentrations remained essentially unchanged by GlgB (V_{max} with GlgB: 0.30 ± 0.02 U·mg^{-1} vs. without GlgB: 0.31 ± 0.01 U·mg^{-1}). In contrast, GlgA2 exhibited a 21.6% increase in maximum activity in the presence of GlgB (V_{max} with GlgB: 0.45 ± 0.01 U·mg^{-1} vs. without GlgB: 0.37 ± 0.02 U·mg^{-1}). Moreover, the catalytic efficiencies (defined as K_{cat}/Primer EC_{50}) of both enzymes increased by at least two orders of magnitude in the presence of GlgB, highlighting the substantial impact of branching on enzyme performance (Fig. 4). Notably, the catalytic efficiency of GlgA2 with GlgB was 6.4-fold higher than that of GlgA1, underscoring a strong dependence of GlgA2 activity on cooperative interactions with GlgB. Taken together, these findings indicate that GlgB significantly enhances the catalytic efficiency and substrate affinity of both GlgA isoenzymes, with a particularly pronounced effect on GlgA2, while GlgA1 activity at higher primer

concentrations appears to be more influenced by the overall primer concentration rather than maximum activation by GlgB alone.

Comparative capacities identify GlgA as the rate-limiting step in *Synechocystis*

To evaluate how coupling to the comparatively slower *Synechocystis* GlgA isoenzymes affects GlgC (as compared to $GlgA^{E.coli}$), we compiled previously reported kinetics parameters for GlgC measured by malachite green (MG) Pi-release assay together with those for GlgA reported above. We compared the intrinsic catalytic capacities on a common flux scale ($\mu M \cdot min^{-1}$) to relate their activities directly. Using the MG assay-derived specific activity of GlgC ($8.9\ U \cdot mg^{-1}$ at 4.98 nM GlgC tetramer) as a benchmark for supply, and the Assay A specific activities (V_{max}) of GlgA1, GlgA2 and $GlgA^{E.\ coli}$ as measures of utilization capacity, we estimated the minimum GlgC concentration required to match GlgA demand under assay conditions (Table 2) [6]. For *Synechocystis*, our calculations indicate that matching the demand of 200 nM GlgA would require on the order of ~3.2 nM GlgC for GlgA1 (≈62 GlgA1 monomers per GlgC tetramer) or ~5 nM GlgC for GlgA2 (≈40 GlgA2 monomers per GlgC tetramer), whereas the highly active $GlgA^{E.\ coli}$ would require over 3.33 μM GlgC tetramer to match 200 nM of $GlgA^{E.coli}$ (≈0.06 : 1). Thus, *Synechocystis* GlgA remains the kinetic bottleneck over a wide range of realistic GlgA:GlgC ratios, while $GlgA^{E.\ coli}$ would be strongly supply-limited by GlgC.

Structural alignment reveals conserved active site geometry despite pronounced global backbone divergence in *Synechocystis* GlgA

To further investigate this difference in utilization capacity between *Synechocystis* and *E. coli* GlgA, we performed a structure-guided motif mapping using AlphaFold models (Fig. 4C). Cα-RMSD-based structural alignment revealed closer overall structural correspondence between $GlgA^{E.\ coli}$ and GlgA2 than between $GlgA^{E.\ coli}$ and GlgA1 (3.19 Å/469 residues vs. 6.06 Å/448 residues), consistent with larger backbone deviations and/or domain-level differences in GlgA1 (Table 3). Despite substantial global backbone differences in both *Synechocystis* GlgA, we managed to identify previously reported conserved residues linked to essential roles in catalysis and substrate positioning in $GlgA^{E.\ coli}$ (Table 4) [23–26]. The active site region was found to be highly conserved: after fitting on residues within 6 Å of key catalytic/binding residues, the active site Cα RMSD was 0.68 Å (GlgA1) and 0.94 Å (GlgA2), and the 10 key residues alone superposed with ≤ 0.35 Å RMSD (Table 3). Within the tight active site pocket, ≤ 6 Å from the 10 key residues, backbone superposition showed that $GlgA^{E.\ coli}$ and GlgA1 are nearly indistinguishable (mean backbone RMSD 0.47 Å; 93.9% of residues ≤ 1.0 Å), with only minor, largely conservative local shifts (≤ 1.32 Å) that are unlikely to account for large kinetic differences (Table 5). In contrast, $GlgA^{E.\ coli}$ vs. GlgA2 displayed a generally conserved pocket (mean 0.65 Å; 83.8% ≤ 1.0 Å) but contained two localized perturbation hotspots: a pronounced deviation centered on the A329–G330 region (A329 → A338 and G330 → T339; backbone RMSD ~3.5 Å) and a second cluster around Q281–I282 (Q281 → R289 and I282 → E290; backbone RMSD ~1.7–2.1 Å) (Table 5). These

Table 3. GlgA active site Cα-RMSD.

	Region	Residues [*n*]	Cα-RMSD [Å]
$GlgA^{E.coli}$	Global	448	6.06
vs.	Key residues only (10)	10	0.35
GlgA1	Active site pocket (6 Å from key residues)	99	0.68
$GlgA^{E.coli}$	Global	469	3.19
vs.	Key residues only (10)	10	0.25
GlgA2	Active-site pocket (6 Å from key residues)	99	0.94

Table 4. GlgA key active site residue position mapping.

E. coli Residue	GlgA1 equivalent	GlgA2 equivalent	Reported Function in $GlgA^{E.\ coli}$
K15	K15	K15	Conserved KXGG loop [25]
G17	G17	G17	Conserved KXGG loop [25]
G18	G18	G18	Conserved KXGG loop [25]
D137	D129	D137	Acceptor (glucan chain) positioning [26]
H161	H152	H166	Major catalytic-geometry/ transition-state contributor [26]
K277	K257	K285	Catalytic contribution [24]
R300	R280	R308	Catalytic phosphate-handling network [26]
K305	K285	K313	Catalytic phosphate-handling network [26]
E377	E358	E388	Glucose positioning [23]
C379	C360	C390	Donor sugar/phosphoglucose recognition [23]

Table 5. Per-residue backbone RMSD (Å) over N, Cα, C, O after a local least-squares fit using the 99 pocket Cα atoms.

Largest local deviations (top 5)				
GlgA$^{E.coli}$ → GlgA1		Backbone RMSD (Å)	Cα deviation (Å)	GlgA$^{E.coli}$ vs. GlgA1 ($n = 99$)
F197	V179	1.32	1.31	Mean 0.47 Å, median 0.40 Å
V6	V6	1.15	1.3	90th percentile 0.83 Å, 95th percentile 1.01 Å
D308	D288	1.08	1.07	Max 1.32 Å
V310	V290	1.05	0.92	93.9% of residues are ≤ 1.0 Å
L198	M180	1.01	0.9	
GlgA$^{E.coli}$ → GlgA2		Backbone RMSD (Å)	Cα deviation (Å)	GlgA$^{E.coli}$ vs. GlgA2 ($n = 99$)
A329	A338	3.56	3.33	Mean 0.65 Å, median 0.45 Å
G330	T339	3.54	3.4	90th percentile 1.23 Å, 95th percentile 1.50 Å
V310	V318	2.13	2.2	Max 3.56 Å
I282	E290	2.05	1.97	83.8% of residues are ≤ 1.0 Å
Q281	R289	1.71	1.61	

deviations combine substantial backbone displacement with non-conservative side-chain changes, consistent with altered loop flexibility and electrostatics at the pocket periphery that could hypothetically modulate active site closure and/or acceptor/donor positioning, all the while the catalytic core itself remains structurally conserved.

GlgA1 produces more-branched glycogen, whereas GlgA2 yields a more linear polymer

To study the products of the glycogen synthesis reaction in detail, we repurposed the Assay A system for preparative purposes by omitting the coupling system components for the spectrophotometric assays, namely LDH and NADH (Fig. 1). To complete the *in vitro* glycogen synthesis pathway, we introduced an upstream ADP-Glc production module by integrating GlgC at a stoichiometric ratio of 1 : 1 GlgA monomer to GlgC tetramer and started the glycogen synthesis reaction via addition of Glc-1P, using starch as the synthesis primer (Assay B).

Products formed in the presence of GlgB were considered predominantly branched glycogen, whereas those produced in its absence were considered amylose-like linear glucans. Polymer synthesis products from Assay B were quantified by both iodine-iodide spectrophotometric staining and enzymatic determination (Fig. 5A), yielding consistent results with no significant differences observed between the two quantification methods. Figure 5B presents the synthesis product yields for both GlgA isoenzymes with and without GlgB. From 1 mL reaction mixtures, GlgA2 in combination with GlgB produced 18.1% more glycogen (1.3 mg) than the GlgA1-GlgB reaction (1.1 mg). Similarly, in the absence of GlgB, GlgA2 synthesized 12.9% more amylose-like polymer (0.233 mg) compared to GlgA1 (0.206 mg). Notably, reactions lacking GlgB demonstrated a substantial decrease in product yield, with an 82.9% reduction for GlgA1 and 81.3% for GlgA2.

Analysis of iodine-iodide absorbance spectra revealed subtle differences in polymer branching between products of the two GlgA isoenzymes in the presence of GlgB (Fig. 5C). Glycogen synthesized by GlgA1 showed an absorbance maximum (λ^{max}) of 450 nm with higher absorbance at lower wavelengths, indicative of a more-branched structure, approximating the profile of highly branched bovine glycogen (λ^{max}: 434 nm). Conversely, GlgA2-derived glycogen exhibited a λ^{max} of 470 nm, suggestive of comparatively fewer branches. The amylose-like polysaccharides generated in the absence of GlgB from both isoenzymes showed λ^{max} values near 546 nm (Fig. 5D), characteristic of linear starch-like molecules, closely matching the profile of the starch standard λ^{max} of 554 nm. We further compared these *in vitro* polymer profiles with glycogen isolated from *Synechocystis* mutants deficient in either GlgA1 (Δ*glgA1*) or GlgA2 (Δ*glgA2*) (Fig. 6A). Glycogen from the Δ*glgA2* mutant displayed a λ^{max} of 470 nm, resembling bovine glycogen (Fig. 6B), whereas glycogen from Δ*glgA1* had a higher λ^{max} of 516 nm, aligning more closely with starch (Fig. 6C).

Although neither mutant-derived glycogen spectrum perfectly matched their respective *in vitro* synthesized products, the glycogen produced *in vivo* by GlgA1 exhibited spectral properties ($\lambda^{max} = 470$ nm) closely resembling those of *in vitro* GlgA1-derived glycogen ($\lambda^{max} = 450$ nm). Both forms demonstrated a higher degree of branching compared to glycogen produced by GlgA2. *In vivo* synthesized glycogen by GlgA2 displayed starch-like characteristics with a notably higher λ^{max} of 516 nm, indicating less branching. This trend of reduced branching was also observed in glycogen synthesized *in vitro* by GlgA2, though less pronounced,

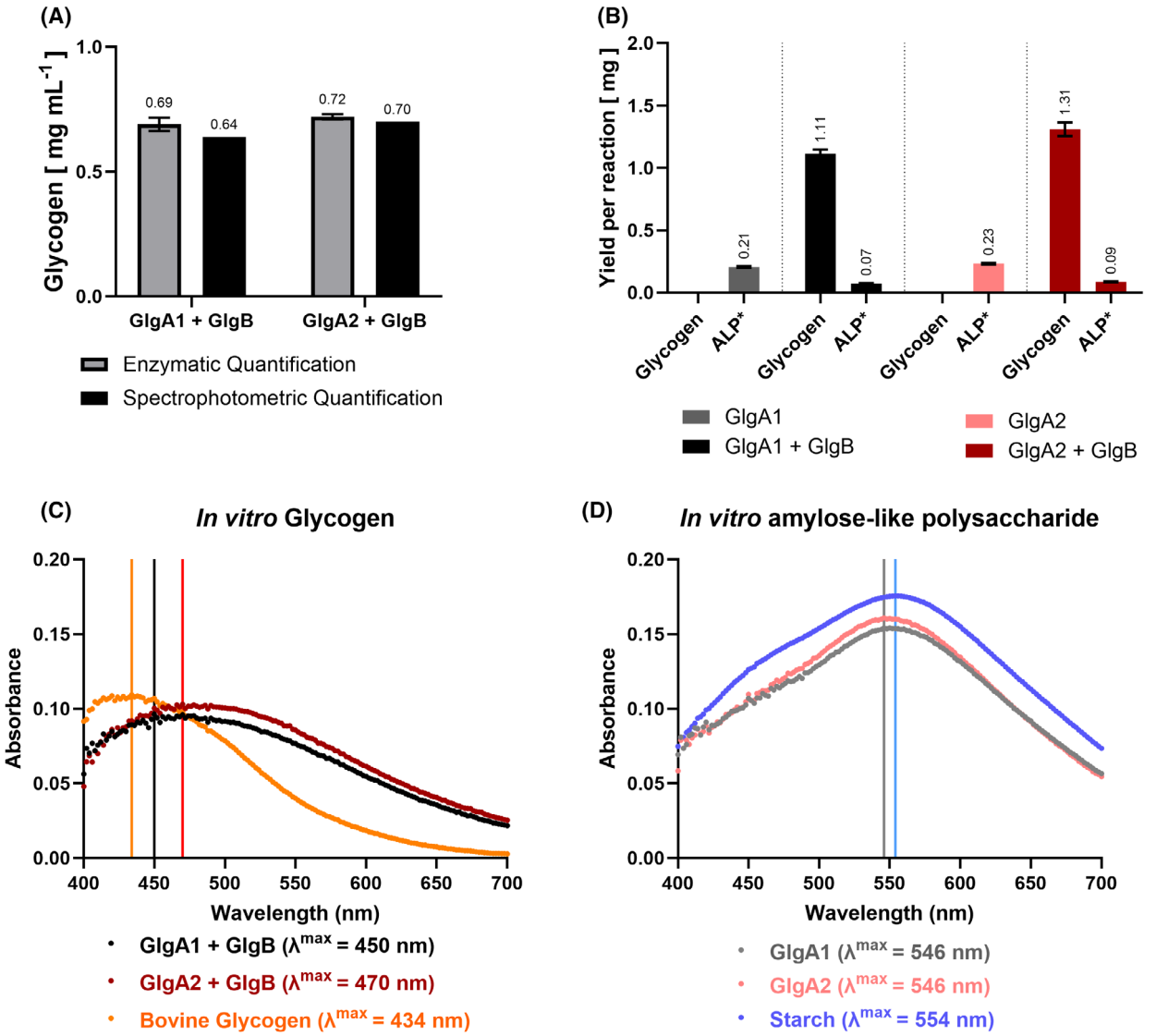

Fig. 5. Characterization of *in vitro* polymer products (Assay B). (A) Comparison of glycogen quantification methods. Pooled glycogen samples from Assay B replicates ($n = 6$) were adjusted to 1 mL volume. Glycogen concentrations were first measured using the iodine-iodide spectrophotometric assay and subsequently validated by an enzymatic rapid glycogen assay. Paired *t*-test analysis yielded a *P* value of 0.2578, indicating no significant difference ($P > 0.05$). (B) Yields of reaction products from Assay B, expressed as mg of product per 1 mL reaction volume. Each data point represents the mean of six replicates ($n = 6$), with standard deviation (SD) shown as error bars. Absorbance spectra between 400 and 700 nm of pooled synthesis products from Assay B. Equal volumes of replicate reactions from (B) were combined, and concentrations were adjusted to 0.5 mg·mL^{-1} for glycogen samples and 0.1 mg·mL^{-1} for amylose-like samples. Maximum absorbance values (λ^{max}) were calculated using the Area Under the Curve (AUC) function in GraphPad Prism, referencing the highest peak identified, and are indicated by vertical lines on the *x*-axis. * Amylose-like Polysaccharides (ALP). (C) Absorbance spectra of glycogen samples from Assay B compared to the bovine glycogen standard. (D) Absorbance spectra of amylose-like samples from Assay B compared to a starch standard.

as reflected by a λ^{max} of 470 nm. Wild-type glycogen showed intermediate properties, with a λ^{max} of 504 nm, positioning it between the two mutant profiles and recapitulating the distinct structural divergences between GlgA1- and GlgA2-derived glycogen *in vivo*. (Fig. 6A).

Modified assay a enables quantification of PGM forward reaction kinetics

To further expand the utility of our assay system, we modified the core assay (Assay A) to examine PGM activity by coupling the PGM reaction to equimolar

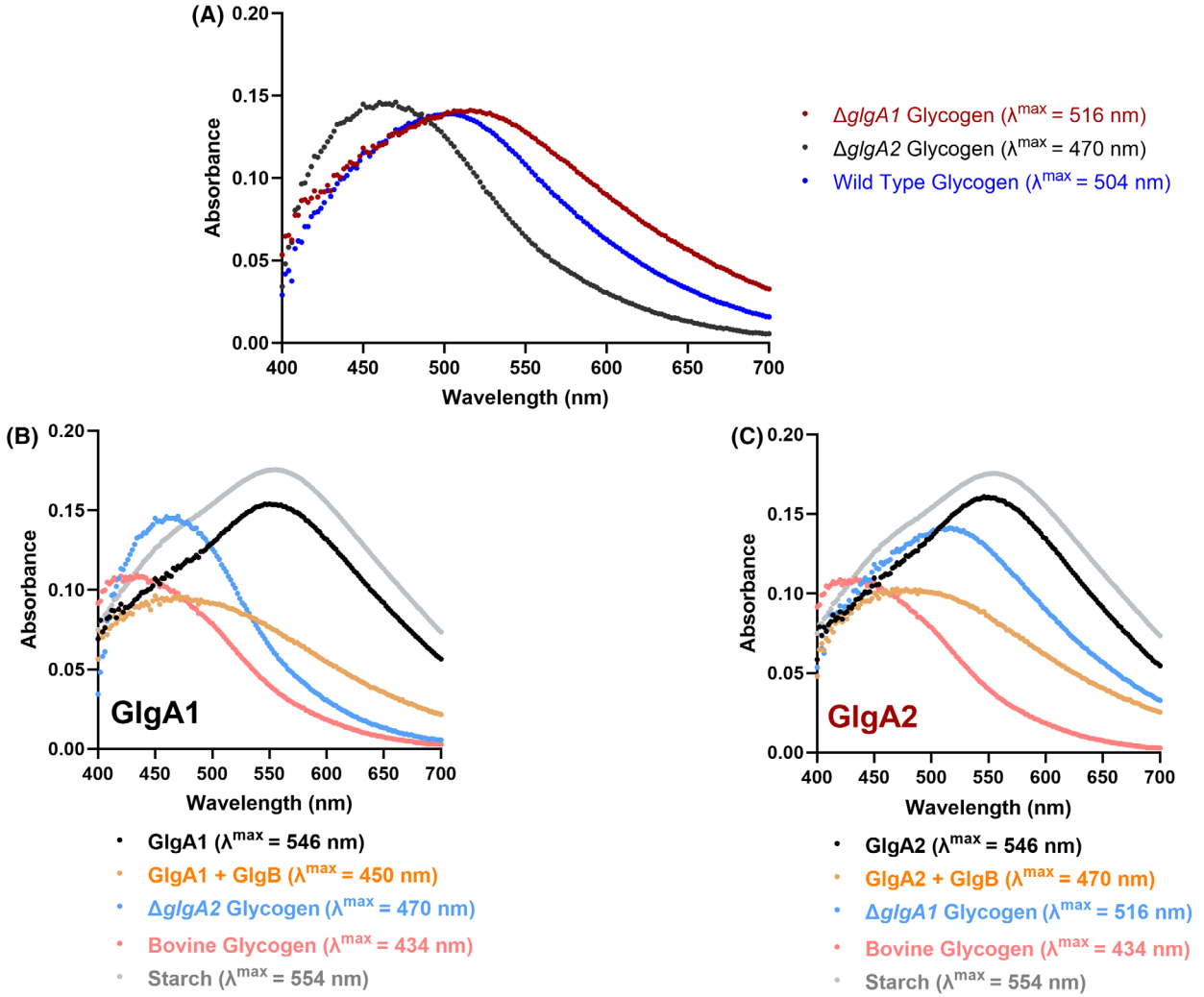

Fig. 6. Comparison of *in vitro* polymer products with *in vivo* glycogen. Absorbance spectra between 400 and 700 nm of pooled synthesis products from Assay B were compared to glycogen extracted from *Synechocystis* wild-type and *glgA*-deficient mutant cultures. Equal volumes of replicate reactions from Assay B or isolated glycogen from *Synechocystis* cultures were combined, and concentrations were adjusted to 0.5 mg·mL^{-1} for glycogen samples and 0.1 mg·mL^{-1} for amylose-like samples. Maximum absorbance values (λ^{max}) were calculated as previously described using the Area Under the Curve (AUC) function in GraphPad Prism. (A) Absorbance spectra of glycogen isolated from Δ*glgA2*, Δ*glgA1*, and wild-type *Synechocystis* cultures. (B) Comparison of GlgA1-derived synthesis products with bovine glycogen, starch, and glycogen isolated from GlgA2-deficient (Δ*glgA2*) *Synechocystis* mutants. (C) Comparison of GlgA2-derived synthesis products with starch, bovine glycogen, and glycogen isolated from GlgA1-deficient (Δ*glgA1*) *Synechocystis* mutants.

GlgC and GlgA$^{E.coli}$ (Assay C) (Fig. 1). PGM catalyzes the reversible interconversion of Glc-1P and Glc-6P. *Synechocystis* bears two genes encoding putative PGM enzymes (*sll0726* and *slr1334*); the *sll0726*-encoded enzyme was selected for this study, as it represents the primary PGM isoform in *Synechocystis* [16]. To ensure substrate turnover was not rate-limited, the coupling enzymes GlgC and GlgA$^{E.coli}$ were included in the reaction at 400 nM each, placing the GlgA:GlgC ratio at 1 : 1, far above the ideal 0.06 : 1 established previously (Table 2).

A titration of PGM was performed to identify the concentration range in which the measured activity reflected intrinsic enzyme catalysis (Fig. 7A). The reaction rate increased linearly with PGM concentration up to the tested concentration of 6.13 nM, indicating that within this range, the observed activity corresponded directly to PGM turnover. Together with the determined dissociation constant (K_d: 6.4 ± 0.25 nM), these results indicate that enzyme concentrations within this range are optimal for reliable kinetic measurements under the applied conditions. Subsequently,

a Glc-6P titration was conducted using 5 nM PGM. As shown in Fig. 7B, the resulting kinetic parameters demonstrated that the assay effectively resolved PGM catalytic properties, yielding a V_{max} of 190 ± 6.6 U·mg^{-1} and a K_m of 1.52 ± 0.16 mM for Glc-6P.

Discussion

We established an *in vitro* model of glycogen synthesis pathway from *Synechocystis* (Fig. 1). This model elucidates critical factors controlling glycogen synthesis, including primer selectivity and the modulatory role of GlgB. Additionally, we demonstrated production of glycogen *in vitro* and characterized structural differences between products synthesized by GlgA1 and GlgA2.

Primer architecture and GlgB cooperation partition elongation labor between GlgA isoenzymes

The kinetic analyses demonstrate that GlgA1 and GlgA2 isoenzymes possess broadly similar catalytic efficiencies despite subtle differences in their kinetic parameters, implying differential optimization potentially aligned with distinct cellular or metabolic contexts. Both isoenzymes can utilize short, linear polysaccharide primers, though less efficiently than branched glycogen, indicating some flexibility in primer selectivity but also emphasizing that primer structure notably influences enzymatic activity. The absence of detectable GlgA activity without an exogenous primer (Fig. 2C) demonstrates that *Synechocystis* GlgA are strictly primer-dependent and therefore unlikely to function as initiating enzymes. Together with the reported requirement for an unidentified protein factor for *de novo* glycogen initiation *in vivo*, our results suggest that initiation may involve an upstream priming/acceptor-generating activity that supplies the first α-glucan substrate for GlgA [27].

The distinct responses of GlgA1 and GlgA2 to starch and glycogen highlight differential primer interactions. Significantly higher concentrations of linear starch were needed to reach activities comparable to those with branched glycogen, indicating that branched primers with more readily accessible nonreducing ends are essential for optimal GlgA binding and activation (Fig. 2C,D). This highlights the role of GlgB in glycogen synthesis, where the inclusion of GlgB markedly enhanced the catalytic activities of both GlgA isoenzymes, albeit to different extents (Fig. 3). GlgA2, which synthesizes longer glucan chains, is suggested to be particularly susceptible to steric hindrance within the growing glycogen network [5,10,28]. The branching activity of GlgB alleviates

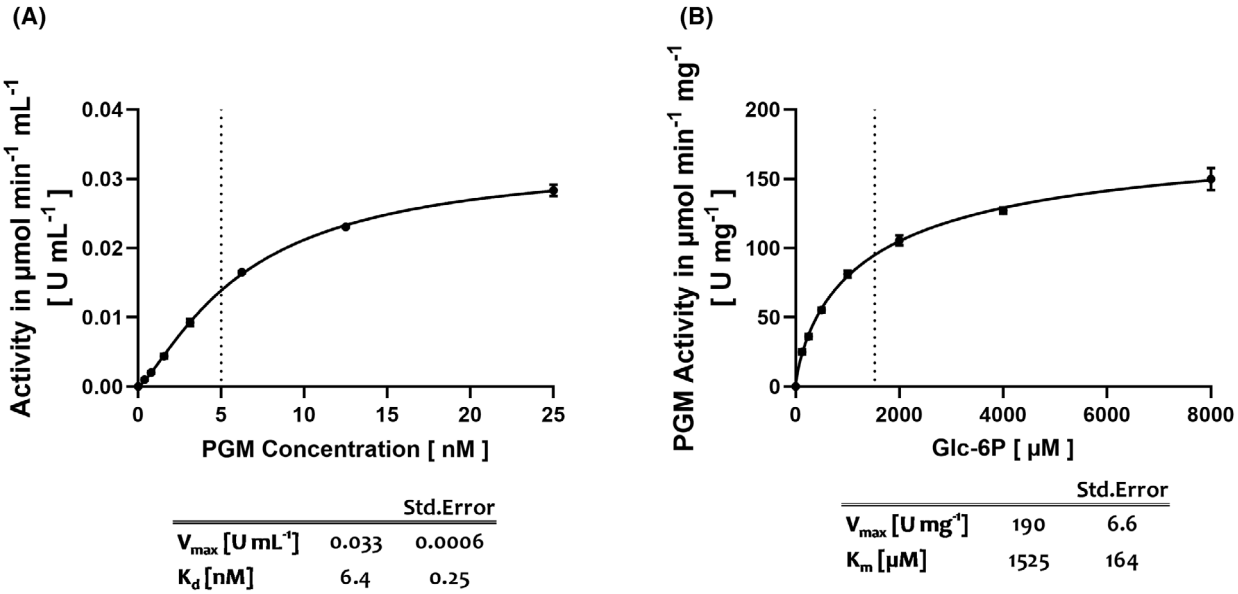

Fig. 7. PGM forward reaction Assays (Assay C). (A) Titration of PGM at the indicated concentrations. Reactions were initiated by the addition of 1 mM Glc-6P. Activity values (U·mL^{-1}) on the y-axis represent the overall enzymatic activity of the coupled pathway, including Glc-1P formation from Glc-6P, subsequent ADP-Glc synthesis, and glycogen polymerization. The dotted line on the *x*-axis denotes the standard PGM concentration used in subsequent assays. (B) Titration of Glc-6P in the presence of 5 nM PGM. The K_m value is indicated by the dotted line on the *x*-axis. Where applicable, each data point represents the mean of independent replicates with the SD shown as error bars ($n = 3$–6).

these steric constraints by creating new branch points, thereby enabling GlgA2 to extend even longer chains more efficiently [10]. Consequently, GlgA2 exhibited a substantially stronger and more persistent activation in the presence of GlgB, indicative of a highly efficient functional cooperativity between the two enzymes (Fig. 3B). This pronounced synergy likely reflects a close coordination of elongation and branching reactions that supports continuous and effective glucan synthesis. In contrast, GlgA1 performs a more dispersive elongation, resulting in the synthesis of glycogen that is inherently more branched than that produced by GlgA2 [5,10]. Accordingly, GlgA1 activity was observed to be increased only up to a defined level and then plateaued in the presence of GlgB, suggesting that the additional branching generated by GlgB does not further stimulate catalysis beyond a certain limit (Fig. 3). Additionally, at elevated GlgB concentrations, a slight decrease in GlgA2 activity was observed (Fig. 3C), an effect absent in GlgA1. This pattern suggests that GlgA2 may be particularly sensitive to steric effects arising from excessive enzyme crowding or suboptimal access to elongation sites despite branching's general role in relieving steric hindrances. Taken together, these observations highlight that GlgA2 engages in significantly more efficient and finely tuned cooperation with GlgB than GlgA1. The iodine-iodide spectra of products formed with GlgB further reinforce that GlgA1 glycogen is more branched than GlgA2 glycogen despite similar primer usage [5,27].

This aligns the observations from our enzyme assays with the physicochemical differences observed between glycogen synthesized by the two GlgA isoenzymes: glycogen produced by GlgA1, both *in vivo* and *in vitro*, is notably more branched than that formed by GlgA2 (Figs 5C and 6A). In the absence of GlgB, both isoenzymes generate amylose-like, largely linear polymers with largely indistinguishable iodine–iodide spectral profiles, likely reflecting some degree of synthesis inhibition or a drastic reduction in GlgA activity to negligible levels over longer durations of sustained synthesis in the absence of branching (Fig. 5D). Taken together with the markedly lower yields of amylose-like polysaccharides in reactions without GlgB, it is reasonable to conclude that branching is also essential to relieve steric hindrances that occur during sustained glycogen synthesis (Fig. 5B,D) [28]. These findings demonstrate that the role of GlgB extends beyond primer branching—it also plays a key role in glycogen structure reorganization for efficient GlgA activity and allows for efficient sustained glycogen synthesis.

The structural distinctions in glycogen produced by each GlgA isoenzyme, in addition to the characteristics of the isoenzymes themselves may reflect specialized physiological roles. For example, the short, highly branched glycogen synthesized by GlgA1 could confer survival advantages under environmental stresses, as observed in various bacteria where such glycogen is degraded more slowly, supporting reduced metabolic rates and prolonged viability, given that the shorter branches are more easily accessible to glycogen degradation enzymes [13]. In *Synechocystis*, the dependence of resuscitation from nitrogen starvation on GlgA1 supports the notion that GlgA1-derived glycogen contributes to adaptability and survival, whereas GlgA2-generated glycogen primarily could serve as a carbon storage molecule during conditions of high carbon flux [14,27,29]. Given that sustained glycogen synthesis occurs under such conditions, it is reasonable to assume that the reorganization of the growing glycogen granule by GlgB is especially crucial to support optimal GlgA2 activity. Since wild-type glycogen exhibits characteristics intermediate between those of GlgA1- and GlgA2-derived glycogen, it is reasonable to conclude that both isoenzymes cooperatively contribute to glycogen synthesis during normal growth, balancing metabolic flexibility with carbon storage needs (Fig. 6A) [10].

Divergent glycogen synthesis control in phototrophs and heterotrophs

Oxygenic phototrophs—including *Synechocystis*—allocate primary control upstream at GlgC, which is activated by 3-PGA and inhibited by Pi [6–9], and diversify elongation via two GlgA isoenzymes with distinct operational biases [5,27]. Additionally, given the roughly comparable *in vivo* expression levels of GlgA monomers and GlgC tetramers during normal heterotrophic growth, our observations also suggest an additional layer of intrinsic regulation of glycogen synthesis via enzyme stoichiometry [29–31]. Our *in vitro* reconstitutions support this proposed architecture in that: (i) GlgB sharply potentiates both GlgA isoenzymes under low-primer conditions but disproportionately enhances GlgA2, (ii) product spectra indicate that GlgA1 yields more highly branched glycogen (lower λ^{max}) than GlgA2, and (iii) at a practical and biologically relevant 1 : 1 GlgC tetramer: GlgA monomer ratio, pathway flux is GlgA-limited due to the lower intrinsic activity of the *Synechocystis* GlgA isoenzymes. In sum, primer/branching governance and modest GlgA catalysis—rather than maximal elongation throughput—determine the glycogen synthesis flux and polymer architecture in *Synechocystis*.

By contrast, in heterotrophic bacteria such as *E. coli*, glycogen synthesis is configured for rapid accumulation.

GlgA$^{E.coli}$ has high catalytic capacity *in vitro* [22,32], and the GlgA–GlgB pair sustains appreciable elongation even when exogenous primer is scarce—under 'unprimed' conditions, GlgB (further facilitated by citrate) supports ~30% of the GlgA$^{E.coli}$ V_{max} otherwise achieved with saturating glycogen primer concentrations [33,34]. *In vivo*, the maltose/maltodextrin network (MalQ/MalP and associated transporters) continually supplies maltooligosaccharide acceptors, minimizing primer limitation and amplifying the impact of a fast GlgA [35,36]. These features indicate an evolutionary reason why *E. coli* GlgC (GlgC$^{E.coli}$) exhibits substantially higher intrinsic activity than the *Synechocystis* isoenzymes, and why GlgA$^{E.coli}$ activity exceeds GlgC$^{E.coli}$ by several fold [6,32,37].

Multiple sequence alignment and structure-guided motif mapping indicate that both *Synechocystis* GlgA enzymes retain the canonical GlgA active site architecture. Residues classically implicated in ADP-glucose binding and catalysis in GlgA$^{E.coli}$—including the N-terminal KXGG signature and other conserved catalytic/structural positions—are preserved at alignment-equivalent sites (Table 4, Fig. 4C) [23–26]. Consistent with this, pocket-restricted superposition (≤ 6 Å from the ten key residues) shows that the immediate catalytic environment is highly conserved, most strikingly for GlgA1, whose tight-pocket backbone differs from GlgA$^{E.coli}$ only marginally (Table 5). Thus, the markedly lower apparent catalytic efficiency of *Synechocystis* GlgA relative to GlgA$^{E.coli}$ is unlikely to reflect altered donor-binding chemistry or loss of catalytic determinants within the pocket itself. Instead, our structural data support a model in which the difference in activity between GlgA$^{E.coli}$ and *Synechocystis* GlgA is due to features of the global GlgA structure that govern how often the enzyme reaches (and maintains) a productive catalytic configuration. The larger whole-structure deviations seen for GlgA1 (GlgA1 vs. GlgA$^{E.coli}$), compared with GlgA2 vs. GlgA$^{E.coli}$, suggest changes in interdomain orientation and/or hinge dynamics. These changes could slow formation of the closed, catalytically competent state and thus reduce overall catalytic activity (Table 3). GlgA2, while globally closer to GlgA$^{E.coli}$, exhibits two localized perturbation hotspots at the pocket periphery that could further tune loop flexibility and electrostatics at the acceptor-facing boundary, thereby modulating primer positioning, processivity, and substrate-gated conformational transitions (Tables 3 and 5). Collectively, these observations argue that divergence in primer binding and conformational dynamics, rather than changes to the conserved catalytic core, provides the most likely explanation for the substantially lower activity of *Synechocystis* GlgA.

Supporting this is a further distinction in synthesis initiation and primer economy. Bacteria do not employ a glycogenin-type protein primer; in some species, glycogen synthesis can initiate *de novo*, and primer pools arise via enzyme-mediated interconversion of maltooligosaccharides [38]. This helps explain why *E. coli* can partly circumvent primer scarcity through GlgB-assisted 'unprimed' synthesis and MalQ/MalP-driven primer provision [34–36]. On the other hand, *Synechocystis* lacking a dedicated maltose circuit, relies more on primer economy and GlgB cooperation to maintain throughput. A similar control logic of GlgA-GlgB coordinated elongation–branching is also documented in higher plants, where multiple starch synthase and branching enzyme isoforms assemble into catalytically competent complexes [39,40]. Additionally, similar GlgA-GlgC catalytic arrangements—higher intrinsic GlgC activity relative to starch/glycogen synthases—were also observed in various higher plants, hinting that these regulatory strategies might be common to photoautotrophs [1,41–45]. Viewed together, these considerations provide a plausible mechanistic rationale: Despite largely working off the same molecular principles, *Synechocystis* GlgA operates in a measured kinetic regime that facilitates efficient GlgB-mediated branch insertion under primer-limited conditions, rather than being tuned for maximal elongation velocity *per se*, contrasting with the primer-rich, high-throughput configuration of *E. coli*.

The coupled assay (Assay B) applications go beyond modeling glycogen synthesis

The coupled assay system developed in this study demonstrates considerable flexibility and can be readily adapted to address a broad range of biochemical questions beyond glycogen synthesis itself. Its modular design allows precise modification of reaction components to target different catalytic processes or synthetic outcomes. For example, scaling the assay for preparative purposes (Assay B, Fig. 5) highlights its utility for large-scale *in vitro* glycogen synthesis, providing new perspectives on glucan structure formation and enzyme cooperation. Beyond analytical use, such adaptations may also serve practical applications, such as generating defined *Synechocystis* glycogen for downstream enzymatic studies—most notably of glycogen phosphorylase—without requiring extensive biomass cultivation.

Apart from applications directly related to glycogen synthesis, the adaptation applied in Assay C (Fig. 7) establishes a powerful approach for investigating phosphoglucomutase (PGM) activity and its

regulation. While the kinetics of the reverse PGM reaction (Glc-1P → Glc-6P) have been thoroughly examined, the forward conversion (Glc-6P → Glc-1P) has received far less attention [16,46]. By coupling GlgC and $GlgA^{E.coli}$, our system enables reliable quantification of this underexplored reaction and could be easily expanded to screen for potential metabolic regulators influencing PGM activity.

Looking ahead, the modularity of the coupled platform provides a direct route to test flux control and compatibility hypotheses by systematically swapping pathway modules *in vitro* (e.g., replacing *Synechocystis* GlgA with a high-turnover synthase such as $GlgA^{E.coli}$) and quantifying how control shifts toward ADP-glucose supply (GlgC) and energy status, as well as how elongation kinetics reshape glucan architecture through competition with branching/debranching. In parallel, an equally informative *in vivo* approach would be to complement a completely GlgA-deficient *Synechocystis* background strain with $GlgA^{E.coli}$ to test whether a fast elongation module is compatible with cyanobacterial glycogen homeostasis and stress physiology. Such a test is particularly interesting because complete loss of glycogen synthase activity in *Synechocystis* is reported to be lethal due to ADP-glucose accumulation, with viability achievable only under specific conditions that redirect carbon flux [47]. Collectively, these applications underscore the assay's versatility as a platform for probing diverse aspects of carbohydrate metabolism and enzymatic regulation in a controlled *in vitro* context, as well as method to complement and inform additional physiological investigations.

Conclusion

Our reconstruction of the *Synechocystis* glycogen biosynthesis pathway *in vitro* resolves glycogen synthesis into a hierarchical control scheme and a context-dependent division of labor between GlgA isoenzymes. Upstream, GlgC governs precursor supply: Its substrate affinity and allosteric effectors tune ADP-glucose availability and thereby gate entry into the pathway [6]. Downstream, GlgA imposes the principal flux limitation. Within this framework, primer architecture and GlgB cooperation partition elongation tasks between GlgA1 and GlgA2—branching density selectively accelerates GlgA2-mediated chain extension, whereas GlgA1 favors shorter, more-branched products—linking flux control to product fine structure. Finally, the coupled assay we established offers a modular platform to quantify control coefficients and to generalize these principles to other nucleotide-sugar polymer pathways, such as resolving PGM forward kinetics.

Acknowledgements

We thank Dr. Christophe Colleoni at the University of Lille for his advice regarding the analysis of our synthesis products. This work was supported by the DFG funded research consortium FOR2816 'The Autotrophy-Heterotrophy Switch in Cyanobacteria: Coherent Decision-Making at Multiple Regulatory Layers', research grant Fo195/16-2. We also acknowledge infrastructural Cluster of Excellence EXC 2124 (Controlling Microbes to Fight Infections, CMFI, grant 390838134) at the Eberhard Karls Universität Tübingen. The author(s) used Chat-GPT 5.2 Thinking for minor phrasing edits and proofreading for mistakes in grammar and spelling. The author(s) reviewed and edited the generated output and assume(s) full responsibility for the content of the publication. Open Access funding enabled and organized by Projekt DEAL.

Author contributions

KL: designed and carried out the experiments and the wrote paper. DB: Assistance with Assay C. SD and KF: conceptualization, supervision, and paper writing. All authors contributed at varying stages in the editing and review of the paper.

Peer review

The peer review history for this article is available at https://www.webofscience.com/api/gateway/wos/peer-review/10.1002/1873-3468.70299.

Data accessibility

Enzymatic data and all figures presented in this study have been deposited here (https://doi.org/10.15490/fairdomhub.1.assay.2758.1) on the data and model management platform FAIRDOMHub [48].

References

1 McFadden GI (2001) Chloroplast origin and integration. *Plant Physiol* **125**, 50–53.
2 Makowka A, Nichelmann L, Schulze D, Spengler K, Wittmann C, Forchhammer K and Gutekunst K (2020) Glycolytic shunts replenish the Calvin–Benson–Bassham cycle as anaplerotic reactions in cyanobacteria. *Mol Plant* **13**, 471–482.
3 Miao X, Wu Q, Wu G and Zhao N (2003) Sucrose accumulation in salt-stressed cells of *agp* gene deletion-mutant in cyanobacterium *Synechocystis* sp. PCC 6803. *FEMS Microbiol Lett* **218**, 71–77.

4 Doello S, Klotz A, Makowka A, Gutekunst K and Forchhammer K (2018) A specific glycogen mobilization strategy enables rapid awakening of dormant cyanobacteria from chlorosis. *Plant Physiol* **177**, 594–603.
5 Yoo S-H, Lee B-H, Moon Y, Spalding MH and Jane J-L (2014) Glycogen synthase isoforms in *Synechocystis* sp. PCC 6803: identification of different roles to produce glycogen by targeted mutagenesis. *PLoS One* **9**, e91524.
6 Lee K, Doello S, Hagemann M and Forchhammer K (2025) Deciphering the tight metabolite-level regulation of glucose-1-phosphate adenylyltransferase (GlgC) for glycogen synthesis in cyanobacteria. *FEBS J* **292**, 759–775.
7 Ballicora MA, Iglesias AA and Preiss J (2003) ADP-glucose pyrophosphorylase, a regulatory enzyme for bacterial glycogen synthesis. *Microbiol Mol Biol Rev* **67**, 213–225.
8 Iglesias AA, Kakefuda G and Preiss J (1991) Regulatory and structural properties of the cyanobacterial ADPglucose pyrophosphorylases. *Plant Physiol* **97**, 1187–1195.
9 Figueroa CM, Kuhn ML, Hill BL, Iglesias AA and Ballicora MA (2018) Resurrecting the regulatory properties of the *Ostreococcus tauri* ADP-glucose pyrophosphorylase large subunit. *Front Plant Sci* **9**, 1564.
10 Fermont L, Szydlowski N and Colleoni C (2022) Determination of glucan chain length distribution of glycogen using the fluorophore-assisted carbohydrate electrophoresis (FACE) method. *J Vis Exp* **181**, e63392.
11 Seibold GM, Breitinger KJ, Kempkes R, Both L, Krämer M, Dempf S and Eikmanns BJ (2011) The *glgB*-encoded glycogen branching enzyme is essential for glycogen accumulation in *Corynebacterium glutamicum*. *Microbiology* **157**, 3243–3251.
12 Wang L, Liu Q, Hu J, Asenso J, Wise MJ, Wu X, Ma C, Chen X, Yang J and Tang D (2019) Structure and evolution of glycogen branching enzyme N-termini from bacteria. *Front Microbiol* **9**, 3354.
13 Wang L and Wise MJ (2011) Glycogen with short average chain length enhances bacterial durability. *Naturwissenschaften* **98**, 719–729.
14 Koch M, Doello S, Gutekunst K and Forchhammer K (2019) PHB is produced from glycogen turnover during nitrogen starvation in *Synechocystis* sp. PCC 6803. *Int J Mol Sci* **20**, 1942.
15 Selim KA, Haase F, Hartmann MD, Hagemann M and Forchhammer K (2018) PII-like signaling protein SbtB links cAMP sensing with cyanobacterial inorganic carbon response. *Proc Natl Acad Sci USA* **115**, E4861–E4869.
16 Neumann N, Friz S and Forchhammer K (2022) Glucose-1,6-bisphosphate, a key metabolic regulator, is synthesized by a distinct family of α-phosphohexomutases widely distributed in prokaryotes. *MBio* **13**, e0146922.
17 Wayllace NZ, Valdez HA, Merás A, Ugalde RA, Busi MV and Gomez-Casati DF (2012) An enzyme-coupled continuous spectrophotometric assay for glycogen synthases. *Mol Biol Rep* **39**, 585–591.
18 Vidal R and Venegas-Calerón M (2019) Simple, fast and accurate method for the determination of glycogen in the model unicellular cyanobacterium *Synechocystis* sp. PCC 6803. *J Microbiol Methods* **164**, 105686.
19 Abramson J, Adler J, Dunger J, Evans R, Green T, Pritzel A, Ronneberger O, Willmore L, Ballard AJ, Bambrick J *et al.* (2024) Accurate structure prediction of biomolecular interactions with AlphaFold 3. *Nature* **630**, 493–500.
20 Thompson JD, Higgins DG and Gibson TJ (1994) CLUSTAL W: improving the sensitivity of progressive multiple sequence alignment through sequence weighting, position-specific gap penalties and weight matrix choice. *Nucleic Acids Res* **22**, 4673–4680.
21 Meng EC, Goddard TD, Pettersen EF, Couch GS, Pearson ZJ, Morris JH and Ferrin TE (2023) UCSF ChimeraX: tools for structure building and analysis. *Protein Sci* **32**, e4792.
22 Holmes E and Preiss J (1979) Characterization of *Escherichia coli* B glycogen synthase enzymatic reactions and products. *Arch Biochem Biophys* **196**, 436–448.
23 Sheng F, Jia X, Yep A, Preiss J and Geiger JH (2009) The crystal structures of the open and catalytically competent closed conformation of *Escherichia coli* glycogen synthase. *J Biol Chem* **284**, 17796–17807.
24 Furukawa K, Tagaya M, Tanizawa K and Fukui T (1994) Identification of Lys277 at the active site of *Escherichia coli* glycogen synthase: application of affinity labeling combined with site-directed mutagenesis. *J Biol Chem* **269**, 868–871.
25 Furukawa K, Tagaya M, Tanizawa K and Fukui T (1993) Role of the conserved Lys-X-Gly-Gly sequence at the ADP-glucose-binding site in *Escherichia coli* glycogen synthase. *J Biol Chem* **268**, 23837–23842.
26 Yep A, Ballicora MA and Preiss J (2004) The active site of the *Escherichia coli* glycogen synthase is similar to the active site of retaining GT-B glycosyltransferases. *Biochem Biophys Res Commun* **316**, 960–966.
27 Kadouche D, Ducatez M, Cenci U, Tirtiaux C, Suzuki E, Nakamura Y, Putaux J-L, Terrasson AD, Diaz-Troya S, Florencio FJ *et al.* (2016) Characterization of function of the *glgA2* glycogen/starch synthase in *cyanobacterium* sp. Clg1 highlights convergent evolution of glycogen metabolism into starch granule aggregation. *Plant Physiol* **171**, 1879–1892.
28 Meléndez R, Meléndez-Hevia E, Mas F, Mach J and Cascante M (1998) Physical constraints in the synthesis

of glycogen that influence its structural homogeneity: a two-dimensional approach. *Biophys J* **75**, 106–114.
29 Plohnke N, Seidel T, Kahmann U, Rögner M, Schneider D and Rexroth S (2015) The proteome and lipidome of *Synechocystis* sp. PCC 6803 cells grown under light-activated heterotrophic conditions. *Mol Cell Proteomics* **14**, 572–584.
30 Wegener KM, Singh AK, Jacobs JM, Elvitigala T, Welsh EA, Keren N, Gritsenko MA, Ghosh BK, Camp DG, Smith RD *et al.* (2010) Global proteomics reveal an atypical strategy for carbon/nitrogen assimilation by a cyanobacterium under diverse environmental perturbations. *Mol Cell Proteomics* **9**, 2678–2689.
31 Kopf M, Klähn S, Scholz I, Matthiessen JKF, Hess WR and Voß B (2014) Comparative analysis of the primary transcriptome of *Synechocystis* sp. PCC 6803. *DNA Res* **21**, 527–539.
32 Fox J, Kawaguchi K, Greenberg E and Preiss J (1976) Biosynthesis of bacterial glycogen: purification and properties of the *Escherichia coli* B ADPglucose:1,4-α-D-glucan 4-α-glucosyltransferase. *Biochemistry* **15**, 849–857.
33 Kawaguchi K, Fox J, Holmes E, Boyer C and Preiss J (1978) De novo synthesis of *Escherichia coli* glycogen is due to primer associated with glycogen synthase and activation by branching enzyme. *Arch Biochem Biophys* **190**, 385–397.
34 Cattaneo J, Chambost JP and Creuzet-Sigal N (1978) Combined action of *Escherichia coli* glycogen synthase and branching enzyme in the so-called "unprimed" polyglucoside synthesis. *Arch Biochem Biophys* **190**, 85–96.
35 Park J-T, Shim J-H, Tran PL, Hong I-H, Yong H-U, Oktavina EF, Nguyen HD, Kim J-W, Lee TS, Park S-H *et al.* (2011) Role of maltose enzymes in glycogen synthesis by *Escherichia coli*. *J Bacteriol* **193**, 2517–2526.
36 Boos W and Shuman H (1998) Maltose/maltodextrin system of *Escherichia coli*: transport, metabolism, and regulation. *Microbiol Mol Biol Rev* **62**, 204–229.
37 Ballicora MA, Sesma JI, Iglesias AA and Preiss J (2002) Characterization of chimeric ADPglucose pyrophosphorylases of *Escherichia coli* and *Agrobacterium tumefaciens*: importance of the C-terminus on the selectivity for allosteric regulators. *Biochemistry* **41**, 9431–9437.
38 Ugalde JE, Parodi AJ and Ugalde RA (2003) *De novo* synthesis of bacterial glycogen: *agrobacterium tumefaciens* glycogen synthase is involved in glucan initiation and elongation. *Proc Natl Acad Sci USA* **100**, 10659–10663.
39 Hennen-Bierwagen TA, Liu F, Marsh RS, Kim S, Gan Q, Tetlow IJ, Emes MJ, James MG and Myers AM (2008) Starch biosynthetic enzymes from developing maize endosperm associate in multisubunit complexes. *Plant Physiol* **146**, 1892–1908.
40 Tetlow IJ, Beisel KG, Cameron S, Makhmoudova A, Liu F, Bresolin NS, Wait R, Morell MK and Emes MJ (2008) Analysis of protein complexes in wheat amyloplasts reveals functional interactions among starch biosynthetic enzymes. *Plant Physiol* **146**, 1878–1891.
41 Pollock C and Preiss J (1980) The citrate-stimulated starch synthase of starchy maize kernels: purification and properties. *Arch Biochem Biophys* **204**, 578–588.
42 Boehlein SK, Shaw JR, Stewart JD, Sullivan B and Hannah LC (2015) Enhancing the heat stability and kinetic parameters of the maize endosperm ADP-glucose pyrophosphorylase using iterative saturation mutagenesis. *Arch Biochem Biophys* **568**, 28–37.
43 Hwang S-K, Hamada S and Okita TW (2006) ATP binding site in the plant ADP-glucose pyrophosphorylase large subunit. *FEBS Lett* **580**, 6741–6748.
44 Baba T, Noro M, Hiroto M and Arai Y (1990) Properties of primer-dependent starch synthesis catalysed by starch synthase from potato tubers. *Phytochemistry* **29**, 719–723.
45 Iglesias AA, Ballicora MA, Sesma JI and Preiss J (2006) Domain swapping between a cyanobacterial and a plant subunit ADP-glucose pyrophosphorylase. *Plant Cell Physiol* **47**, 523–530.
46 Alford JT, Borisova-Mayer M, Mayer C and Forchhammer K (2025) Diverse metabolic control of phosphoglucomutases by bisphosphorylated sugars in heterotrophic bacteria. *Microb Physiol* **35**, 50–64.
47 Díaz-Troya S, Roldán M, Mallén-Ponce MJ, Ortega-Martínez P and Florencio FJ (2020) Lethality caused by ADP-glucose accumulation is suppressed by salt-induced carbon flux redirection in cyanobacteria. *J Exp Bot* **71**, 2005–2017.
48 Wolstencroft K, Krebs O, Snoep JL, Stanford NJ, Bacall F, Golebiewski M, Kuzyakiv R, Nguyen Q, Owen S, Soiland-Reyes S *et al.* (2017) FAIRDOMHub: a repository and collaboration environment for sharing systems biology research. *Nucleic Acids Res* **45**, D404–D407.
49 Chen X, Schreiber K, Appel J, Makowka A, Fähnrich B, Roettger M, Hajirezaei MR, Sönnichsen FD, Schönheit P, Martin WF *et al.* (2016) The Entner–Doudoroff pathway is an overlooked glycolytic route in cyanobacteria and plants. *Proc Natl Acad Sci USA* **113**, 5441–5446.
50 Gründel M, Scheunemann R, Lockau W and Zilliges Y (2012) Impaired glycogen synthesis causes metabolic overflow reactions and affects stress responses in the cyanobacterium *Synechocystis* sp. PCC 6803. *Microbiology* **158**, 3032–3043.

Redox control and substrate specificity of the glycogen catabolic isoenzymes in *Synechocystis* sp. PCC 6803

Niels Neumann[1,2], Sofía Doello, Kenric Lee[2], Bill Kauderer, Karl Forchhammer[2]*

[1]Institute of Cell Biology, University of Tübingen, Auf der Morgenstelle 15, 72076 Tübingen, Germany

[2]Interfaculty Institute of Microbiology and Infection Medicine, University of Tübingen, Auf der Morgenstelle 28, 72076 Tübingen, Germany

*Corresponding author, karl.forchhammer@uni-tuebingen.de

Running title:

Redox control and substrate specificity of the glycogen catabolic isoenzymes in *Synechocystis* sp. PCC 6803

Key words:

Glycogen; cyanobacteria; thioredoxin; reactive oxygen species (ROS), glycogen phosphorylase; glycogen debranching enzyme, enzyme catalysis, metabolic regulation

Abstract

Glycogen serves as the main carbon storage polymer in many organisms and is widespread across all domains of life. In cyanobacteria, glycogen degradation is crucial for metabolic transitions during dark phases or during resuscitation from nitrogen starvation. Like many other cyanobacteria, *Synechocystis* sp. PCC 6803 possesses multiple homologues of glycogen catabolizing enzymes, though their specific roles and regulatory mechanisms are only partially understood. Here we demonstrate through biochemical analysis that the glycogen phosphorylase GlgP1, known to promote high temperature acclimation, is uniquely regulated by a C-terminal redox switch found certain cyanobacteria. This is the first evidence of redox regulation of a prokaryotic glycogen degrading enzyme. Notably, GlgP1 is activated via oxidation by reactive oxygen species and inactivated by reducing agents, with thioredoxin being the most effective inhibitor tested. The physiological implications of this redox regulation are discussed. Additionally, a biochemically characterization of the two glycogen debranching isoenzymes GlgX1 and GlgX2 revealed that only GlgX1 exhibits debranching activity, while GlgX2 does not. Mutant analysis confirmed that GlgX1 plays an essential role in glycogen mobilization, being crucial for resuscitation from chlorosis and survival during extended dark periods. In contrast the physiological function of GlgX2 remains unclear.

Introduction

Glycogen is the primary carbon storage compound in animals, fungi and most bacteria. It is a glucose polymer linked at position α-1,4 with branches at position α-1,6. In bacteria, particularly free-living strains, glycogen is usually built up under conditions of carbon surplus and degraded when energy or carbon availability becomes limited [1-3]. In cyanobacteria glycogen plays a key role in carbon metabolism and is tightly coupled to a photoautotrophic lifestyle: During daylight excess fixed CO_2 is stored as glycogen which is subsequently broken down at night when metabolism switches to a heterotrophic mode. This essential role is further underscored by the fact that glycogen metabolic enzymes are conserved in all known cyanobacterial strains [4]. Beyond providing energy during dark phases, glycogen degradation is also crucial for acclimation to environmental stress, particularly nitrogen starvation, which is a frequent challenge in marine and terrestrial ecosystems [5]. Adaptation to nitrogen starvation in non-diazotrophic cyanobacteria triggers a genetically determined program, called chlorosis, where cells enter a state of dormancy, enabling them to outlive long periods of nitrogen deprivation. Once combined nitrogen sources become available again, cells can resuscitate within 48 hours, a process primarily fueled by the rapid breakdown of accumulated glycogen which provides the building blocks for re-establishing metabolic processes. [6-8]. Glycogen breakdown requires the coordinated action of glycogen phosphorylase (GlgP) and glycogen debranching enzyme (GlgX): GlgP

catalyzes the transfer of orthophosphate to the non-reducing ends of glycogen, releasing glucose-1-phosphate (Glc-1P) which is considered the rate limiting step in glycogen turnover [9]. This processive reaction halts once GlgP reaches the last four glucose residues left on a branch. In prokaryotes those remaining glucose units are hydrolyzed by "direct" debranching enzymes, releasing maltotetraose, which is further processed by maltodextrin phosphorylase (MalP) and by a-1,4-glucanotransferase (MalQ) [10]. The released Glc-1P is converted to Glc-6P by phosphoglucomutase (PGM) enabling its entry into different metabolic pathways including the Embden–Meyerhof–Parnas (EMP), the Entner-Doudoroff (ED) and the oxidative-pentose-phosphate (OPP) pathway.

Like many other cyanobacteria, the unicellular model organism *Synechocystis* sp. PCC 6803 (from now *Synechocystis*) encodes multiple isoenzymes involved in glycogen catabolism, including the glycogen phosphorylases *sll1356* (*glgP1*) and *slr1367* (*glgP2*) as well as the glycogen debranching enzymes *slr0237* (*glgX1*) and *slr1857* (*glgX2*). Previous studies have shown that GlgP2 is responsible for glycogen degradation during the dark and during resuscitation from chlorosis [8]. In contrast, GlgP1 does not contribute to glycogen degradation under those conditions but has been implicated in high temperature acclimation [11]. The roles of GlgX1 and GlgX2 have so far not been investigated and it is unclear whether these enzymes exhibit distinct enzymatic activities or physiological roles in *Synechocystis*. The need for cyanobacteria to switch between autotrophic and heterotrophic metabolic states implies a tight regulation of glycogen catabolism to prevent a premature degradation. While our previous work identified PGM as a key regulator of glycogen metabolism during chlorosis and resuscitation, the divergent roles of GlgP1 and GlgP2 imply additional regulatory mechanisms governing these enzymes [12].

In this study, we address these critical gaps by characterizing the biochemical properties of these isoenzymes, uncovering a novel redox-regulatory switch in GlgP1 and establishing a clear functional hierarchy in glycogen catabolism.

Results

Activity of GlgP1 is redox regulated

Synechocystis encodes two isoforms of glycogen phosphorylases, the product of *glgP1* (*sll1356*) and *glgP2* (*slr1367*). Previous studies showed that GlgP2 is essential for glycogen degradation during the night and for recovery from nitrogen starvation, whereas GlgP1 appears dispensable under these conditions but was shown to contribute to growth at elevated temperatures [8, 11]. However, the biochemical activity and regulation of GlgP1 and GlgP2 have not been characterized to date.

To determine the enzymatic activity of GlgP1 and GlgP2 we purified the respective recombinant proteins overexpressed in *Escherichia coli.* Since glycogen phosphorylases require pyridoxal phosphate (PLP) as an essential co-factor, we measured UV/Vis absorbance to ensure that both enzymes show equal loading with PLP (**Figure S1**). GlgP activity was assessed by coupling the formation of glucose-1-phosphate (Glc-1P) from glycogen to the NADPH-producing reactions of phosphoglucomutase (PGM) and glucose-6-phosphate dehydrogenase (G6PDH). Reactions contained 10 mM KH_2PO_4 (saturating concentration; data not shown) and varying amounts of oyster-derived glycogen (0.1–1%) which was used to start the reaction. Both enzymes exhibited robust in vitro activity and were capable of glycogen degradation. While GlgP1 and GlgP2 showed comparable K_m values for glycogen, GlgP1 displayed a higher overall catalytic efficiency (**Figure 1A and B**, **Table 1**).

Inspired by the findings of Florencio, Pérez-Pérez [13] who identified GlgP2 as a putative target of thioredoxin A (TrxA), we investigated whether reducing conditions affect the activity of GlgP1 and GlgP2. Therefore, we pre-incubated enzyme reactions with 5 mM dithiothreitol (DTT) for 30 minutes prior to initiation by glycogen addition. Strikingly under reducing conditions GlgP1 did not follow standard Michaelis-Menten kinetics anymore but showed an allosteric/sigmoidal kinetic curve. Its Catalytic efficiency of GlgP1 dropped to 7.5% of the original activity due to a markedly increased $K_{0.5}$ and a reduced k_{cat}. In contrast GlgP2 activity remained unaffected by DTT treatment (**Figure 1A and B**, **Table 1**).

To further quantify the redox sensitivity of GlgP1, we performed a DTT titration, incubating the enzyme with 0.5 to 10 mM DTT for 30 minutes. As shown in **Figure 1C**, treatment with 5 mM DTT was sufficient to achieve maximum inhibition of GlgP1 and higher DTT concentrations did not lead to further activity loss. GlgP1 treated with 5 mM DTT was therefore used as a reference for a fully reduced enzyme in all subsequent experiments. Conversely, treatment of the purified enzyme with hydrogen peroxide did not enhance GlgP1 activity, suggesting that the untreated protein is already fully oxidized under native purification conditions (data not shown).

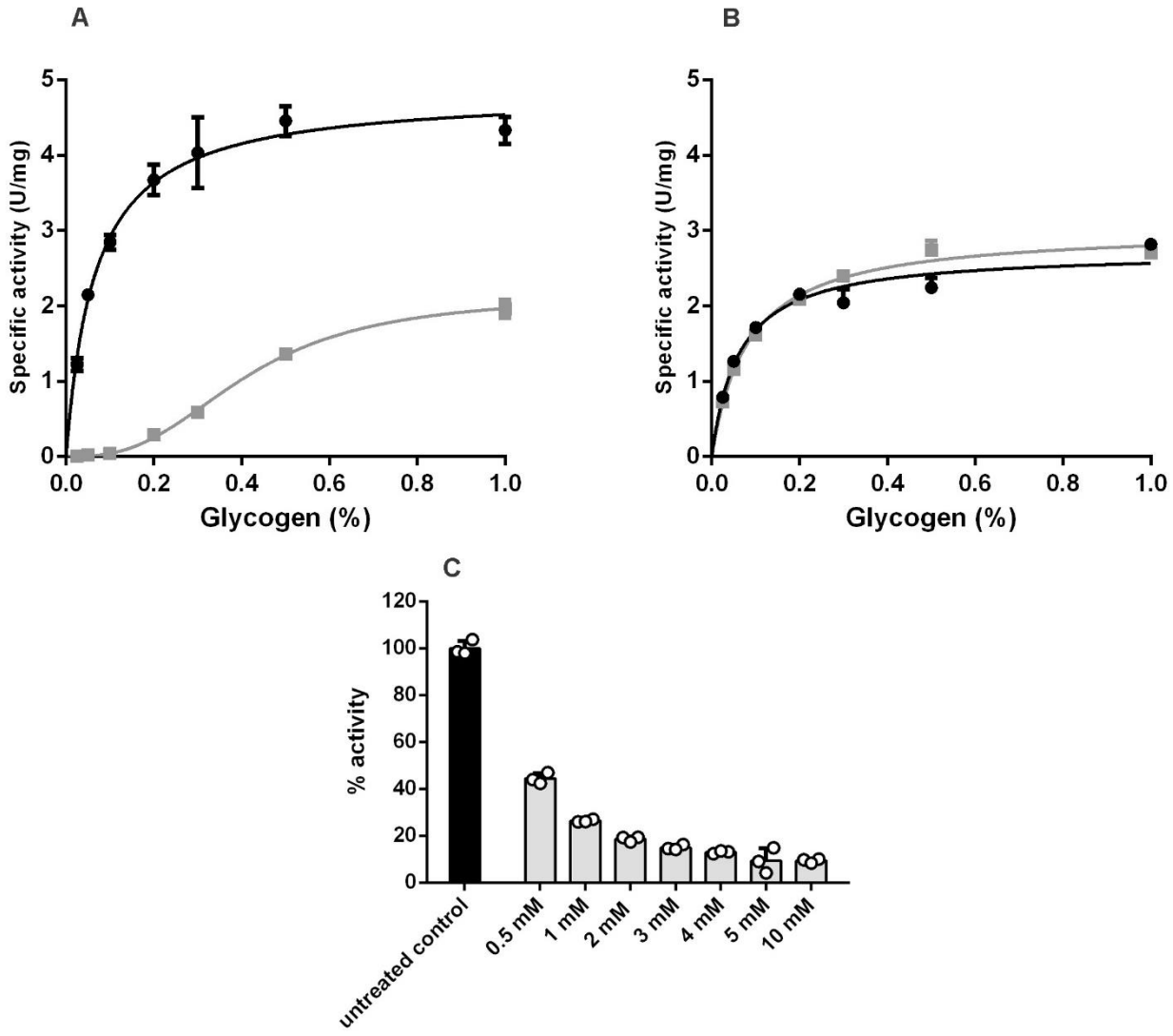

Figure 1: GlgP1 is strongly inhibited under reducing conditions

(A, B) Enzyme kinetics of GlgP1 (A) and GlgP2 (B) with or without 30 min pre-incubation with 5 mM DTT: untreated (black) and DTT-treated (light grey). (C) Relative GlgP1 activity at 0.1% glycogen following 30 min pre-incubation with increasing DTT concentrations, normalized to untreated control (black, set to 100%). Data represent mean ± SD from at least three independent replicates.

Table 1: Kinetic parameters of GlgP1 and GlgP2 with and without treatment with 5 mM DTT

	GlgP1			GlgP2		
Treatment	k_{cat} (s^{-1})	K_M or $K_{0.5}$ (mM)	Kcat/K_m or $K_{0.5}$ (mM^{-1} s^{-1})	k_{cat} (s^{-1})	K_M (mM)	K_{cat}/K_M (mM^{-1} s^{-1})
Untreated	6.56 ± 0.16	0.07 ± 0.01	93.71	4.44 ± 0.14	0.06 ± 0.01	74.00
5 mM DTT	2.90 ± 0.08	0.41 ± 0.09	7.07	4.94 ± 0.09	0.08 ± 0.01	61.75

Values represent the mean ± standard deviation (SD) from triplicate measurements

GlgP1 is selectively inhibited by TrxA and reactivated under oxidizing conditions

To further investigate the redox regulation of GlgP1, we compared the response of GlgP1 and GlgP2 to various reducing agents, including both thiol-dependent and thiol-independent compounds. Enzyme reactions (25 nM GlgP1 or GlgP2) were pre-incubated for 30 minutes with 5 mM DTT, 5 mM tris(2-carboxyethyl)phosphine (TCEP), 5 mM glutathione (GSH), or 5 mM cysteine. In addition, we tested recombinant thioredoxin A (TrxA; product of *slr0623*), applied in its reduced (TrxA_red) or oxidized (TrxA_ox) form at 2.5 µM. Enzymatic activity was assayed using 10 mM KH_2PO_4 and 0.1% oyster glycogen, and untreated enzyme served as a reference control.

Consistent with our previous observations, DTT strongly inhibited GlgP1 activity. Remarkably, TrxA_red also caused substantial inhibition, reducing GlgP1 activity to ~20% of the untreated control. TCEP, despite having a comparable redox potential (–0.29 V) to DTT (–0.33 V), showed moderate inhibition (~40% remaining activity). In contrast, GSH, cysteine, and TrxA_ox had no significant effect on GlgP1 (**Figure 2A**). None of the tested treatments, including DTT and TrxA_red, substantially affected GlgP2 activity (**Figure 2B**), underscoring a specific redox sensitivity unique to GlgP1.

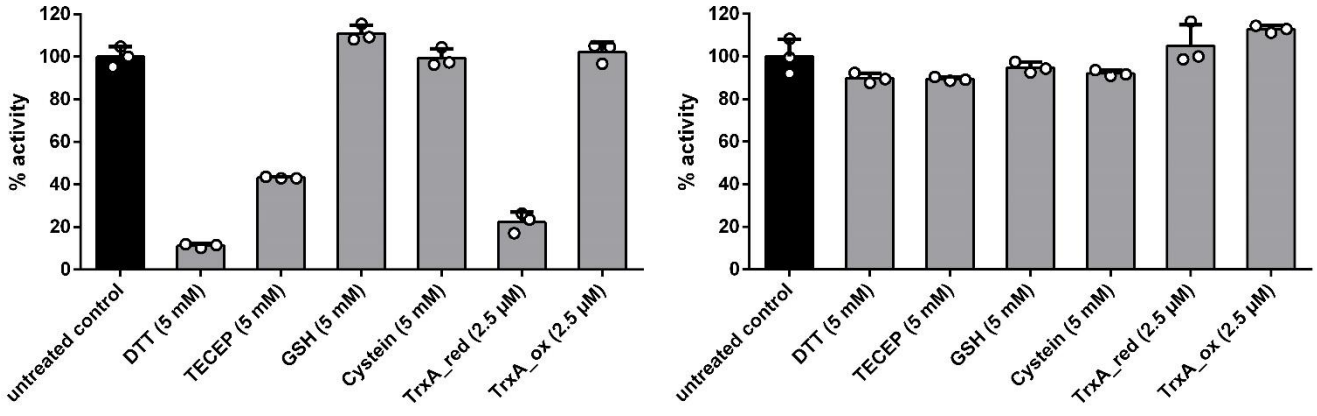

Figure 2: GlgP1 activity is specifically modulated by TrxA

(A) GlgP1 activity after 30 min pre-incubation with various reducing agents (light grey), including DTT, TCEP, GSH, cysteine, and reduced TrxA (TrxA_red); untreated control (black) set to 100%. (B) Same treatments applied to GlgP2. Bars represent mean ± SD of at least three independent replicates.

We next asked whether the inhibition of GlgP1 by reduction could be reversed through oxidation. To this end, GlgP1 was first fully reduced with 5 mM DTT, and subsequently treated with various oxidizing agents for 30 minutes at room temperature. Tested oxidants included oxidized DTT (DTT_ox), glutathione disulfide (GSSG) (5 mM each), and TrxA_ox (10 µM), as well as the stronger oxidants $CuCl_2$ (5 µM) and H_2O_2 (25 µM), for which optimal concentrations were determined in prior titrations (data not shown).

Compared to the untreated enzyme (set to 100% activity), DTT-reduced GlgP1 retained only ~10% residual activity. Upon oxidation, H_2O_2 and GSSG showed the strongest reactivation effects, restoring activity to ~65% and ~50%, respectively. $CuCl_2$ treatment led to partial recovery (~30%), while DTT_ox yielded only modest reactivation (~20%). TrxA_ox did not increase activity beyond that of the reduced control (**Figure 3**).

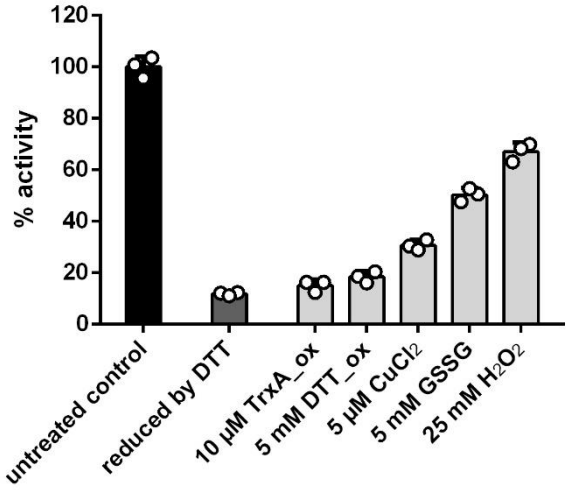

Figure 3: Oxidizing agents restore GlgP1 activity following reductive inhibition

GlgP1 activity under the following conditions: untreated control (black, 100%), DTT-reduced (dark grey), and post-treatment with various oxidants (light grey): oxidized DTT (DTT_ox), GSSG, TrxA_ox, $CuCl_2$, and H_2O_2. Data represent mean ± SD from at least three replicates.

Together, these results demonstrate that GlgP1 activity is redox-sensitive and can be partially reactivated following reductive inhibition. The pronounced effect of TrxA_red, despite its low concentration compared to the other reducing agents tested, suggests a targeted and specific redox interaction between GlgP1 and TrxA. GlgP2, in contrast, appears largely insensitive to redox modulation under the tested conditions, further highlighting functional divergence between the two isoforms.

GlgP1 C-Terminal Redox Switch Regulates Enzyme Activity and Diurnal Viability

To identify the regulatory site responsible for redox control of GlgP1 we aligned the amino acid sequence of GlgP1 and GlgP2, revealing a high overall sequence identity of 62%. By looking for prominent cysteine residues which might form disulfide bonds, we discovered a distinctive motif in the C-terminal domain of GlgP1 featuring two cysteine residues at position 837 and 842. Structural prediction using AlphaFold 3 suggests that this region forms a surface exposed hairpin loop potentially stabilized by a disulfide bond between the cysteines C837 and C842 (**Figure 4A**). A comparative sequence analysis across species indicated that this motif is unique to specific cyanobacterial strains (**Figure S2**).

To assess whether this domain is in fact responsible for redox regulation, we generated a C837S point mutant to mimic a constitutively reduced state. The activity of GlgP1 C837S matched that of the fully reduced GlgP1 WT. However, in contrast to the WT enzyme this variant did not respond to treatment with H_2O_2, confirming the redox sensitivity of this cysteine **(Figure 4B)**.

To determine whether the reduced activity of the C837S variant was due to impaired dimerization, we constructed a GlgP1 variant lacking the entire C-terminal domain (GlgP1ΔC-term) and examined its enzymatic activity as well as its oligomeric state via mass photometry. Interestingly, GlgP1ΔC-term displayed enzymatic activity comparable to the C837S mutant, while its ability to dimerize was not negatively affected **Figure 4C, Figure S4A and B**). These findings demonstrate that the C-terminal region of GlgP1 functions as a redox-sensitive regulatory element essential for full enzymatic activity, but not for dimer formation.

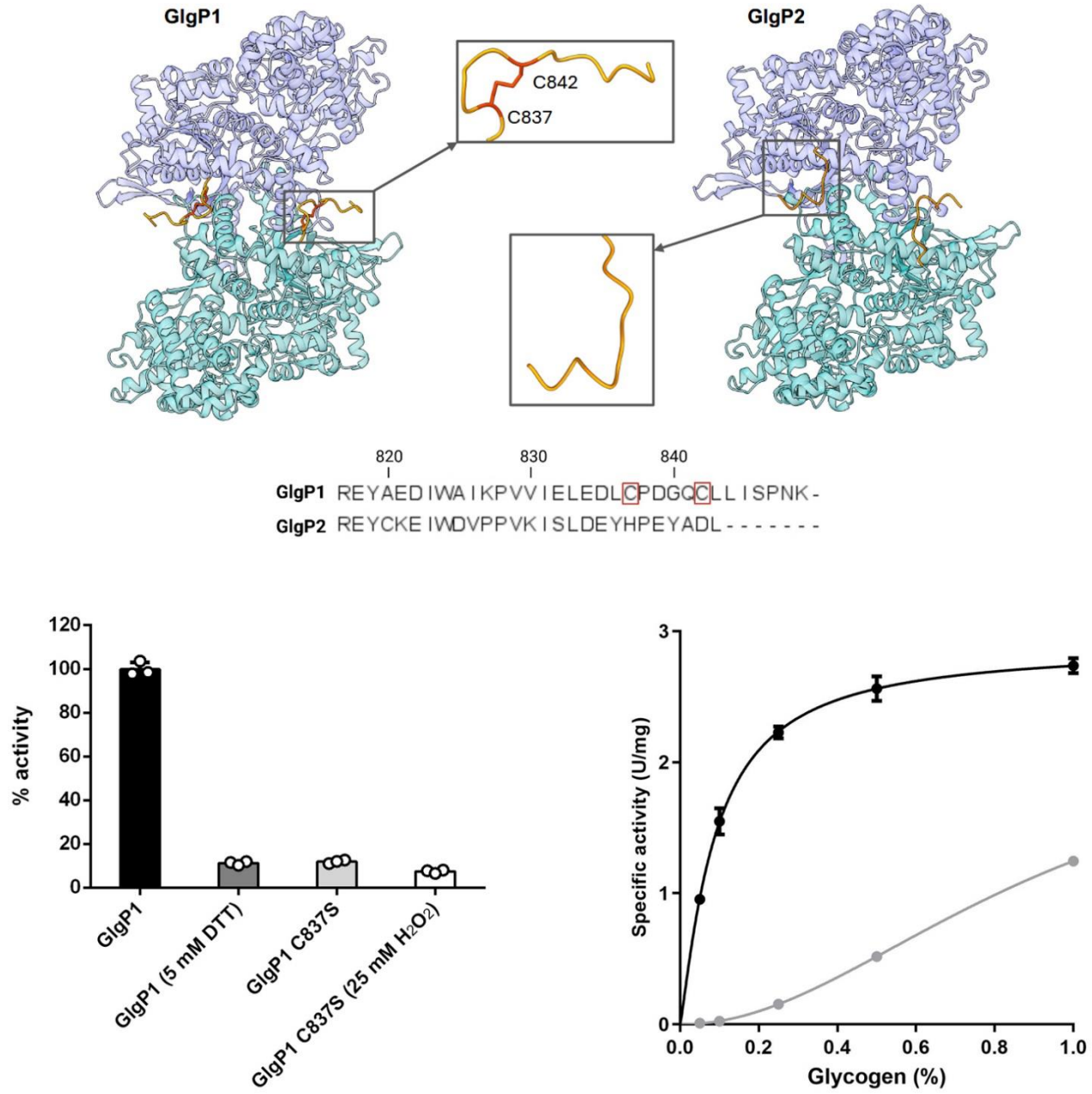

Figure 4: A C-terminal redox switch controls GlgP1 activity

(A) Predicted GlgP1 structure (AlphaFold) highlighting the C-terminal region with Cys837 and Cys842 forming a putative disulfide bond. Sequence alignment shows the absence of these residues in GlgP2. (B) Relative GlgP1 activity: WT (black, untreated = 100%), DTT-reduced WT (dark grey), untreated C837S variant (light grey), and H_2O_2-treated C837S (white). Data represent mean ± SD of at least three replicates. (C) Enzyme kinetics of GlgP1 (black) and GlgP1 (GlgP1ΔC-term)

To explore the physiological relevance of this redox regulation, we generated *Synechocystis* knockout strains lacking either or both glycogen phosphorylase isoenzymes and assessed their viability under a 12-hour light/dark cycle using a drop-plate assay. While the ***glgP2*** knockout showed a mild growth defect, the ***glgP1*** knockout grew similarly to the wild type (**Figure 5**). However, the growth impairment observed in the ***glgP2*** mutant was significantly worsened in the double knockout, indicating that both isoenzymes contribute to survival under diurnal conditions. These results suggest that GlgP1 can partially compensate for the loss of GlgP2, underscoring the physiological importance of redox regulation of GlgP1 in fluctuating light environments.

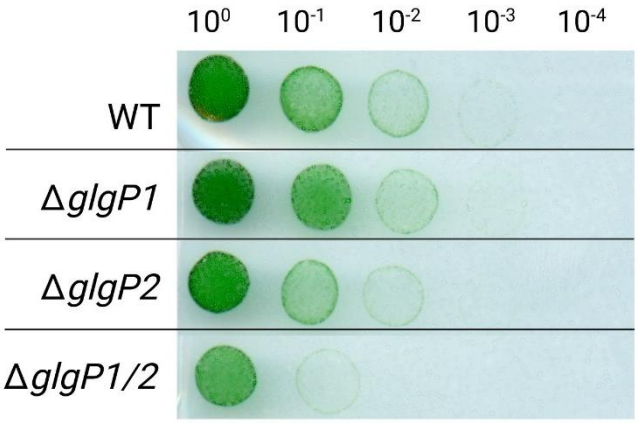

Figure 5: Both glycogen phosphorylases contribute to survival in darkness

Spot assays of *Synechocystis* WT and *glgP* mutants (*ΔglgP1*, *ΔglgP2*, double knockout) under 12 h light/12 h dark cycle. Dilution series indicated in the top row.

GlgX1 is essential for recovery from chlorosis

Complete glycogen degradation requires not only glycogen phosphorylase activity (GlgP) but also the action of a glycogen debranching enzyme. Similar to GlgP1 and GlgP2, *Synechocystis* encodes two annotated isoforms of glycogen debranching enzymes, *glgX1* (*slr0237*) and *glgX2* (*slr1857*). However, their physiological roles and biochemical activities have not yet been characterized.

To gain insight into their function we generated knockout mutants for both *glgX1* and *glgX2* and assessed their phenotypes under various growth conditions using a drop-plate assay (**Figure 6**). Under continuous light or a 12 h light–dark cycle, both mutants exhibited growth comparable to the wild type (**Figure 6A and B**). However, upon resuscitation from nitrogen chlorosis, the *glgX1* mutant displayed a noticeable growth impairment, whereas the *glgX2* mutant remained unaffected (**Figure 6C**). This phenotype became more pronounced under a 12 h light–dark resuscitation regime (**Figure 6D**) or following extended chlorosis (**Figure 6E**). These results suggest that GlgX1 plays a critical role under conditions

that require efficient mobilization of glycogen, specifically during recovery from chlorosis and long-term darkness. In contrast, GlgX1 appears to be dispensable under normal diurnal conditions, where glycogen turnover demands are lower. The physiological role of the paralogue GlgX2 remains elusive, as its deletion did not affect viability under any of the tested conditions.

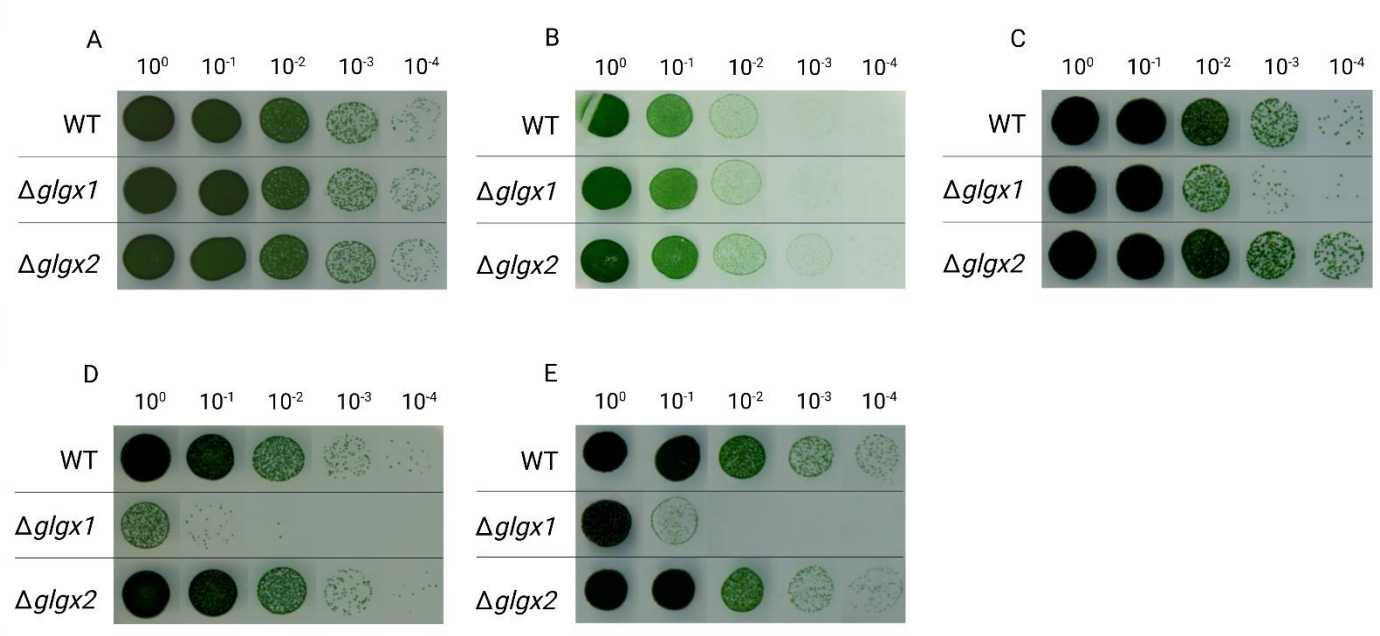

Figure 6: GlgX1 is essential for recovery from chlorosis and survival in darkness

Spot assays of WT, ΔglgX1, and ΔglgX2 strains under various conditions: (A) continuous light, (B) 12 h light/12 h dark cycle, (C) resuscitation after 14 days chlorosis (constant light), (D) resuscitation after 14 days chlorosis (light/dark), (E) resuscitation after 21 days chlorosis (constant light), (F) recovery after 14 days darkness (constant light). Dilution series indicated above.

GlgX1 promotes GlgP1 and GlgP2 activity, particularly on native glycogen

To further investigate the functional role of GlgX1 and GlgX2, we overexpressed strep-tagged versions of both enzymes in *E. coli* and tested their effects *in vitro* using the established GlgP activity assay. Alongside oyster glycogen, we included glycogen purified from nitrogen-starved *Synechocystis* cultures (both at 0.1% final concentration) to examine how glycogen origin influences enzymatic activity. To facilitate comparison, the activity of GlgP1 and GlgP2 with oyster glycogen and without GlgX addition were set to 100%. Addition of GlgX1 increased GlgP1 activity to 128% with oyster glycogen. When *Synechocystis* glycogen was used as substrate, GlgP1 activity dropped to 65% without GlgX1 but was restored to 117% in its presence (**Figure 7A**). For GlgP2, GlgX1 increased activity to 132% with oyster glycogen and from 40% to 89% with *Synechocystis* glycogen (**Figure 7B**). In contrast, GlgX2 had no significant effect on GlgP activity under any of the tested conditions (**Figure 7A and B**). This experiment yielded two major findings: First, without GlgX1 addition using *Synechocystis* derived

glycogen gives rise to generally lower GlgP activities as compared to oyster glycogen (60 % activity for GlgP1 and 40 % activity for GlgP2). Second, addition of GlgX1 enhanced the overall degradation of *Synechocystis* derived glycogen much stronger than degradation of oyster glycogen. While GlgX1 increased activity on oyster glycogen by 28% (GlgP1) and 32% (GlgP2), it boosted activity on *Synechocystis* derived glycogen by 80% and 121%, respectively. Altogether, these results suggest that *Synechocystis* glycogen is more dependent on debranching activity for efficient degradation, and that GlgP2, in particular, benefits strongly from the presence of GlgX1. In contrast, GlgX2 appears to be inactive or non-functional under these assay conditions, further supporting a dominant role for GlgX1 in glycogen catabolism.

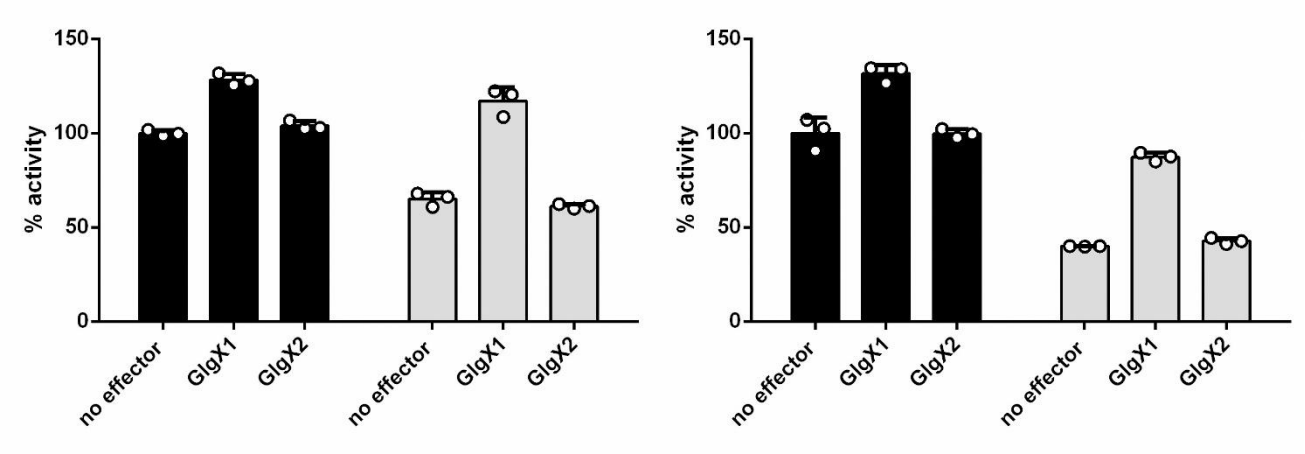

Figure 7: GlgX1 enhances GlgP activity, particularly on Synechocystis-derived glycogen

(A, B) Relative activity of GlgP1 (A) and GlgP2 (B) with or without GlgX1 or GlgX2, using either oyster glycogen (black bars) or Synechocystis glycogen (grey bars). Activities normalized to GlgP alone with oyster glycogen (set to 100%). Data are mean ± SD from at least three replicates.

In addition to testing GlgX activity, we also examined whether GlgX1 or GlgX2 might be subject to redox regulation, as previously shown for GlgP1. To this end, both debranching enzymes were pre-treated with either DTT (5 mM) or H_2O_2 (25 mM) and then added to the GlgP2 assay, using GlgP2 as a redox-insensitive background. Neither GlgX1 nor GlgX2 showed any change in activity following treatment, suggesting that, unlike GlgP1, the debranching enzymes are not redox-regulated under the tested conditions (**Figure S5**).

Discussion

Glycogen metabolism and its tight regulation is pivotal for cyanobacteria to survive in an ever-changing environment. Understanding the functions and regulatory mechanism of glycogen-associated enzymes is therefore essential for deciphering cyanobacterial physiology. In this study we investigated the glycogen phosphorylase isoenzymes GlgP1 and GlgP2 as well as the glycogen debranching isoenzymes GlgX1 and GlgX2 in *Synechocystis*. We demonstrate that GlgP1 is regulated via a C-terminal redox switch marking the first report of such a mechanism of glycogen phosphorylases in prokaryotes. Additionally, we show that GlgX1 is essential for recovery from chlorosis and enhances glycogen degradation by GlgP activity in dependence of the used glycogen source, whereas the function of GlgX2 remains elusive.

Redox regulation of GlgP1: A Novel Mechanism in Bacterial Glycogen Phosphorylases

Previous studies established that GlgP2 but not GlgP1 is the primary glycogen phosphorylase responsible for glycogen degradation during the night and resuscitation from nitrogen starvation [8], whereas GlgP1 was shown to play a role in high temperature adaptation[8, 11]. These distinct functions suggested different regulatory mechanisms for the two isoenzymes. Here we confirm that both purified GlgP isoenzymes are active *in vitro,* exhibiting standard Michaelis-Menten kinetics, with GlgP1 displaying a higher overall catalytic efficiency. However, GlgP1 activity is strongly decreased in the presence of reducing agents, adopting a sigmoidal kinetic profile. We identified a unique C-terminal extension in cyanobacterial GlgPs, with GlgP1 containing a conserved cysteine pair (C837 and C842) that forms a regulatory disulfide bond absent in GlgP2. Substitution of C837 with serine resulted in an enzyme activity resembling that of fully reduced GlgP1, underscoring the functional importance of this disulfide bond for enzymatic activation. Truncation of the entire C-terminal domain yielded a similar effect, producing an enzyme with reduced activity comparable to the fully reduced wild-type GlgP1. This suggests that the C-terminal region, and specifically the redox-sensitive cysteines, plays a critical role in regulating GlgP1 activity. The sigmoidal kinetics in the reduced state suggest a diminished glycogen affinity, while an impact on the dimer formation of GlgP1 could be excluded. Although the C-terminal extension appears to be conserved among cyanobacterial GlgPs (Figure S2), the redox-active cysteine motif is restricted to a subset of both diazotrophic and non-diazotrophic strains that are not closely related phylogenetically. This patchy distribution suggests that the motif may have been acquired through horizontal gene transfer rather than by vertical inheritance along a shared evolutionary trajectory. Redox regulation of glycogen metabolizing enzymes has been rarely described in bacteria. A previous study reported redox-dependent modulation of an starch specific amylase in the cyanobacterium *Nostoc* sp. PCC7119 [14]. In humans, an isoenzyme-specific redox regulation of the brain glycogen phosphorylase (bGP) was shown, where the oxidized state affects binding of the activator

AMP – an interaction not known to occur in bacterial GlgPs [15]. Unlike bGP, *Synechocystis* GlgP1 is activated under oxidizing conditions, revealing a distinct and previously unrecognized redox-regulatory mechanism in bacterial glycogen metabolism.

Proposed role of redox -activated GlgP1

The fact that GlgP1 is active only under oxidizing conditions raises questions on the potential role of GlgP1 and under which situations it gets activated. By testing different reducing agents that are present in the cells we could show that reduction and inactivation of GlgP1 was especially effective with TrxA, an m-type thioredoxin which has been shown to be essential in *Synechocystis* [16]. Thioredoxin has been assumed before to play a role in regulation of glycogen metabolism: A proteomic approach by Florencio, Pérez-Pérez [13] revealed that TrxA potentially interacts with several glycogen-associated enzymes in *Synechocystis*, including the glycogen synthatse GlgA2, phorphoglucomutase 1 (PGM1), and the glycogen brancing enzyme (GlgB). Curiously, GlgP1 was not identified in this study. Moreover, the OpcA protein, which regulates the activity glucose-6-phosphate dehydrogenase (G6PDH), is an additional TrxA target. Here, we show that GlgP1 gets re-activated by oxidation, most effectively by H_2O_2 and GSSG. While H_2O_2 is a common ROS species, GSSG is formed as a product of ROS scavenging by GSH and therefore closely connected to ROS formation. Thereby, a low GSH/GSSG ratio is an indicator for high oxidative stress. Being exclusive to cyanobacteria and the fact that regulation was especially effective with TrxA and H_2O_2/GSSG strongly indicates a connection of GlgP1 to photosynthetic activity. TrxA as a part of the ferredoxin/thioredoxin system is known to provide the biochemical link between light reactions and the regulation of carbon metabolism in photoautotrophic organisms [17]. Reactive oxygen species are byproducts of the photosynthetic electron transport chain, whose formation increases with light intensity and temperature, a feature encountered by all photosynthetically active organisms.

We also showed that both glycogen phosphorylases are able to contribute to night-time survival, with *glgp2* being the isoenzyme that likely contributes more to glycogen degradation in the dark, consistent with its expression levels. Despite being downregulated during the night, residual *glgp1* could also contribute to glycogen degradation in the dark, and might also be metabolically important for the transition from night to day. A previous study addressed the potential role of GlgP1, showing that GlgP1 is important for survival at high temperatures and that GlgP1 is only active during illumination [11]. High temperature has been shown to cause strong ROS formation in bacteria and in nature high temperature and high light are often associated with one another [18]. High temperatures have a negative influence on photosynthesis by increasing the oxygenase activity of RuBisCo and due to the fact that CO_2 shows a lower water solubility at higher temperatures than O_2 [19]. This increases the demand of ribulose-1,5-BP due to a higher rate of photorespiration. Several studies have shown that glycogen degradation can contribute to replenish the ribulose-1,5-BP pool by shuffling carbon through the OPP

pathway to stabilize photosynthesis [20]. This mechanism appears to be especially important during the "restart" of photosynthesis after the night phase, where it has been shown that glycogen degradation at the end of the dark phase can fill up the depleted ribulose-1,5-BP pools, leading to a faster start of photosynthesis while glycogen free mutants show a strong delay [21]. We assume that the same pathway contributes to ribulose-1,5-BP formation during heat stress. Furthermore, it was shown that survival at higher temperature and high ROS formation is dependent on the availability of GSH [22, 23]. Reduction of GSSG by glutathione reductase is dependent on NADPH, which can either be formed by linear photosynthetic electron transport or in the OPP fueled by glycogen catabolism. The oxygen-evolving complex of PSII has also been shown to be prone to heat damage, which would inhibit NADPH formation by linear electron transport, making the OPP the only source of NADPH [24].

GlgX1 is the key glycogen debranching enzyme in *Synechocystis*

It is estimated that roughly one-third of a glycogen granule is accessible to glycogen phosphorylase (GlgP) without the need to remove α-1,6-linked branches [25]. Therefore, glycogen debranching enzymes are crucial for a complete glycogen degradation. Despite their importance, little is known about their function in cyanobacteria, and the roles of the two GlgX isoenzymes in *Synechocystis* have remained unexplored. Here, we identify GlgX1 (Slr0237) as the primary glycogen debranching enzyme in *Synechocystis*. While neither the *glgX1* nor *glgX2* knockout strains showed growth defects under standard diurnal conditions, the *glgX1* mutant was severely impaired in surviving prolonged darkness. This suggests that during normal night periods, partial glycogen degradation by glycogen phosphorylases is sufficient to meet basal metabolic needs. In contrast, when glycogen reserves must be mobilized for extended periods, as during prolonged darkness, debranching activity becomes essential for accessing the full glycogen pool (**Figure 6**). A pronounced phenotype was also observed for the *glgX1* mutant during recovery from nitrogen starvation, particularly after extended chlorosis or under day-night resuscitation. This highlights the distinct metabolic demands of resuscitation, which relies not just on energy generation but also on anabolic processes requiring carbon skeletons. Glycogen degradation during resuscitation thus appears more dependent on complete access to stored glycogen via GlgX1 activity, whereas nocturnal metabolism may tolerate limited breakdown.

In contrast, *glgX2* deletion had no detectable effect under any tested condition, and GlgX2 showed no activity *in vitro*. Debranching enzymes are notoriously difficult to annotate with confidence, as their glycoside hydrolase domains can overlap functionally with those of transglycosylases or other carbohydrate-active enzymes. Thus, GlgX2 may possess a yet-undiscovered specificity or function unrelated to classical debranching activity.

Cooperativity of GlgP and GlgX depends on enzyme isoform and glycogen architercture

Our *in vitro* assays confirmed that GlgX1 enhances GlgP activity, but this effect strongly depended on the source of glycogen. Enhancement was more pronounced with glycogen isolated from *Synechocystis* than with commercially available oyster glycogen, suggesting that the structure of native glycogen is more reliant on debranching activity for efficient degradation. Notably, GlgP2 activity showed a greater dependence on GlgX1 than GlgP1, but only when *Synechocystis* derived glycogen was used. This could reflect differences in branching pattern or other structural features specific to *Synechocystis* glycogen. In eukaryotes, glycogen is known to undergo post-synthetic modifications that influence degradability and a smilar complexity might exist in cyanobacteria [26]. *Synechocystis* possesses two glycogen synthases, both contributing to glycogen biosynthesis [27]. Previous studies have shown that glycogen branching patterns differ slightly between single synthase mutants, whereas the wild type contains a mixture of both [28]. Future work should explore whether GlgP1 and GlgP2 show different preferences or efficiencies depending on which synthase produced the glycogen.

In contrast to GlgP1, GlgX1 and GlgX2 did not exhibit any detectable redox regulation (**Figure S5**), indicating that the primary level of control during glycogen breakdown lies with the GlgP enzymes themselves. The preferential stimulation of GlgP2 by GlgX1, combined with the similar resuscitation phenotypes observed in the respective knockout mutants, suggests that GlgP2 and GlgX1 function as a coordinated enzymatic pair during metabolic recovery from chlorosis. Further investigation is needed to uncover potential regulatory mechanisms governing this GlgP2-GlgX1 axis. Nonetheless, our findings provide new insight into the functional specialization of glycogen catabolic enzymes in cyanobacteria and highlight the sophisticated regulation that underpins carbon reserve utilization in *Synechocystis*. Whether these regulatory principles extend to other cyanobacterial species or are conserved across broader phylogenetic boundaries remains an open question for future research.

Methods

Cultivation of *Synechocystis*

All *Synechocystis* sp. PCC 6803 strains used in this study were grown in BG_{11} supplemented with 5 mM $NaHCO_3$, as described previously [29]. A list of the strains used in this study is provided in **Table S1**. Cultivation was performed with continuous illumination (40–50 µmol photons m^{-2} s^{-1}) and shaking (130–140 rpm) at 27°C if not stated otherwise. Induction of nitrogen starvation and resuscitation was induced as described previously [30, 31]. If mutants or strains containing antibiotic markers were used, the precultures were propagated with the appropriate concentration of antibiotics. Biological replicates were inoculated with the same precultures but propagated, nitrogen starved, and resuscitated independently in different flasks under identical conditions.

Isothermal, Single-Reaction DNA Assembly

Cloning was performed as described by Gibson, Young [32] using E. coli NEB10β cells (details in Table S2). All primers and plasmids used are shown in **Table S3** and **Table S4** in the supplemental material, respectively.

Cultivation of *Escherichia coli*

If not otherwise stated *E. coli* was grown in Luria-Bertani medium at 37°C. For growth on plates, 1.5% (w/v) agar-agar was added. For cells containing plasmids, the appropriate concentration of antibiotics was used. All *E. coli* strains used in this study are listed in **Table S2**.

Protein purification

The plasmids used for protein overexpression are shown in **Table S4**. *Escherichia coli* Rosetta-gami (DE3) (details **Table S2**) was used for the overexpression of all proteins. All purified proteins were tagged at the C-terminus with a Strep-tag. For overexpression, cells were cultivated in 2xYT (3.5% tryptone, 2% yeast extract, 0.5% NaCl; 1L of culture in 5L flasks) at 37 °C until reaching exponential growth (OD_{600} 0.6-0.8). Protein overexpression was induced by adding 75 µg/L anhydrotetracycline, followed by incubation at 20°C for 16 h. Cells were harvested by centrifugation at 4000 g for 10 min at 4 °C. Cell disruption was performed by sonication in 40 mL of lysis buffer (100 mM Tris-HCl pH 8, 150 mM NaCl, 10 mM $MgCl_2$). Lysis buffers were supplemented with DNAse I, and cOmplete™ protease inhibitor cocktail (Roche, Basel). The cell lysate was centrifuged at 40,000 g for 45 min at 4°C and the supernatant was filtered with a 0.22 µM filter.

For purification of the strep tagged proteins a 5 mL Strep-Tactin XT column (GE Healthcare, Illinois, USA) was used. The cell extracts were loaded onto the column with a peristaltic pump followed by

washing with washing buffer (50 mM Tris-HCl pH 8.0, 150 mM NaCl) and elution with elution buffer (50 mM Tris-HCl pH 8.0, 150 mM NaCl, and 50 mM biotin).

GlgP and GlgX enzymatic assays

Buffer for enzymatic reactions was composed of 50 mM HEPES-KOH pH 7.5, 10 mM $MgCl_2$, 1 mM $NADP^+$, 5 mM KH_2PO_4, 1U/µl phosphoglucomutase from rabbit muscle (P3397, Merck), 10 µM Glucose-1,6-bisphosphate and 1 U/mL G6PDH from *Saccharomyces cerevisiae* (G6378, Merck). For GlgP1/2 activity, 2,5 µg of Strep-tagged purified protein was added to each reaction. Reaction was started by the addition of glycogen. Reactions were carried out in a total of 300 µl in a 96-well microplate. Absorption change at 340 nm was continuously measured for 15 min at 30 °C in a TECAN Spark® Multiplate reader (Tecan Group AG, Männedorf, Switzerland). For determining GlgX activity, 15 µg of GlgX1 and GlgX2 Strep-tagged purified protein were added to the GlgP assay mastermix respectively.

Redox Treatments

For reduction, purified enzymes were incubated with the indicated concentrations of reducing agents for 30 minutes at room temperature, followed by enzymatic activity measurement as described above.

For reoxidation experiments, GlgP1 was first reduced with 5 mM DTT for 30 minutes to ensure full reduction of cysteine residues. Excess DTT was subsequently removed using a HiTrap Desalting Column (Cytiva) connected to a peristaltic pump and pre-equilibrated with buffer (50 mM Tris-HCl, pH 7.5, 150 mM NaCl). Eluted protein fractions were immediately used for oxidation. For reoxidation, the reduced GlgP1 protein was incubated for 30 minutes at room temperature with one of the following oxidizing conditions: 25 mM hydrogen peroxide (final ~30 mM), 10 µM oxidized thioredoxin A (TrxA), 5 mM oxidized DTT, 5 µM $CuCl_2$, or 5 mM oxidized glutathione (GSSG). Residual oxidants were removed by a second buffer exchange using the same desalting column setup. Enzymatic activity was subsequently assayed under standard conditions.

Mass Photometry Analysis.

Protein samples were diluted with buffer (50 mM Tris-HCl pH 7.5, 5 mM MgCl2) to aconcentration of 100 nM. Microscope coverslips (No. 1.5H, 24x5, Marienfeld, Germany) were cleaned 3 times by immersion in isopropanol (HPLC grade) and Milli-Q water. CultureWell gaskets (3 mm DIA x 1 mm Depth, Grace Bio-Labs, Bend, OR, USA) were assembled on the clean coverslips. 5 µL of buffer were added to a gasket's well, the focal position was identified and secured in place with an autofocus system based on total internal reflection for the entire measurement. 5 µL of diluted protein were then added to

the same well and movies of 60 s duration were recorded. Each sample was measured at least three times independently. A calibration measurement was performed to correlate contrast with mass. Images were processed and analyzed using the DiscoverMP v2022 R1 software as described in [33]

Spot viability assay

Serial dilutions of chlorotic cultures were prepared (10^0, 10^{-1}, 10^{-2}, 10^{-3}, 10^{-4}, and 10^{-5}), starting with an OD_{750} of 1.5 µL of these dilutions, dropped on solid BG_{11} agar plates, and cultivated at 50 µmol photons m^{-2} s^{-1} and 27°C for 5 to 7 d.

Statistical analysis

Statistical details for each experiment can be found in the figure legends. GraphPad PRISM was used to perform one-sided ANOVA to determine the statistical significance. Asterisks (*) in the figures symbolize the p-value: One asterisk represents $p \leq 0.05$, two asterisks $p \leq 0.01$, three asterisks $p \leq 0.001$, and four asterisks $p \leq 0.0001$

Data availability statement

All data are included in this manuscript or in supportive information

Author CRediT Statement

Niels Neumann, investigation, methodology, formal analysis, visualization, writing original draft. **Sofia Doello: conceptualization, supervision, review and editing. Kenric Lee**: investigation. **Bill Kauderer**: investigation. **Karl Forchhammer,** conceptualization, validation, supervision, writing – review and editing, project administration, funding acquisition.

Acknowledgments

This work was supported by the DFG funded research consortium FOR2816 “The Autotrophy-Heterotrophy Switch in Cyanobacteria: Coherent Decision-Making at Multiple Regulatory Layers”. We also acknowledge infrastructural funding via the Cluster of Excellence (EXC2124) “Controlling Microbes to Fight Infections”

References

1. Henrissat, B., E. Deleury, and P.M. Coutinho, *Glycogen metabolism loss: a common marker of parasitic behaviour in bacteria?* Trends in Genetics, 2002. **18**(9): p. 437-440.
2. Wang, L. and M.J. Wise, *Glycogen with short average chain length enhances bacterial durability.* Naturwissenschaften, 2011. **98**(9): p. 719.
3. Preiss, J., *Bacterial Glycogen Synthesis and its Regulation.* Annual Review of Microbiology, 1984. **38**(1): p. 419-458.
4. Beck, C., et al., *The diversity of cyanobacterial metabolism: genome analysis of multiple phototrophic microorganisms.* BMC Genomics, 2012. **13**(1): p. 56.
5. Vitousek, P.M. and R.W. Howarth, *Nitrogen limitation on land and in the sea: How can it occur?* Biogeochemistry, 1991. **13**(2): p. 87-115.
6. Sawers, R.G., *Dormancy: Illuminating How a Microbial Sleeping Beauty Awakens.* Current Biology, 2016. **26**(21): p. R1139-R1141.
7. Neumann, N., S. Doello, and K. Forchhammer, *Recovery of Unicellular Cyanobacteria from Nitrogen Chlorosis: A Model for Resuscitation of Dormant Bacteria.* Microb Physiol, 2021: p. 1-10.
8. Doello, S., et al., *A Specific Glycogen Mobilization Strategy Enables Rapid Awakening of Dormant Cyanobacteria from Chlorosis.* Plant Physiol, 2018. **177**(2): p. 594-603.
9. Alonso-Casajús, N., et al., *Glycogen Phosphorylase, the Product of the glgP Gene, Catalyzes Glycogen Breakdown by Removing Glucose Units from the Nonreducing Ends in Escherichia coli.* Journal of Bacteriology, 2006. **188**(14): p. 5266-5272.
10. Ball, S., et al., *The evolution of glycogen and starch metabolism in eukaryotes gives molecular clues to understand the establishment of plastid endosymbiosis.* Journal of Experimental Botany, 2011. **62**(6): p. 1775-1801.
11. Fu, J. and X. Xu, *The functional divergence of two glgP homologues in Synechocystis sp. PCC 6803.* FEMS Microbiology Letters, 2006. **260**(2): p. 201-209.
12. Doello, S., N. Neumann, and K. Forchhammer, *Regulatory phosphorylation event of phosphoglucomutase 1 tunes its activity to regulate glycogen metabolism.* The FEBS Journal. **n/a**(n/a).
13. Florencio, F.J., et al., *The diversity and complexity of the cyanobacterial thioredoxin systems.* Photosynthesis Research, 2006. **89**(2): p. 157-171.
14. Reyes-Sosa, F.M., F.P. Molina-Heredia, and M.A. De la Rosa, *A novel α-amylase from the cyanobacterium Nostoc sp. PCC 7119.* Applied Microbiology and Biotechnology, 2010. **86**(1): p. 131-141.
15. Mathieu, C., et al., *An Isozyme-specific Redox Switch in Human Brain Glycogen Phosphorylase Modulates Its Allosteric Activation by AMP.* J Biol Chem, 2016. **291**(46): p. 23842-23853.
16. Navarro, F. and F.J. Florencio, *The cyanobacterial thioredoxin gene is required for both photoautotrophic and heterotrophic growth.* Plant Physiol, 1996. **111**(4): p. 1067-75.
17. Schürmann, P. and B.B. Buchanan, *The ferredoxin/thioredoxin system of oxygenic photosynthesis.* Antioxid Redox Signal, 2008. **10**(7): p. 1235-74.
18. Marcén, M., et al., *Oxidative stress in E. coli cells upon exposure to heat treatments.* Int J Food Microbiol, 2017. **241**: p. 198-205.
19. Brooks, A. and G.D. Farquhar, *Effect of temperature on the CO2/O2 specificity of ribulose-1,5-bisphosphate carboxylase/oxygenase and the rate of respiration in the light.* Planta, 1985. **165**(3): p. 397-406.
20. Makowka, A., et al., *Glycolytic Shunts Replenish the Calvin-Benson-Bassham Cycle as Anaplerotic Reactions in Cyanobacteria.* Mol Plant, 2020. **13**(3): p. 471-482.
21. Shinde, S., et al., *Glycogen Metabolism Supports Photosynthesis Start through the Oxidative Pentose Phosphate Pathway in Cyanobacteria.* Plant Physiol, 2020. **182**(1): p. 507-517.
22. Suginaka, K., et al., *Effect of Intracellular Glutathione on Heat-induced Cell Death in the Cyanobacterium, Synechocystis PCC 6803.* Biosci Biotechnol Biochem, 1999. **63**(6): p. 1112-5.

23. Cameron, J.C. and H.B. Pakrasi, *Essential role of glutathione in acclimation to environmental and redox perturbations in the cyanobacterium Synechocystis sp. PCC 6803.* Plant Physiol, 2010. **154**(4): p. 1672-85.
24. Allakhverdiev, S.I., et al., *Heat stress: an overview of molecular responses in photosynthesis.* Photosynth Res, 2008. **98**(1-3): p. 541-50.
25. Meléndez-Hevia, E., T.G. Waddell, and E.D. Shelton, *Optimization of molecular design in the evolution of metabolism: the glycogen molecule.* The Biochemical journal, 1993. **295 (Pt 2)**(Pt 2): p. 477-483.
26. Prats, C., T.E. Graham, and J. Shearer, *The dynamic life of the glycogen granule.* Journal of Biological Chemistry, 2018. **293**(19): p. 7089-7098.
27. Koch, M., et al., *PHB is Produced from Glycogen Turn-over during Nitrogen Starvation in Synechocystis sp. PCC 6803.* Int J Mol Sci, 2019. **20**(8).
28. Yoo, S.-H., et al., *Glycogen Synthase Isoforms in Synechocystis sp. PCC6803: Identification of Different Roles to Produce Glycogen by Targeted Mutagenesis.* PLOS ONE, 2014. **9**(3): p. e91524.
29. Rippka, R., et al., *Generic Assignments, Strain Histories and Properties of Pure Cultures of Cyanobacteria.* Journal of General Microbiology, 1979. **111**(1): p. 1-61.
30. Schlebusch, M. and K. Forchhammer, *Requirement of the Nitrogen Starvation-Induced Protein Sll0783 for Polyhydroxybutyrate Accumulation in Synechocystis sp. Strain PCC 6803.* Applied and Environmental Microbiology, 2010. **76**(18): p. 6101-6107.
31. Klotz, A., et al., *Awakening of a Dormant Cyanobacterium from Nitrogen Chlorosis Reveals a Genetically Determined Program.* Curr Biol, 2016. **26**(21): p. 2862-2872.
32. Gibson, D.G., et al., *Enzymatic assembly of DNA molecules up to several hundred kilobases.* Nat Methods, 2009. **6**(5): p. 343-5.
33. Kofinova, Z., et al., *Measuring Protein-Protein Interactions and Quantifying Their Dissociation Constants with Mass Photometry.* Current Protocols, 2024. **4**(1): p. e962.
34. Jumper, J., et al., *Highly accurate protein structure prediction with AlphaFold.* Nature, 2021. **596**(7873): p. 583-589.

Supporting Figures:

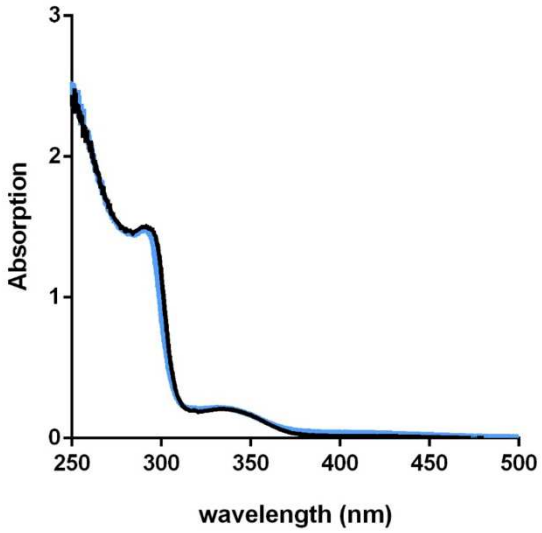

Figure S1: PLP loading confirmed for GlgP1 and GlgP2 by absorbance spectra

UV/Vis spectra of purified GlgP1 (black) and GlgP2 (blue). Absorbance at 280 nm reflects aromatic residues; absorbance at 335 nm indicates PLP in its enolimine form.

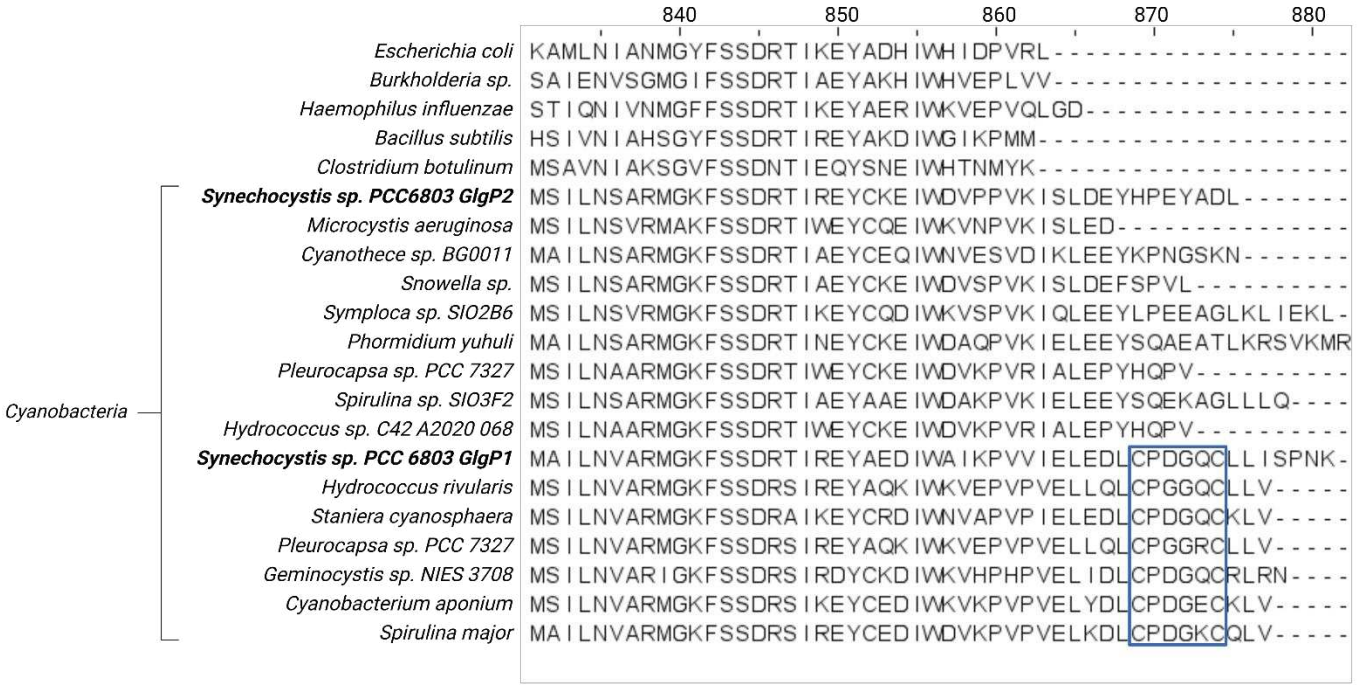

Figure S2: The GlgP1 redox switch is conserved in select cyanobacteria

Sequence alignment of the GlgP1 C-terminal region from various bacterial species. Conserved cysteine motif in GlgP1 homologues is highlighted in a blue box

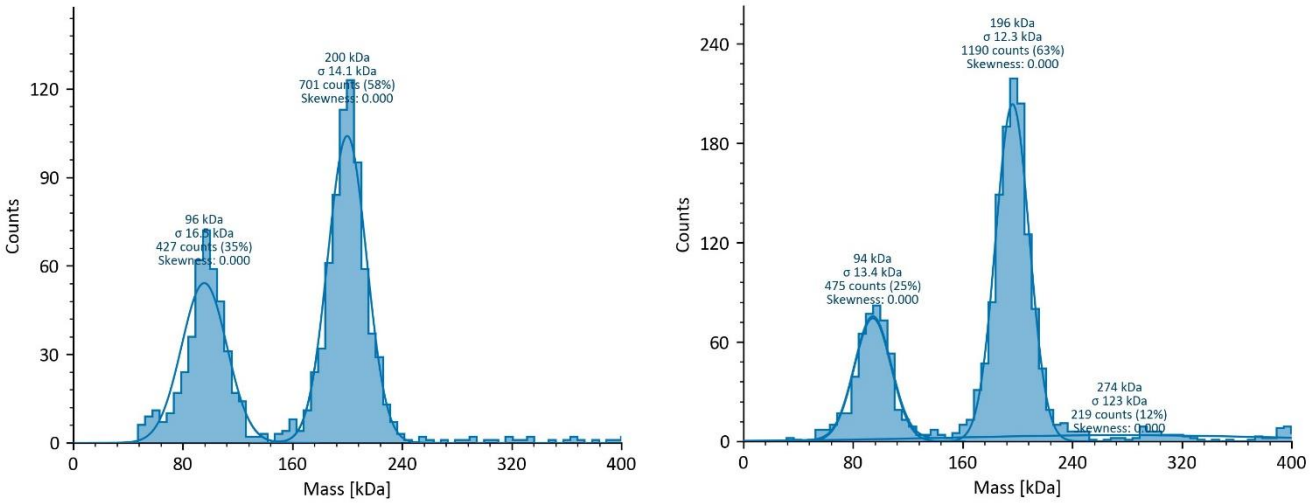

Figure S3: Mass photometry analysis of the oligomeric state of WT GlgP1 ang GlgP1ΔC-term.

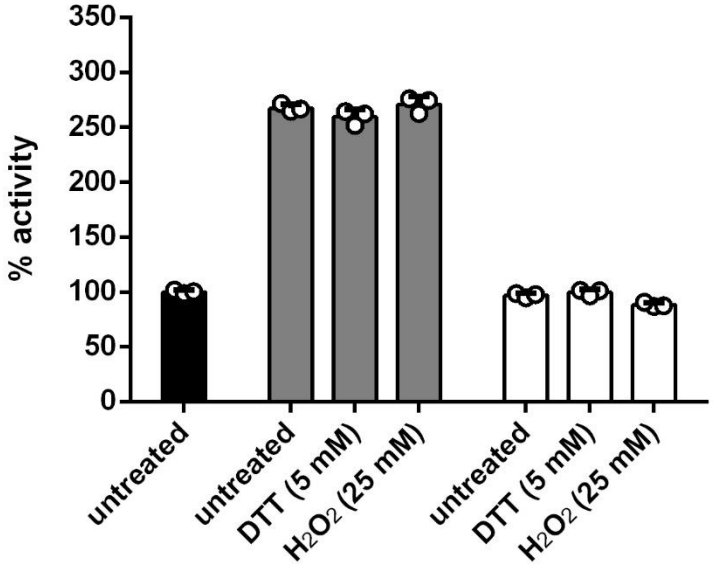

Figure S4: GlgX1 and GlgX2 activity is not influenced by redox state

Relative GlgP2 activity in the presence of GlgX1 or GlgX2 pre-treated with either DTT or H_2O_2. Control reactions without GlgX (dark grey), with GlgX1 (light grey), and with GlgX2 (white). *Synechocystis* glycogen was used as substrate. Data are mean ± SD of at least three replicates

Supporting tables

Table S1: List of cyanobacterial strains used in this study

Strain	Genotype	Reference
Synechocystis sp. PCC 6803	Wildtype	Pasteur culture collection
Δ*glgp1*	*Sll1356::Kan*^{R}	Doello, Klotz (2018)
Δ*glgp2*	*Slr1367::Spec*^{R}	Doello, Klotz (2018)
Δ*glgp1/2*	*Sll1356::Kan*^{R}*; Slr1367::Spec*^{R}	Doello, Klotz (2018)
Δ*glgx1*	*Slr0237::Spec*^{R}	This study
Δ*glgx2*	*Slr1857::Kan*^{R}	This study

Table S2: List of strains used for cloning and protein overexpression

Strain	Genotype	Description
E. coli NEB10β	Δ(ara-leu) 7697 araD139 fhuAΔlacX74 galK16 galE15 e14-Φ80dlacZΔM15 recA1 relA1 endA1 nupGrpsL(StrR) rphspoT1 Δ(mrr-hsdRMS-mcrBC)	Molecular cloning
E. coli Rosetta gami (DE3)	Δ(ara-leu)7697 ΔlacX74 ΔphoA PvuII phoR araD139 ahpC galE galK rpsL (DE3) F'[lac$^+$ lacI^q pro] gor522::Tn10 trxB pLysSRARE (Cam^R, Str^R, Tet^R)	Protein overexpression

657 **Table S3: List of primers**

658

Primer	Sequence (5'- 3')
pASKC_glgp1_fw	CTAGAAATAATTTTGTTTAACTTTAAGAAGGAGATATACAAATGGAGCACCTTCCCATGGC
pASKC_glgp1_rev	GGTCTTATTTTTCGAACTGCGGGTGGCTCCAGCTAGCCATTTTATTAGGAGAAATTAACAAAC
pASKC_glgp2_fw	TAGAAATAATTTTGTTTAACTTTAAGAAGGAGATATACAAATGATTGATCAATCTACCCTAAAC
pASKC_glgp2_rev	GTCTTATTTTTCGAACTGCGGGTGGCTCCAGCTAGCCATTAAATCGGCGTATTCGGGATGG
pASKC_glgx1_fw	TAGAAATAATTTTGTTTAACTTTAAGAAGGAGATATACAAGTGCCACAGTTGATATCTGTTC
pASKC_glgx1_rev	GGTCTTATTTTTCGAACTGCGGGTGGCTCCAGCTAGCCATTTTTGCCATTAACACCACAG
pASKC_glgx2_fw	TAGAAATAATTTTGTTTAACTTTAAGAAGGAGATATACAAATGGAACGCATAGATATTCATC
pASKC_glgx2_rev	GGTCTTATTTTTCGAACTGCGGGTGGCTCCAGCTAGCCATTTTAGCCAGTAAAATAACAAC
pET15b_trxA_fw	CAGCAGCGGCCTGGTGCCGCGCGGCAGCCATATGCTCGAGATGAGTGCTACCCCTCAAGTTTC
pET15b_trxA_rev	CCCTCAAGACCCGTTTAGAGGCCCCAAGGGGTTATGCTAGTTATTGCTCAGCGGTGGCAGCAGCCAAC
Glgp1_C837S_fw	AGAAGACCTCTCTCCCGATGGTC
Glgp1_C837S_rev	AATTCAATTACCACGGGTTTG
pASKC_glgP1_ΔCterm_fw	TAGAAATAATTTTGTTTAACTTTAAGAAGGAGATATACAAATGGAGCACCTTCCCATGGC
PASKC_glgP1_ΔCterm_rev	TCTTATTTTTCGAACTGCGGGTGGCTCCAGCTAGCCATTAATTCAATTACCACGGGTTTG
GlgX1_DS_fw	CAAGGTAGTCGGCAAATAATCTAATTTACTGAGTTTTTGCCC
GlgX1_DS_rev	CGGCCAGTGAATTCGAGCTCGGTACCCGGGGATCCTCTAGCAATGTTAGATAAACTACATTG
GlgX1_Spec_fw	GAATCTGAACAATTTTTGGAATTGCCTGAGCTCTTGACCGAACGCAGCGGTGGTAAC
GlgX1_Spec_rev	GTTACCACCGCTGCGTTCGGTCAAGAGCTCAGGCAATTCCAAAAATTGTTCAGATTC
GlgX1_US_fw	GACCATGATTACGCCAAGCTTGCATGCCTGCAGGTCGACTTGGGGCAGGCAAGGCCATTGAC
Glgx1_US_rev	CCACTGCGCCGTTACCACCGCTGCGTTCGGTCAAGAGCTCAGGCAATTCCAAAAATTGTTC
GlgX2_DS_fw	GTTATCTTGGCAAATCATCTATTGTCTTAAATTTCCCTTTC
GlgX2_DS_rev	ATACCGCACAGATGCGTAAGGAGAAAATACCGCATCAGGCGCCATTCGCCATTCAGGCTGC
GlgX2_Kan_fw	GAGGCATTTTAGCAGGACACCCGAACCGAACAGGCTTATGTC
GlgX2_Kan_rev	CATTACTTTCCAAGTTGTGCCTCAGAGTTTGTAGAAACGCAAAAAG
GlgX2_US_fw	GACCATGATTACGCCAAGCTTGCATGCCTGCAGGTCGACTATCCCCGGATATTCTTCCCC
GlgX2_US_rev	GACATAAGCCTGTTCGGTTCGGGTGTCCTGCTAAAATGCCTC
GlgX2_prom_fw	TGCGTTTCTACAAACTCTGAGGCACAACTTGGAAAGTAATG
GlgX2_prom_rev	GAAAGGGAAATTTAAGACAATAGATGATTTGCCAAGATAAC

659

660 **Table S4: List of used plasmids**

Plasmid Name	Description	Resistance Marker	Source/Reference
pASK IBA5plus	Template for pASKC construction	Ampicillin	IBA Lifesciences (Göttingen, Germany)
pASKC	Overexpression with C-terminal Strep-tag	Ampicillin	This study
pASKC_glgp1	Expression of C-terminal Strep-tagged *Synechocystis* GlgP1 in *E.coli*	Ampicillin	This study
pASKC_glgp2	Expression of C-terminal Strep-tagged *Synechocystis* GlgP2 in *E.coli*	Ampicillin	This study
pASKC_glgp1_C837S	Expression of C-terminal Strep-tagged *Synechocystis* GlgP1 C837S in *E.coli*	Ampicillin	This study
pASKC_glgp1ΔC-term	Expression of C-terminal Strep-tagged Synechocystis GlgP1ΔC-term in *E.coli*	Ampicillin	This study
pASKC_glgx1	Expression of C-terminal Strep-tagged *Synechocystis* GlgX1 in *E.coli*	Ampicillin	This study
pASKC_glgx2	Expression of C-terminal Strep-tagged *Synechocystis* GlgX2 in *E.coli*	Ampicillin	This study
pASKC_trxA	Expression of C-terminal Strep-tagged *Synechocystis* TrXA in *E.coli*	Ampicillin	This study
pUC19_glgx1_KO	Replacement of *slr0237* for $Spec^R$ in *Synechocystis* sp. PCC 6803	Ampicillin	This study
pUC19_glgx2_KO	Replacement of *slr1857* for Kan^R in *Synechocystis* sp. PCC 6803	Ampicillin	This study

661

662